Flight Mechanics and Performance of Direct Lift Control

Applying Control Allocation Methods to a Staggered Box-Wing Aircraft Configuration

Varriale, C.

DOI
10.4233/uuid:8b868c52-f34f-4307-8fc0-b1176eaf9d04

Publication date
2022

Document Version
Final published version

Citation (APA)
Varriale, C. (2022). *Flight Mechanics and Performance of Direct Lift Control: Applying Control Allocation Methods to a Staggered Box-Wing Aircraft Configuration*. [Dissertation (TU Delft), Delft University of Technology]. https://doi.org/10.4233/uuid:8b868c52-f34f-4307-8fc0-b1176eaf9d04

Flight Mechanics and Performance of Direct Lift Control

Applying Control Allocation Methods to a Staggered Box-Wing Aircraft Configuration

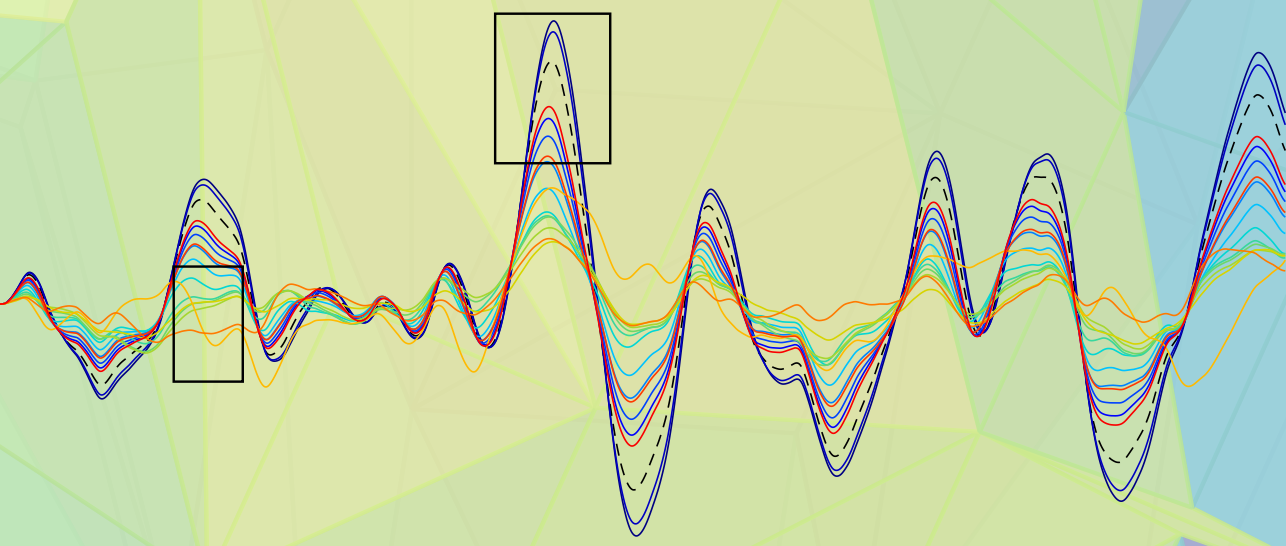

Carmine Varriale

Propositions

accompanying the PhD dissertation

Flight Mechanics and Performance of Direct Lift Control

Applying Control Allocation Methods
to a Staggered Box-Wing Aircraft Configuration

by

Carmine Varriale

These propositions are regarded as opposable and defendable, and have been approved as such by the promotors prof. dr. ir. Leo L.M. Veldhuis and prof. dr. ir. Mark Voskuijl

1. Direct Lift Control is completely irrelevant to the environmental sustainability of future aviation (Ch. 1 and Ch. 7)
2. For commercial transport applications, Control Allocation methods with closed-form solutions should always be preferred to those based on numerical iterations, as safety must precede optimality at all costs (Ch. 5 and Ch. 7)
3. Drag in trimmed cruise conditions is the only flight mechanics performance parameter worth investigating for commercial transport aircraft (Ch. 6)
4. Global optimization methods using complex physical models should be adopted only to obtain results, not explanations (Ch. 4)
5. Trusting the results of flight mechanics simulations is always a leap of faith, since complete validation is basically impossible
6. Geometric interpretations are the only truly effective way to convey a given concept, as they combine the perfection of mathematics with the beauty of art
7. Source code should always be as well written as a book, and it should be obligatorily integrated in scientific publications to improve the understanding of a task, approach, or entire discipline
8. Artificial Intelligence is dumb
9. The most important personal skill required to stay healthy and strong during a PhD research project, as if on a windy bicycle journey, is being able to realize when to ride at constant speed and when to ride at constant power
10. The outcome of every PhD research project is fundamentally twofold: the acquired knowledge for the human kind, which is almost insignificant, and the acquired comprehension of the human self, which is completely life-changing

Flight Mechanics and Performance of Direct Lift Control

Applying Control Allocation Methods to a Staggered Box-Wing Aircraft Configuration

FLIGHT MECHANICS AND PERFORMANCE OF DIRECT LIFT CONTROL

APPLYING CONTROL ALLOCATION METHODS TO A STAGGERED BOX-WING AIRCRAFT CONFIGURATION

Dissertation

for the purpose of obtaining the degree of doctor
at Delft University of Technology,
by the authority of the Rector Magnificus prof. dr. ir. T.H.J.J. van der Hagen,
chair of the Board for Doctorates,
to be defended publicly on
Tuesday 1st March 2022 at 10am

by

Carmine VARRIALE

Master of Science in Aerospace Engineering,
Università degli Studi di Napoli *Federico II*, Naples, Italy
Born in Naples, Italy

This dissertation has been approved by the promotor.

Composition of the doctoral committee:

Rector Magnificus	chairperson
Prof. dr. ir. L.L.M.Veldhuis	Delft University of Technology, *promotor*
Prof. dr. ir. M.Voskuijl	Netherlands Defence Academy, *copromotor*
Independent members:	
Prof. dr. ir. M. Mulder	Delft University of Technology
Prof. dr.-ing. F. Holzapfel	Technical University of Munich, Germany
Prof. dr. A. Frediani	University of Pisa, Italy
Prof. dr. J. Rauleder	Georgia Institute of Technology, USA
Dr. ir. G.H.N. Looye	German Aerospace Center, Germany
Prof. dr. ing. G. Eitelberg	Delft University of Technology, *reserve member*

This research has been funded by the European Union Horizon 2020 Research and Innovation Program, under Grant Agreement No.723149 – PARSIFAL.

Keywords: Direct Lift Control, Control Allocation, Flight Mechanics, Box-Wing

Printed by: Ridderprint

Front & Back: In the foreground: altitude response of a staggered box-wing aircraft in turbulent atmosphere, for different reference positions of the Control Center of Pressure. In the background: a stylized close-up view of a three-dimensional convex hull representing a generic Effective Action Set for the traditional “three-moment” Control Allocation problem.

ISBN 978-94-6366-510-0

An electronic version of this dissertation is available at
`http://repository.tudelft.nl/`.

A mio fratello Matteo,
ai miei genitori,
a nonna Ninna.

Per sviluppare una mente completa,
studia la scienza dell'arte,
studia l'arte della scienza.
Sviluppa i tuoi sensi,
impara soprattutto a vedere.
Comprendi che tutto è connesso.

To develop a complete mind,
study the science of art,
study the art of science.
Develop your senses,
especially learn how to see.
Understand that everything is connected.

SUMMARY

The objective of the present dissertation is to show how redundant control surfaces can be exploited to shape an aircraft dynamic behavior and obtain desired flight mechanics performance. This is achieved by introducing novel approaches and methods for flight mechanics and control, mainly revolving around original implementations of traditional formulations of the Control Allocation (CA) problem. Control surfaces and, more in general, control effectors are defined as redundant if they are capable to independently control the same motion axis of the aircraft.

Redundant effectors can be linked together, and to the pilot input, in many ways according to different optimality criteria and/or performance objectives. In particular, the research presented in this dissertation focuses on the possibility to achieve Direct Lift Control (DLC). The latter is intended as the ability to use control effectors to alter the aircraft lift "without, or largely without, significant change in the aircraft incidence, and ideally is meant not to generate pitching moment."

The ability to do so is essentially dependent on the position of the Control Center of Pressure (CCoP), which is the center of pressure of aerodynamic forces solely due to control surface deflections. In case of a single control surface dedicated to DLC, the CCoP coincides with the control surface itself. In case of redundant control surfaces, their deflections can be coordinated to induce the position of the CCoP towards some preferred location, as allowed by the architecture of the aircraft and the available control effectiveness.

All of the studies presented in this dissertation make use of a staggered box-wing aircraft configuration, referred to as the PrandtlPlane (PrP), as the main application test case for flight simulation analyses. The PrP has been conceived and designed for transonic commercial flight within the PARSIFAL project, funded by the European Union in the scope of the Horizon 2020 Research and Innovation Program. The peculiar geometry of the staggered box-wing allows to position multiple control surfaces both fore and aft the aircraft center of gravity, hence representing the perfect platform to experiment with new CA methods and DLC.

The scientific interest in box-wing aircraft, as well as in other disruptive and unconventional configurations, is justified by the necessity to address the future needs of the aviation sector in terms of traffic increase and, most importantly, environmental sustainability. The more fundamental scientific interest in DLC is justified by the necessity to investigate flight control techniques revolving around the possibility to modulate an aircraft lift in a fast and precise way, as it is believed that this can lead to increases in tracking performance, safety and comfort on board.

In this context, the concepts and methods proposed in the following chapters are applicable to any aircraft configuration, regardless of its shape and number of control effectors. As a matter of fact, though, they have been conceived to exploit the possibility of practically employing some form of DLC, hence expressing their full potential when

applied to aircraft configurations featuring control surfaces both fore and aft the center of gravity. These include the staggered box-wing geometry of the PrP, but are not limited to it.

The first three chapters of the dissertation are dedicated to establishing the societal, scientific, and technical background underlying the subsequent research studies. Chapter 1 moves from the many challenges that the aviation market is called to face in the present and near future, to introduce unconventional aircraft configurations as a potential solution for the sustainability of the sector. Focusing on the particular characteristics of the box-wing, it then proceeds to illustrate the fundamental theory of DLC, providing derivations and examples. It elaborates on the motivation, the scope and objective on the present dissertation, and presents a synthetic outline of the latter.

Chapter 2 presents an overview of the CA problem for redundant control effectors. It focuses on the philosophy behind the most popular approaches, and illustrates the characteristics and performance of the algorithms used for the following technical analyses. It dedicates significant attention to the geometric interpretation of CA, by introducing concepts such as the Effective Actions Set (EAS) and the Attainable Actions Set (AAS), in light of the relevance it is going to have in some of the proposed studies.

Chapter 3 presents an overview of the various components behind the flight mechanics model used in all of the subsequent analyses, introducing the adopted conventions and the equations behind the most important models. It provides a more detailed characterization of the PrP, as designed within the PARSIFAL project, and describes the software environment developed to perform the necessary flight simulations and gather the relevant results.

Chapter 4 evaluates the mission performance of the PrP aircraft model, to characterize such a disruptive aircraft concept from an operational standpoint and compare it to state-of-the-art competitors with a conventional tube-and-wing geometry. On the solid ground of optimal control theory, but with consistent injection of rules and procedures typical of realistic aeronautical operations, it presents a generic approach to aircraft mission performance assessment. It shows that the PrP is indeed competitive in terms of fuel consumption per number of passengers, although this comes at the price of a relatively low maximum range.

Chapter 5 compares the performance of different CA methods on the optimum control surface layout of a box-wing aircraft, and proposes a slight improvement on the most traditional arrangement of control surfaces on the PrP. It formulates a design problem aimed at positioning and sizing a given number of control surfaces under the constraints of adequate flying qualities, with the objective to achieve minimum total control surface span width. Flying qualities are evaluated through the simulation of a number of maneuvering tasks, which are performed by exploiting different CA methods. Results allow to make considerations on the correlation between the volume of the AAS of each CA method and the final total control surface span width.

Chapter 6 presents a trim problem formulation which employs forces and moments due to the aircraft control surfaces as decision variables. It shows how to use the geometry of the AAS to define linear equality and inequality constraints for the control forces decision variables. It defines control authority on the basis of control forces and moments, and interprets it geometrically as a distance within the AAS. It proposes novel

trim applications to maximize control authority about the lift and pitch axes, and a "balanced" control authority. In all cases, control forces and moments are mapped to control surface deflections at every solver iteration through a CA method. Results show that the method is able to capitalize on the angle of attack or the throttle setting to obtain the control surface deflections which maximize control authority in the assigned direction. The chapter also explores more conventional trim applications for minimum total drag and for assigned angle of elevation, proving the flexibility of the proposed method.

Chapter 7 presents a CA approach aimed at altering the characteristics of the transient response of an aircraft by exploiting the properties of the CCoP. The approach is based on a weighting matrix to prioritize control effectors, and is implemented in three application studies to evaluate the dynamic performance of the PrP: a simple pull-up maneuver, a trajectory tracking task, and an altitude holding task in turbulent atmosphere. Results show that, in the best-case scenario, the aircraft is able to completely cancel the non-minimum phase behavior typical of pitch dynamics, hence achieving a sharp initial response to longitudinal commands. If compared to a standard CA method, the proposed formulation results in improved tracking precision, better disturbance rejection, and a significant reduction in perceived overall acceleration when flying in turbulent atmosphere, contributing to an improved feeling of comfort for passengers on board.

Chapter 8 presents a comprehensive, top-level recap of the main aspects and topics covered within the dissertation. It reflects on the classic meaning of DLC, and what it means to achieve it with redundant control surfaces that are not expressly dedicated to it. With some considerations on the needs of aviation market, it speculates on the practical role of unconventional aircraft configurations in the near future. It synthesizes the main results achieved in the previous chapters and provides answers to the research questions formulated in Chapter 1. Lastly, it provides suggestions for improvements and future research studies.

CONTENTS

Summary ix

Table of contents xiii

Acronyms xvii

Symbols xix

1 Introduction 1
- 1.1 Direct Lift Control. . . . 8
  - 1.1.1 Two conceptual examples 11
  - 1.1.2 General longitudinal response 16
  - 1.1.3 Summary 19
- 1.2 The opportunity with redundant effectors 21
- 1.3 Motivation, objective and scope 23
- 1.4 Outline 24

2 Control Allocation 27
- 2.1 The problem with redundant effectors 28
- 2.2 Fundamental Control Allocation problem 30
- 2.3 Geometric interpretation 31
- 2.4 Notable approaches. . . . 33
  - 2.4.1 Generalized inverses and ganging 36
  - 2.4.2 Weighted Pseudo Inverse 37
  - 2.4.3 Direct Allocation 38
- 2.5 The Attainable Actions Set 40
- 2.6 Conclusions. . . . 44

3 Flight mechanics model 45
- 3.1 The PrandtlPlane 46
- 3.2 Disciplinary sub-models 47
  - 3.2.1 Geometry 48
  - 3.2.2 Aerodynamics 51
  - 3.2.3 Propulsive system 57
- 3.3 Flight dynamics 57
  - 3.3.1 Flight Control System 59
  - 3.3.2 Equations of motion 60
- 3.4 Conclusions. . . . 62

4 Mission performance 65
- 4.1 Introduction 66
  - 4.1.1 Optimal control theory. . . . 67

4.2 Mission model . . . 68
4.2.1 Capture conditions . . . 68
4.2.2 Constraints . . . 69
4.2.3 Mission phase stereotypes . . . 70
4.2.4 Mission cost index . . . 72
4.3 Simplified flight mechanics model . . . 72
4.3.1 Point-mass equations of motion . . . 73
4.3.2 Simplified aerodynamic model . . . 74
4.3.3 Propulsive model . . . 74
4.3.4 Control variables . . . 75
4.3.5 Optimal control solver . . . 77
4.4 Simulations and results . . . 77
4.4.1 Design range performance . . . 79
4.4.2 Harmonic range performance . . . 81
4.4.3 Top-level mission performance summary . . . 82
4.5 Conclusions . . . 83

5 Control surface layouts **87**
5.1 Introduction . . . 88
5.2 Optimization framework . . . 90
5.2.1 Aerodynamic analysis . . . 91
5.2.2 Flight Control System architecture . . . 91
5.2.3 Flying Qualities constraints . . . 95
5.2.4 Objective function . . . 97
5.3 Applications and results . . . 98
5.3.1 Impact of Control Allocation methods . . . 99
5.3.2 Exploration of new Control Surface layouts . . . 104
5.4 Conclusions . . . 108

6 Trim and control authority **111**
6.1 Introduction . . . 112
6.1.1 Control Authority . . . 115
6.2 Trim problem formulation . . . 116
6.2.1 Assigned trim parameters . . . 117
6.2.2 Trim controls and bounds . . . 117
6.2.3 Linear constraints due to the AAS geometry . . . 118
6.2.4 Non-linear constraints . . . 118
6.2.5 Solution and algorithm . . . 119
6.3 Applications and results . . . 119
6.3.1 Maximum control authority . . . 120
6.3.2 Minimum aerodynamic drag . . . 125
6.3.3 Assigned pitch angle . . . 127
6.4 Conclusions . . . 130

7 Transient dynamic response **133**
7.1 Introduction . . . 134
7.2 Flight Control System architecture . . . 135
7.3 Novel Control Allocation formulation . . . 137
7.3.1 Inducing the position of the Control Center of Pressure . . . 137
7.3.2 Control effectiveness matrix augmentation . . . 139
7.3.3 Weighted prioritization . . . 140
7.4 Applications and results . . . 141
7.4.1 Trim condition . . . 142
7.4.2 Pull-up maneuver . . . 142
7.4.3 Altitude shift maneuver . . . 147
7.4.4 Altitude hold in turbulent atmosphere . . . 148
7.5 Conclusions . . . 150

8 Conclusions and recommendations **153**
8.1 Conclusions . . . 154
8.2 Reflection . . . 158
8.2.1 Direct Lift Control with redundant effectors . . . 158
8.2.2 Applications to box-wing aircraft . . . 158
8.3 Recommendations . . . 160

Acknowledgements **163**

Glossary **165**

References **171**

Curriculum Vitæ **189**

List of Publications **193**

ACRONYMS

AAS	Attainable Actions Set
ACS	Admissible Controls Set
AFCS	Automatic Flight Control System
BADA	Base of Aircraft Data
BWB	Blended Wing Body
CA	Control Allocation
CAS	Calibrated Airspeed
CCoP	Control Center of Pressure
CFD	Computational Fluid Dynamics
CI	Cost Index
CPACS	Common Parametric Aircraft Configuration Schema
CPC	Conventional Pitch Control
CS	Control Surface
CSR	CeRAS Short Range
CWPI	Constrained Weighted Pseudo Inverse
DA	Direct Allocation
DLC	Direct Lift Control
DOC	Direct Operating Costs
DoF	Degree of Freedom
EAS	Effective Actions Set
FAP	Final Approach Point
FCS	Flight Control System
FQs	Flying Qualities
ICAO	International Civil Aviation Organization
ICR	Instantaneous Center of Rotation
ISA	International Standard Atmosphere
LCR	Linear Constraint Representation
MMG	Multi-Model Generator
NDI	Non-linear Dynamic Inversion
ODE	Ordinary Differential Equation
OEI	One Engine Inoperative
PrP	PrandtlPlane
PSI	Pseudo Inverse
RANS	Reynolds Averaged Navier-Stokes
RMS	Root Mean Square
TRL	Technology Readiness Level
UML	Unified Modelling Language
WPI	Weighted Pseudo Inverse
XDSM	Extended Design Structure Matrix

SYMBOLS

Roman letters

A	generic aerodynamic action, N or N·m
a	generic acceleration, m/s^2
$\mathcal{A}$	control authority
B	control effectiveness matrix, 1/rad
b	reference wing span, m
BPR	engine bypass ratio
C	dimensionless coefficient
$\bar{c}$	aerodynamic mean chord, m
D	drag force, N
e	span efficiency factor
F	generic force, N
f	generic function
G	ganging matrix
g	gravitational acceleration, m/s^2
H	gearing matrix
h	altitude, m
I	identity matrix
J	inertia tensor, kg·m^2
$\mathcal{J}$	objective function
L	lift force, N
$\mathcal{L}$	roll moment, N·m
M	Mach number
m	mass, kg
$\mathcal{M}$	pitch moment, N·m
N	number of elements
n	load factor
$\mathcal{N}$	yaw moment, N·m
P	generalized inverse matrix
p	roll rate, rad/s
q	pitch rate, rad/s
q_∞	asymptotic dynamic pressure, Pa
R	range, km
r	yaw rate, rad/s
S	reference wing area, m^2
T	thrust force, N
t	time, s
$TSFC$	thrust-specific fuel consumption, g/(N·s)
u	longitudinal speed, m/s
$\boldsymbol{u}$	control variables
V	airspeed, m/s
v	lateral speed, m/s
W	weighting matrix
w	vertical speed, m/s
X	longitudinal force, N
x_α	position of the neutral point, m
x_δ	position of the Control Center of Pressure (CCoP), m
x_m	position of the maneuver point, m
Y	lateral force, N
Z	normal force, N

Greek letters

α	angle of attack, rad
β	angle of sideslip, rad
χ	heading angle, rad
δ	control surface deflection, rad
η	dimensionless span-wise position
γ	flight path angle, rad
μ	bank angle, deg
ν	control objective
ω	angular velocity, rad/s
φ	roll angle, rad
ψ	yaw angle, rad
ρ_∞	asymptotic density, kg/m^3
$\boldsymbol{\sigma}$	state variables
$\boldsymbol{\tau}$	trim controls
τ_δ	control device efficiency
θ	pitch angle, rad

Subscripts and superscripts

a	aerodynamic reference frame
ail	aileron
b	body reference frame

ch	convex hull
cmd	command
cr	cruise condition
dir	directional
e	Earth reference frame
ele	elevator
eng	engine
eq	equality
fin	final condition
har	harmonic
ineq	inequality
ini	initial condition
lat	lateral
lb	lower bound
lon	longitudinal
mo	maximum operative
mto	maximum at take-off
oe	operative empty
pax	passengers
p	mission phase
pil	pilot
rud	rudder
tr	trim condition
ub	upper bound
w	wind reference frame
zf	zero fuel
zl	zero lift

1

INTRODUCTION

If we have learned one thing
from the history of invention and discovery,
it is that, in the long run, and often in the short one,
the most daring prophecies seem laughably conservative.

Arthur C. Clarke
The Exploration of Space
1951

I have not the smallest molecule of faith
in aerial navigation other than ballooning [...].
I would not care to be a member of the Aeronautical Society.

William Thomson, Lord Kelvin
Letter to Baden Powell
1896

Before 2020, commercial transport aviation had been experiencing a tremendous and steady market expansion in the past few decades. As shown in Figure 1.1, worldwide air traffic had more than doubled since the beginning of the new millennium, and an analogous forecast was expected to hold for the following twenty years. In multiple occasions, the industry had already been able to prove its resilience to global catastrophic events — the attacks of 9/11, the financial crisis of 2008 — making its growth appear seemingly unstoppable [1, 2]. The global COVID-19 pandemic has definitely shocked the aviation industry with literally unprecedented intensity, as shown by the steep drop — and only partial recovery, as of 2021 — in the air traffic metrics reported in Figure 1.2.

Nevertheless, the aviation sector is expected to eventually recover and continue its growth on a global scale [2]. According to the most conservative forecasts, this should

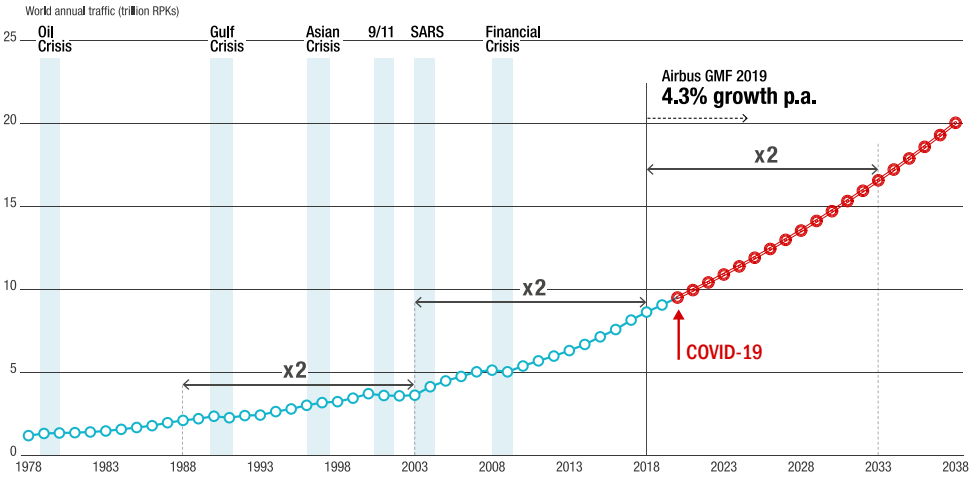

Figure 1.1 Historic trend and forecast, before the COVID-19 pandemic, of world annual traffic in Revenue Passenger Kilometers. September 2019[1] (© Airbus) [1].

happen by the end of the decade [3]. For the most optimistic predictions, an almost complete recovery could also be envisioned in the time span of two to four years [4]. On one hand, this is certainly owing to the constantly improving socio-economic background of the main players and customers of the commercial aviation industry. On the other hand, it is also undoubtedly due to the capability of the sector to overcome major challenges at national and international system level. The profound changes we have been witnessing in the past years about the logistics, comfort and safety of boarding an airplane are only a few possible examples. But in an ever changing global scenario, while some of these challenges seem to belong to the past, new ones are already awaiting at the doors of the immediate future.

Whilst the average passenger number per flight has increased by twenty since 2002, air traffic has not been spreading uniformly around the world. Many cities acting as international hubs, especially for large aircraft, have developed or consolidated an infrastructure based on multiple airports. This is where 70% of long-haul passengers and 35% of short-haul passengers concentrate. But the same has not happened for smaller cities — the endpoints in the hub-and-spoke distribution paradigm — for which a significant expansion is hindered by logistic and financial limitations [1].

In light of these trends, the growth in future passenger demand is predicted to remain unmatched by the increase in available and new airport connections. This raises reasonable concerns about the potential congestion of future aviation traffic, especially for short and medium range routes [5]. A possible passenger leak towards other means of transportation is envisioned in this range segment, where the competition is already fierce in many aspects. One of these, and probably the most fundamental factor that is going to determine the success of aviation in the future transport market, is undoubtedly

[1] The COVID-19 annotation has been added and the 2020-2038 segment has been colored in red at the moment of writing this dissertation.

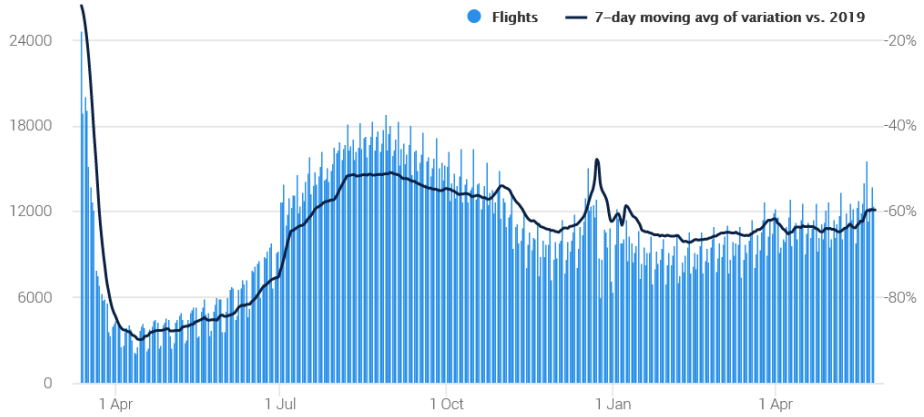

a) European traffic variation from March 13th 2020 to May 26th 2021 (© Eurocontrol[2]).

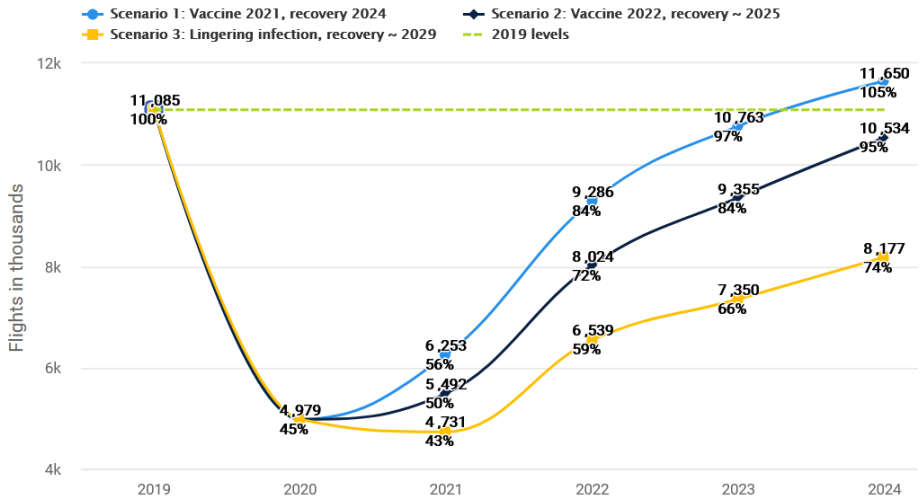

b) European traffic forecast for 2021-2024, with three scenarios depending on the progress and efficacy of vaccination campaigns (© Eurocontrol[3]).

Figure 1.2 Impact of the COVID-19 pandemic on the aviation market in Europe.

the environmental impact [6].

Commercial aviation is well known to be among the major contributors of greenhouse gas emissions in the global transport sector. Reducing the carbon imprint is regarded as the biggest and hardest challenge the sector has to face in the immediate fu-

[2]Source: `https://www.eurocontrol.int/covid19`. Accessed on: June 9th, 2021

[3]Source: `https://www.eurocontrol.int/publication/eurocontrol-forecast-update-2021-2024`. Accessed on: June 9th, 2021.

ture, if it wants to survive and stay competitive. Crucial improvements have to be implemented systematically and in the short term, "since the continuing growth in passenger and freight activity could outweigh all mitigation measures", if the latter are not effective enough [7].

At the same time, present aviation is demanded to comply with ever more stringent constraints on emissions and noise, in order to meet the ambitious and necessary sustainability goals that have been set to keep the sector competitive and the planet alive. Clean renewable energy sources have definitely been drawing the attention of researchers and investors. As a matter of fact, they represent the most straightforward and immediate way to achieve more sustainable operations, being tied to the development of more efficient engines or novel forms of propulsions, such as hydrogen or distributed (hybrid-)electric propulsive systems. Moreover, the consolidated know-how available for state-of-the-art aircraft architectures is supposed to make the integration of new subsystem technologies easier, faster, less risky and more cost-effective, at least in the short and medium term.

On the other hand, only looking at propulsive efficiency may not be enough [8–11]. Incremental innovation is, by definition, more prudent than radical revolution, and the history of aviation has not failed to demonstrate this concept throughout the last century. But it is also apparent that incremental improvements are not sufficient anymore to safeguard the needs of our future. Several recent analyses suggest that the well-refined, conventional tube-and-wing aircraft configuration seems to have reached its maximum potential, and its inherent performance and efficiency is deemed stagnant nowadays [12–14]. What is the way forward then?

Disruptive aircraft configurations have lately received renewed attention as a possible solution towards the sustainable future of commercial aviation. These are unconventional and highly innovative aircraft designs, which attempt to reshape the aviation market by abandoning the traditional paradigm of the slender fuselage connected to a cantilever wing. With such aircraft designs, potential benefits can be achieved in essentially two, non-mutually exclusive ways: a straightforward, inherent improvement in aero-propulsive performance, and the capability to exploit innovative operations and piloting techniques. As shown in Figure 1.3, some examples of disruptive aircraft designs are represented by the Blended Wing Body (BWB) [15], the more recent Flying-V concept [16], and a wide range of aircraft employing non-planar wing geometries [17, 18].

The present dissertation finds its main application subject in an innovative box-wing aircraft configuration, referred to as the PrP and shown in Figure 1.4. Brought to fame by an intuition of Ludwig Prandtl, the box-wing geometry uses two full-size, upper and lower wings, which are connected at the wing tips in a way to create a closed box. As in the case of other multi-wing architectures, its aerodynamic behavior is heavily influenced by the vertical distance between the two wings. But regardless of the value of this parameter, the box-wing has been known for almost a century as the "best wing system" for induced drag performance. This is in light of the fact that the box-wing geometry generates the least possible induced drag, for a given span and lift [19]. Such fundamental optimal behavior is retained even if the box-wing is swept and/or staggered, since the induced drag of a multi-plane is independent of the stream wise position of its elements, as stipulated by Munk's stagger theorem [20].

Interestingly, these notable properties have been formally proven for every possible multi-wing configuration only in very recent times [21]. But already in the past few years, they have constituted the scientific ground of several engineering research efforts. The latter have been mainly aimed at integrating the complex box-wing geometry into complete aircraft architectures [22, 23]. This is certainly not a trivial task, since many top-level traditional design practices have to be completely reconsidered in this case. For example, the double wing-fuselage connection creates a structurally over-constrained system. This can lead to a lighter structure, with smaller wing chords, but also to aeroelastic and fuel capacity problems [17]. Additionally, maximizing the wings vertical stagger prevents the propulsive units to be placed under the front wings, because of ground clearance concerns. Obviously, these particular considerations are always accompanied by overarching evaluations of the mass, balance and stability characteristics of the complete aircraft design [24].

One of the most down-to-earth arguments that has led to believe in box-wing aircraft configurations as potential contenders for the sustainable future of aviation maintains that their geometry is “not too unconventional”. For this reason, unlike in the case of other disruptive aircraft concepts, such as BWBs or the Flying-V, it has been argued that it could be easier for the box-wing to be accepted by the general public. Moreover, given its resemblance to a tube-and-wing aircraft with a very large horizontal tail, the adoption of the PrP for commercial transport aircraft could be expected not to involve a complete revolution in the procedures and facilities already available for aircraft certification and operations.

With its swept wings and the wide-body fuselage, the PrP has been conceived for commercial transonic applications. The horizontal stagger between the wings allows the necessary sweep angle for transonic flight, without affecting the minimum induced drag performance of the box-wing system [20]. At the same time, it allows the installation of redundant control surfaces both fore and aft of the aircraft center of gravity. While posing an interesting design challenge, this opportunity sets the PrP apart from most other disruptive aircraft configurations. It allows the aircraft to make use of unconventional piloting techniques, among which, in particular, innovative forms of DLC.

Such control strategy allows the pilot to modulate the aircraft lift directly, without necessarily generating a pitch moment to alter the aircraft angle of attack. For this rea-

a) Airbus ZEROe BWB concept (© Airbus) **b)** TU Delft Flying-V concept

Figure 1.3 Two examples of disruptive aircraft configurations.

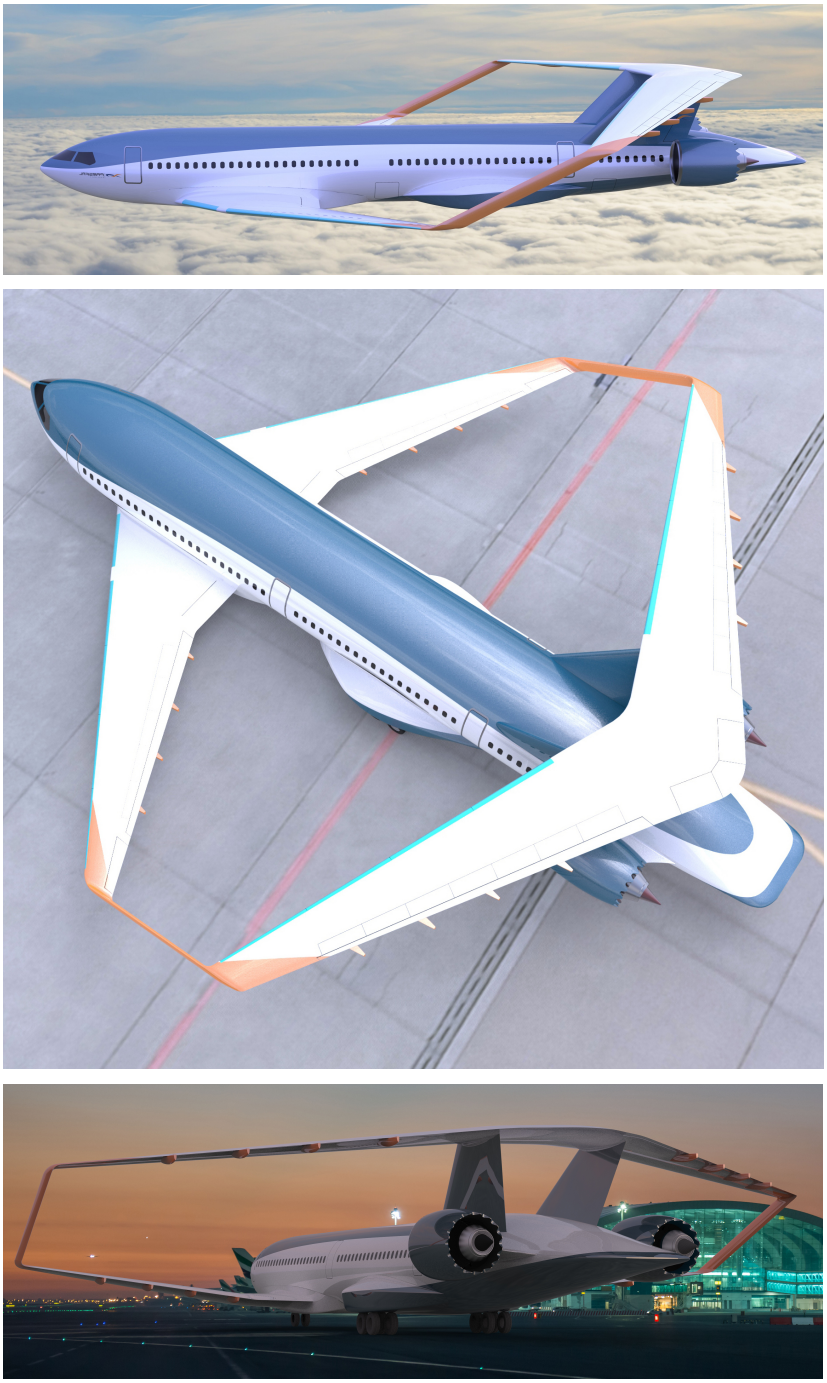

Figure 1.4 Renderings of the PrandtlPlane (PrP) aircraft configuration (parsifalproject.eu).

son, it also allows the pilot to have precise control over the aircraft vertical dynamics. As lift acts perpendicularly to the aircraft velocity vector, by definition, DLC is theoretically the fastest and most effective way to obtain a change in aircraft trajectory. As explained in more detail in the following Section 1.1, the possibility to implement DLC usually results in improved handling qualities and trajectory tracking precision. As introduced in Section 1.2, the availability of redundant control surfaces makes it possible to partially or completely decouple the control of pitch and vertical dynamics. If this is the case, DLC effectively represents an additional, independent degree of freedom to control the vertical dynamics of the aircraft, and can be exploited to achieve some performance gains also in terms of aerodynamic efficiency — trim drag in cruise conditions, for example — and control power — or control authority.

While it is certainly improper to state that DLC contributes significantly to the environmental impact of the PrP, it should be easy to understand that any available control strategy concurs to shaping the dynamic characteristics of the aircraft configurations which are able to employ it. As it is necessary, on one side, to investigate disruptive aircraft designs to ensure the sustainability of the future aviation sector, it is equally important, on the other side, to demonstrate that such new aircraft concepts could be practically operated with similar — and hopefully better — flying qualities, as compared to current ones. To the author's knowledge, only a single research study has explicitly focused on proposing and evaluating new, DLC-specific flying qualities criteria [25]. The study has been applied to two conventional aircraft models, for which a pilot stick displacement causes the simultaneous deflection of flaps — on the main wing — and elevators — on the horizontal tail. The two control surfaces are linked through a simple mechanical linkage, as shown in Figure 1.5. The study also quantifies the impact of the gearing ratios between the two movables and the pilot stick on the DLC flying qualities of the aircraft.

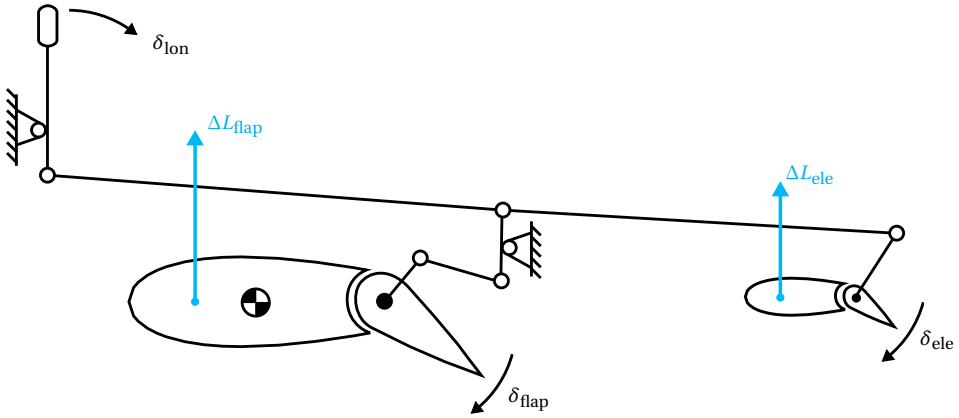

Figure 1.5 Mechanical linkage between the pilot command stick, the front flap and the tail elevator to achieve DLC of conventional aircraft configurations. Adapted from [25].

Moving from this example, the focus of the present dissertation lies exclusively on the flight mechanics of DLC, to the extent that such control strategy can be obtained

by control surfaces lying both in front and after the aircraft center of gravity. With this intention in mind, the PrP configuration is only treated as a mere application case for all the studies proposed in the following chapters. The staggered box-wing geometry simply provides a practical and flexible platform to test the developed methods, and is justified by the necessary exploration of innovative aircraft concepts to ensure the environmental sustainability of future aviation operations.

The proposed methods and formulations explore the implications of DLC on the various aspects of aircraft design, trim and dynamic response, while being completely independent of the aircraft shape under investigation. For the sake of generality, whenever the context allows it throughout the whole dissertation, the discussion will revolve around the broader concept of control effector, rather than being restricted to control surfaces only. A control effector is here intended as any physical device which is able to generate control forces and/or moments on the aircraft, in a sufficiently small time span, for the sake of maneuvering flight [26]. The nomenclature "control effectors" includes aerodynamic control surfaces, throttle and thrust vectoring systems, but also devices for active flow control, variable camber airfoils, or integrated architectures such as the propulsive empennage concept employed by the Delft University Unconventional Configuration (DUUC) aircraft.

A detailed presentation of the the fundamental characteristics of DLC is provided in the next section.

1.1. DIRECT LIFT CONTROL (DLC)

DLC is defined as the capability to use control effectors to alter the aircraft lift "without, or largely without, significant change in the aircraft incidence, and ideally is meant not to generate pitching moment" [27]. In the case of DLC, the lift unbalance caused by control effectors can rapidly result in a translational acceleration — dependent on the aircraft mass — and hence in a variation of the aircraft trajectory, through alteration of the flight path angle. This is synthetically expressed by the following Equation 1.1, making use of the time-scale separation principle.

$$\delta \rightarrow \Delta L(\delta) \rightarrow \dot{w} \propto 1/m \rightarrow \Delta\gamma \tag{1.1}$$

This is fundamentally opposed to Conventional Pitch Control (CPC) of all airplanes with traditional architecture, which revolves around the use of a tail elevator to generate a small, dislocated control lift. In this case, such lift contribution is only relevant insofar it produces a significant pitch moment and gives raise to some angle of attack dynamics. In the case of CPC, the control lift generated by the effectors is used to alter the aircraft pitch moment, which in turn determines a change in attitude, in angle of attack, and finally a variation of the aircraft lift. This ultimately results in some evolution of the trajectory, which tends to become more sluggish with the increase of the aircraft moment of inertia about its lateral axis [27, 28]. The time delay of the trajectory response achieved with CPC should be evident in Equation 1.2.

$$\delta \rightarrow \Delta L(\delta) \rightarrow \Delta\mathcal{M} \rightarrow \dot{q} \propto 1/J_{yy} \rightarrow \Delta\theta \rightarrow \Delta\alpha \rightarrow \Delta L(\alpha) \rightarrow \Delta\gamma \tag{1.2}$$

As a very indirect control technique, CPC also results in the classic, undesired non-minimum phase behavior of pitch dynamics, with the initial aircraft response — due to

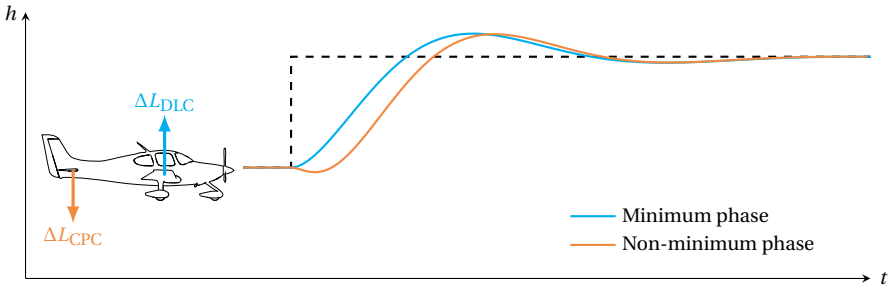

Figure 1.6 Qualitative comparison between a minimum phase and non-minimum phase altitude response, respectively associated with generic DLC and CPC pilot inputs.

control effectors dynamics — being opposite to the much larger steady-state response — due to angle of attack dynamics. This is qualitatively represented in Figure 1.6, where the inherent delay of CPC is made evident by comparison with DLC. In the case of CPC, a pull-up maneuver is initiated with a deflection of the tail elevator. Such maneuver results first in a small downward acceleration — with related altitude loss — due to the lift unbalance caused by the elevator upward deflection, and only then in a climb, due to the increase in lift due to the angle of attack. Together with the inherent lag of pitch dynamics, this behavior can be problematic in all flight conditions where fast, precise control is desired or strictly required.

The definition of DLC reported at the beginning of this section is very general and fundamental, and does not entail any practical implementation of the control system architecture which is supposed to make such control strategy available to the pilot. For this reason, many types of aircraft configurations can be said to have DLC capabilities, although in very different forms and for very different applications.

Helicopter pilots, for example, are able to control vertical dynamics directly through the collective control. This usually takes the form of a lever in the rotorcraft cockpit, and makes it possible to change the pitch angle of all the rotor blades at the same time, hence modulating the lift generated by them. For fixed-pitch propellers, as the ones typically used on the remotely piloted “drones” of common use, the vertical force is controlled simply through the alteration of the propeller speed. Two examples of these configurations are shown in Figure 1.7. What all these aircraft designs have in common is the ability to modify the lift force through some control action on the propulsive units. In the aforementioned cases, pilot commands result in the alteration of the thrust supplied by a set of rotors or propellers. To some extent, the vertical force produced by a thrust vectoring system may also be included in the same definition of DLC, although alternative designations are also common, such as “powered lift” or “direct thrust” control. Two examples of these cases are shown in Figure 1.8.

A radically different way to achieve DLC, and the only one of interest for the present dissertation, is through the deflection of control surfaces located at key positions of the aircraft geometry. For conventional aircraft configurations, existing implementations of such forms of DLC can be traced to the use of flaps and spoilers [28–31]. For conventional aircraft operations, flaps are typically only used as lift augmentation systems, and not as

a) Bell 412 helicopter **b)** Quadcopter "drone"

Figure 1.7 Examples of rotorcraft configurations achieving DLC through various forms of thrust control.

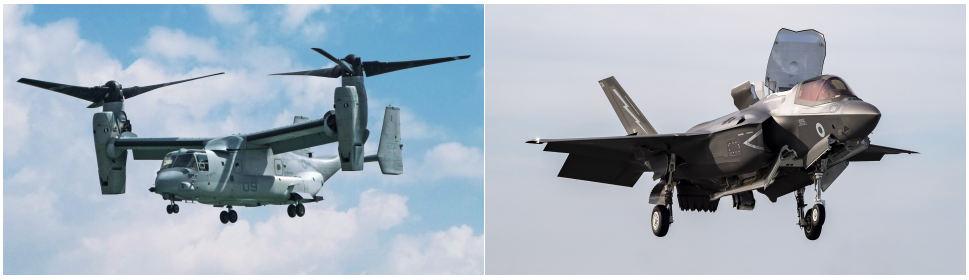

a) Bell Boeing V-22 Osprey tiltrotor aircraft **b)** Lockheed Martin F-35 Lightning II

Figure 1.8 Examples of aircraft configurations achieving DLC through various forms of thrust vectoring.

control effectors. Therefore, they have no role in maneuvering flight. On the other hand, a few experimental vehicles and in-flight simulators have been equipped with the possibility to employ DLC through the deflection of modified trailing-edge flaps on the main wing. Examples are provided by the Advanced Technologies Testing Aircraft Systems (ATTAS) of DLR, based on a VFW-Fokker 614 airframe [31], or the Lockheed L-1329 JetStar, also employed in military operations under the designation of Lockheed C-140 [32].

Beyond operating as airbrakes, at full deflection upon landing, over-the-wing spoilers can also be deflected by a specified, moderate angle to control the aircraft airspeed and descent rate. Thanks to their position close to the aircraft center of gravity, the change in pitch moment due to spoilers deflection is usually small, although not completely negligible [28, 33]. The downside of this type of operation lies in the fact that they must first be biased upwards, hence reducing the static lift and increasing the drag generated by the wing. The best know aircraft to use DLC for commercial operations is with no doubt the Lockheed L-1011 TriStar [28]. This 200 ton, three-engine, 250-passenger airliner used its four inboard spoilers to employ DLC during approach and landing phases. Inboard spoilers were biased upwards in coordination with the deployment of trailing-edge flaps, so that the steady-state change in lift due to the displacement of both types of effectors would roughly cancel. Outboard spoilers were left to be used for roll coordination and air braking, since their deflection would result in a significant pitch contribution, which would deteriorate (or completely countervail) the benefits of DLC.

DLC was implemented to increases the pitch axis control bandwidth, in order to improve the aircraft flight response to pilot commands, remove the non-minimum phase behavior, and reduce the aircraft sensitivity to external disturbances. It was integrated in the Flight Control System (FCS) through cross-feeds with the pitch control channel and the α-based autothrottle, giving the L-1011 arguably the most advanced — and complex — autolanding system of its time. Results from simulated and piloted flights report a four-time reduction in the energy absorbed by gusts, significant reduction in touchdown dispersions, a two-fold reduction in touchdown vertical speed, increase in pilot acceptability, cost and weight savings due to the relief of the CPC system, "large improvements in terms of safety" and "vast improvement in ride comfort". Figure 1.9 shows an advertising pamphlet by Trans World Airlines, boasting the L-1011 as the "the smoothest plane in the air" and "the only widebody with DLC".

Nowadays, it is common for both heavy airliners and gliders to use over-the-wing spoilers to track an assigned flight path without altering the pitch attitude significantly. Additionally, spoilers can also be used to counteract turbulence and wind shear effects in proximity of the ground, and can be operated asymmetrically, on left and right wings, to cooperate with ailerons in maintaining the wings levelled or performing roll maneuvers. Two modern examples of over-the-wing spoilers in use are shown in Figure 1.10.

Other advanced applications of DLC are common in flight scenarios where maneuvering precision and response quickness are critical, like aircraft carrier landings, station keeping, or air docking for refueling [34–37]. Unconventional and/or unmanned aircraft configurations usually allow more design freedom, hence innovative solutions like over-the-wing propellers, distributed propulsion and active flow control have also started attracting the interest of researchers as plausible ways to practically implement some forms of DLC [38, 39]. The present dissertation does not cover the DLC capabilities of such novel and agile propulsion systems, but rather focuses exclusively on the use of trailing-edge mounted control surfaces.

In the following Section 1.1.1, some peculiar aspects of the longitudinal dynamics of DLC are gently introduced by means of two conceptual examples. Following a classic derivation, the general response to a longitudinal control input is then formally presented in Section 1.1.2, where the dependency of DLC dynamic performance on key aerodynamic parameters is highlighted. Lastly, Section 1.2 presents the innovative opportunity provided by the staggered box-wing geometry of the PrP to implement DLC through the use of trailing edge control surfaces.

1.1.1. TWO CONCEPTUAL EXAMPLES

Consider a generic lifting body, equipped with some sort of movable device which allows it to achieve different dynamic responses. Rather than focusing on the practical realization of such control device, the purpose is now to show how different ways to generate control lift can impact the characteristics of the dynamic response.

For the sake of a clear and fundamental derivation focused on the conceptual analysis of the short transient behavior triggered by the control device, some simplifying assumptions are made [27]. The dynamic contribution of rotational inertia is neglected in a quasi-steady approximation: $J_{yy}\dot{q} \approx 0$. A linear aerodynamic model with constant stability derivatives is adopted. The effect of pitch rate q on the lift coefficient is neglected, as

1

TWA flies the L-1011 the world's most advanced widebody. Here's why.

From the moment you step aboard TWA's L-1011, you'll have the feeling you're in a very special plane.

You'll be particularly impressed by the spaciousness of the passenger cabin—19' wide and 8' high—with two aisles, indirect lighting, and comfortable seats. But the real beauty of the L-1011 lies in the things you don't see.

Offspring of the SST

When America embarked on the SuperSonic Transport program, considerable resources were put behind the development of new technology. Much of this has been incorporated into the L-1011, making it the most advanced widebody in the world.

The L-1011's advanced flight control system derives from the SST program.

"TWA's L-1011 fleet is another reason why you're going to like us."
—J. E. Frankum, TWA Chief Pilot

The smoothest plane in the air

The L-1011 is the only widebody with a flying horizontal stabilizer, for smoother takeoffs.

In the air, the L-1011's computerized autopilot—the most advanced of any aircraft—works to provide the smoothest flight.

And because the L-1011 is the only widebody with direct lift control (automatic adjustment of lift and pitch), it's smoother on landing, too.

An all-weather aircraft

Most widebodies have a 2-part autoland system. Only the L-1011 has a 4-part autoland system, making it more sophisticated than other aircraft.

In addition, the L-1011 has instrumentation so advanced it was granted a special Category IIIA clearance—the ability to land in all weather.

Passenger comfort

Inside TWA's L-1011, everything has been designed to make a long flight seem shorter.

The L-1011 is equipped with three Rolls-Royce high-bypass engines—the quietest of their kind.

At your fingertips are controls for reading lights, air outlets, and entertainment. Drinks, stereo music, and full-length movies help the time fly by.

So if you're planning a trip coast to coast, plan to fly on TWA's L-1011, today's most advanced widebody.

You're going to like us

TWA

Figure 1.9 Adverting pamphlet of the Lockheed L-1011 TriStar by Trans World Airlines, 1980.

a) Boeing B737-800 during descent for approach **b)** Glider during a descent flight phase

Figure 1.10 Examples of aircraft configurations achieving DLC through over-the-wing spoilers.

well as all higher order derivatives, unsteady effects ($\dot{\alpha}$), and contributions that depend on the longitudinal development of the flow. Pitch rotations and flight path variations are considered small. Moreover, the airspeed V is assumed constant, and the deflection of the control device is assumed to happen instantaneously. With these assumptions, the equations of motion used to characterize the vertical and rotational dynamics of the lifting body reduce to those in Equation 1.3.

$$\begin{cases} m\dot{w} = q_\infty S\left(C_{L_\alpha}\Delta\alpha + C_{L_\delta}\delta\right) \\ 0 = C_{L_\alpha}\bar{x}_\alpha\Delta\alpha + C_{L_\delta}\bar{x}_\delta\delta + C_{\mathcal{M}_q}q \end{cases} \tag{1.3}$$

These equations express the variation of flight parameters from an equilibrium condition in straight and level flight, and represent the starting point for the derivations presented in the current and following section. In the equations, $\bar{x}_\alpha$ is the longitudinal position of the neutral point with respect to the aircraft center of gravity. Analogously, $\bar{x}_\delta$ is the longitudinal position of the CCoP, which is the application point of lift generated through control devices. The overbar notation signifies that both variables have been nondimensionalized with respect to the mean aerodynamic chord length $\bar{c}$. The vertical acceleration $\dot{w}$ is exclusively due to a change in lift force, which in turn can be caused by both a variation of the angle of attack α and the displacement of the control device δ. It is also assumed that a positive displacement $\delta > 0$ results in an upward shift of the lift curve, and is able to impart an upward heave motion to the lifting body.

In the two following examples, some characteristics of the dynamic evolution sparking out of a unit step input on the control device are assumed *a priori*. This unusual approach allows to easily derive the vertical dynamics evolution of the lifting body, together with the conditions that allow to obtain it, in some particular flight scenarios.

PURE HEAVE MOTION

The basic kinematics of an upward translation with no alteration in rotational attitude are shown in Figure 1.11. As it can be seen in the figure, this type of motion results in a decrease of the angle of attack which is only due to the change in trajectory. In particular, $\Delta\alpha$ is equal and opposite in sign to the variation of flight path angle γ, as summarized by Equation 1.4.

$$q = \dot{\theta} = 0 \quad \Rightarrow \quad \Delta\alpha + \Delta\gamma = 0 \quad \Rightarrow \quad \Delta\alpha = -\Delta\gamma \approx -\frac{w}{V} \tag{1.4}$$

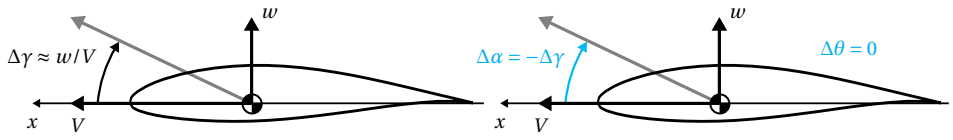

Figure 1.11 Basic kinematics of a hypothetical pure heave maneuver with no rotation about the pitch axis.

During such maneuver, the lift coefficient increases because of the action of the control device, but also decreases in light of the reduction of the angle of attack, as represented in Figure 1.13a. Because of this behavior, a pure heave maneuver should not be thought of as the ideal outcome of a DLC input, since part of the new lift generated by the control device is lost by the reduction in angle of attack, which is a direct consequence of the necessity to maintain a constant pitch attitude.

In light of the latest additional assumptions, the system of equations of motion assumes the form reported in the following Equation 1.5.

$$\begin{cases} \dfrac{m}{q_\infty S}\dot{w} + \dfrac{C_{L_\alpha}}{V} w = C_{L_\delta}\delta \\ \dfrac{C_{L_\alpha} x_\alpha}{V} w = C_{L_\delta} x_\delta \delta \end{cases} \tag{1.5}$$

In the first equation, it can be seen that the term due to the vertical speed w — which is responsible for the reduction of the angle of attack — results in a damping action for vertical dynamics. This indicates that the dynamic evolution of vertical speed is damped by aerodynamic forces due to the upward motion of the airfoil. The equation for vertical dynamics allows to find the vertical speed and acceleration responses to a unit step input of the control device in an unequivocal manner. These are expressed in the following Equation 1.6, and represented in Figure 1.13b.

$$\delta(t) = 1 \quad \Rightarrow \quad \dot{w}(t) = V\frac{C_{L_\delta}}{C_{L_\alpha}} K e^{-Kt} \quad \Rightarrow \quad w(t) = V\frac{C_{L_\delta}}{C_{L_\alpha}}\left(1 - e^{-Kt}\right) \tag{1.6}$$

where $K = q_\infty S C_{L_\alpha}/mV$. The vertical acceleration response is sharp but damped, as expected. The vertical speed increases to the maximum achievable value reported in Equation 1.7, which depends on the efficiency of the control device τ_δ.

$$w_{t\to+\infty} = V\frac{C_{L_\delta}}{C_{L_\alpha}} = -\tau_\delta V \tag{1.7}$$

By imposing that the evolution of $\dot{w}$ must be the same for both the equations of vertical and rotational dynamics, it is possible to formulate the condition required to obtain such type of dynamics. This results in Equation 1.8, which shows that the position of the CCoP is also a function of time. In particular, the CCoP has to move from its initial position towards the aircraft center of gravity, as it would be expected in a maneuver that results in no rotation about the pitch axis. The time history of the CCoP position is shown in Figure 1.13c, assuming $\bar{x}_\alpha < 0$ for a statically stable lifting body.

$$\bar{x}_\delta = \bar{x}_\alpha K e^{-Kt} \tag{1.8}$$

CONSTANT ANGLE OF ATTACK

According to the classic definition reported at the beginning of Section 1.1, DLC maneuvers should result in no significant variation of the angle of attack. It feels intuitive, then, to also investigate this type of motion. Assuming that the arising dynamics is characterized by no variation of α automatically implies that the lifting body has to accompany the heave motion with some rotation about the pitch axis. In particular, the pitch rotation about the body axis has to be equal in magnitude and sign to the change in flight path angle. This is shown in Figure 1.12 and expressed by the following Equation 1.9.

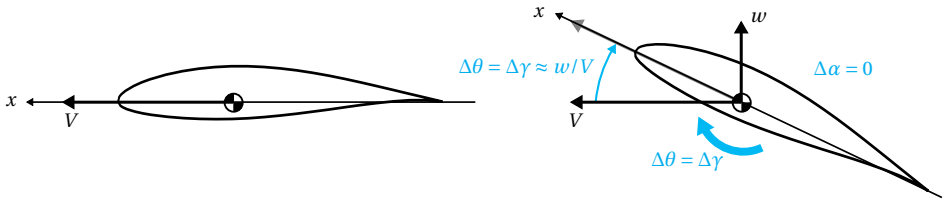

Figure 1.12 Basic kinematics of a hypothetical heave maneuver at constant angle of attack.

$$\Delta\alpha = 0 \quad \Rightarrow \quad \Delta\theta = \Delta\gamma \approx \frac{w}{V} \quad \Rightarrow \quad q \approx \frac{\dot{w}}{V} \tag{1.9}$$

This control strategy is classically referred to as "Pure DLC", since the capability to generate lift with changes in the angle of attack is completely unexploited [27]. On the lift curve, it can be represented as in Figure 1.14a. In this case, the total lift and pitch coefficients are altered only by means of the control device, and the system of dynamic equations can be further simplified to the one in Equation 1.10.

$$\begin{cases} m\dot{w} = q_\infty S C_{L_\delta}\delta \\ 0 = C_{L_\delta}\bar{x}_\delta\delta + C_{\mathcal{M}_q}\dfrac{\dot{w}}{V} \end{cases} \tag{1.10}$$

As done in the previous example, solving the equation for vertical dynamics allows to obtain the evolution of vertical speed and acceleration as a result of a unit step input on the control device. They are reported in Equation 1.11, which shows that the vertical speed increases linearly with time, and is hence theoretically unbounded.

$$\delta(t) = 1 \quad \Rightarrow \quad \dot{w} = \frac{q_\infty S C_{L_\delta}}{m} \quad \Rightarrow \quad w(t) = \frac{q_\infty S C_{L_\delta}}{m}\, t \tag{1.11}$$

The dynamic behavior of Pure DLC is graphically summarized in Figure 1.14b. By recalling that $\Delta\theta \approx w/V$, it should be clear that this type of motion is not suitable for long sustained maneuvers, as the rotation needed to neutralize the variation in angle of attack would be unbounded as the vertical speed. In a similar fashion, extrapolating this conceptual result to large values of $\Delta\theta$ would be inconsistent with the assumptions made at the beginning of Section 1.1.1 and with Equation 1.9.

As done in the previous example, the condition required to achieve such type of dynamics is obtained by imposing that the evolution of $\dot{w}$ must be the same for both the

equations of vertical and rotational dynamics. This is expressed by the following Equation 1.12

$$\bar{x}_\delta = -\frac{q_\infty S C_{\mathcal{M}_q}}{mV} \tag{1.12}$$

where the term on the right-hand side can be traced to a simplified expression of the maneuver margin [40]. This is the distance between the maneuver point and the aircraft center of gravity, and can be expressed as in the following Equation 1.13

$$\bar{x}_m = \bar{x}_\alpha + \frac{q_\infty S}{mV} C_{\mathcal{M}_q} = \bar{x}_\alpha - \frac{q_\infty S l}{mV^2} \frac{C_{\mathcal{M}_\delta}}{\tau_\delta} \tag{1.13}$$

where $\tau_\delta = \partial \alpha_{zl} / \partial \delta < 0$ is the efficiency of the control device, and l is a suitable equivalent longitudinal distance — for conventional aircraft configurations, it would be related to the distance between the center of gravity and the horizontal tail, for example.

Combining the previous two equations shows that, in order to achieve vertical dynamics at constant angle of attack — or, in other words, Pure DLC — the control device must be able to drive the CCoP to a position which falls ahead of the aircraft neutral point, by a distance equal to the maneuver margin. This is expressed in the following Equation 1.14, and the simple time history of the position of the CCoP is shown in Figure 1.14c.

$$\bar{x}_\delta = \bar{x}_\alpha - \bar{x}_m \tag{1.14}$$

Moving on the path traced by the latter two examples, it should feel intuitive to envision an even more effective type of longitudinal response to a DLC input, in which the rotation of the lifting body contributes positively to the lift generation provided by the control device. In such a case, the heave motion would benefit from an initial input due to the control-dependent contribution of lift, and then from an additional boost due to angle of attack dynamics. In the next section, the general expression of the vertical response is formally derived, and the aerodynamic conditions to obtain a certain type of longitudinal dynamics are presented.

1.1.2. GENERAL LONGITUDINAL RESPONSE

In order to characterize the longitudinal response in the most general way, by closing the system of Equation 1.3 while retaining all of its elements, it is once again necessary to assume that $q \approx \dot{w}/V$. This kinematic assumption expresses the fact that a pitch rotation accompanies the heave motion of the lifting body, in an attempt to obtain no variation in angle of attack. Due to flow reorganization and delays due to its longitudinal development, it is allowed in this case to retain that $\Delta\alpha \neq 0$, hence the present derivation is more general than the one obtained by imposing Equation 1.9. With these hypotheses, combining the two dynamic equations results in the expression of the vertical response to an input on the control device, which is reported in Equation 1.15.

$$\frac{\dot{w}}{\delta} = \frac{q_\infty S}{m} C_{L_\delta} \left(\frac{\bar{x}_\alpha - \bar{x}_\delta}{\bar{x}_\alpha + \frac{q_\infty S}{mV} C_{\mathcal{M}_q}} \right) = \frac{q_\infty S}{m} C_{L_\delta} \left(\frac{\bar{x}_\alpha - \bar{x}_\delta}{\bar{x}_m} \right) \tag{1.15}$$

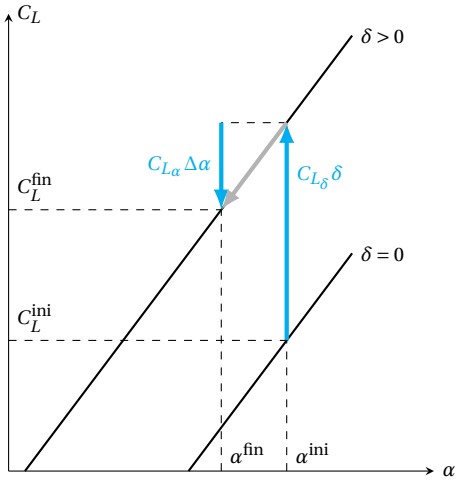

a) Lift coefficient and angle of attack variation

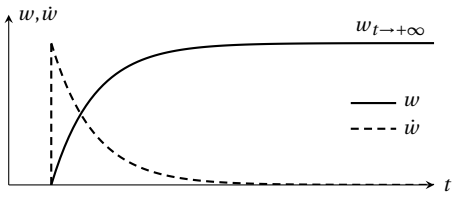

b) Time histories of vertical speed and acceleration

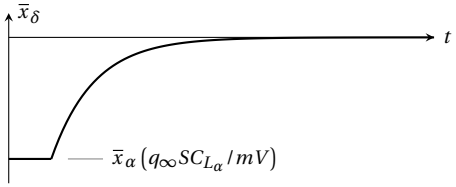

c) Time history of the Control Center of Pressure

Figure 1.13 Characterization of a hypothetical DLC maneuver resulting in pure heave motion, with no rotation about the pitch axis, in response to a unit step input on the control device.

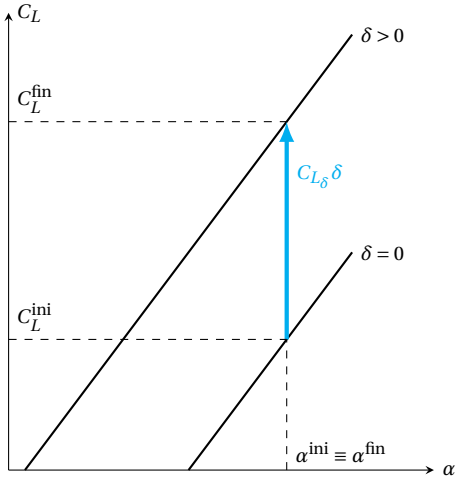

a) Lift coefficient and angle of attack variation

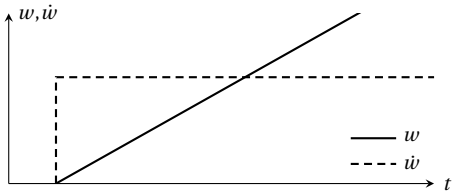

b) Time histories of vertical speed and acceleration

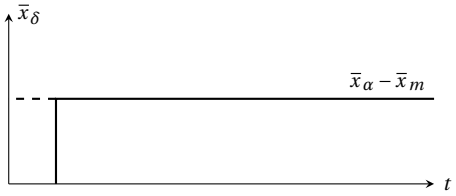

c) Time history of the Control Center of Pressure

Figure 1.14 Characterization of a hypothetical DLC maneuver resulting in vertical and rotational motion at constant angle of attack, in response to a unit step input on the control device. This behavior can also be referred to as Pure DLC.

The term at the denominator, playing the role of a scale factor for the distance between the CCoP and the neutral point, has been previously introduced in Equation 1.13 as a simplified expression of the maneuver margin.

Equation 1.15 shows how the vertical response is, in general, majorly influenced by the relative position of the CCoP with respect to the neutral point [27]. The position of the center of gravity also plays a role, to the extent that it impacts the static and maneuver stability of the aircraft. In the next section, the characteristics of the dynamic response are briefly presented for various notable positions of the CCoP.

ROLE OF THE CONTROL CENTER OF PRESSURE (CCOP)

The CCoP has been introduced in the previous section as the center of pressure of the aerodynamic forces generated solely by displacing the aircraft control effectors. In this section, the vertical dynamics of the aircraft is qualitatively described for notable arrangements of the CCoP and the neutral point. Once again, this is done without focusing on any specific aircraft configuration or practical implementation of DLC. All of the aircraft design parameters can be retained fixed, but the control device is supposed to be able to shift the application point of the control lift it generates [27]. The different dynamic behaviors are represented in Figure 1.15 for a hypothetical pull-up maneuver.

The most classic case of CPC is obtained with a control force very far aft the aircraft center of gravity, and is characterized by the CCoP roughly coinciding with the location of the control effector itself. As explained before, when the CCoP falls aft of the neutral point, the initial and steady-state vertical acceleration responses are discordant in sign. This condition results in the conventional, undesired non-minimum phase pitch behavior shown in Figure 1.15a, and already discussed at the beginning of Section 1.1.

As the CCoP advances towards the neutral point, the magnitude of the adverse initial response increases, while the one of the steady-state response decreases. The theoretically maximum difference occurs when the CCoP is aft of the neutral point by a distance equivalent to the maneuver margin (Figure 1.15b). In this condition, control lift acts sufficiently close to the neutral point to have a significant impact on the aircraft initial vertical acceleration. At the same time, it is also sufficiently far aft of the neutral point to trigger a significant aircraft rotation about its center of gravity, counteract the aerodynamic damping due to pitch rotation, and start a relevant angle of attack dynamics, which in turn causes an opposing vertical acceleration.

By further advancing the CCoP, the magnitude of the steady-state acceleration response keeps decreasing, until vanishing when the CCoP coincides with the neutral point itself, as shown in Figure 1.15c. In this condition, the angle of attack dynamics triggered by the pitch rotation of the aircraft is just sufficient to neutralize the large initial vertical acceleration.

If the CCoP moves fore of the neutral point, the initial and steady-state acceleration responses are concordant in sign. Consequently, in order to perform an actual pull-up maneuver, the control device has to be displaced in the opposite direction of the previous cases. Only in this case it is possible to properly talk about DLC. In particular, if the CCoP is fore of the neutral point by a distance equivalent to the maneuver margin, the steady-state acceleration response is theoretically equal to the initial one. Such behavior coincides with how “Pure DLC” has been characterized in Section 1.1.1, and is represented in Figure 1.15d.

If the CCoP is between the neutral point and the Pure DLC position, the angle of attack dynamics tends to dampen the initial peak response (Figure 1.15e). A longitudinally stable aircraft can achieve this behavior if the CCoP coincides with the center of gravity, for example. A longitudinal maneuver with this very particular configuration would result in the pure heave vertical dynamics presented in Section 1.1.1. If the CCoP is in front of the Pure DLC position, the angle of attack dynamics tends to further feed the initial peak response, as in the case of a canard wing configuration (Figure 1.15f).

1.1.3. SUMMARY

As compared to CPC, the most notable case of "Pure DLC" allows the pilot to have faster and more precise control of the aircraft lift and trajectory, by canceling any response delay due to non-minimum phase dynamics. Even if at the cost of limited control power, DLC represents an additional, independent degree of freedom in vertical axis dynamics, and can be exploited to improve aircraft performance in many different ways. This is especially true for larger aircraft, for which the longitudinal response to CPC tends to be inherently sluggish because of the large moment of inertia about the later axis.

A few examples — some of which may seem rather speculative at this stage — are provided in the following list:

- DLC results in improved vertical maneuver precision, which can have important consequences on
  - the dispersion of the aircraft position and vertical speed at touch-down, with significant impact on the design and weight of landing gears;
  - aerodynamic efficiency, as it can be used to make small altitude adjustments without alteration of an optimally trimmed attitude;
  - obstacle avoidance, in cases of emergency;
- DLC results in faster vertical maneuvers, with consequences on
  - the aircraft response quickness to the pilot inputs, with reduced chance to incur in the undesired phenomenon of pilot-in-the-loop oscillations;
  - the capability to reject high-frequency external disturbances — such as turbulence — with improved comfort on board and reduction of structural stress due to fatigue;
- DLC results in additional control authority, and can be used to
  - improve the transient response obtained with CPC, without altering the stability and short period characteristics of the aircraft;
  - achieve steeper descent profiles and/or facilitate the implementation of continuous descent schedules in modern air traffic management operations, leading to important reductions of fly-over noise in urban areas.

In light of this short overview, DLC can be beneficial in all flight scenarios when fast and precise trajectory tracking is of great importance. Extreme scenarios where this

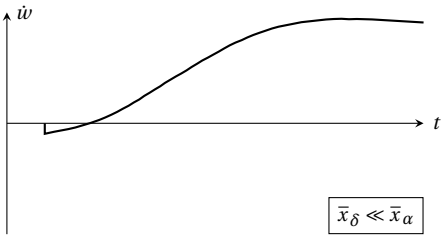

a) CCoP very far behind the neutral point

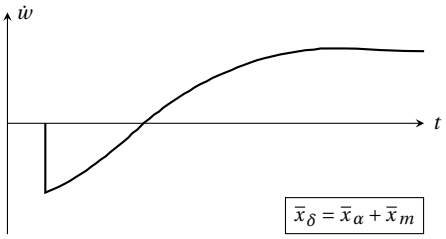

b) CCoP one maneuver margin behind the neutral point

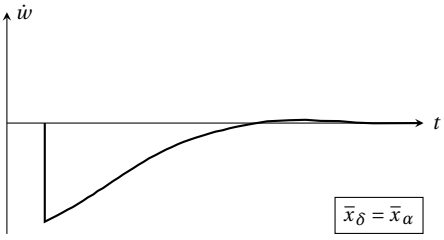

c) CCoP coincident with the neutral point

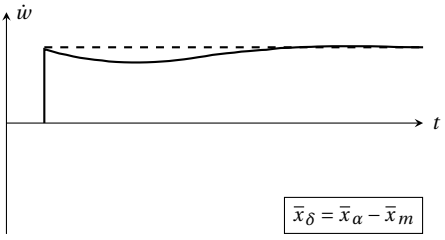

d) CCoP one maneuver margin in front of the neutral point (Pure DLC)

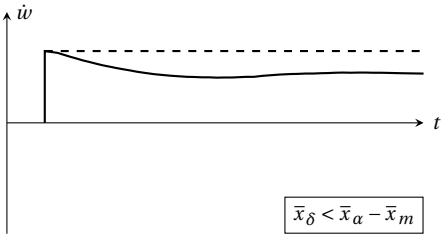

e) CCoP between the neutral point and the Pure DLC position

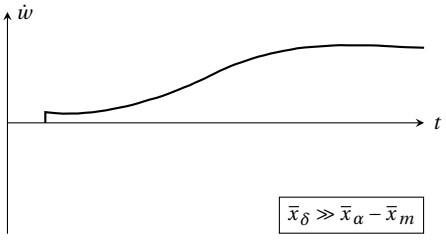

f) CCoP very far ahead of the Pure DLC position

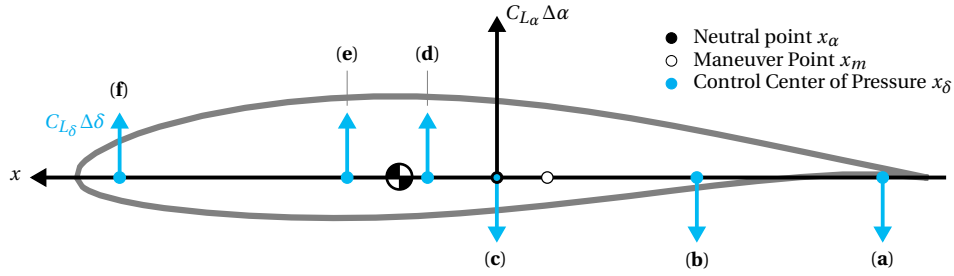

Figure 1.15 Time histories of the vertical acceleration response to a unit step input on a hypothetical control device which is able to impose different positions of the CCoP [27].

might be the case are landings on complex terrains or short/narrow runways, in-flight refueling or remote sensing applications. When redundant control surfaces are also available, the possibility to achieve DLC can also aid in rearranging aerodynamic loads along the wings, in order to obtain better aerodynamic efficiency in steady flight, and ultimately improved mission performance.

1.2. THE OPPORTUNITY WITH REDUNDANT EFFECTORS

As mentioned earlier, CPC is attained when a single effector controls the aircraft rotational and vertical dynamics by means of pitch moment generation. This set-up has two very important implications. Firstly, having only one effector dedicated to longitudinal control, independently of its location, prevents any ruling on the position of the CCoP. Secondly, and consequently, longitudinal control characteristics are tightly connected to longitudinal dynamic stability [27]. As a simple proof of the latter statement, it should be sufficient to consider that the aircraft transient response, after any kind of longitudinal control input, is heavily influenced by the characteristics of the short period motion, which in turn is characterized by stability parameters such as the maneuver margin. Equivalently, it should be intuitive to realize that a higher longitudinal stability results in a stiffer transient response, smaller stability in high maneuverability, and instability in a diverging response to any longitudinal input.

By adding more degrees of freedom than needed for motion control about a given axis, redundant effectors make it possible to break the connection between the stability and control characteristics of an aircraft. When these are perfectly uncoupled, the former only depend on clean aerodynamics, mass and balance properties, while the latter only depend on the effectors themselves and the architecture of the FCS. With restriction to longitudinal flight, in the example of a whole commercial mission, it could be possible to express the gearing ratio between front and rear control surfaces as a function of the position of the aircraft center of gravity. In this case, while the stability of the aircraft would evolve accordingly to the emptying of the fuel tanks, control characteristics would stay constant by design.

Control effectors can be said to be redundant if they are capable to independently control the same motion axis. Redundant effectors can be linked together, and to the pilot input, in different ways to drive the position of the CCoP and achieve desired dynamic properties. This definition does not imply that some of such effectors are not necessary at all. For example, high- and low-speed ailerons are surely redundant effectors for the roll control of conventional aircraft architectures. Each pair of ailerons is required in different flight phases, but high-speed ailerons, in the inboard section of the wing, can also be linked to the low-speed ones, to improve the roll control power of the aircraft. Alternatively, high-speed ailerons could be linked to move symmetrically, in response to longitudinal commands and in conjunction with the tail elevators and/or over-the-wing spoilers. In this case, they would contribute to the rotational and vertical dynamics of the aircraft, becoming redundant in the pitch and vertical axes.

It has already been shown in Figure 1.5 how front and rear longitudinal effectors could be coordinated through a simple mechanical linkage to achieve DLC flying qualities in the case of a a conventional aircraft configuration [25]. The staggered box-wing geometry of the PrP introduces innovative ways to exploit various levels of control sur-

face redundancy. This is especially true for pitch and vertical dynamics in the longitudinal plane. A synthetic representation of the main control forces in play along the vertical axis, and a comparison with the case of a conventional aircraft configuration, is represented in the free-body diagrams of Figure 1.16. The sketch of Figure 1.16b has been realized with a staggered box-wing in mind, but it can easily be interpreted as a generic bi-wing aircraft layout, which is capable to employ DLC in the way it is of interest in the scope of this dissertation.

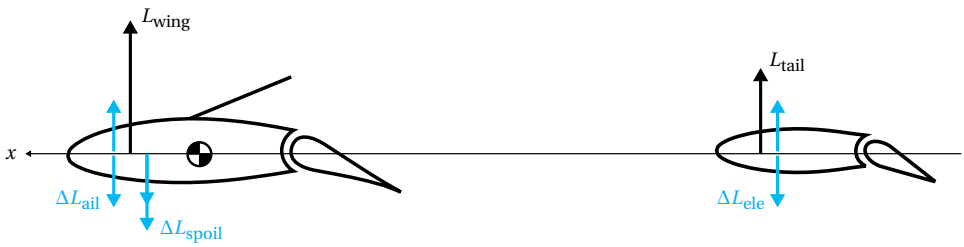

a) Conventional aircraft geometry, with one main wing equipped with ailerons and over-the-wing spoilers, and a smaller horizontal tail wing equipped with elevators

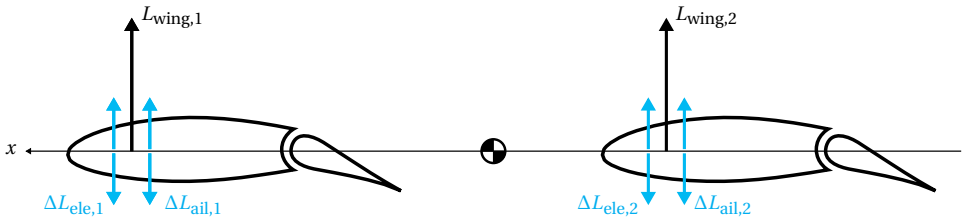

b) Staggered box-wing geometry, with two main wings equipped with inboard (elevators) and outboard (ailerons) control surfaces

Figure 1.16 Vertical aerodynamic forces generated by wings and control effectors, for two generic aircraft configurations.

A mechanical linkage system is the most straightforward and traditional way to constrain the relative motion of any number of control effectors, and link them to the pilot input device. Historically, it can be said to represent the first instance of a FCS. Conceptually, from the most high-level perspective, a mechanical linkage realizes two fundamental operations: gearing and ganging. Although similar in meaning, a different connotation is given to these concepts in the present dissertation. Gearing is defined as linking a control effector to the pilot input command, by means of a constant gearing ratio. On the other hand, ganging is the operation of constraining the motion of one control effector with respect to another one.

Gearing and ganging strategies are both essential for the realization of a mechanical linkage, and explicit ganging may be desired for fly-by-wire ones as well. In all cases, both approaches and their combination clearly have an impact on the position of the CCoP, and hence on the type of transient response that can be achieved in maneuvering flight.

The major drawback of these strategies lies in the fact that gearing ratios and ganging matrices need to be selected *a priori*, and usually need to be tailored to — and optimized for — different flight scenarios. This can result in inefficient control, and clearly hinders the potential range of achievable dynamic responses.

One of the several, more advanced approaches that can be used to calculate the control effectors position required to perform a given maneuvering task is represented by CA methods [41]. These algorithms are in charge of distributing the FCS commands to a given set of control effectors, in the most efficient way possible, according to some optimization criterion. CA methods are going to be the core mathematical instrument underlying the different approaches presented in the following chapters of this dissertation. In particular, in an effort to diverge from classic flight control studies, several attempts are going to be made to evaluate the performance of well-established and novel CA methods in the scope of multi-disciplinary analyses, including top-level considerations on aircraft design.

1.3. MOTIVATION, OBJECTIVE AND SCOPE

The work presented in this dissertation is partially motivated by the interests of the PARSIFAL[4] project[5], funded by the European Union within the Horizon 2020 Research and Innovation Program. The objective of the project was to design a transonic PrP aircraft configuration, with a payload capacity of about 300 passengers, to be competitive in the short and medium range sector. Among other tasks, and springing from early preliminary studies [42, 43], advanced flight mechanics and control concepts were to be explored, with the ambition to obtain performance benefits with respect to conventional aircraft configurations of similar category.

The main motivation of this study lies in the necessity to investigate innovative flight control techniques revolving around the possibility to modulate an aircraft lift in a fast and precise way, without spoiling its aerodynamic efficiency. Such control techniques are, in principle, rather independent of the aircraft geometry, and can therefore be implemented for both conventional and unconventional configurations. But in a more practical sense, this research is motivated by the intention to quantify the innovative flight mechanical behavior of DLC on the basis of a innovative realization of it, such as the staggered box-wing geometry of the PrP.

The objective of the dissertation is to show how redundant control surfaces, located fore and aft the aircraft center of gravity, can be exploited to shape an aircraft dynamic behavior and obtain desired flight mechanics performance. This is achieved by introducing novel flight control methods, mainly revolving around original implementations of traditional formulations of the CA problem. The simulation of several different flight scenarios attempts to provide multiple examples to support the significance of the present research effort in different aspects of aeronautical engineering. Various effects of implementing DLC with trailing-edge control surfaces are analyzed: from the improvement of open-loop handling qualities, to top-level mission performance; from optimal trim conditions for maximum control authority, minimum drag, or an assigned pitch angle,

[4] Prandtlplane ARchitecture for the Sustainable Improvement of Future AirpLanes (PARSIFAL)
[5] Homepage: `https://parsifalproject.eu/`

to the achievement of desired transient dynamic responses. Various flight mechanics performance indices are monitored in different studies, from fundamental parameters, such as control authority or tracking precision, to more practical ones, such as agility quickness or comfort level on board.

In light of the aforementioned motivations and objectives, the present dissertation attempts to answer the following research questions:

1. What is the impact of different Control Allocation (CA) methods on the design of a control surface layout and on the sizing of redundant control surfaces, for a given aircraft configuration? (Chapter 5)

2. How can redundant control surfaces be fully exploited to obtain maximum control authority about one or more specified motion axes in trim conditions? (Chapter 6)

3. How can the concept of Control Center of Pressure (CCoP) be leveraged to shape the aircraft transient response in a controlled manner and remove the typical non-minimum phase behavior of pitch dynamics? (Chapter 7)

The concepts and methods proposed in the following chapters are applicable to any aircraft configuration, regardless of its shape and number of control effectors. As a matter of fact, though, they have been conceived to exploit the possibility of practically employing DLC, hence expressing their full potential when applied to aircraft configurations featuring control surfaces both fore and aft the center of gravity. These include the PrP, but are not limited to it.

1.4. OUTLINE

The present dissertation consists of eight main chapters. A conceptual flow chart of its outline is represented in Figure 1.17.

Following the introduction, Chapter 2 presents an overview of the CA problem for redundant control effectors. The most popular approaches and algorithms are illustrated in detail, and relevant properties, such as the AAS, are explored in the scope of the upcoming applications.

Chapter 3 illustrates the models and methods developed to perform the subsequent analyses and gather relevant results. All studies have been performed by means of flight simulation, hence significant space is devoted to the description of the implemented software framework.

A mission performance study of the PrP aircraft model is then presented in Chapter 4, to characterize such disruptive aircraft concept from an operational standpoint. By making comparisons with a potential competitor aircraft with conventional tube-and-wing geometry, this chapter proves that box-wing aircraft configurations can be competitive in modern and future market scenarios.

In the core part of the dissertation, and using a more complex and detailed flight mechanics model, Chapter 5 deals with the problem of positioning and sizing redundant control surfaces on a box-wing aircraft geometry. In order to obtain good flight mechanics performance, it is indeed first necessary to have a good aircraft design. In this chapter,

the impact of various classic CA algorithms on the optimum control surface arrangement is evaluated by correlating aircraft design parameters to the inherent properties of the CA approaches.

The trim problem is then comprehensively analyzed in Chapter 6. A general trim formulation based on the concept of the AAS is here presented, with many applications for maximum control authority, minimum drag and assigned pitch angle.

Lastly, an in-depth study on the aircraft transient response to longitudinal commands is presented in Chapter 7, where a novel CA approach based on the definition of the CCoP is presented. Several applications performing different flight tasks show how being able to induce the position of the CCoP can result in performance benefits such as tracking precision, handling qualities, disturbance rejection and improved comfort on board.

Finally, a comprehensive overview of the work is presented in Chapter 8, with considerations on the practical development of box-wing aircraft configurations, and on the implementation of DLC in case of redundant control surfaces. The research questions are answered, conclusions are drawn, and an outlook on future research perspectives is given.

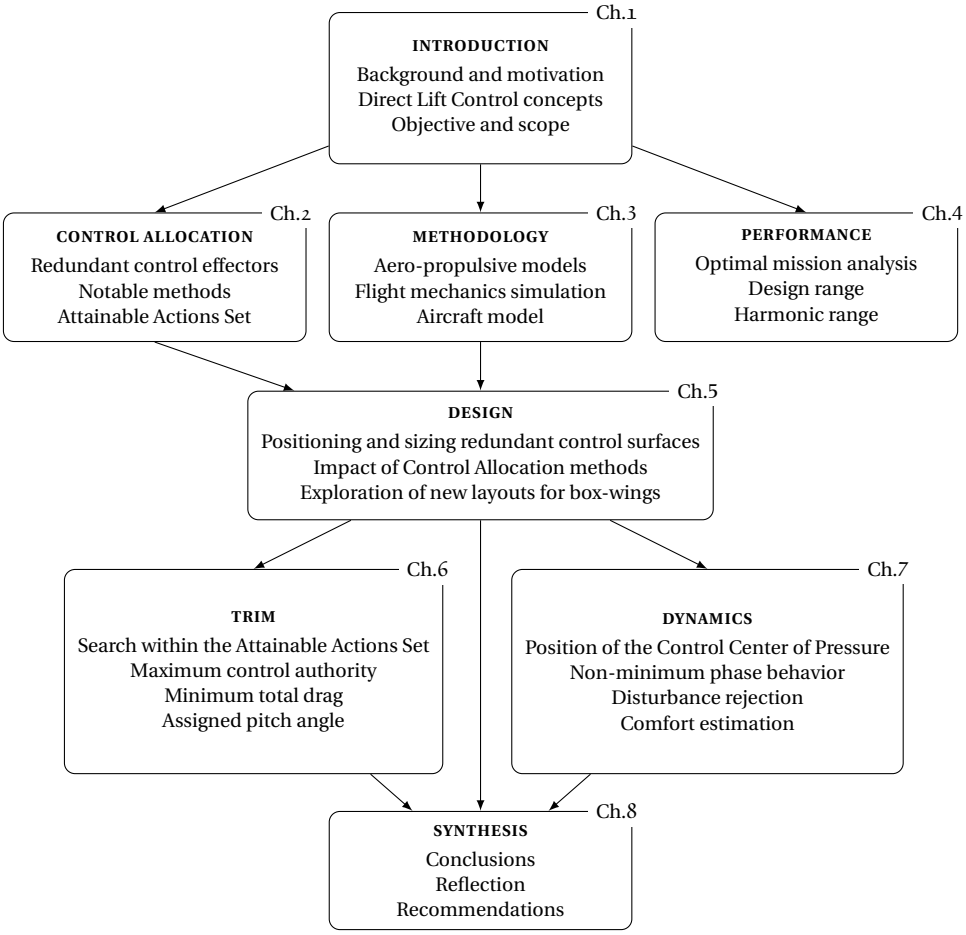

Figure 1.17 Flow chart of the present dissertation.

2

CONTROL ALLOCATION

A book cannot by itself teach how to play.
It can only serve as a guide, and the rest
must be learned by experience.

Jose Raul Capablanca
Chess Fundamentals
1921

Mathematics will take care of everything
if we just believe.

Wayne Durham
Aircraft Control Allocation
2017

The possibility to install multiple control surfaces, as in the case of box-wing configurations, raises an important question about the architecture of the FCS. FCSs based on mechanical linkages traditionally rely on a collection of cables, rods and pulleys to transmit the control input from the pilot to the control surfaces. Those based on a fly-by-wire system feature an electronic layer between the pilot interface and the actuated effectors, hence allowing the implementation of arbitrarily complex automatic control laws and augmentation systems. In all cases, it is often, if not always, necessary to constrain the relative motion of some control effectors. But doing so according to some predefined, discretional design criterion can be an inefficient solution towards the achievement of optimal control characteristics in every flight scenario. This chapter introduces and reviews the main concepts and methods relative to Control Allocation (CA), a more advanced technique used to calculate the optimal effectors displacements necessary to achieve an assigned control goal.

The following Section 2.1 presents an overview of the flight control problem in presence of redundant control effectors, and defines the fundamental CA problem formulation. Section 2.3 provides its geometric interpretation, by introducing the concepts of Control Space and Action Space. An overview of notable CA approaches is presented in Section 2.4, with focus on the methods used in the upcoming chapters. Lastly, Section 2.5 formally defines the key concept of Attainable Actions Set (AAS), which is going to have an important role in several subsequent applications.

2.1. THE PROBLEM WITH REDUNDANT EFFECTORS

The most conventional aircraft configurations dedicate one set of control effectors to each motion axis. One or two elevators control the pitch axis, one pair of ailerons controls the roll axis, and a rudder controls the yaw axis. As for translational dynamics, a propulsive effector is normally employed to control the longitudinal axis, while there is usually no way to directly control the lateral axis. Some existing solutions to control the translation about the vertical axis — basically DLC — have been presented in Section 1.1.

If two or more effectors are devoted to control the same motion axis, as in the classic case of ailerons, these are constrained to move together according to some rule. They will then be displaced as a single "virtual" effector. The total number of virtual effectors is lower than the number of actual effectors, and it should match the number of axes to be controlled. In the case of conventional control techniques, revolving around the roll, pitch, and yaw moments about the aircraft center of gravity, this number is three.

The process of constraining the relative motion among two or more actual effectors, hence defining the set of virtual effectors, is here referred to as "ganging". A ganging matrix G can be designed to establish a simple linear relationship between the real effectors $\boldsymbol{u}$ and the virtual ones $\overline{\boldsymbol{u}}$, as shown in Equation 2.1. For example, for an aircraft with two ailerons, two elevators and a rudder, virtual and actual control effectors could be intuitively related through a conventional ganging matrix as shown in Equation 2.2. In this case, a displacement of the virtual aileron effector corresponds to an opposite motion of the actual ailerons, while a displacement of the virtual elevator corresponds to a concordant motion of the actual ones. Lastly, the virtual rudder coincides with the real rudder.

$$\boldsymbol{u} = G\overline{\boldsymbol{u}} \tag{2.1}$$

$$\begin{Bmatrix} u_{\text{ail},1} \\ u_{\text{ail},2} \\ u_{\text{ele},1} \\ u_{\text{ele},2} \\ u_{\text{rud}} \end{Bmatrix} = \begin{bmatrix} 1 & 0 & 0 \\ -1 & 0 & 0 \\ 0 & 1 & 0 \\ 0 & 1 & 0 \\ 0 & 0 & 1 \end{bmatrix} \begin{Bmatrix} \overline{u}_{\text{ail}} \\ \overline{u}_{\text{ele}} \\ \overline{u}_{\text{rud}} \end{Bmatrix} \tag{2.2}$$

The virtual effectors can then be linked to the pilot inputs through a gearing matrix H, as shown in Equation 2.3. In the most simple case of H being a diagonal matrix of constant gearing ratios, each pilot input is mapped to only one set of virtual effectors, and is completely decoupled from the other ones. Continuing on the previous example, if the pilot input commands are normalized in the $[-1,+1]$ interval, while the virtual ailerons, elevators and rudders are respectively limited to $\pm 45\,\text{deg}$, $\pm 30\,\text{deg}$, $\pm 60\,\text{deg}$, a possible gearing matrix can assume the simple form reported in the following Equation 2.4. This

gearing matrix maps the position limits of the pilot input controls to the position limits of the virtual effectors.

$$\overline{\boldsymbol{u}} = H\boldsymbol{u}_{\text{pil}} \quad \Rightarrow \quad \boldsymbol{u} = GH\boldsymbol{u}_{\text{pil}} \tag{2.3}$$

$$\begin{Bmatrix} \overline{u}_{\text{ail}} \\ \overline{u}_{\text{ele}} \\ \overline{u}_{\text{rud}} \end{Bmatrix} = \begin{bmatrix} \frac{\pi}{4} & 0 & 0 \\ 0 & \frac{\pi}{6} & 0 \\ 0 & 0 & \frac{\pi}{3} \end{bmatrix} \begin{Bmatrix} u_{\text{lat}} \\ u_{\text{lon}} \\ u_{\text{dir}} \end{Bmatrix} \tag{2.4}$$

Gearing and ganging operations are representative of a mechanical FCS architecture, and are clearly not an optimal approach to link the pilot inputs to all the available effectors. Primarily, it is immediate to realize that the ganging operation reduces the number of control Degrees of Freedom (DoFs) of the aircraft. This fact is simply represented by G having more rows than columns. At the same time, it limits the capability of the effectors to control other motion axes. In the previous example, the elevators are incapable of aiding with roll control, and the ailerons are incapable to provide pitch or yaw control.

In more general terms, if the control effectiveness matrix of the actual effectors is defined as in Equation 2.5, control forces can be approximated as in Equation 2.6. In these two relations, the symbol $\boldsymbol{A}$ indicates a generic resultant aerodynamic action with the dimensions of a force (lift, drag, forces in body axes) or moment (roll, pitch or yaw). This notation is necessary, in the present and following chapters, to congregate quantities that have different dimensions but serve the same conceptual purpose: the calculation of the total control effectiveness of the aircraft effectors, about either all of its axes of motion or only the ones that are relevant for a specific investigation.

$$B = \frac{\partial C_{\boldsymbol{A}}}{\partial \boldsymbol{u}} = \begin{bmatrix} \partial C_{A_1}/\partial u_1 & \partial C_{A_1}/\partial u_2 & \dots & \partial C_{A_1}/\partial u_{N_{\boldsymbol{u}}} \\ \partial C_{A_2}/\partial u_1 & \partial C_{A_2}/\partial u_2 & \dots & \partial C_{A_2}/\partial u_{N_{\boldsymbol{u}}} \\ \vdots & \vdots & \ddots & \vdots \\ \partial C_{A_{N_{\boldsymbol{A}}}}/\partial u_1 & \partial C_{A_{N_{\boldsymbol{A}}}}/\partial u_2 & \dots & \partial C_{A_{N_{\boldsymbol{A}}}}/\partial u_{N_{\boldsymbol{u}}} \end{bmatrix} \tag{2.5}$$

$$\Delta C_{\boldsymbol{A}} \approx B\boldsymbol{u} = BG\overline{\boldsymbol{u}} \tag{2.6}$$

In light of Equation 2.6, the combined effectiveness BG of symmetrically ganged effectors is null on lateral-directional axes, while effectors ganged anti-symmetrically have no authority on longitudinal dynamics (if drag effects are not accounted for). As a matter of fact, the capability of each effector to affect the control of all motion axes can be seen as an unwanted coupling effect, as in the case of adverse yaw dynamics triggered by the deployment of ailerons. On the other hand, it can also be a beneficial source of available control power, if exploited properly.

The problem with ganging matrices, and to a smaller extent with gearing ratios, is that they need to be selected *a priori* and somewhat arbitrarily, and usually need to be optimized for different flight scenarios. For example, high-speed ailerons are ganged to move anti-symmetrically to provide roll control in cruise phases, but can also be ganged to move symmetrically, in order to work as air-brakes after landing. Similarly, gearing ratios for all control surfaces can be expressed as a function of the airspeed, when considerations on the pilot effort on the control stick are also necessary. The necessity to calculate multiple ganging and gearing matrices to be employed in different flight phases

generally hinders the potential range of achievable aircraft dynamic responses. Furthermore, while it can be rather intuitive to gang effectors on a conventional aircraft, it may not be so straightforward for unconventional aircraft geometries. Configurations such as the BWB, with all control surfaces along the trailing edge, the Flying-V, with no clear separation between elevators and ailerons, and box-wings, with redundant control surfaces both in front and behind the center of gravity, all pose interesting challenges for the design of the control surface layout and the FCS [44, 45].

2.2. FUNDAMENTAL CONTROL ALLOCATION PROBLEM

One of a few more advanced approaches to calculate the control effectors displacements required to perform a given maneuvering task is represented by CA methods. As shown in Figure 2.1, these methods typically use the output of an overarching flight control law to calculate the displacement of all control effectors, on the basis of the available control effectiveness and according to a prescribed optimality criterion. In these regards, CA methods allow a neat separation between the definition of the control logic and the distribution of the control effort to the effectors. They differ from multi-input multi-output control approaches, since the latter typically combine both of the aforementioned tasks, at the cost of additional modeling complexity.

The baseline, generic CA problem consists in finding the value of the control effectors displacements $\boldsymbol{u}$ which solve the following Equation 2.7.

$$B\boldsymbol{u} = \boldsymbol{\nu} \tag{2.7}$$

In this simple relation, $\boldsymbol{\nu}$ is an array of control objectives to be achieved by displacing the effectors. Reference values for $\boldsymbol{\nu}$ are typically the output of the control law, and can represent control forces and moments as well as angular rates, in the most common applications. If B is the effectiveness matrix defined in terms of aerodynamic actions (forces and moments) as in Equation 2.5, then $\boldsymbol{\nu}$ is an array of control forces and/or moments to be generated by the effectors. In all of the applications presented in this dissertation, the elements of $\boldsymbol{\nu}$ are picked from the set of aerodynamic control force and moment coefficients shown in Equation 2.8, on the basis of the application of interest.

$$\boldsymbol{\nu} = \left\{\Delta C_L,\ \Delta C_D,\ \Delta C_X,\ \Delta C_Y,\ \Delta C_Z,\ \Delta C_{\mathcal{L}},\ \Delta C_{\mathcal{M}},\ \Delta C_{\mathcal{N}}\right\} \tag{2.8}$$

The number of elements of $\boldsymbol{\nu}$ and the number of rows of B depend on which control actions are commanded by the flight control law and are allocated to the effectors. The most classic CA problem is referred to as the “three moment problem”, since it allocates the roll, pitch and yaw moments (or angular accelerations) to a given set of effectors [41]. In principle, the latter could be anything ranging from control surfaces to thrust vectoring mechanisms [46, 47].

The number of elements of $\boldsymbol{u}$ and the number of columns of B depend on the number of effectors that are chosen to take part in the allocation problem. If the number of control effectors $N_{\boldsymbol{u}}$ is equal to the number of control objectives $N_{\boldsymbol{\nu}}$, the B matrix is square and the solution is unique. The effectors positions can be immediately determined by matrix inversion. This is generally the case for conventional aircraft configurations with ganged control surfaces. If the aircraft configuration has more control effectors than strictly required to achieve the control objectives, the B matrix is not square

and cannot be inverted to immediately solve Equation 2.7. In this case, the solution to the CA problem may not be unique. In other words, the same control objectives could be achieved in more than one way because of the redundant control DoFs of the aircraft.

CA methods define an analytic or algorithmic function f_{CA} to calculate the optimal effectors displacements $\boldsymbol{u}$ that obtain the required control objectives $\boldsymbol{\nu}$, on the basis of the available effectiveness B and, optionally, other flight or design parameters. The generic solution to the CA problem may be expressed as in Equation 2.9.

$$\boldsymbol{u} = f_{CA}(B, \boldsymbol{\nu}, \dots) \tag{2.9}$$

The selected effectors can be treated as completely independent from one another or as virtually ganged within the CA method itself. For some applications, as in the example of rudders on a V-tail aircraft configuration, the latter approach may be desired. If the rudders are left completely free to move, any given CA method would make them deflect symmetrically, as elevators, in order to exploit their significant pitch moment effectiveness due to the cant angle of the V-tail. This could be undesired, as it would reduce directional control authority. In order to avoid incurring in this type of behavior, selected groups of control effectors can be ganged to move in a specified way, and the CA problem can be solved only for the virtual effectors, as shown in Equation 2.10.

$$\boldsymbol{u} = G\overline{\boldsymbol{u}} \;\Rightarrow\; \boldsymbol{\nu} = B\boldsymbol{u} = BG\overline{\boldsymbol{u}} \;\Rightarrow\; \overline{\boldsymbol{u}} = f_{CA}(BG, \boldsymbol{\nu}, \dots) \;\Rightarrow\; \boldsymbol{u} = G\overline{\boldsymbol{u}} \tag{2.10}$$

The same considerations on the uniqueness of the solution hold, but must be expressed in terms of the ganged effectiveness matrix BG.

A geometric interpretation of the overall CA problem is presented in the next section, before moving on to an overview of the many techniques available to obtain these types of solutions.

2.3. GEOMETRIC INTERPRETATION

Before venturing into the geometric interpretation of Equation 2.9, it is necessary to clarify a few preliminary definitions [41]. As already mentioned with the introduction of Equation 2.8, the case in which the CA objectives are control forces and moments is considered for the remainder of this dissertation. In other words: $\boldsymbol{\nu} = \Delta C_{\boldsymbol{A}}$. If $N_{\boldsymbol{A}}$ aerodynamic control actions are allocated onto $N_{\boldsymbol{u}}$ control effectors, the following concepts can be introduced:

Control Space is a Cartesian axis system in the $\mathbb{R}^{N_{\boldsymbol{u}}}$ space, with a control effector displacement varying on each axis. Each combination of control effectors displacements is resented by a point in Control Space.

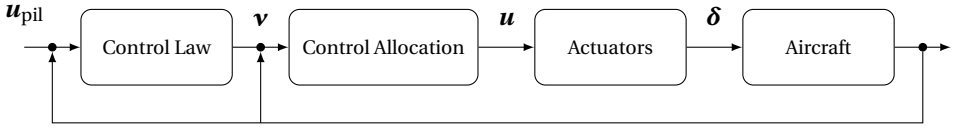

Figure 2.1 Top-level block scheme of a FCS employing CA methods.

Action Space is a Cartesian axis system in the $\mathbb{R}^{N_A}$ space, with a control aerodynamic action — force or moment, dimensional or dimensionless — varying on each axis. Each resultant control action generated by a combination of effectors displacements is represented by a point in Action Space.

The Admissible Controls Set (ACS) is the set of all possible effectors displacements admitted by the physical realization of the FCS and the aircraft architecture.

The Effective Actions Set (EAS) is the set of all control forces and moments that can be, in principle, generated by the effectors.

The nomenclature chosen for the Action Space and the EAS represents an original tentative to expand the well-established designations of "Moment Space" and "Moments Set". The use of the latter are dominant in the field, since early studies of the CA problem focused exclusively on the "three moment problem" already mentioned in the previous section. Other attempts to include different types of control objectives have been made in the past, opting for the obvious designation of "Objective Set" [48, 49]. This was deemed too abstract in the scope of the present dissertation, for which a nomenclature closer to flight dynamics applications has been chosen.

In any case, in light of these definitions, it should be intuitive to understand that the EAS is a function of the Admissible Controls Set (ACS) and of the specified flight condition. Due to non-linearities and possible coupling effects in the aerodynamic model, it is usually hard to characterize the EAS in Action Space. One notable analytic effort has been presented for pairs of left-right control surfaces, for which the roll and pitch moments are linear with the deflection, but the yaw moment is quadratic due to the contribution of drag [50]. A numeric application in the maritime engineering field can be seen in [51], while a more recent work defines and exploits the concept of robust EAS, with applications to fighter aircraft with uncertainties in their control effectiveness [52].

If control forces and moments are linearized with respect to the effectors positions, the control effectiveness matrix B defines a linear function which maps the ACS to an approximation of the EAS, according to Equation 2.11. The goodness of such approximation obviously depends on how accurately the linearized aerodynamic model represents the non-linear one for the selected flight condition.

$$\begin{aligned} B\colon\ & \mathbb{R}^{N_u} \to \mathbb{R}^{N_A} \\ & \boldsymbol{u} \mapsto \Delta C_{\boldsymbol{A}} = B\boldsymbol{u} \end{aligned} \tag{2.11}$$

If the effectors positions are simply bounded, the ACS is a hyper-rectangle in Control Space (a rectangle in $\mathbb{R}^2$, a parallelepiped in $\mathbb{R}^3$). If B is constant and the ACS is a convex set, it can be proven that the EAS is a bounded convex polytope in $\mathbb{R}^{N_A}$ (a polygon in $\mathbb{R}^2$, a polyhedron in $\mathbb{R}^3$) [53], as shown in Figure 2.2. The convexity of the EAS guarantees the existence of a well defined internal, boundary and external region of its geometry. The algorithm to construct the EAS, given a constant B matrix and the saturation limits of the effectors positions, is described in [41] for $N_A = 2$ and $N_A = 3$. For some applications presented in this dissertation, it has been generalized to any number of dimensions of the Action Space.

While it is always straightforward to associate every point in the ACS to its counterpart in the EAS, the opposite is not trivial, and sometimes not even possible. This is exactly the objective of the CA problem: to associate a given point in Action Space, either inside or outside of the EAS, to a point belonging to the ACS. If the prescribed point in Action Space belongs to the interior of the EAS, there is at least one combination of effectors positions which maps to it. If it belongs to the boundary of the EAS, one or more effectors are at their limit positions. In both of these cases, the CA method should be able to find the optimal combination of effectors displacements, although, unfortunately, this is not always the case.

On the other hand, if the prescribed point in Action Space belongs to the exterior of the EAS, the effectors are uncapable to generate the corresponding combination of control forces and moments, and the best alternative solution must be found, according to some criterion. Common criteria are the minimization of the allocation error, the minimization of the control effort, or the preservation of the direction of the prescribed resultant action in Action Space. The following section presents a few CA methods in more detail, after a small overview of the most common CA approaches and applications.

2.4. NOTABLE APPROACHES

A vast variety of CA methods is available in scientific literature. Most of them rise from the formulation of an optimization problem, but may differ in both the main idea behind the formulation, and the algorithm to implement it. A broad and detailed survey of CA approaches, algorithms and applications is presented in [54], for both linear and nonlinear physical models and not only pertaining to the field of aeronautics. A survey and evaluation of optimization methods for the most classic approaches is provided in [55].

The most straightforward approach to solve Equation 2.7 for $\boldsymbol{u}$ consists in finding a matrix P for which the following Equation 2.12 holds.

$$\boldsymbol{u} = P\boldsymbol{v} \tag{2.12}$$

The P matrix is usually referred to as a generalized inverse of B — since $BP = I$ must hold — and can be defined in many different ways to give desired characteristics to the CA problem. A brief presentation of generalized inverses is given in the following Section 2.4.1.

The most intuitive, optimization-based formulation is targeted at minimizing the difference between the requested and the generated control objectives. This is usually referred to as the "error minimization problem", and its baseline formulation is reported in Equation 2.13, where the p-norm can be chosen according to the application study.

$$\begin{aligned} \min_{\boldsymbol{u}} \quad & \|\boldsymbol{v} - B\boldsymbol{u}\|_p \\ \text{subj. to} \quad & \boldsymbol{u}_{\text{lb}} \leq \boldsymbol{u} \leq \boldsymbol{u}_{\text{ub}} \end{aligned} \tag{2.13}$$

An evaluation study on the effect of the p-norm on the type of solutions provided by common optimization algorithms is presented in [56].

An additional step, which builds on top of the solution $\boldsymbol{u}^*$ of the previous equation, aims at achieving the same control objectives while driving the effectors towards a reference position $\boldsymbol{u}_{\text{ref}}$. If $\boldsymbol{u}_{\text{ref}}$ represents the neutral position of the effectors, this approach

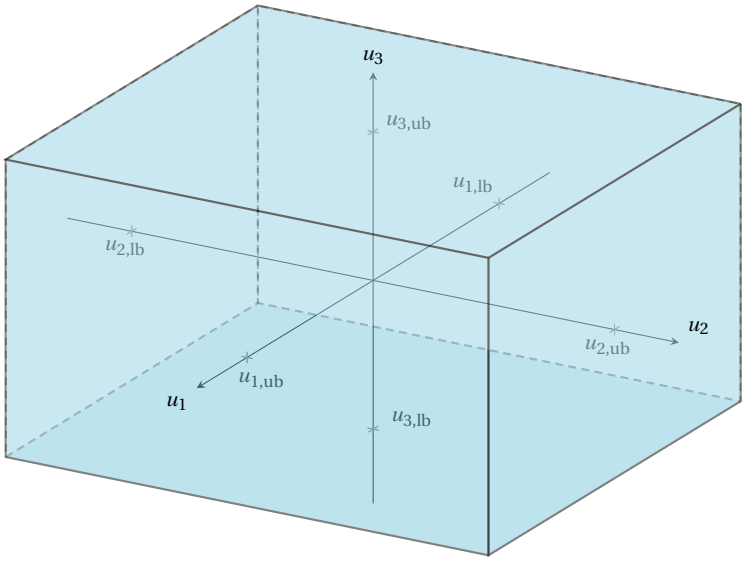

a) Admissible Controls Set (ACS) in $\mathbb{R}^3$: $\boldsymbol{u} = [u_1,\ u_2,\ u_3]$

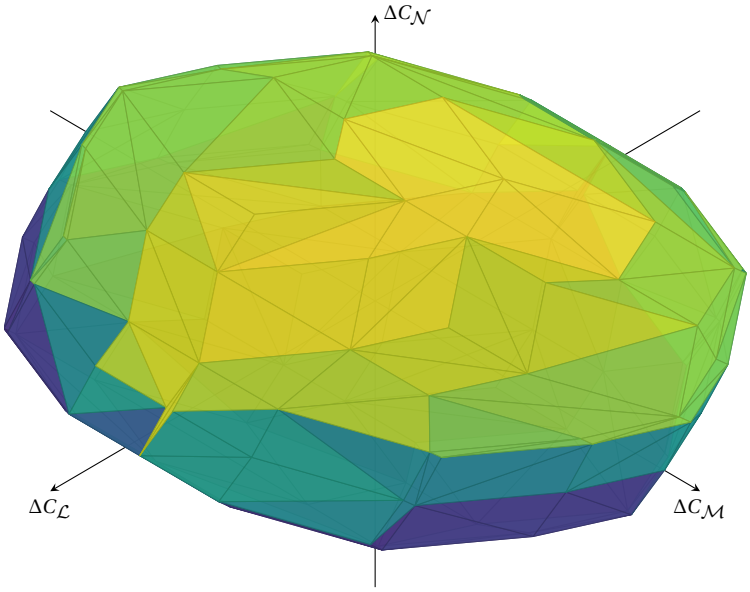

b) Effective Actions Set (EAS) in $\mathbb{R}^3$: $\boldsymbol{\nu} = \left[\Delta C_{\mathcal{L}},\ \Delta C_{\mathcal{M}},\ \Delta C_{\mathcal{N}}\right]$

Figure 2.2 Illustrative geometry of a generic "three moment" CA problem with three control effectors.

results in the minimum control effort solution. For this reason, it is usually referred to as the "effort minimization problem" and its baseline formulation is reported in Equation 2.14.

$$\begin{aligned} \min_{\boldsymbol{u}} \quad & \|\boldsymbol{u} - \boldsymbol{u}_{\text{ref}}\|_p \\ \text{subj. to} \quad & B\boldsymbol{u} = B\boldsymbol{u}^* \\ & \boldsymbol{u}_{\text{lb}} \leq \boldsymbol{u} \leq \boldsymbol{u}_{\text{ub}} \end{aligned} \tag{2.14}$$

By combining the two former philosophies, "mixed allocation" methods attempt to achieve minimum control error while also optimizing a secondary objective, at the same time. The latter is given minor importance thanks to a scaling factor ε, but the formulation of the optimization problem in a single stage greatly improves the quality of its solutions and the time efficiency to achieve them. In the most common formulation, reported in Equation 2.15, the secondary objective is again control effort, but several original approaches have also been presented, trying to minimize control drag [57], or structural loads on the wing [58].

$$\begin{aligned} \min_{\boldsymbol{u}} \quad & \|\boldsymbol{v} - B\boldsymbol{u}\|_p + \varepsilon\|\boldsymbol{u} - \boldsymbol{u}_{\text{ref}}\|_p \\ \text{subj. to} \quad & \boldsymbol{u}_{\text{lb}} \leq \boldsymbol{u} \leq \boldsymbol{u}_{\text{ub}} \end{aligned} \tag{2.15}$$

Lastly, "direct" allocation methods rely on the geometry of the EAS, hence setting themselves apart from all of the aforementioned approaches. The principles behind these methods are going to be presented in more detail in Section 2.4.3.

For any given CA method, the most prominent application in aeronautics is the so called "three moment" CA problem, where the roll, pitch and yaw moments (or angular rates) constitute the vector of control objectives to be allocated. Applications to problems with four, more or different control objectives have also been explored in the past [48, 49], but are becoming more popular with the development of new, unconventional aircraft configurations [59]. Several fundamental works have also explored cascaded or compound formulations, where one of the above mentioned approaches is applied recursively to selected groups of independent effectors, which are assigned decreasing levels of execution priority [41, 53].

A more advanced implementation of CA methods is referred to as "incremental" or "frame-wise". Incremental formulations do not calculate the absolute position of the effectors, but rather the relative deviation from the position calculated in the previous time step [41, 60]. Such discrete-time techniques are much closer to realistic implementations in actual flight control computers, and allow to also include rate limits of the effectors actuators in the problem statement. Most importantly, these formulations are inherently suitable to exploit local control effectiveness, which is based on the current state of the aircraft, including the effectors positions themselves. On the other hand, they also result in history-dependent solutions, meaning that the effectors positions at one instant depend on the whole series of CA problems solved before. This can be due to the employment of a varying local effectiveness matrix during the frame-by-frame solution, or simply to the properties of the solving algorithm. For this reason, incremental CA approaches usually need additional filters, or extra allocation steps exploiting the null-space of the B matrix, to drive the effectors to some preferred position [41].

Several research efforts have focused on evaluating the practical implications of the differences in performance among these formulations and their solution algorithms. A comprehensive study, relying on a high-fidelity wind-tunnel database for a BWB aircraft model, estimates the impact of classic CA methods on trim drag and control surface design [61, 62]. Others have also proposed modifications of classic CA methods to solve specific engineering problems. From a multi-stage frame-wise direct method to minimize aerodynamic drag [48], to the inclusion of aerodynamic interactions among the effectors [46]. From the exploitation of local control effectiveness in a non-incremental approach to improve the CA of non-linear effectors [63], to the inclusion of information on actuator dynamics in the CA problem formulation [64].

While it is definitely important to study the mathematical and numerical properties of the different CA approaches, implementations and solutions, the scope of this dissertation is focused more on flight mechanics than on flight control. For this reason, some of the methods presented in this section are merely used or only slightly modified in the following sections. The intention behind the presented applications is to explore the possibilities for innovative dynamic responses, enabled by the ability to exploit redundant controls on an unconventional box-wing aircraft configuration.

The next three sections present in more detail some well known CA methods, with very different characteristics and performance, which have been employed in the applications presented further on in this dissertation.

2.4.1. GENERALIZED INVERSES AND GANGING

Generalized inverses are a vast category of matrices P which solve the most simple, linear formulation of the inverse CA problem. This has already been introduced in Equation 2.12, and is reported here for convenience.

$$\boldsymbol{u} = P\boldsymbol{\nu} \tag{2.16}$$

A generalized inverse matrix can be expressed, with no loss of generality, as

$$P = Q\,[BQ]^{-1} \tag{2.17}$$

where Q is an auxiliary matrix which can have arbitrary values, as long as BQ is invertible. Such freedom of choice allows generalized inverses to grant very diverse characteristics to the CA problem, since they can easily be tailored to different applications of interest.

On the other hand, the same flexibility comes at the price of some important drawbacks. As a consequence of their simple formulation, all generalized inverse methods do not hold any information about the effectors positions saturation limits. For this reason, solutions of Equation 2.16 may not actually be admissible for the given aircraft architecture, in case of large demanded control objectives. Additionally, it can be proven that control effectors displacements resulting from any generalized inverse formulation cannot form a basis for their respective Control Space [41]. This means that the control effectors positions resulting from Equation 2.16 are never able to cover the entirety of the ACS, but only a subspace of it. When such subspace is mapped to Action Space through the B matrix, the obtained set of control objectives is not capable to cover the entirety of the EAS. This has important consequences on the actual control authority that can be exploited by such CA methods, and is going to be discussed in more detail in Section 2.5.

In light of these limitations, an interesting strategy to assemble the P matrix may be targeted to provide admissible solutions for specified control objectives $\boldsymbol{\nu}$. This approach can be repeated as many times as necessary, to obtain and store different P matrices which cover different regions of Action Space. Alternatively, a numeric optimization problem may be designed to find the auxiliary matrix Q which results in the largest set of admissible controls.

Once a desired generalized inverse matrix has been obtained by any means, its implementation to solve the CA problem requires no computational time or resources at all, since all is required to find the control effectors displacement is a simple matrix multiplication. Because of this, it is common to employ generalized inverse formulations in iterative approaches, such as daisy-chain or "cascaded" methods. In short, these approaches consist in prioritizing entire groups of effectors, and distributing the control objective to secondary groups only when the primary ones have reached their saturation limits. They can be used to improve the quality of the solutions provided by a given CA method, and increase the control power it is able to exploit.

As mentioned already in Section 2.1, gearing and ganging control effectors are possible ways to model a mechanical linkage between the pilot inputs and the effectors displacements. At the end of Section 2.2, it has also been shown how any type of CA problem can include a given set of pre-ganged effectors, by exploiting the ganged effectiveness matrix BG. A particular occurrence of such possibility is represented by a generalized inverse matrix P obtained by choosing the ganging matrix G as the auxiliary matrix Q, as shown in the following Equation 2.18.

$$Q = G \quad \Rightarrow \quad P = G(BG)^{-1} \quad \Rightarrow \quad \boldsymbol{u} = P\boldsymbol{\nu} = G(BG)^{-1}\boldsymbol{\nu} \tag{2.18}$$

Such P matrix represents a linear expression of the generic f_{CA} function which solves the CA problem with ganged effectors. This can be easily seen by left-multiplying both terms the second equality in Equation 2.10 by P.

In this scope, ganging control effectors can also be intended as one of the simplest CA methods possible. Because of the properties of the generalized inverse and the arbitrariness in the choice of the ganging matrix, it should be understandable that such CA method is not able to achieve optimal performance, in general. This is also going to be shown in Section 2.5.

2.4.2. WEIGHTED PSEUDO INVERSE (WPI)

A particular expression for a generalized inverse matrix can be found by solving the optimization problem reported in Equation 2.19. In this relation, $W_{\boldsymbol{u}}$ is a weighting matrix used to prioritize the effectors, and $\boldsymbol{u}_{\text{ref}}$ is a preferred combination of effectors displacements. Both of these parameters need to be prescribed according to some criterion.

$$\begin{aligned} \min_{\boldsymbol{u}} \quad & \| W_{\boldsymbol{u}}(\boldsymbol{u} - \boldsymbol{u}_{\text{ref}}) \|^2 \\ \text{subj. to} \quad & B\boldsymbol{u} - \boldsymbol{\nu} = 0 \end{aligned} \tag{2.19}$$

The particular expression of P resulting from such problem is usually referred to as the Weighted Pseudo Inverse (WPI), and is reported in the following Equation 2.20. By comparison with Equation 2.17, it can be seen that the weighted control effectiveness matrix

also takes the role of the auxiliary matrix Q in this case.

$$P = W_{\boldsymbol{u}}^{-1} B^T \left(B W_{\boldsymbol{u}}^{-1} B^T \right)^{-1} \tag{2.20}$$

The WPI matrix is a very common choice when it is desired to allocated the given control objectives while obtaining minimum control effort with respect to a reference combination of effectors displacements.

The most basic formulation of such approach consists in not prioritizing any of the effectors, and using their neutral position as the reference one. This variation of the WPI method is usually referred to as the Moore-Penrose Pseudo Inverse (PSI), and can be obtained by setting $W_{\boldsymbol{u}} = I$ and $\boldsymbol{u}_{\text{ref}} = \mathbf{0}$. Another classic approach consists in prioritizing the effectors that can afford broader position excursions. This could be achieved, for example, by setting the elements on the diagonal of $W_{\boldsymbol{u}}$ equal to $W_{ii} = 1/|u_{i,\text{ub}} - u_{i,\text{lb}}|$. This is a convenient method to introduce information about the effectors saturation limits in all CA problems based on a generalized inverse matrix.

In general, the control effectors displacements which solve the WPI and PSI problems can be expressed as in the following Equation 2.21 [54], for a diagonal weighting matrix.

$$\boldsymbol{u} = \boldsymbol{u}_{\text{ref}} + W_{\boldsymbol{u}}^{-1} B^T \left(B W_{\boldsymbol{u}}^{-1} B^T \right)^{-1} (\boldsymbol{\nu} - B\boldsymbol{u}_{\text{ref}}) \tag{2.21}$$

As for any other CA method based on generalized inverse matrices, such closed-form solution makes these approaches very robust and reliable in every application. This is proven by the fact that a cascaded PSI method has been implemented on the actual FCS of the Lockheed Martin X-35 demonstrator first [65], and the Lockheed Martin F-35 Lightning II fighter jet later [66]. On the other hand, the simplicity of its formulation comes at the price of sub-optimal allocation performance, as already explained in the previous section.

An alternative WPI formulation, including upper and lower bounds for the effectors directly in the optimization problem, is reported in Equation 2.22. For this formulation, generally referred to as Constrained Weighted Pseudo Inverse (CWPI), the analytic solution is not available anymore, and the CA problem must be solved via an iterative algorithm.

$$\begin{aligned} \min_{\boldsymbol{u}} \quad & \| W_{\boldsymbol{u}} (\boldsymbol{u} - \boldsymbol{u}_{\text{ref}}) \|^2 \\ \text{subj. to} \quad & B\boldsymbol{u} - \boldsymbol{\nu} = 0 \\ & \boldsymbol{u}_{\text{lb}} \leq \boldsymbol{u} \leq \boldsymbol{u}_{\text{ub}} \end{aligned} \tag{2.22}$$

2.4.3. DIRECT ALLOCATION (DA)

The Direct Allocation (DA) method has been explicitly conceived on the basis of the geometric representation of the EAS itself. The logic behind the baseline approach could be summarized as follows [41, 55]. For a prescribed control objective $\boldsymbol{\nu}$ in Action Space:

1. the half-line from the origin passing through $\boldsymbol{\nu}$ is calculated;
2. the intersection between the half-line and the EAS geometry is found;
3. the combination of effectors positions which generates the control objective at the intersection is calculated;

- if $\boldsymbol{\nu}$ is inside or on the boundary of the EAS, the solution from step 3 can be scaled down to achieve exactly $\boldsymbol{\nu}$;
- if $\boldsymbol{\nu}$ is outside of the EAS,hence being infeasible, the solution from step 3 can be used, which preserves the direction of $\boldsymbol{\nu}$ in Action Space.

By definition, DA is hence capable to attain all of the prescribed control objectives within the EAS or on its boundary [41].

The method is usually formulated as the optimization problem shown in the following Equation 2.23. In this relation, the auxiliary variable $\boldsymbol{w} \equiv \boldsymbol{u}$ is used to indicate the candidate solution, and the scale factor ρ is used to evaluate the control objectives in the same direction of $\boldsymbol{\nu}$.

$$\left.\begin{array}{ll} \max\limits_{\rho,\boldsymbol{w}} & \rho \\ \text{subj. to} & B\boldsymbol{w} = \rho\boldsymbol{\nu} \\ & \boldsymbol{u}_{\text{lb}} \leq \boldsymbol{w} \leq \boldsymbol{u}_{\text{ub}} \end{array}\right\} \Rightarrow \begin{cases} \boldsymbol{u} = \boldsymbol{w}/\rho, & \text{if} \quad \rho > 1 \\ \boldsymbol{u} = \boldsymbol{w}, & \text{if} \quad 0 \leq \rho \leq 1 \end{cases} \tag{2.23}$$

Several iterative algorithms have been proposed for the solution of such problems. They are usually slow and hard to implement, as they require the geometric construction of (parts of) the EAS. In its most computationally efficient formulation, DA is reshaped into the smallest standard linear programming equivalent problem, also relying on an iterative algorithm for its solution [55]. This formulation yields several advantages over the original, geometry based ones, and is going to be used in the remainder of the present dissertation. Most importantly, it can be scaled to any number of control objectives, allocating both forces and moments at the same time, without loss of computational efficiency. On the other hand, its solution relies on an iterative algorithm, which may not be sustainable for real-time computation at very high-frequency ($\approx 100\,\text{Hz}$) . Additionally, for frame-wise formulations, solutions depend on the entire history of previous results, while in general, they may depend on the initial guess assigned at the first iteration [41]. These non-deterministic properties make its certification for practical applications extremely time consuming and costly, if not impossible at all. As a matter of fact, to the author's knowledge, the DA method has not been employed for any online application yet.

The DA method takes into account effectors saturation limits and preserves directionality in Action Space for unattainable desired moments, but does not allow any prioritization of effectors via weighting matrices. Its behavior is therefore basically complementary to the one of generalized inverse methods. It is important to remark that the solutions of the DA method are unique as long as any combination of N_A columns of B is linearly independent. This means that DA cannot be applied directly to problems involving failed actuators, which result in a full column of zeroes in B. Also, particular attention should be placed to symmetric effectors, such as a pair of elevators, if only longitudinal forces and moments are allocated. In this case, in order to respect the symmetry of the problem and avoid numerical complications, it would be recommended to define a single virtual elevator, and formulate the CA problem as in Equation 2.10.

2.5. THE ATTAINABLE ACTIONS SET (AAS)

In the previous sections, the fundamental CA problem has been presented as having the goal to associate every point in Action Space to a combination of feasible positions of the effectors in the ACS. But not all CA methods are capable of returning admissible effectors positions for every control objective, even if the latter falls in the interior or on the boundary of the EAS. In other words, not all CA methods are capable of mapping the EAS in its entirety back to the ACS.

The subset of the EAS which a CA method can trace to feasible positions of the effectors is here referred to as the Attainable Actions Set (AAS). The AAS is, in general, a subset of the EAS. Control objectives of the EAS which are outside of the AAS are unattainable by the given CA algorithm, despite being actually attainable by the control power available to the aircraft. For a given B matrix, and given characteristics of the effectors, this is only dependent on the formulation of the CA problem. A CA method which is capable to attain the entirety of EAS is commonly referred to as "optimal". This is the case of the DA method, for example. Otherwise, it is referred to as "sub-optimal", as in the case of the generalized inverse methods, including the WPI and its variations. It can be proven that there cannot exist an optimal CA method with an analytic, closed-form solution [41]. In other words, no generalized inverse matrix can result in a AAS which coincides with the full EAS. Therefore, CA optimality must come at the price of robustness.

In Figure 2.3, the AAS of the DA method is compared to the one of the PSI method, and to the EAS corresponding to the same B matrix and effectors saturation limits. For both examples with a 2D and 3D Action Space, the DA method is able to attain the complete EAS, while the PSI method only attains a subset of it. This means that a large set of prescribed control objectives, all near the boundary of the EAS and theoretically achievable in light of the control effectiveness of the aircraft, are not practically attainable using the PSI method, because the latter is not capable of mapping them to an admissible set of control effectors positions $\boldsymbol{u}$.

Numerical data is obtained by using a box-wing aircraft model, with four pairs of control surfaces on the main wings — two on the front wing and two on the rear wing, in the inboard and outboard regions — and two rudders on a V-tail. More information on the aircraft model is given in Section 3.1, in the next chapter. The same aircraft architecture has been used also to evaluate the AASs of different ganging strategies. In a similar way to the previous example, the geometries of the AASs are compared to the one of the EAS in Figure 2.4. To easily reference the main results of this application, control surfaces are labelled as Inboard (I) or Outboard (O), and as belonging to the Front wing (F), the Rear wing (R), or the Vertical tail (V), on the Port (P) and Starboard (S) side of the aircraft. They are conveniently ordered as shown in the following Equation 2.24.

$$\boldsymbol{u} = \{u_{\mathrm{IFP}},\ u_{\mathrm{IFS}},\ u_{\mathrm{OFP}},\ u_{\mathrm{OFS}},\ u_{\mathrm{IRP}},\ u_{\mathrm{IRS}},\ u_{\mathrm{ORP}},\ u_{\mathrm{ORS}},\ u_{\mathrm{VP}},\ u_{\mathrm{VS}}\}^T \tag{2.24}$$

The 2D allocation problem of the lift force and pitch moment coefficients using different ganging logics is represented in Figure 2.4a. In this case, the G_1 ganging matrix associates a pilot lift command to a concordant deflection of all outboard control surfaces, which act as trailing-edge flaps/spoilers. At the same time, it associates a pitch command to a discordant deflection of front and rear inboard control surfaces, which act as elevators. This approach completely decouples the two sets of inboard and outboard control

surfaces, assigning them to entirely different control functions, and indeed results in a relatively small AAS. The G_2 matrix drastically increases the volume of the AAS by demanding a concordant deflection of all control surfaces for a given lift command, and a discordant deflection for all front and rear control surfaces for a given pitch command. For this 2D problem in the longitudinal plane, rudders are never used. With reference to the vector of effectors displacement shown in Equation 2.24, these ganging logics are summarized in the following Equation 2.25.

$$\begin{aligned} \boldsymbol{u} &= G_i \begin{Bmatrix} u_L \\ u_{\mathcal{M}} \end{Bmatrix} \quad \text{for } i = 1,2 \text{with} \\ G_1 &= \begin{bmatrix} 0 & 0 & 1 & 1 & 0 & 0 & 1 & 1 & 0 & 0 \\ 1 & 1 & 0 & 0 & -1 & -1 & 0 & 0 & 0 & 0 \end{bmatrix}^T \\ G_2 &= \begin{bmatrix} 1 & 1 & 1 & 1 & 1 & 1 & 1 & 1 & 0 & 0 \\ 1 & 1 & 1 & 1 & -1 & -1 & -1 & -1 & 0 & 0 \end{bmatrix}^T \end{aligned} \tag{2.25}$$

A similar approach has been adopted for the "three moment" allocation problem in the 3D Action Space shown in Figure 2.4b. The ganging matrices for this example are reported in the following Equation 2.25. In the case of G_3, the outboard control surfaces respond to a roll command and act as ailerons, the inboard ones respond to pitch commands and act as elevators, and the rudders respond to yaw commands as it would be expected. In the case of G_4, the inboard control surfaces also aid with roll control, and the outboard control surfaces also aid with pitch control.

$$\begin{aligned} \boldsymbol{u} &= G_i \begin{Bmatrix} u_{\mathcal{L}} \\ u_{\mathcal{M}} \\ u_{\mathcal{N}} \end{Bmatrix} \quad \text{for } i = 3,4 \text{with} \\ G_3 &= \begin{bmatrix} 0 & 0 & 1 & -1 & 0 & 0 & 1 & -1 & 0 & 0 \\ 1 & 1 & 1 & 1 & -1 & -1 & -1 & -1 & 0 & 0 \\ 0 & 0 & 0 & 0 & 0 & 0 & 0 & 0 & -1 & -1 \end{bmatrix}^T \\ G_4 &= \begin{bmatrix} 1 & -1 & 1 & -1 & 1 & -1 & 1 & -1 & 0 & 0 \\ 1 & 1 & 0 & 0 & -1 & -1 & 0 & 0 & 0 & 0 \\ 0 & 0 & 0 & 0 & 0 & 0 & 0 & 0 & -1 & -1 \end{bmatrix}^T \end{aligned} \tag{2.26}$$

Both these examples show that there exist some ganging strategies which are able to attain a large part of the EAS, also outperforming the generalized inverse resulting from the WPI method. On the other hand, they also show how the AAS can vary significantly as a function of the chosen ganging matrix. The latter remains dictated by considerations on the practical implementation of the FCS and on the role which is (arbitrarily) assigned to each control effector in a given flight scenario.

For several applications presented in the following chapters, the volume of the AAS, in relation to the one of the corresponding EAS, is often used as a criterion to choose the most appropriate CA method to be implemented. In a similar way, it is a characteristic parameter which can be used to compare given performance metrics achieved with different CA methods, as done in Chapter 5.

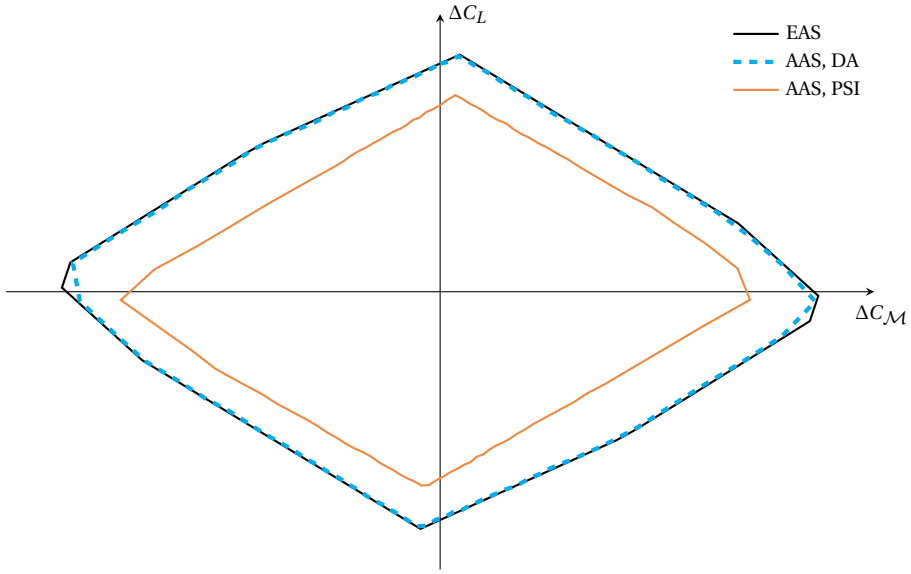

a) Lift force and pitch moment allocation in $\mathbb{R}^2$

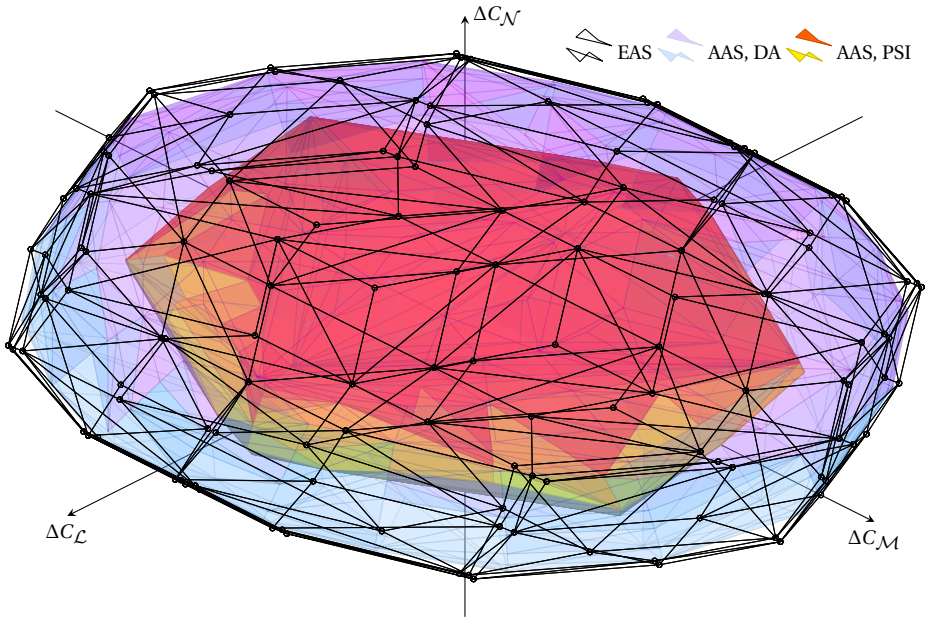

b) "Three moment" allocation in $\mathbb{R}^3$

Figure 2.3 Comparison of the EAS with the AASs of two classic CA methods, for a box-wing aircraft with four pairs of control surfaces (two on the front and two on the rear wing) and two rudders on a V-tail, at $\alpha = 0\,\text{deg}$, $\beta = 0\,\text{deg}$ and $M = 0.5$.

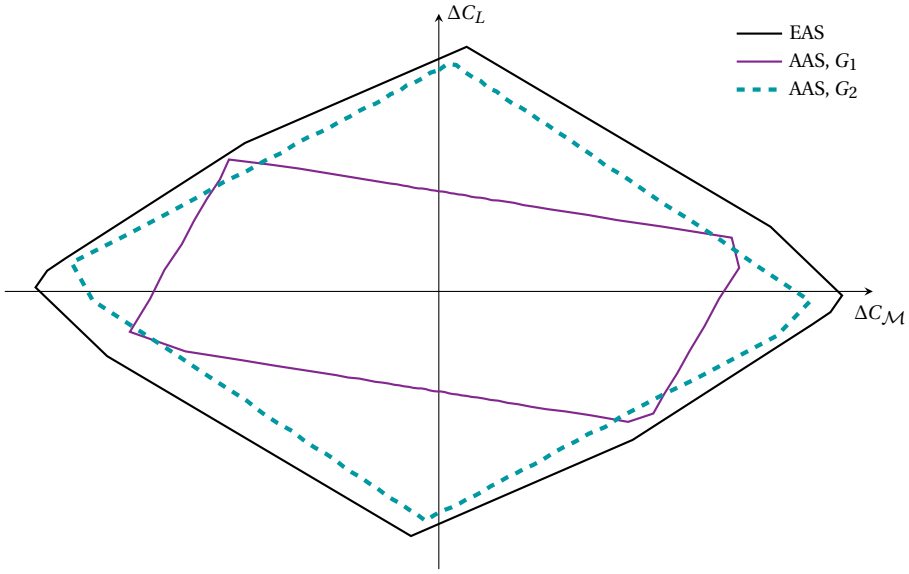

a) Lift force and pitch moment allocation in $\mathbb{R}^2$

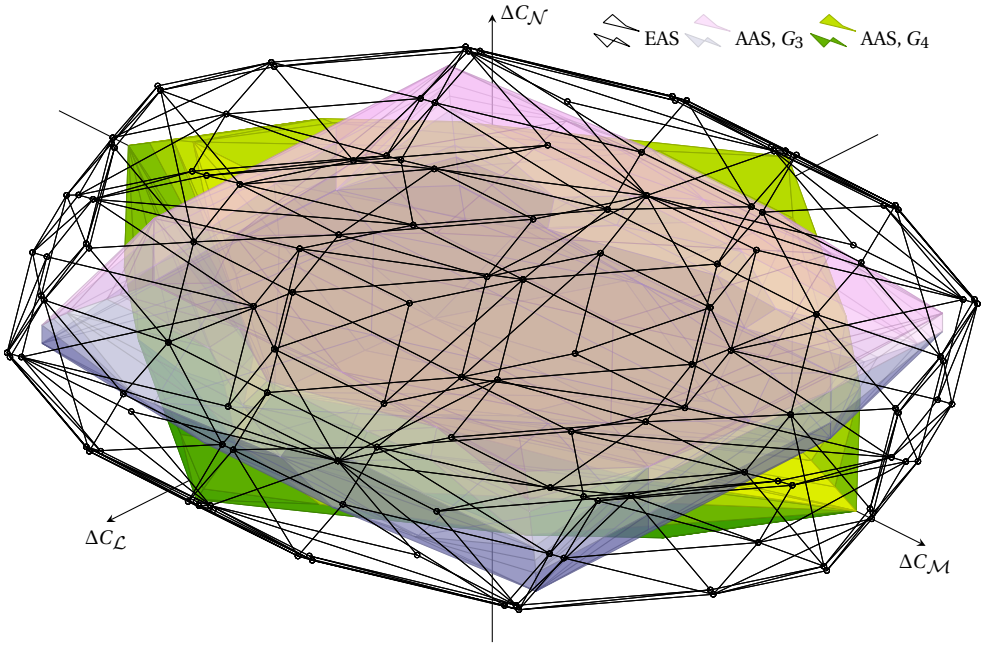

b) "Three moment" allocation in $\mathbb{R}^3$

Figure 2.4 Comparison of the EAS with the AASs of different ganging strategies, for a box-wing aircraft with four pairs of control surfaces (two on the front and two on the rear wing) and two rudders on a V-tail, at $\alpha = 0\,\text{deg}$, $\beta = 0\,\text{deg}$ and $M = 0.5$.

2.6. CONCLUSIONS

This chapter has presented an overview of the CA problem, which has the purpose of distributing an assigned control objective to a set of redundant effectors. From a more general perspective, a geometric interpretation of the fundamental CA problem has been provided, introducing the concepts of ACS and EAS. The main ideas behind classic CA approaches and formulations have been outlined, and the properties and formulations of three particular methods has been presented in more detail. Lastly, it has been shown that CA methods are, in general, capable of returning admissible effectors positions for only a subset of the EAS, referred to as the AAS. The AAS has been presented as an important property of the CA method itself, which can be used as a performance metric to compare different CA methods for the same control effectiveness matrix and effectors saturation limits.

Arbitrarily ganging the effectors has been introduced as the conventional, but rather arbitrary technique to solve the CA problem. It can be cast as a CA method based on generalized inverse matrices, but is fundamentally equivalent to the creation of a mechanical linkage among the effectors. Ganging can result in rather inefficient allocation if the choice of the ganging matrix is not sensible for the specific flight scenario.

The WPI method is also based on a generalized inverse matrix formulation, but the resulting control effectors displacements solve the fundamental CA problem while minimizing the total control effort. Since the outcome of this method is the solution of an optimization problem, there is no arbitrariness in its value. The WPI presents a closed-form solution, hence being easier to implement in real applications, but is not capable to exploit the entire EAS of the aircraft.

Lastly, the DA method is formulated on the basis of the geometry of the EAS. For this reason, its AAS coincides with the corresponding EAS, hence the method is capable to extract all available control power from the effectors. Contrarily to the previous two approaches, the solution can only be obtained with an iterative procedure, hence requiring much more computational resources.

These CA methods have been presented in detail in this chapter, as they are going to be employed systematically in the remainder of this dissertation. They have been chosen in light of the very different properties they present. The dynamic characteristics and flight performance they achieve allow to make several considerations on the impact that these CA formulations have on other aeronautic disciplines, such as control surface sizing, trim or transient response.

3

FLIGHT MECHANICS MODEL

Part of the inhumanity of the computer is that
once it is competently programmed and working smoothly,
it is completely honest.

Isaac Asimov
Change! Seventy-One Glimpses of the Future
1981

Man can't help hoping, even if he is a scientist.
He can only hope more accurately.

Karl A. Menninger
Love Against Hate
1942

After having introduced the core mathematical methods underlying all the applications presented in this dissertation, the present chapter focuses on delineating the main models and tools used and developed to perform the required flight simulations.

The following Section 3.1 presents the top-level design and geometric parameters of the PrP aircraft configuration, which has been used as the main test case throughout the entire dissertation. As it will be evident in the following sections, the methods and models used to characterize it are completely physics based and aircraft configuration-agnostic. Hence, they are applicable to any other aircraft geometry, in principle. Section 3.2 dives into the characterization of external forces on the aircraft. It presents the main workflow used to model the geometry of the PrP and its potential competitors with conventional architecture, and obtain their aerodynamic and propulsive models.

Section 3.3, presents the most relevant characteristics of the overarching flight mechanics model, which synthetizes and coordinates all of the aspects presented in the

previous sections. In particular, Section 3.3.1 discusses the modeling of the FCS, including considerations on pilot commands, auto-pilots and trim. Lastly, Section 3.3.2 focuses on the formulation of the dynamic equations of motion, based on a multi-body physics approach.

3.1. THE PRANDTLPLANE (PRP)

As already mentioned in Chapter 1, disruptive aircraft configurations are becoming increasingly popular in modern research studies, from concepts for future commercial operations to unmanned aircraft systems applications. This is due to the inherent performance benefits that they may allow to obtain, but also to their potential capability of reshaping the aeronautical sector in a more profound way. These capabilities are going to be required to meet the necessarily ambitious sustainability goals which the aviation sector is demanded to face in the next decades [1, 6], since the well-refined tube-and-wing aircraft configuration seems to have reached its performance and efficiency limit [12, 13, 67, 68].

While the concepts and approaches introduced in the present dissertation are applicable to any aircraft configuration, in principle, the proposed investigations focus on a commercial transport box-wing aircraft model, referred to as the PrandtlPlane (PrP). In the case of the PrP, the box-wing is employed to achieve minimum induced drag performance, but is also substantially swept and staggered to account for transonic effects [19, 20, 22]. The front wing is attached to the lower part of the fuselage, while the rear one is connected to a twin vertical tail. This is in order to provide a significant vertical stagger, which critically affects the aerodynamic efficiency of the box-wing [19, 21]. Overall, such complex wing system is integrated in a modern wide-body aircraft design, with the purpose of obtaining higher payload and better aerodynamic efficiency than conventional, single-wing aircraft with the same wing span.

The specific aircraft category under examination targets high passenger capacity in the short and medium range segment. This version of the PrP has been designed within the scope of the Prandtlplane ARchitecture for the Sustainable Improvement of Future AirpLanes (PARSIFAL) project, in the attempt to address the forecasted increase in air passenger demand in such range segment [5]. For this purpose, the PrP aims to board a greater number of passengers than the current aircraft flying in these range segments, but without modifying their overall dimensions. The latter requirement is necessary to satisfy slot constraints for the already existing airports, which is important since the available ground infrastructures are not expected to grow as fast as the passenger traffic they should accommodate in the near future [69]. This objective translates into adopting two top-level design requirements, according to which the wingspan must not exceed 36 m, and the wheel span must not exceed 9 m. These values are aimed to place the PrP in the ICAO Aerodrome Reference Code C category, the same one adopted for the most common aircraft models flying nowadays: the Airbus A320 and the Boeing 737.

In summary, the market target of the PrP is to match the dimensions and fuel consumption of A320/B737 category aircraft, and the payload capacity of A330/B767 category ones [67, 70, 71]. With a passenger capacity about double the one of the most widespread aircraft models, and with their same wingspan, the main objective of the PrP is to sustain the forecasted increase in passenger traffic, while retaining the use of ex-

Table 3.1 Selected top-level aircraft requirements for the PrP.

Variable	Value	Description
b	36 m	Maximum wing span for ICAO Aerodrome Ref. C
R_{har}	4000 km	Maximum range at maximum payload (harmonic range)
M_{cr}	> 0.78	Minimum Mach number at cruise
h_{cr}	11 km	Initial cruise altitude
N_{pax}	250 – 308	Number of passengers, depending on cabin configuration
N_{eng}	2	Number of engines

isting ground infrastructures, thus attempting to relieve pressure on congested airports. By exploiting the unique aerodynamic properties of the box-wing, and integrating its geometry in a transonic commercial aircraft architecture, the PrP strives to be competitive in the modern and future commercial aviation market.

The reference set of top-level aircraft requirements that have guided the development and improvement of the PrP configuration throughout the PARSIFAL project is reported in Table 3.1. The several studies presented in the following chapters have had different sub-versions of the PrP as a test case, following its design process during the course of the project itself. For this reason, a consistent and detailed summary of the aerodynamic and propulsive performance of the aircraft model cannot be shown at this stage. Instead, selected characteristics of the PrP will be disclosed in the chapter where they are required. Nevertheless, all of the proposed applications retain the fundamental characteristics of the staggered box-wing configuration. The most relevant one, in the scope of this dissertation, is the possibility to install multiple control surfaces on the main wings, both fore and aft the aircraft center of gravity.

3.2. DISCIPLINARY SUB-MODELS

The following sections provide an overview of the techniques and tools used to characterize the aerodynamic and propulsive models of the PrP and its competitor aircraft configurations. These workflows and approaches have been selected to promote, as far as possible, physics-based analyses that are not tailored to a specific aircraft configuration. This criterion is important to allow fair evaluation and comparisons of any flight performance metric of interest.

Since the PrP design has been in continuous development throughout the time span of the PARSIFAL project, it is impossible to provide a single, complete and consistent characterization of its performance at this stage. For this reason, the present section focuses on the description of methods and approaches used to create the disciplinary sub-models that constitute the global flight mechanics model of the aircraft. Relevant data resulting from these analyses is conveniently presented in the chapter or section where they are needed.

As explained more in depth in the following sections, the aircraft aerodynamics is characterized in terms of the global aerodynamic actions — forces and moments — expressed in body axes as a tabular function of the angle of attack, angle of sideslip, Mach

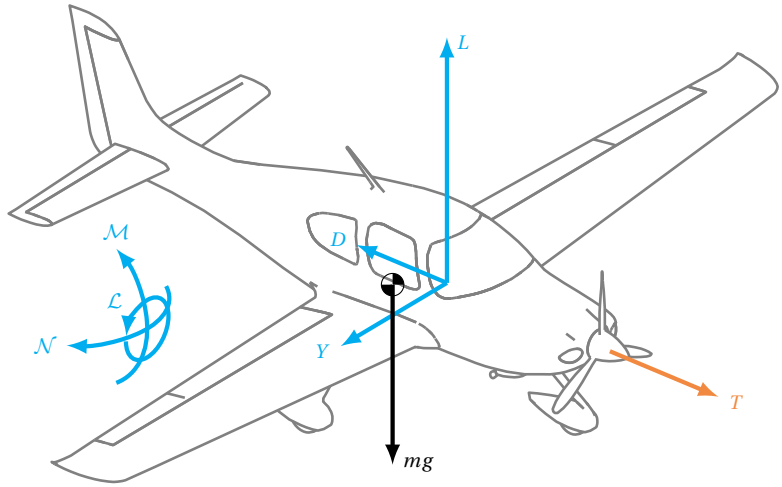

Figure 3.1 Free body diagram representing the result of the adopted disciplinary models. All forces are applied, all moments are pure torques. The scheme remains valid for all number of propulsive units, and for any aircraft configuration.

number, body angular rates and control surface deflections (always modelled as plain flaps). Forces are applied at an assigned, fixed reference point close to the quarter of the mean aerodynamic chord. Due to time constraints, it has been impossible to generate more refined aerodynamic models, also including unsteady effects or detailed modelling of local phenomena, such as gaps, slots, interferences and interactions. At the same time, such high-level of detail was deemed unnecessary for flight mechanics and control applications on an aircraft configuration at conceptual/preliminary design stage.

The total propulsive actions generated by each engine results in a thrust force which is function of altitude, Mach number and throttle setting. The thrust force vector is applied at a given reference point in proximity of the engine itself, and oriented according to the engine mounting angles. The resulting moment due to pure torques and all applied forces is then expressed with respect to the aircraft center of gravity, which can slightly move as a consequence of fuel consumption. Methods to characterize the mass, balance and inertia models have been made available by various partners of the PARSIFAL project, and therefore are not described here.

A representative free-body diagram which can be used as a reference for the following sections is shown in Figure 3.1, in the case of a conventional aircraft configuration.

3.2.1. GEOMETRY

During the conceptual and preliminary design phases, aircraft geometry models are not mature and detailed enough to support medium- or high-fidelity disciplinary analyses (aerodynamics, mass and balance, propulsion integration,...). Nevertheless, an aircraft geometry model has to be generated with the available information, with the aim of refining it in future, more detailed studies. In the scope of this dissertation, the geometric representation of the aircraft has been necessary as a means to provide a sufficiently de-

tailed aerodynamic model, including the effects of control surfaces deflections and the propulsive system. The geometry model presented in this section has been conceived to support low- and medium-fidelity aerodynamic analyses, such as the ones provided by vortex-lattice and panel methods. At the same time, it can serve as a starting point to be refined for higher fidelity Computational Fluid Dynamics (CFD) analyses.

For all of the proposed applications, the aircraft geometry is automatically modelled and meshed using the Multi-Model Generator (MMG), a Knowledge Based Engineering toolbox developed in-house [72–74] and built on top of the ParaPy software libraries[1]. The MMG provides automatic geometry modeling and meshing capabilities, which are completely aircraft configuration-agnostic and can be easily interfaced with selected aerodynamic solvers. To this end, the MMG facilitates aircraft designers in the modelling of diverse aircraft configurations, and in the fast preparation of input files for further disciplinary analyses, such as aerodynamic, weight and balance or propulsive studies.

In order to generate the aircraft geometry, conceptual design information must be provided to the MMG in the form of numerical values and option strings. This can be done in one of the following three formats:

- a Common Parametric Aircraft Configuration Schema (CPACS) based representation of the aircraft [75];
- a JSON[2] input format generated specifically to capture relevant conceptual design information, necessary for geometry generation;
- a MATLAB[3] output file generated by the Aircraft Design Initiator.

The Initiator is an in-house conceptual aircraft design tool, which synthesizes a feasible aircraft configuration from assigned top-level aircraft requirements. It makes use of several, nested design iteration loops, implementing design and analysis methods of increasing fidelity: from handbook methods, to semi-empirical rules, to physics based calculations. It can be used to obtain complete and consistent aircraft models — including geometry and performance — for further evaluation, optimization and sensitivity studies [76–79]. Although the Initiator can be used to synthesize conventional or unconventional aircraft designs, including box-wing configurations, the PrP geometry used in this dissertation has been provided by the technical consortium of the PARSIFAL project.

Conceptual design data is processed by the MMG, and the geometric model of different aircraft components is created using pre-defined, high-level primitives [80], such as:

- wings: swept and tapered wings, with or without kinks, trapezoidal wings, curved leading and trailing edges as for BWBs, connecting wing elements, like side-wings in box-wing configurations;
- fuselages: either with or without wing fairings, depending on the level of detail of the available conceptual design data;

[1] `https://www.parapy.nl/`
[2] `https://www.json.org/`
[3] `https://www.mathworks.com/products/matlab.html`

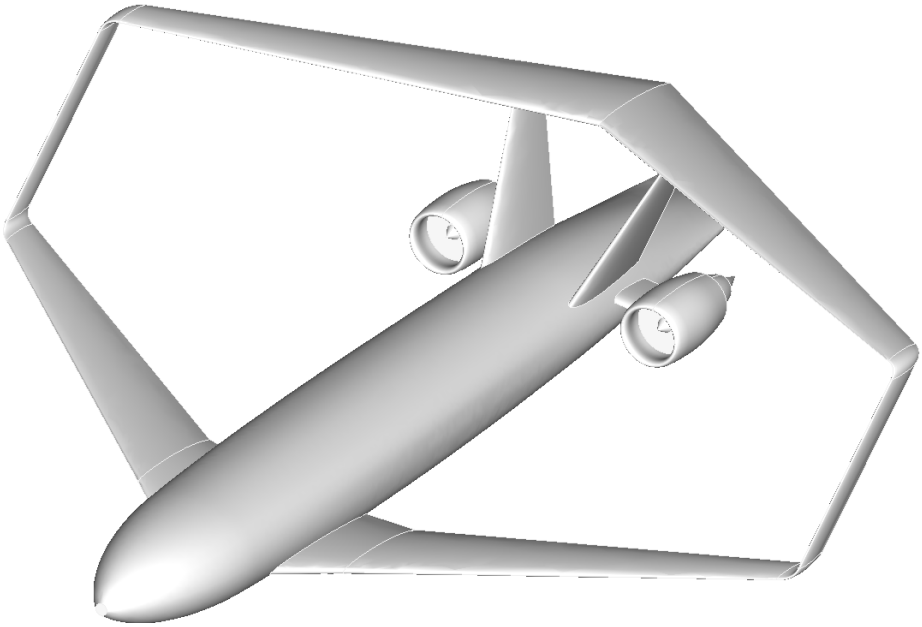

Figure 3.2 PrP aircraft model, as rendered in the Multi-Model Generator.

- movable surfaces: the MMG can generate a movable surface and deflect it, as necessary for different aerodynamic solvers on any type of wing described above. In the current state, only plain movables are modelled;

- turbofan engines and nacelles: the external geometry is modelled to make it possible to include the effects of these components in the aerodynamic analysis and allow for engine integration design studies.

After all components are instantiated, their shapes are fused and merged together, on the basis of conceptual design information, using classic geometric operations. Figure 3.2 shows the final version of the PrP, as rendered in the user interface of the MMG.

During the geometry generation phase, the MMG creates an ontology of the whole aircraft topology. In other words, it retains information about the relationship between geometry primitives, such as edges and facets, and their corresponding functional elements, such as wings, fuselages or engines. In this way, it is able to further process the aircraft geometry and generate a structured or unstructured mesh for an assigned aerodynamic solver. For example, a structured mesh of the whole aircraft geometry is automatically generated by systematically splitting each surface primitive and placing equal number of nodes on the opposite edges of all quadrilateral facets. The whole splitting and meshing process is independent of the actual geometry of the aircraft, and can therefore be used to perform meshing irrespective of the aircraft configuration. An example of surface mesh automatically generated by the MMG is shown in Figure 3.3.

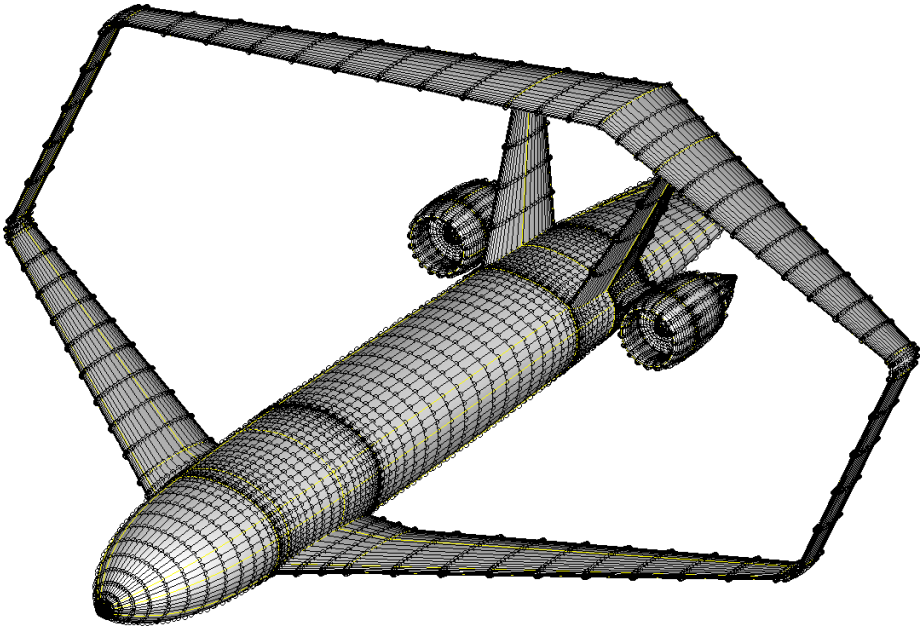

Figure 3.3 Example of a structured surface mesh of the PrP geometry, automatically generated by the MMG.

In addition to the mesh model, a discretized wake model may also be necessary to perform some type of aerodynamic analyses. The MMG can automatically generate both a flexible and rigid wake model, depending on the mesh type and the aircraft topology. A particular mention is required for the treatment of movable surfaces at the trailing edge of a wing element. After the movable geometries are generated and deflected, a gap is created between the movable surface and the fixed part of the wing, which can become problematic when resolving the wake in that region. In order to avoid complications, the MMG automatically constructs transition surfaces between the movable and fixed parts, as shown in Figure 3.4. This is deemed acceptable — and even preferable when exporting the geometry to aerodynamic solvers based on vortex-lattices and 3D panel distributions — for the flight mechanics and control applications presented in this dissertation.

With such a bottom-up approach, the MMG can generate, pre-process and mesh the geometry of practically any aircraft configuration. This configuration-agnostic behavior makes the use of the tool extremely beneficial in the conceptual design phase of unconventional aircraft. For this reason, even though the analysis tools and approaches used to characterize the aircraft aerodynamic and propulsive models have changed on the basis of the application, as mentioned in the following chapters, the geometry of the aircraft has always been treated with such tool.

3.2.2. AERODYNAMICS

In order to perform non-linear flight mechanics simulations, an extensive aerodynamic database is needed to reproduce the aircraft dynamic behavior in different regions of the

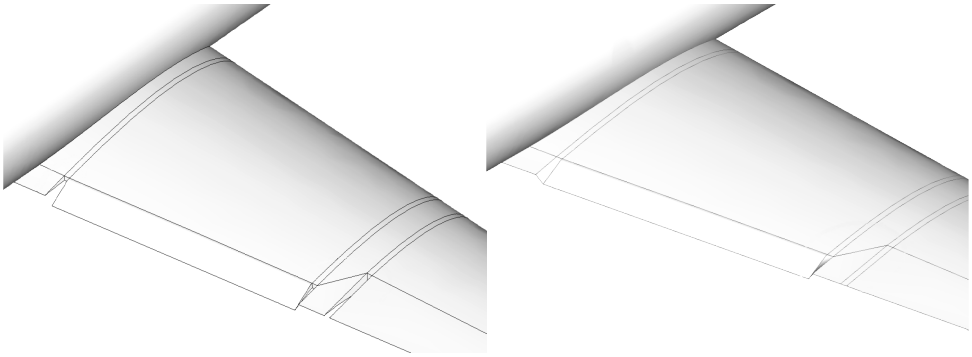

a) With gaps, without transition surfaces **b)** Without gaps, with transition surfaces

Figure 3.4 Automatic generation of transition surfaces in movables gaps to support different types of aerodynamic analyses.

flight envelope. Depending on the application of interest, this database should model the dependency of the aerodynamic forces on a certain set of flight and configuration parameters [81]. The time required to generate it depends on the level of fidelity of the aerodynamic analyses used: possible examples range from handbook and semi-empirical methods, to CFD techniques such as panel methods or Reynolds Averaged Navier-Stokes (RANS) equations, to wind-tunnel test campaigns. In practice, irrespectively of the fidelity level, the large number of aerodynamic analyses needed — from several hundreds to a few thousands — makes the production of the aerodynamic database a critical bottleneck in the design and analysis process [82, 83].

The first step to be taken before generating such a database is to understand what effects must be included in the analysis, as required by the specific application under investigation. On the basis of this modeling choice, the type of aerodynamic solver that has to actually perform the analysis can be chosen. For the present research effort, two main considerations have been made. Firstly, the PrP has been in the conceptual/preliminary design stage during the entire development of the analyses presented in this dissertation. In this time span, relatively fast aerodynamic analyses were needed to assess a given PrP design, or to be included in an iterative design loop. Secondly, the purpose of the proposed analyses is not to provide a detailed aerodynamic characterization of any given aircraft configuration. It is to explore innovative applications of DLC, as allowed by the non-conventional geometry of the staggered box-wing aircraft, but also as applicable to any other aircraft configuration, in principle.

To this extent, the aerodynamic analysis serves the only purpose of providing a consistent set of forces and moments, expressed as a function of the main flight parameters and allowing to perform meaningful flight simulations. The functional dependencies that must be captured for this purpose are surely the ones on the angle of attack, the angle of sideslip, and the control surface deflections. The dependency on the Mach number is strictly necessary only for the mission performance estimation of Chapter 4, as compressibility effects are not necessarily important for the fundamental flight control studies presented in the other chapters. Since the aircraft dynamics are always studied

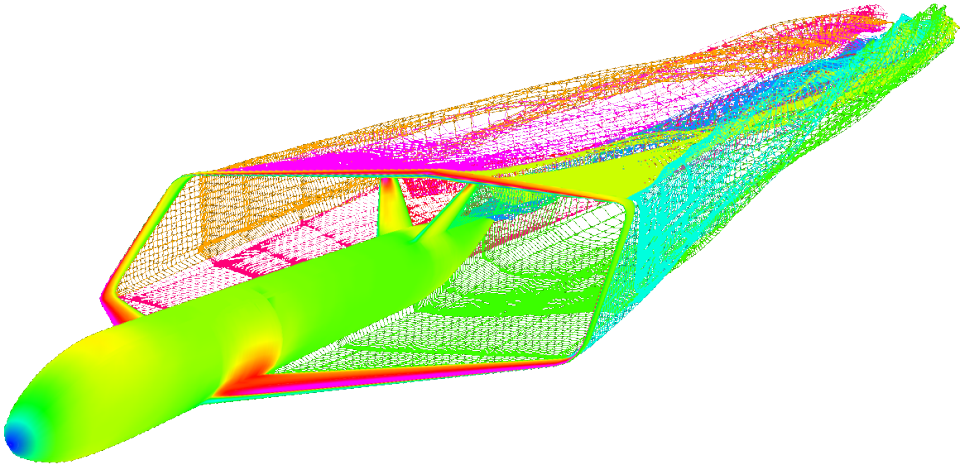

Figure 3.5 VSAERO simulation results for the PrP, using aircraft geometry and wake models generated by the MMG. Clean aircraft configuration, steady simulation with $\alpha = 3\,\text{deg}$, $\beta = 0\,\text{deg}$, $M = 0.3$.

in flight conditions far away from the flight envelope boundaries, a linear quasi-steady aerodynamic model is deemed suitable for all the proposed applications.

In light of these considerations, the commercial 3D panel method VSAERO[4,5] has been employed in most of the applications presented in the following chapters, in light of the attractive trade-off it offers between computational time and solution accuracy [84]. In the specific application presented in Chapter 5, for which the required computational effort has been the most significant impediment to the gathering of results, the simpler open-source vortex lattice method AVL[6,7] has been employed.

Panel methods can be used to calculate the flow field around a watertight geometry, in the hypotheses of steady, irrotational and inviscid flow. In the specific case of VSAERO, the potential flow around the assigned geometry is corrected in a series of iterations accounting for boundary layer effects. The solver uses integral boundary layer equations to alter the original geometry and recalculate the potential flow field around it. Additionally, it accounts for compressibility effects using the Karman-Tsien rule or the Prandtl-Glauert correction [85]. A visualization of a converged flow field around the PrP, as determined by a VSAERO simulation, is shown in Figure 3.5. Vortex lattice methods are simpler panel methods, which additionally neglect the effect of thickness of the assigned geometry. For this reason, the latter are only appropriate for representing thin lifting surfaces, and are most accurate for small values of the angles of attack.

Panel methods of different fidelities are probably the most common choice for flight mechanics studies at conceptual or preliminary design stage, especially for flight at low Reynolds numbers and/or experimental vehicle geometries [86–96]. They are certainly

[4] Vortex Separation Aerodynamics (VSAERO)
[5] `https://www.amiaerollc.com/Software.html`
[6] Athena Vortex Lattice (AVL)
[7] `http://web.mit.edu/drela/Public/web/avl/`

attractive in light of the relatively small time and effort required for the modelling and analysis process. Additionally, the pre- and post-processing operations for the appropriate software tools are usually easy to automate, as it has been done to assemble the workflow here presented. This allows to easily perform many parameter sweeps — which is especially important for a great number of control surfaces, as in the case of the PrP — and characterize the aircraft aerodynamic model in steady, quasi-steady, symmetric and/or asymmetric flight conditions.

On the other hand, panel methods are unsuitable for accurate estimations, especially when capturing local aerodynamic phenomena due to complex geometries, flow separation, compressibility, friction and/or aerodynamic interactions. Possible examples are wing-fuselage intersection regions, effects of gaps and slots in control surface geometry, and basically everything related to drag not dependent on lift. Quantifying these effects in general terms is almost impossible, as they depend on the given aircraft geometry, the flight conditions under observations, the specific solver in use, and are usually sensitive to the mesh characteristics. Overlooking on the impossibility to model stall-related phenomena, several applications on conventional aircraft geometries report satisfying match with other methods at low angles of attack and subsonic flight [86, 92, 94, 96]. On the other hand, discrepancies in both the values and slopes of aerodynamic forces and moments, with drag being basically always underpredicted, are also regularly reported in literature [87–91, 95].

Figure 3.6 shows the aerodynamic efficiency of a preliminary version of the PrP configuration, with no vertical tail or control surfaces. The curve corresponding to VSAERO simulations results in a maximum efficiency of $L/D = 23.7$. A more reliable value of $L/D = 19.4$ (about 18% less) is obtained with high-fidelity RANS analyses available within the PARSIFAL project [97, 98]. It can be seen how the two approaches start differing quite significantly at higher angles of attack, due to different ways to model flow transition and separation effects. While the RANS analysis predicts incipient stall around $\alpha = 3\,\text{deg}$, the panel method is not capable to capture anything related to it, and returns solutions up to $\alpha = 6\,\text{deg}$ with questionable reliability.

In the scope of the present dissertation, the main advantage of using panel methods and adopting their low/medium fidelity lies in their robustness and quickness when performing large numbers of evaluations in different flight conditions. On the other hand, the smooth trends in the variation of aerodynamic forces and moments returned by panel methods are only reliable as long as the underlying aerodynamics is actually linear. Since the flight mechanics formulations presented in the following chapters can be applied to any aircraft configuration, obtaining the most accurate numerical values for the aerodynamic model of the PrP is of little to no interest in this case. In light of these considerations, the aforementioned limitations of panel methods have been deemed acceptable for the purpose of the proposed flight mechanics applications.

As for many other flight mechanics applications making use of the aforementioned assumptions, a vast aerodynamic database is generated for the PrP in the form of look-up tables [91, 99]. The database for steady aerodynamics expresses the six dimensionless aerodynamic actions on the aircraft as tabular functions of α, β, M and control surface deflections $\boldsymbol{\delta}$. In particular, the aerodynamic model can be conceptually divided into the following three contributions:

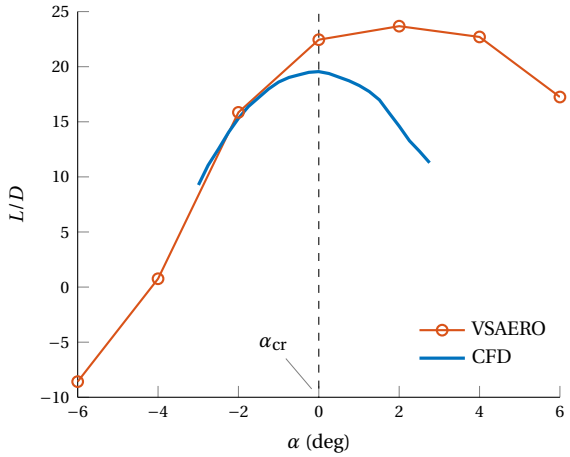

Figure 3.6 Aerodynamic efficiency of a preliminary PrP clean configuration, at $M = 0.3$. Comparison between VSAERO and high-fidelity CFD analyses [97, 98].

- the steady aerodynamic actions due to the clean aircraft configuration, with no control surface deflected, expressed as a function of α, β and M;
- the control aerodynamic actions obtained through the deflection of control surfaces, expressed with respect to the clean aircraft configuration as a function of α, β, M and $\boldsymbol{\delta}$;
- the quasi-steady derivatives of the aerodynamic actions with respect to the roll, pitch and yaw angular rates, as a function of α, β and M.

Each aerodynamic action is then expressed as in Equation 3.1, exploiting the assumption of superposition of effects.

$$C_F = \underbrace{C_{F_0}\left(\alpha,\beta,M,\boldsymbol{\delta}=\mathbf{0}\right)}_{\text{steady, clean}} + \underbrace{\sum_{i=1}^{N_{\boldsymbol{\delta}}} \Delta C_F\left(\alpha,\beta,M,\delta_i\right)}_{\text{steady, control effectors}} + \underbrace{\sum_{\omega=p,q,r} C_{F_\omega}\left(\alpha,\beta,M,\boldsymbol{\delta}=\mathbf{0}\right)\omega}_{\text{unsteady, clean}} \tag{3.1}$$

This model assumes linear dependence of the aerodynamic actions on the angular rates p, q, r, and decouples the aerodynamic models for the clean aircraft and its control surfaces. Quasi-steady derivatives with respect to angular rates are calculated with a second order finite difference formula, for each flight condition and for an assigned position of the aircraft center of gravity. For a given flight condition, the differential actions due to control surface deflections are determined by subtracting the aerodynamic actions generated by the clean configuration from the ones obtained with a single control surface deflected. In this way, it also disregards possible interaction effects between control surfaces. As explained in the previous section, movable surfaces are modelled in the MMG as plain flaps, and their deflection obtained by geometry deformation. This is sufficient as long as they are required to act as primary control surfaces.

Table 3.2 Comparison of numerical values of dimensionless q- and $\dot{\alpha}$-derivatives, as obtained by high-fidelity RANS computations on a preliminary version of the PrP. Reference condition: $h = 3048\,\text{m}$, $M = 0.5$, $\alpha = 0\,\text{deg}$ [97, 98].

C_{L_q}	$C_{L_{\dot{\alpha}}}$	$C_{\mathcal{M}_q}$	$C_{\mathcal{M}_{\dot{\alpha}}}$
4.76	1.65	-25.47	-2.461

Unsteady aerodynamic effects, in the form of the so-called "acceleration derivatives" — with respect to $\dot{\alpha}$, $\dot{\beta}$, $\dot{q}$ or higher order terms [100–102] — have not been included in the model. The purpose of these quantities is to model the time delay which is necessary for the flow to develop in the longitudinal ($\dot{\alpha}$) and lateral ($\dot{\beta}$) directions [100, 101, 103]. Because the pressure field does not adjust to the aircraft shape instantaneously, the quasi-steady model of Equation 3.1 formally becomes less and less accurate as flight maneuvers get faster. On the other hand, it must also be noted that the condition that has been refereed to as Pure DLC in Section 1.1, results in vertical motion with $\dot{\alpha} = 0$.

The decision to not include these effects has been partially motivated by the impossibility to calculate them in the chosen physics-based analysis framework [85]. An additional motivation lies in the order of magnitude of $\dot{\alpha}$-derivatives for lift and pitch coefficients, as compared to q-derivatives for the box-wing aircraft. Some indicative values, calculated within the PARSIFAL project for a preliminary and incomplete version of the PrP, are summarized in Table 3.2 [97, 98]. It can be seen that the $\dot{\alpha}$-derivatives are ≈ 5 to 10 times smaller than the q derivatives, in this reference flight condition. For these reasons, neglecting unsteady effects is believed to have only a minor impact on the numerical results presented in Chapters 5 and 7, but does not diminish in any way the validity of any of the proposed flight mechanics applications.

Lastly, it is worth mentioning that the CFD techniques used to calculate unsteady derivatives usually require to simulate some type of harmonic motion of the aircraft within the aerodynamic solver. This is not representative of any realistic flight scenario, and is applicable to flight mechanics studies only with several assumptions. Overcoming the "severe limits on the motion rates and motion forms for which" [101] the unsteady derivatives so calculated are applicable to realistic flight maneuvers, together with the complexity required to implement sophisticated unsteady formulations in the flight mechanics model, has been deemed well beyond the scope of this dissertation [101, 102].

The high-level of automation injected in the aerodynamic analysis workflow can affect the capability to capture detailed or very specific phenomena which may be of interest for a particular application. In these cases, or if the aerodynamic solver is not capable to capture desired characteristics because of modelling limitations, semi-empirical methods can be used. They represent a simple and quick resource to augment, or modify, the aircraft aerodynamic model in conceptual and preliminary design stage, but should not be preferred for higher-fidelity analyses in more advanced design stages, obviously. Semi-empirical methods do not require any computational effort, as they are usually based on statistical datasets or handbook rules. They are typically unreliable, or even not existent, for straightforward applications to unconventional aircraft configurations, and therefore must be used with care. Small modifications to the aerodynamic model of

Equation 3.1, based on semi-empirical methods, have been necessary in Chapter 4, to model the lift and drag increase due to complex flaps, and the transonic drag effects due to control surfaces.

3.2.3. PROPULSIVE SYSTEM

The propulsive model of the PrP is generated by an in-house, physics-based method for turbofan engine sizing, referred to as GTpy [104]. This tool takes the required thrust, a reference design flight condition and a few engine geometric requirements as input, and performs a physics based design and sizing of the whole engine assembly, including the nacelle. It builds up on the gas turbine performance simulation method GSP [105], and connects it to a design methodology based on thermodynamic cycle calculations [106]. Moving from the assigned reference flight condition, regarded as the engine design point, GTpy generates engine thrust and fuel flow maps in off-design conditions, as a function of altitude, Mach number and corrected fan speed. The dependency on the latter parameter is then mapped to a normalized excursion of the pilot throttle command, as summarized in Equation 3.2.

$$\begin{cases} T = T(M, h, \delta_T) \\ TSFC = TSFC(M, h, \delta_T) \end{cases} \tag{3.2}$$

The propulsive system of the PrP configuration has been designed according to specific performance and size requirements, among which the ability to deliver at least 180 kN of thrust at take-off. The thrust variation with Mach number and altitude is shown in Figure 3.7, for the maximum throttle condition. Each engine has a *BPR* of 11, although alternative designs with very large *BPR* up to 18 have also been explored within the PARSIFAL project [107]. In light of the low/medium fidelity adopted to generate both the aerodynamic and propulsive models, the forces and moments resulting from these analyses are completely uncoupled and do not interact. For example, there is no aerodynamic effect of mass flow through the engine on the aerodynamics of nearby elements. On the other hand, the geometry of the nacelles is included in the aerodynamic analysis of the PrP at the latest stages of the PARSIFAL project, hence the aerodynamic effects of their shape and position is indeed taken into account.

3.3. FLIGHT DYNAMICS

Once generated and parsed, the aerodynamic and propulsive databases have to be integrated, together with other relevant information, into the global flight mechanics model of the aircraft. The purpose of a flight mechanics model is to calculate the solution of the aircraft dynamics equations of motion, and the time evolution of relevant parameters in some specified flight scenario. The solution of the flight dynamics equations of motion can be carried out with simplified analytical models, or through numerical simulations. The flight mechanics analysis can have the objective to assess the flight performance of the aircraft, its stability and control characteristics, or its flying and handling qualities. It is obviously an essential process in the evaluation of the aircraft operational behavior, and a fundamental one to support aircraft design and optimization studies.

For all of the applications presented in this dissertation, the flight mechanics model

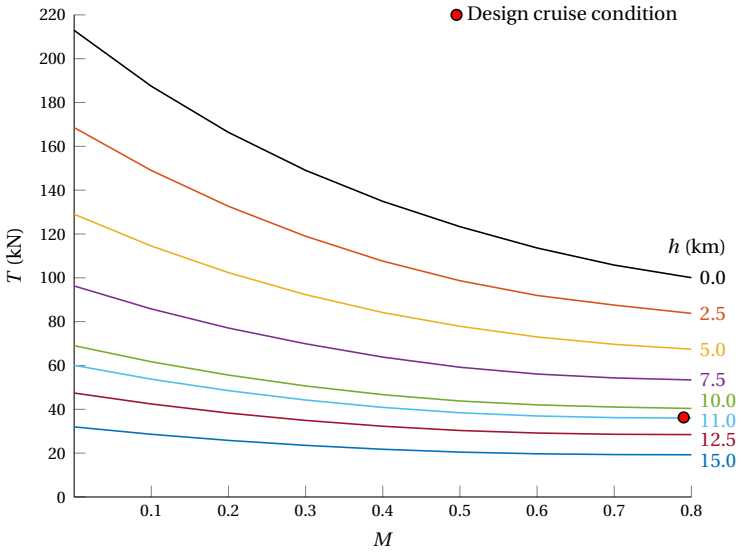

Figure 3.7 Maximum available thrust of the PrP as a function of Mach number and altitude, excluding the effects of nacelles drag.

of the PrP and its competitor aircraft has been developed in a MATLAB/Simulink environment referred to as PHALANX[8]. PHALANX is a modular toolbox for non-linear, 6 DoFs flight simulation and analysis. Its main purpose is to provide a framework of synthesis and analysis functions, with the objective to quickly and automatically generate a complete flight mechanics model of a given aircraft, starting from the datasets and information pertaining to its disciplinary sub-models. Each baseline flight mechanics model can always be manually tailored to the specific application, while retaining the possibility to rely on an ample array of functions to assess its performance.

The practical implementation of the flight mechanics model consists of a small network of interconnected disciplinary modules. The fidelity of each module depends on its underlying model and dataset, making PHALANX a data-driven toolbox. The fidelity of the resulting flight mechanics analyses will then depend on the fidelity of the input models. Such flexible structure, together with the capability to operate regardless of the aircraft configuration, allow PHALANX to be implemented consistently at different stages of the design process, and to make fair comparisons among application cases. The toolbox has been used in previous works for studies on novel aircraft configurations, like the BWB [108], the DUUC — featuring the propulsive empennage concept [109] — and the PrP itself [42, 43].

A block-scheme overview of PHALANX is shown in Figure 3.8. From this top-level perspective, PHALANX links a simple pilot module to a FCS module, which allows to design custom Automatic Flight Control System (AFCS) architectures on the basis of the application. The FCS takes charge of determining the position of the control effectors

[8] Performance, Handling Qualities and Load Analysis Toolbox (PHALANX)

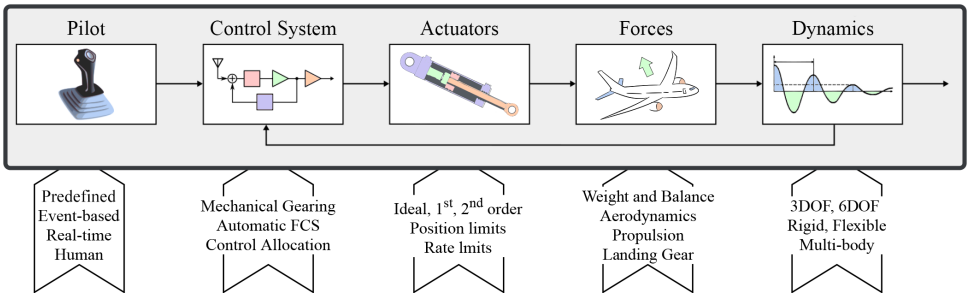

Figure 3.8 Block scheme overview of the PHALANX flight mechanics model.

at every time step of the simulation, also using CA methods, if necessary. Together with the other flight parameters, the control effectors positions are used to access the aerodynamic and propulsive databases, and calculate the external forces acting on the aircraft at every time step of the simulation. Once these are known, the equations of motion can be solved numerically, and the aircraft state can be propagated to the following time step and fed back for control purposes.

The following sections present an overview of the FCS and flight dynamics module of PHALANX.

3.3.1. FLIGHT CONTROL SYSTEM (FCS)

The FCS module connects the pilot and autopilot models to the aircraft control effectors. It provides a flexible but robust baseline architecture, which is easy to customize for every particular application. The specific AFCSs developed for the presented applications are going to be presented in more detail in the appropriate chapters, while this section only gives an overview of the baseline PHALANX module in question. A top-level scheme of the FCS architecture in PHALANX is shown in Figure 3.9

Pilot commands can be modelled in multiple ways. In the most common case, the time histories of the pilot inputs on the control stick and/or the throttle can be defined explicitly before the time simulation is launched. A slightly more advanced approach consists in triggering pre-defined pilot maneuvers on the basis of specific simulation events. Possible examples are represented by a pull-up maneuver during the take-off run when the decision speed is reached, or a flare maneuver when reaching a minimum altitude. Additionally, PHALANX can be interfaced with external hardware, such as a joystick or a joypad, which gives a human user the ability to inject pilot commands in real time. This can be useful for testing or prototyping a new model, or to record visualizations in external simulators as FlightGear[9].

Pilot commands are transmitted to the effectors either through a basic mechanical gearing chain, or through an arbitrarily complex control law. They can also be mixed with inputs from an AFCS, or be left completely unused, leaving the whole burden of the control task to the latter. The mechanical gearing branch maps the normalized pilot inputs, ranging in the $[-1,1]$ interval, to the control surface deflections and the throttle

[9] `https://www.flightgear.org/`

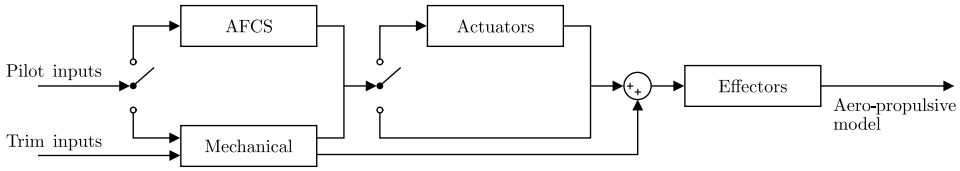

Figure 3.9 Block scheme overview of the baseline FCS architecture in PHALANX.

setting, making use of a ganging matrix and appropriate gearing ratios. While the throttle effector ranges in the $[0,1]$ by default, the gearing ratios for control surfaces have to be calculated automatically on the basis of their saturation limits and the chosen ganging matrix. The standard approach in PHALANX is to associate the maximum input on the pilot stick to the saturation limit of each control surface.

Control inputs, coming from either the mechanical gearing branch or the AFCS one, are then input to the actuator models, which regulate the motion of the control effectors. Actuators can be modeled as ideal systems, with no delay or oscillations, or first and second order systems, depending on the application. They can be assigned both a position saturation limit, and a rate saturation limit as well.

Because the mechanical gearing chain does not necessitate any control logic, it can also be conveniently used to trim the aircraft model at specified initial flight conditions. A trim branch runs through the mechanical gearing chain in parallel to the aforementioned one, and has the objective to overlay constant trim commands to the ones that are calculated at runtime. The trim branch takes its inputs in the form of constant pilot commands on the stick and throttle, which have to be calculated before any simulation by a selected trim routine. It outputs constant effectors positions, which supposedly keep the aircraft trimmed in case of no additional pilot or auto-pilot inputs. The trim effectors positions are not affected by actuator dynamics and are summed to the runtime values obtained through the pilot or AFCS models.

Several trim methods are available in PHALANX, in the form of different optimization problem formulations. Chapter 6 formally introduces the trim problem, presents an original formulation and illustrates several application studies in detail. For this specific approach, the mechanical gearing trim branch is replaced by one based on CA.

3.3.2. EQUATIONS OF MOTION

The external forces and moments — as calculated using the models introduced in Section 3.2, for example — act on the aircraft body and determine the evolution of all flight parameters in time. In order to propagate the aircraft state in PHALANX, the system of Ordinary Differential Equations (ODEs) describing aircraft dynamics is not encoded explicitly in the flight mechanics model, but generated through a multi-body dynamics reference framework. This acts as the flight simulation core of PHALANX, and is developed by exploiting the Simscape Multibody Dynamics library in Simulink[10]. With this approach, it is possible to model complex phenomena like relative motion of aircraft parts — as the center of gravity due to fuel consumption — or wing flexibility, and mea-

[10] https://nl.mathworks.com/products/simscape-multibody.html

sure local flight parameters at specific aircraft locations.

In the baseline flight mechanics model, the main aircraft body is modelled as a constant mass with inertia. A prescribed variable mass can also be included, in order to form a body compound. This is necessary when the effects of fuel consumption on the performance to study are relevant. The variable mass is treated as a point, but its contribution to the overall balance and inertia of the compound is automatically calculated by the framework, making use of the Huygens-Steiner theorem [110]. The simulation can be allowed to have 6 DoFs, or limited to a vertical plane, hence only granting the aircraft its longitudinal 3 DoFs. Alternatively, it is always possible to define custom dynamic models, as done in Chapter 4 for a point mass mission optimization study.

In all cases, a flat and non-rotating Earth model is assumed. The equations of motion are rendered in the aircraft body reference frame, exploiting classic kinematic transformations from a Cartesian, topocentric reference frame. These approximations are acceptable for almost all types of flight mechanics studies, also in light of the small spatial and temporal scale of classic flight simulations. They are also acceptable for mission performance evaluations, as long as the purpose of the investigation is to assess and compare aircraft performances on a generic mission profile, rather than studying real-world point-to-point navigation problems. The International Standard Atmosphere (ISA) model is adopted, together with the assumption of constant gravitational acceleration and still air.

Initial values of all necessary parameters must be explicitly assigned or calculated via a trim routine. Flight parameters in the wind reference frame — such as the angle of attack, angle of sideslip, or the flight path angle — are calculated at the end of each time iteration, using the latest value of the aircraft states in body axes. Both of these reference frames are represented in Figure 3.10, together with the aerodynamic reference frame. The system of dynamic equations is closed by expressing aero-propulsive forces as functions of the various flight and control variables, as shown in Equations 3.1 and 3.2.

In principle, this framework also allows to model each aircraft component as a separate, individual body, characterized by its own properties and disciplinary sub-models. The position and orientation of each component can be independently defined with respect to an inertial reference frame, and rigidly — or elastically — connected to the other parts, if necessary, to form the aircraft assembly as a whole. Local flight parameters, such as the angle of attack or the airspeed, can be measured at runtime. And if each component is associated to its corresponding aerodynamic dataset, every aircraft part is able to generate its own aerodynamic actions from its own position relative to the aircraft center of gravity. In this way, it is possible to exploit the difference in local speed and incidence to artificially simulate unsteady aerodynamic effects. This could be the case, for example, of the aerodynamic pitch damping due to the horizontal tail plane. Such approach has been used to study the longitudinal dynamics of the DUUC, for which three separate aerodynamic models based on CFD datasets, were available for the aircraft wing, fuselage and horizontal tail [109].

In the most simple case, when the aircraft compound only features one body, and it has no moving parts or variable mass components, the underlying equations of motion reduce to the classic 6 DoFs rigid body dynamic equations, written in the body reference frame as in Equation 3.3. In this case, and if not specified otherwise in the remainder of

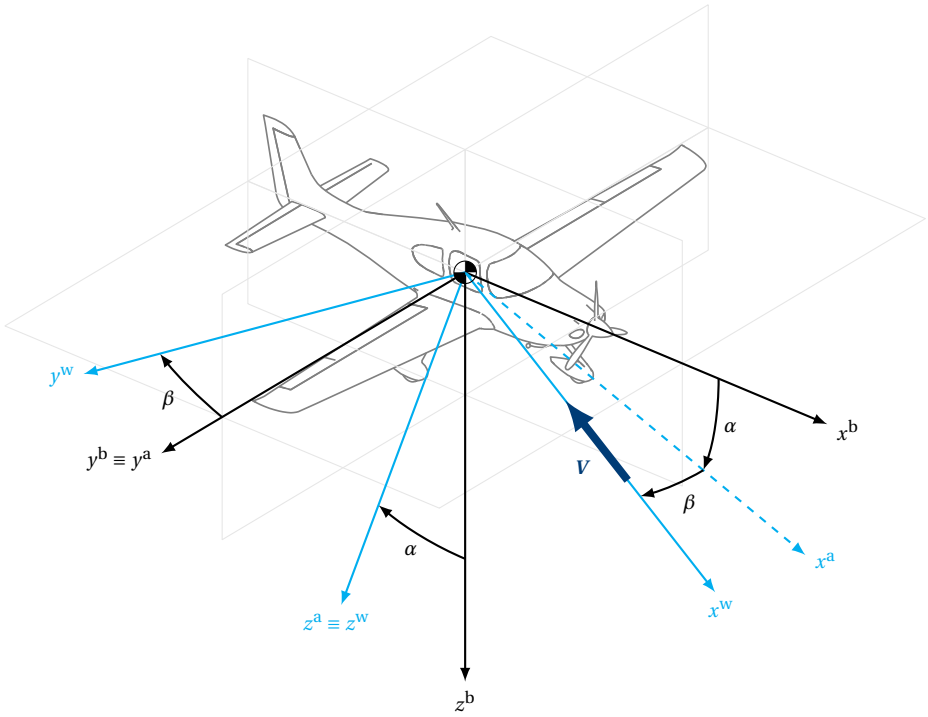

Figure 3.10 Body, wind and aerodynamic reference frames, with definition of the angle of attack α and the angle of sideslip β.

this dissertation, the "b" superscript indicating that the X, Y, Z forces and the $\mathcal{L}, \mathcal{M}, \mathcal{N}$ moments are expressed in the body reference frame is omitted.

$$\begin{Bmatrix} \dot{u} \\ \dot{v} \\ \dot{w} \end{Bmatrix} + \begin{Bmatrix} p \\ q \\ r \end{Bmatrix} \times \begin{Bmatrix} u \\ v \\ w \end{Bmatrix} = \frac{q_\infty S}{m} \begin{Bmatrix} C_X\left(\alpha, \beta, M, p, q, r, \boldsymbol{\delta}\right) \\ C_Y\left(\alpha, \beta, M, p, q, r, \boldsymbol{\delta}\right) \\ C_Z\left(\alpha, \beta, M, p, q, r, \boldsymbol{\delta}\right) \end{Bmatrix} + g \begin{Bmatrix} -\sin\theta \\ \cos\theta \sin\varphi \\ \cos\theta \cos\varphi \end{Bmatrix}$$
$$J \begin{Bmatrix} \dot{p} \\ \dot{q} \\ \dot{r} \end{Bmatrix} + \begin{Bmatrix} p \\ q \\ r \end{Bmatrix} \times J \begin{Bmatrix} p \\ q \\ r \end{Bmatrix} = q_\infty S \begin{Bmatrix} bC_{\mathcal{L}}\left(\alpha, \beta, M, p, q, r, \boldsymbol{\delta}\right) \\ \bar{c} C_{\mathcal{M}}\left(\alpha, \beta, M, p, q, r, \boldsymbol{\delta}\right) \\ bC_{\mathcal{N}}\left(\alpha, \beta, M, p, q, r, \boldsymbol{\delta}\right) \end{Bmatrix} \tag{3.3}$$

3.4. CONCLUSIONS

This chapter has presented an overview of the tools and approaches used to characterize the various aspects of a complete aircraft flight mechanics model. These are necessary to perform significant flight dynamics simulations and analyses, and to estimate the aircraft performance within an acceptable level of accuracy. Emphasis has been placed on the added value of physics-based approaches, which can be employed to perform fair comparisons among different aircraft configurations. The proposed overall analysis

workflow has been presented as highly automated, in order to streamline the design and evaluation process, and leave small margin for human error. On the other hand, specific studies always require customizations of the baseline models presented in this chapter. These particular modifications to the flight mechanics model are going to be presented in the following chapters, in the scope of the particular application they have been tailored for.

The PrP has been presented as the main test case for all the flight control methods proposed in the following chapters. Its design has been in continuous development, within the PARSIFAL project, throughout the time period that led to this dissertation. For this reason, low/medium fidelity tools have been chosen to characterize its aerodynamic and propulsive models, and a complete and consistent overview of the aircraft performance at this stage has not been presented. For this research, the relevance of the PrP lies in the geometry of its staggered box-wing, which allows innovative applications of DLC. With this scope in mind, relatively little importance has been placed on the actual numerical values resulting from the aerodynamic and propulsive analyses. The latter mainly serve the purpose of providing a consistent set of external forces and moments, expressed as a function of the most relevant flight and configuration parameters. Rather than to characterize the performance of the specific aircraft in detail, they make it possible to perform flight simulations to test and evaluate the methods proposed in the following chapters.

4

MISSION PERFORMANCE

Sometimes you're ahead, sometimes you're behind.
The race is long, and in the end,
it's only with yourself.

Larry Mann
The Big Kahuna
1999

Simplicity does not precede complexity, but follows it.
Optimization hinders evolution.

Alan J. Perlis
Epigrams in Programming
1982

Once the properties of box-wing aircraft have been introduced in Chapter 1, and the philosophy behind the development of the PrP configuration have been outlined in Chapter 3, the present chapter attempts to characterize the PrP from an operational standpoint. Its objective is to assess the optimal mission performance of the PrP, and compare it to the one of a competitor aircraft with conventional tube-and-wing geometry. This is done by making use of the definition, modeling and simulation of operational, globally optimal mission profiles for different aircraft models. A simplified point-mass model is used for all the analyses performed in this chapter, in order to leverage the full power of optimal control theory.

After the brief introduction to the problem of mission performance optimization provided in the following Section 4.1, Section 4.2 presents a generalized approach to create a mission model in the framework of an optimal control study. A simplified flight mechanics model is presented in Section 4.3 for the PrP and a candidate competitor aircraft,

Parts of this chapter have been published in the MDPI Aerospace journal in 2020 [111].

together with an overview of the numerical approach implemented to perform flight simulations. Trajectories, time histories and top-level performance metrics are then presented in Section 4.4, for missions with design and harmonic ranges. Lastly, conclusions and limitations for the present study are presented in Section 4.5.

4.1. INTRODUCTION

The determination of optimal aircraft trajectories and the quantification of related performance metrics have always been of fundamental interest for all aircraft operators. In particular, commercial aviation stakeholders have in mission performance optimization one of the most natural ways to gain an economic advantage over their competitors, by seeking minimum operative costs and maximum profits. On the other hand, in more recent times, several scientific investigations have also employed trajectory analysis and optimization techniques for proposing the development of a more sustainable aviation ecosystem.

The most common approach, in these regards, is to explore innovative mission schedules and air traffic management procedures, and assess their impact on the mission performance of state-of-the-art aircraft models [112, 113]. But with unconventional aircraft configurations rising in popularity as one of the feasible solutions for a more sustainable future aviation, it should be equally relevant to evaluate the mission performance of such disruptive geometries. This can be done with respect to currently available regulations, but also with respect to innovative mission profiles. In the latter case, specific mission schedules or procedures can be tailored to the aircraft configuration of interest, in order to exploit its peculiar properties and the new piloting techniques it allows.

In the particular example of box-wing aircraft, the optimal induced drag characteristics are nowadays well established from a theoretical and experimental standpoint, and confirmed by multiple static aerodynamic analyses. Additionally, it has already been mentioned how the staggered box-wing geometry allows an efficient and practical implementation of DLC. In light of these properties, it seems intuitive to expect the PrP to have a performance advantage on mission schedules with longer climb or descent segments, or in general when flying at higher angles of attack. As a matter of fact, it is in these scenarios of relatively low flight speed that induced drag effects on mission performance become more relevant. On the other hand, detailed and configuration-specific studies should be carried out in any case to prove that the control surface deflections required to fly the given mission profile do not undermine the optimal induced drag performance of the clean box-wing too much.

A wide variety of approaches is available in literature to model well-established, realistic commercial mission schedules. For example, the Base of Aircraft Data (BADA) airline procedure model prescribes a set of mission speed schedules as a function of the aircraft altitude, in tabular format [114]. A very different approach uses the notion of capture conditions and flight objectives to define flight phases in a more operational, yet conceptual, fashion [115]. Flight objectives are variables that are kept constant throughout a phase, whereas capture conditions determine the termination of a given flight phase. This approach has been selected for the present study, as it can be easily paired with a completely physics-based, aircraft configuration-agnostic flight mechanics model. It is presented in more detail in Section 4.2.

For all of these types of models and applications, global optimization techniques deliver the most accurate and comprehensive results [116]. These complex mathematical methods aim at finding the optimal value of a cost function, resulting from the evolution of a given dynamic system over a certain period of time. They are usually computationally expensive in their numerical implementation, and hence require simplified models for the dynamic simulation of the system of interest. The equations of motion that are typically used for global mission optimization usually represent the aircraft as a simple point-mass dynamic system, with selected states and control variables [117–119]. In almost all cases, these reduced-order dynamic models disregard the relation between rotational dynamics and control surfaces, and assume attitude angles as the top-level control variables for aircraft dynamics [120]. Moreover, they neglect all aspects related to rotational trim, unless some form of trimmed lift and drag polars are provided in the underlying aerodynamic model. Notably, optimal control applications for mission analysis of unconventional aircraft configurations have not been found in the available scientific literature.

The theoretical background underlying the selected mission simulation approach, and a brief state-of-the-art review of relevant mission optimization applications is presented in the following sections.

4.1.1. OPTIMAL CONTROL THEORY

Originating from the calculus of variations, optimal control theory has become the cornerstone of modern aircraft trajectory optimization [116, 121–124]. The goal of any optimal control problem is to find the time histories of the states $\boldsymbol{\sigma}^*(t)$ and of the controls $\boldsymbol{u}^*(t)$ that minimize the cost functional $\mathcal{J}$ to $\mathcal{J}^*$, while respecting the problem constraints [123, 125, 126]. In the most general Bolza formulation, the cost functional $\mathcal{J}$ is composed of the Mayer end-cost term Ma and the Lagrange running cost La, as shown in Equation 4.1 [123, 125, 126].

$$\mathcal{J}(\boldsymbol{\sigma}, \boldsymbol{u}, t) = \sum_{\mathrm{p}=1}^{N_\mathrm{p}} \left[\mathrm{Ma}^\mathrm{p}\left(\boldsymbol{\sigma}^\mathrm{p}_{t_\mathrm{ini}}, t^\mathrm{p}_\mathrm{ini}, \boldsymbol{\sigma}^\mathrm{p}_{t_\mathrm{fin}}, t^\mathrm{p}_\mathrm{fin}\right) + \int_{t^\mathrm{p}_\mathrm{ini}}^{t^\mathrm{p}_\mathrm{fin}} \mathrm{La}\left(\boldsymbol{\sigma}(t), \boldsymbol{u}(t), t\right) \right] \tag{4.1}$$

Several gradient-based methods exist for solving such a continuous-time optimal control problem. They are usually categorized as direct or indirect methods, on the basis of the set of optimal control equations, and as shooting or collocation methods, on the basis of the set of variables that are discretized [122–124]. For the present application, a direct collocation method has been adopted. The main reason behind the choice of a direct method is the ease and flexibility guaranteed for the formulation of different problems, with no need to provide unintuitive initial guesses and derive different optimality conditions for each slight problem adaptation. The main reason for choosing a collocation method is the relative robustness of this approach. In any case, the choice of the optimal control solver is not expected to affect any high-level conclusion on the performance of the PrP.

Direct collocation methods have been successfully applied to commercial aircraft trajectory optimization, for both conventional mission studies and novel formation flight performance assessments [118, 127, 128]. These studies use either the lift coefficient or the flight path angle as a control variable, hence allowing for discontinuities in the time

histories of the angle of attack and/or the aircraft attitude angles. Moreover, they implement the well-established parabolic drag polar model, for the purpose of simplicity and robustness of the underlying aerodynamic model. Another study on an existing commercial aircraft configuration [129] makes use of BADA as its underlying flight mechanics model [114, 130]. This can be quite restricting, or even inapplicable, for a disruptive aircraft geometry.

The following sections describe the abstraction process required to model and link diverse, realistic mission segments within the domain of multi-phase optimal control theory. Particular emphasis is placed on the injection of common piloting techniques and aeronautical practices in the mission mathematical model. These are required to make the modelled mission realistic from an operational point of view, in the current state of air traffic management regulations.

4.2. MISSION MODEL

A commercial aircraft mission profile is inherently composed of several flight phases with different characteristics. For this reason, multi-phase optimal control methods are naturally applicable to mission performance analysis problems. This section aims at presenting a general method to translate an intuitive and realistic aircraft trajectory model to its multi-phase optimal control problem-compatible counterpart.

4.2.1. CAPTURE CONDITIONS

In order to simulate realistic commercial aviation flight procedures, flight phases are often characterized by a certain subset of constant flight parameters, referred to as *flight objectives*, and flight phase termination conditions, referred to as *capture conditions* [115]. Flight objectives serve the purpose of modeling classic pilot procedures, to some extent. Examples include cruise flight at constant Mach number and altitude, or climb at constant Calibrated Airspeed (CAS). Capture conditions ensure the convergence of the whole mission simulation, through proper linkage of flight phases.

If a *capture variable* — a flight parameter that is "monitored to determine the junction of the current segment with an adjacent one" [115] — reaches a specified threshold value, the capture condition is satisfied and the simulation switches to the new mission phase. Examples of capture variables are altitude for a climb phase, speed for a take-off ground roll phase, or heading angle for a turn phase. Their respective threshold values could be the initial cruise altitude, the lift-off speed, and the desired route heading, for instance. Specific capture conditions for each relevant flight phase are presented in more detail in Section 4.2.3.

The fulfilment of a capture condition, and consequent adequate linkage of neighboring phases, is automatically guaranteed when the capture variable behaves monotonically. Choosing a capture variable which behaves monotonically during a specific flight phase is therefore a sufficient condition to obtain a well defined linkage criterion for that phase. On the other hand, a capture condition could also be achieved if the corresponding capture variable is not monotonic. This would make the linkage criterion less robust and the phase connection more unpredictable [115]. Although imposing capture conditions and prescribing flight objectives is necessary only for time-stepping, locally opti-

mal trajectory simulations, this is not strictly the case for integral, globally optimal control approaches. Nonetheless, the concepts of capture conditions and flight objectives are an intuitive and realistic representation of real-life operations, and are thus adopted in the current methodology, using them wherever applicable.

4.2.2. CONSTRAINTS

The aircraft flight envelope is limited in several ways by physical considerations. Firstly, the aircraft is not allowed to fly within a specified tolerance of its stall speed. Practically, this limit will not be sought by any trajectory optimization algorithm, because of the low speed combined with the high drag penalty which characterize this flight regime. Secondly, structural limitations bound the aircraft within a minimum and maximum value of the aircraft load factor. In common commercial mission operations, these limit conditions are rarely approached and are therefore not included in the present framework. The last main limitation is represented by the high-speed buffet onset boundary. Due to the limitations of the 3D panel method used for generating the aerodynamic database, this effect cannot be properly captured, and it has been replaced by the explicit prescription of a M_{mo} value.

Physical and operational limitations can be injected in the optimal control framework as various forms of constraints on flight variables. In the first place, the set of differential-algebraic equations of motion is the most fundamental physical constraint that the system has to comply with. These are referred to as *dynamic constraints* and synthetically expressed in terms of state and control variables in Equation 4.2.

$$\dot{\boldsymbol{\sigma}}^{\text{p}} = f\left(\boldsymbol{\sigma}^{\text{p}}(t), \boldsymbol{u}^{\text{p}}(t), t\right) \quad \forall \text{p} = 1, \ldots, N_{\text{p}} \tag{4.2}$$

Additionally, *path constraints* can be imposed to continuously restrict the trajectory during each mission phase. In general, these constraints can be formulated as in Equation 4.3, where the inequality constraint can become an equality constraint if the same lower and upper bounds are imposed.

$$\text{lb}^{\text{p}}_{\text{path}} \leq \mathcal{C}^{\text{p}}_{\text{path}}(\boldsymbol{\sigma}(t), \boldsymbol{u}(t), t) \leq \text{ub}^{\text{p}}_{\text{path}} \quad \forall \text{p} = 1, \ldots, N_{\text{p}} \tag{4.3}$$

In a similar way, *bound constraints* can be imposed to limit variables between a fixed minimum and maximum value, at all times. It must be underlined that bounds are mathematically equivalent to path constraints, if the constraint function coincides with the bounded variable. From a numerical solver standpoint, though, they are treated in a substantially different way. Constraints generally increase problem complexity whereas tighter bounds decrease it.

In a different manner, *phase endpoint constraints* can be imposed on time and state variables to constrain their values at the interface between two phases. They can be formulated directly, as an explicit prescription of desired values, or indirectly, by defining an event constraint function, as shown in Equation 4.4.

$$\text{lb}^{\text{p}}_{\text{event}} \leq \mathcal{C}^{\text{p}}_{\text{event}}\left(\boldsymbol{\sigma}^{\text{p}}_{t_{\text{ini}}}, t^{\text{p}}_{\text{ini}}, \boldsymbol{\sigma}^{\text{p}}_{t_{\text{fin}}}, t^{\text{p}}_{\text{fin}}\right) \leq \text{ub}^{\text{p}}_{\text{event}} \quad \forall \text{p} = 1, \ldots, N_{\text{p}} \tag{4.4}$$

A specific, indispensable instance of phase endpoint constraints are *phase linkage constraints*. These ensure that time and states are continuous at phase interfaces, by requiring that the state variables and time should be equal at the end of phase p and at the

start of phase p + 1.

$$t^{\mathrm{p}}_{\mathrm{fin}} = t^{\mathrm{p+1}}_{\mathrm{ini}} \quad \text{and} \quad \boldsymbol{\sigma}^{\mathrm{p}}_{\mathrm{fin}} = \boldsymbol{\sigma}^{\mathrm{p+1}}_{\mathrm{ini}} \quad \forall \mathrm{p} = 1, \ldots, N_{\mathrm{p}} - 1 \tag{4.5}$$

This result is obtained by modeling $\mathcal{C}^{\mathrm{p}}_{\mathrm{event}}$ as the difference between two phases trajectories at their common interface, and setting both the lower and upper bounds equal to zero. Periodic variables, such as the heading angle, are instead linked by using a sinusoidal function. The optimal control transcription method adopted for the current work, described in Section 4.3.5, does not allow setting event constraints as a function of control variables. For this reason, the continuity of the controls at phase interfaces cannot be guaranteed.

Lastly, selected *mission boundary conditions* are imposed on the aircraft states and controls. These concern the initial condition of the first phase and final condition of the last phase. For commercial aviation missions, like all of those presented in this chapter, a mission boundary condition is imposed to ensure that the overall distance flown at the end of the mission equals the specified mission range. Another mission boundary condition ensures that the aircraft arrives at its destination at its zero-fuel weight, while the initial take-off mass of the aircraft is determined accordingly by the solver, and limited by an imposed upper bound on the m_{mto} value. In this way, the aircraft is driven to burn all and only the necessary fuel for the mission profile of interest, in an attempt to simulate the most efficient mission planning possible. On the other hand, this approach is not well suited to take into account missions with multiple legs and stop-overs, and regulatory contingency fuel requirements are disregarded for simplicity.

4.2.3. MISSION PHASE STEREOTYPES

In order to easily create a consistent, well-posed mission profile model for optimal control problem formulations, typical flight operations and piloting schedules have been formalized in so called *phase stereotypes*. These are specific mission segments definitions and implementations, based on only few top-level parameters, which collect and couple all relevant sets of constraints and capture conditions relative to each phase. Their formulation is synthetically presented in Table 4.1.

On the highest level, a nominal commercial aviation mission can be divided into a take off, climb, cruise, approach, and landing phase [129]. A critical mission profile may also include a holding (or loitering) phase, and a diversion phase to another airport [131]. On a more-detailed level, each of those phases can be in turn broken down into more specific, shorter flight segments.

In the proposed implementation, climb and descent are substantially mirrored phases, the latter terminating at a specified Final Approach Point (FAP). Cruise stereotypes can be used to assemble a variable number of level flight segments connected by step climb segments. Their length and duration are flexibly determined on the basis of the other mission phases, in order to match the prescribed total mission range. Similarly, the airspeed and/or Mach number are also left free to be determined by the optimizer, although being limited by the M_{mo} value. The possibility to employ continuous cruise-climb schedules has not been employed since this flight strategy is not allowed by conventional air traffic management rules.

Table 4.1 Summary of mission phase stereotypes formulations.

Phase	Segment	Flight Objectives	Capture Condition	Path constraints	Event constraints
Take-off [132]	Level ground roll	$q = 0$	V_{rot}	—	—
		$(\gamma, \chi, \mu) = (\gamma, \chi, \mu)_{\text{runway}}$			
	Pitched ground roll	$(\gamma, \chi, \mu) = (\gamma, \chi, \mu)_{\text{runway}}$	$L = mg$	—	—
	Initial climb out	$\chi = \psi_{\text{runway}}$	h_{screen}	—	—
Climb [128, 133–135]	CAS-limited	—	$h = 3048\,\text{m}$	$\text{CAS} < 129\,\text{m/s}$	—
	Level acceleration	$\gamma = 0$	CAS	—	—
	Acceleration	$\dot{\text{CAS}} = 0$	M	—	—
	Deceleration	$\dot{M} = 0$	h_{cr}	$M < M_{\text{mo}}$	—
Cruise [132, 136, 137]	Level flight	$\gamma = 0$	—	$M < M_{\text{mo}}$	—
	Step climb	—	—	$M < M_{\text{mo}}$	—
				$\dot{h}_{\text{avg}} > 500\,\text{ft/min}$	
				$\dot{h}_{\text{avg}} < 1500\,\text{ft/min}$	
Descent [128, 133–135]	Acceleration	$\dot{M} = 0$	CAS	$M < M_{\text{mo}}$	—
	Deceleration	$\dot{\text{CAS}} = 0$	$h = 3048\,\text{m}$	—	—
	Level deceleration	$\gamma = 0$	$\text{CAS} = 129\,\text{m/s}$	—	—
	CAS-limited	—	h_{FAP}	$\text{CAS} < 129\,\text{m/s}$	—
Landing [138]	Approach	$\dot{\gamma} = 0$	h_{flare}	—	—
		$\chi = \psi_{\text{runway}}$			
	Flare/round out	$\chi = \psi_{\text{runway}}$	h_{runway}	—	$\gamma = \gamma_{\text{runway}}$
					$\mu = \mu_{\text{runway}}$

4.2.4. MISSION COST INDEX

The mission cost functional is set to minimize a linear combination of the total flight time and fuel consumption, both good indicators of an aircraft's Direct Operating Costs (DOC) [118]. By defining a Cost Index (CI) as in Equation 4.6, and prescribing its value for a given mission, the monetary impact of fuel usage can be traded off against the one of turnaround time [129].

$$\mathrm{CI} = \frac{\mathrm{Timecost[\$/s]}}{\mathrm{Fuelcost[\$/kg]}} \tag{4.6}$$

The overall mission cost can then simply be determined as in Equation 4.7, where assigning a value of the CI corresponds to prescribing an operative strategy to fly the given aircraft model.

$$\mathcal{J} = \left(m_{\mathrm{ini}}^{1} - m_{\mathrm{fin}}^{N_\mathrm{p}}\right) + \mathrm{CI}\left(t_{\mathrm{fin}}^{N_\mathrm{p}} - t_{\mathrm{ini}}^{1}\right) \tag{4.7}$$

A null CI, for which there is no cost associated to having a high mission duration, drives the trajectory to its minimum-fuel solution. Contrarily, the trajectory tends to its minimum-time solution as the CI tends to infinity, since the cost of mission time is deemed way higher than the one of burning fuel. Finally, in case the CI is prescribed a finite non-zero value, the resulting trajectory will minimize both fuel usage and mission time, with the assigned relative importance and in relation to the units of measurement used to express Equation 4.6. For example, if CI = 1 kg/s the cost for burning 1 kg of fuel is assumed to be the same of the one for spending 1 s more in flight.

In the remainder of the chapter, the first (CI = 0 kg/s) and last (CI = 1 kg/s) scenarios are going to be analyzed. For brevity, they are going to be referred to as the *efficient* and *balanced* trajectories, respectively.

4.3. SIMPLIFIED FLIGHT MECHANICS MODEL

As mentioned in Chapter 3, the PrP version implemented in the current work has been designed for a range of 4000 km, with the same wingspan of an Airbus A320, and approximately double its passenger capacity. Because of its vast popularity over similar range segments, an aircraft resembling the A320, the common research CeRAS Short Range (CSR) model, has been identified within the PARSIFAL project as a possible competitor of the PrP [139]. Such aircraft model has been developed as part of the CeRAS project[1,2] [140], and its most relevant top-level design parameters are compared to those of the PrP in Table 4.2.

For both aircraft in this specific study, the flight mechanics model presented in Chapter 3 has required some simplifications and modifications. These are mostly owed to the necessity of containing the computational effort demanded by the optimal control solver. For this reason, the generic multi-body model presented in the previous chapter is temporarily sacrificed in favor of a more pragmatic point-mass model. The following sections briefly outline the major characteristics of the modified flight mechanics model, and present relevant aspects of the aero-propulsive model of both aircraft in more detail.

[1] Central Reference Aircraft data System (CeRAS)
[2] `https://ceras.ilr.rwth-aachen.de`

Table 4.2 Top-level design parameters of the PrP and CSR aircraft.

Parameter	Unit	PrP	CSR
m_{mto}	kg	125 000	79 000
m_{zf}	kg	98 000	62 000
m_{oe}	kg	69 000	42 000
S	m^2	266.7	122.4
b	m	36	34.1
M_{cr}	–	0.79	0.79
h_{cr}	km	11	11
N_{pax}	–	308	150

4.3.1. POINT-MASS EQUATIONS OF MOTION

The aircraft attitude and instantaneous trajectory are obtained in the wind reference frame, previously depicted in Figure 3.10, and indicated by the "w" superscripts. The adopted equations of motion are reported in Equation 4.8, where the "ae" subscript indicates aerodynamic force contributions, and the "gd" subscript indicates ground reactions. They identify the aircraft as a point-mass with 6 DoFs and variable weight. Rotations about the wind axes are obtained in terms of the body angular rates p, q, r, which are treated as top-level control variables for the aircraft dynamic system. This approach is proven to be more accurate and less computationally demanding than an approach based on the body Euler angles [141]. The latter can be easily calculated from the body rotational rates using the classic kinematic auxiliary equations [142]. Further details behind the choice of state and control variables, and their impact on computational efficiency, are given in Section 4.3.4.

$$\dot{\boldsymbol{\sigma}} = \begin{Bmatrix} \dot{x}^{\text{e}} \\ \dot{y}^{\text{e}} \\ \dot{h} \\ \dot{\psi} \\ \dot{V} \\ \dot{\gamma} \\ \dot{\mu} \\ \dot{\alpha} \\ \dot{\beta} \\ \dot{m} \end{Bmatrix} = \begin{Bmatrix} V\cos\gamma\sin\chi \\ V\cos\gamma\cos\chi \\ V\sin\gamma \\ \frac{1}{mV\cos\gamma}\left[T\cos\alpha\sin\beta + \left(Z^{\text{w}}_{\text{gd}} + L\right)\sin\mu + \left(Y^{\text{w}}_{\text{ae}} + Y^{\text{w}}_{\text{gd}}\right)\cos\mu\right] \\ \frac{1}{m}\left[T\cos\alpha\cos\beta - \left(D + X^{\text{w}}_{\text{gd}}\right)\right] - g\sin\gamma \\ \frac{1}{mV}\left[T\sin\alpha + \left(Z^{\text{w}}_{\text{gd}} + L\right)\cos\mu - \left(Y^{\text{w}}_{\text{ae}} + Y^{\text{w}}_{\text{gd}}\right)\sin\mu - mg\cos\gamma\right] \\ p\cos\alpha\cos\beta + q\sin\beta + r\sin\alpha\cos\beta \\ \frac{1}{\cos\beta}\left(q\cos\alpha - p\sin\beta - \dot{\gamma}\right) \\ \dot{\chi} + p\sin\alpha - r\cos\alpha \\ -T\cdot TSFC \end{Bmatrix} \tag{4.8}$$

These equations are simplified even more for every particular mission phase. For example, coordinated flight is obtained by setting $\beta = 0$, level flight is enforced by setting $\gamma = 0$, and two-dimensional flight in a vertical plane can be obtained by imposing

$\dot{\psi} = \beta = 0$. In a similar way, the ground reaction forces are calculated for the on-ground flight phases by solving for vertical and transverse equilibrium ($\dot{\gamma} = \dot{\psi} = 0$) while they are automatically set to zero in airborne phases.

4.3.2. SIMPLIFIED AERODYNAMIC MODEL

The baseline aerodynamic dataset has been generated for both the PrP and the CSR using the same workflow outlined in Chapter 3. In the present study, α ranges from -6 deg to 6 deg, β ranges from -3 deg to 3 deg, both in steps of 3 deg, and Mach numbers between $M = 0$ and $M = 0.8$ have been analyzed. For the latter, five data points were used to model the PrP, whereas four for the CSR.

The lift and drag polars of the clean PrP and CSR configurations, corresponding to the first term in the aerodynamic model of Equation 3.1, are shown in Figure 4.1. While the PrP exhibits a clear increase in drag at high angles of attack and/or Mach numbers, the CSR seems to be able to contain its drag divergence, at least within the range of angles of attack and Mach numbers analyzed. Despite VSAERO results were expected not to be reliable for the high-transonic regime, data points for $M = 0.8$ are necessary to allow interpolations of the aerodynamic dataset at least up to the design cruise Mach number, equal to $M = 0.79$ for both aircraft. Anticipating the requirements for the optimal control problem solver, presented in Section 4.3.5, all the tabular data output from VSAERO has been interpolated using a twice continuously differentiable spline function.

In light of the simplified flight mechanics model used, it has not been necessary to evaluate the aerodynamic contribution due to control surfaces. To simulate the deployment of high-lift devices, a constant lift and drag coefficient increase has been added to the aerodynamic dataset during the take-off and landing mission phases. The lift coefficient increase at a given angle of attack is assumed to be $\Delta C_L^{\text{flap}} = 0.6$, on the basis of a conservative representation of the $C_{L_{\max}}$ values reported in [143]. The same value is taken for the PrP and the CSR. For the former, preliminary VSAERO lift coefficient data due to flaps indicate that this value is feasible. For the latter, existing references indicate that this value is reasonable and even somewhat conservative [144]. In a similar fashion, the drag increase due to high-lift devices is taken as $\Delta C_{D_0}^{\text{flap}} = 0.055$, for both the PrP and CSR [144].

4.3.3. PROPULSIVE MODEL

The propulsive model for both aircraft has been created by exploiting the same workflow outlined in Section 3.2.3. No modifications have been made for the specific application. While the PrP has been designed with a tailor-made propulsive system, the CSR has been equipped with a modern CFM LEAP-1 engine model [145]. The available thrust maps and the *TSFC* maps at maximum throttle are shown for both aircraft in Figures 4.2 and 4.3. The maximum thrust available for the PrP is about double the one available for the CSR, in light of the similar difference in weight between the two aircraft. Both engine models feature a *BPR* equal to 11, with comparable *TSFC* maps. In particular, the design point *TSFC* of the CSR is 4.8% higher than its counterpart for the PrP.

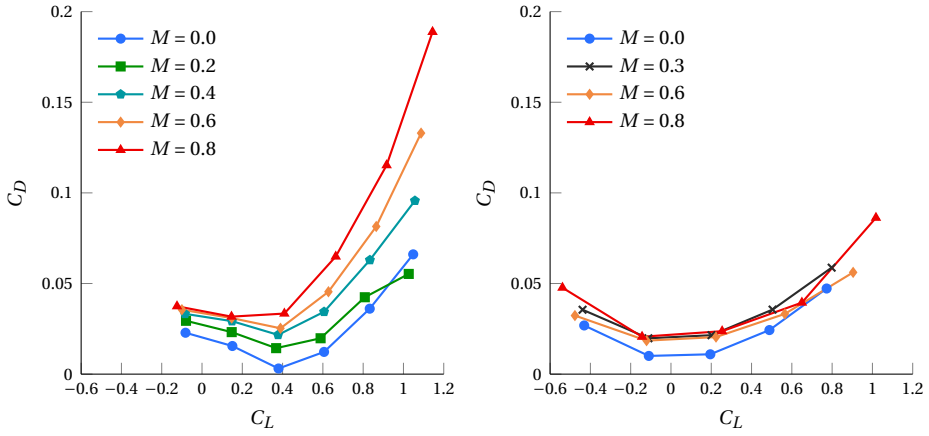

a) PrandtlPlane (PrP) **b)** CeRAS Short Range (CSR)

Figure 4.1 Lift-drag polar of the PrP and CSR for different values of the Mach number.

4.3.4. CONTROL VARIABLES

The selection of states and controls that has been chosen for this work is synthesized in Table 4.3. The body rotational rates p, q, r are used to control the aircraft attitude at all times. Preferring these over the attitude angles allows to prevent the insurgence of instantaneous discontinuities in the aircraft attitude time histories. This is easily done by setting appropriate bounds on p, q, r themselves. Additionally, this choice is advantageous as the body rates have an explicit impact on the aerodynamic model described in Section 3.2.2, and hence eliminate the need for computationally costly matrix transformations.

On the other hand, bang-bang control can occur in light of the linear dependence of aerodynamic forces on the body rotational rates, presented in Equation 3.1. This control strategy is typically not representative of aircraft mission performance simulations, as it can give rise to unrealistic oscillations in the time history of several flight parameters. In an attempt to discourage the excessive use of bang-bang control, the penalization term shown in Equation 4.9 is added to the objective functional of Equation 4.7.

$$\mathcal{J}_{\boldsymbol{u}} = C_{\boldsymbol{u}} \int_{t_{\text{ini}}}^{t_{\text{fin}}} \left(p^2 + q^2 + r^2\right) \mathrm{d}t \tag{4.9}$$

The constant $C_{\boldsymbol{u}}$ is a measure of the severity of the control penalization. Generally, setting a very small value for $C_{\boldsymbol{u}}$ suffices, for it makes the equations of motion non-linear in the controls. As a result, the impact of such term on $\mathcal{J}^*$ is negligible [146].

Table 4.3 Selected grouping of flight parameters into state and control variables.

State variables $\boldsymbol{\sigma}$	Control variables $\boldsymbol{u}$
h, m, V, x^{e}, y^{e}, μ, γ, χ, α, β	δ_T, p, q, r

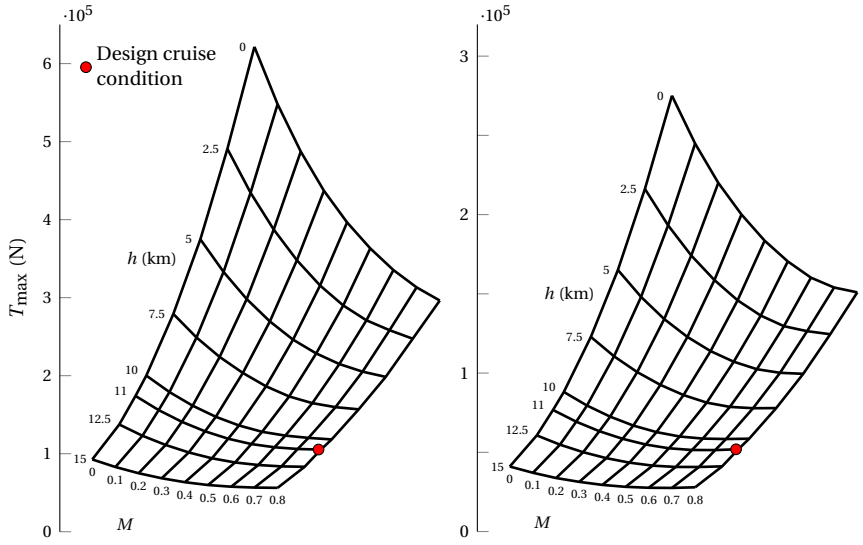

a) PrandtlPlane (PrP) **b)** CeRAS Short Range (CSR)

Figure 4.2 Maximum available thrust carpet plots for the PrP and CSR.

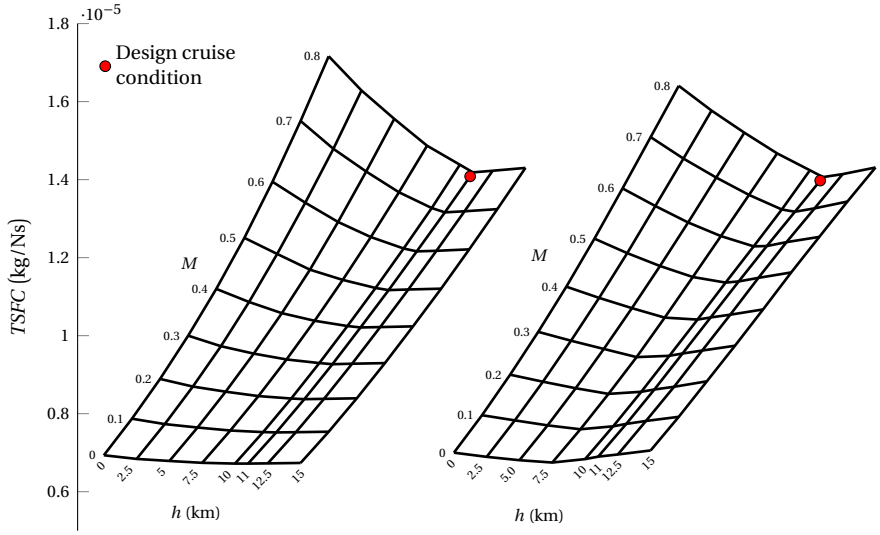

a) PrandtlPlane (PrP) **b)** CeRAS Short Range (CSR)

Figure 4.3 Thrust specific fuel consumption carpet plots at max thrust for the PrP and CSR.

Lastly, the engine throttle setting δ_T is assumed the same for all engines, hence allowing no differential thrust. Throttle usage is not penalized in the present applications. The default bound constraints used for the applications presented in this chapter are reported in Table 4.4.

Table 4.4 Default bound constraints imposed on state and control variables.

Variable	Unit	Lower bound	Upper bound
h	km	0	14
V	m/s	0	330
m	kg	m_{zf}	m_{mto}
α	deg	-6	+9
β	deg	-3	+3
γ	deg	-25	+25
μ	deg	-30	+30
δ_T	–	0	1
p, q, r	deg/s	-5	+5

4.3.5. OPTIMAL CONTROL SOLVER

For this specific application, PHALANX serves the purpose of a frame environment, which contains the execution flow of the optimal control transcription solver and the non-linear programming optimizer.

To solve the trajectory optimization problem outlined so far, the commercial optimal control transcription software GPOPS-II[3,4] has been used. This software employs a Legendre-Gauss-Radau (LGR) direct pseudo-spectral (orthogonal) collocation method and serves as an optimal control transcription program with built-in mesh refinement and error quantification [147]. At the lowest level, the open-source IPOPT[5,6] is used as non-linear programming optimization program [148].

A schematic overview of the execution flow of the simulation framework is shown in Figure 4.4, in the form of a Unified Modelling Language (UML) activity diagram. The figure also shows which parts of the program are owned by which software application, keeping in mind that the whole execution flow is contained in the PHALANX environment.

4.4. SIMULATIONS AND RESULTS

In the following sections, the mission performance of the PrP and its competitor aircraft are compared and discussed on the basis of several case studies, all complying with current air traffic management practices. All application studies are completely

[3] General Purpose Optimal Control Software (GPOPS-II)
[4] `https://www.gpops2.com/`
[5] Interior Point Optimizer (IPOPT)
[6] `https://github.com/coin-or/Ipopt`

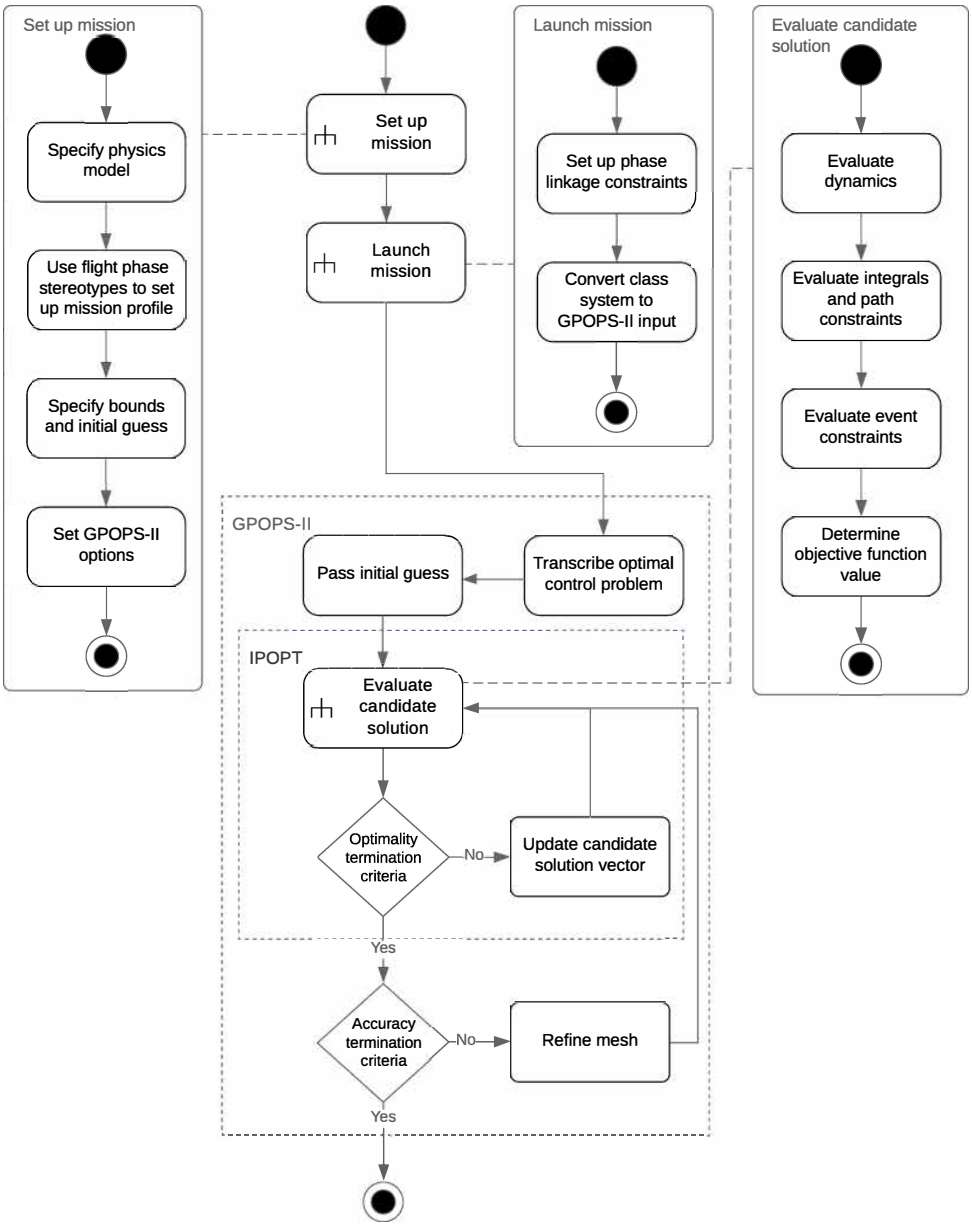

Figure 4.4 UML activity diagram of the trajectory optimization program in PHALANX.

characterized by 2D flight, for which the equations of motion are obtained by setting $y^e = \mu = \beta = p = r = 0$, and $\chi = 90\,\text{deg}$, in order to make the aircraft fly in the x^e direction.

In every case, both aircraft fly the same mission profile, schematically summarized in Table 4.1, in chronological order from top to bottom. In particular, the following values are assigned: $V_{\text{rot}} = 50\,\text{m/s}$, $h_{\text{screen}} = 50\,\text{m}$, $h_{\text{cr}} = 11\,\text{km}$, $h_{FAP} = 610\,\text{m}$, $h_{\text{flare}} = 15\,\text{m}$, $h_{\text{runway}} = 0\,\text{m}$. During ground roll phases, the rolling friction coefficient is assumed to be constant and equal to 0.02 [149]. Despite these parameters are all necessary to simulate the required missions, the phases for take-off, landing, first climb out, and terminal descent represent an extremely small part of the entire mission profile. For this reason, the assigned numerical values bear a small impact on the resulting optimal mission profile and the related top-level performance metrics of both aircraft.

The following section presents the design mission optimal trajectories of both the PrP and the CSR aircraft for two CIs: a fuel *efficient* flight strategy (CI = 0 kg/s), and a *balanced* flight strategy (CI = 1 kg/s). Section 4.4.1 focuses on the fuel consumption and mission duration over a specified (design) range. Section 4.4.2 deals with off-design performance, namely with finding the the maximum range at maximum payload and fuel capacity (harmonic range) for both aircraft. Lastly, a top-level overview of the most relevant performance metrics is given in Section 4.4.3.

4.4.1. DESIGN RANGE PERFORMANCE

The design range requirement is fulfilled by imposing that the distance travelled at the final time instant is $x^e(t_{\text{fin}}) = 4000\,\text{km}$. The corresponding efficient and balanced trajectories are displayed in Figure 4.5, for both the PrP and CSR, in the case of an imposed altitude of 11 km. This value was indicated as a top-level aircraft requirement within the PARSIFAL project, as reported in Table 4.2.

For the fuel efficient trajectory (CI = 0 kg/s), the CSR immediately reaches and maintains the prescribed initial cruise altitude, whereas the PrP seems to postpone it by adopting a very small rate of climb in the last segment of the climb phase. This indicates that the fuel-optimal cruise altitude of the PrP is actually lower than the imposed 11 km, which was indicated as a top-level aircraft requirement within the PARSIFAL project. As shown in Figure 4.7, the efficient trajectory of the PrP is flown at a significantly lower Mach number than the one chosen by the CSR. This is because the C_L for minimum drag of the PrP is much higher than the one of the CSR, as it can be appreciated in Figure 4.1. Since the difference in wing loading is not so drastic, this makes the PrP fly at higher angles of attack and, therefore, lower speeds than its competitor.

For the balanced trajectory (CI = 1 kg/s), the PrP makes use of one step climb, whereas the CSR maintains its initial altitude throughout the whole cruise phase. The reason for this different behavior can be sought in the relative importance given to fuel consumption in the case of the two aircraft models. While the mission duration is comparable for both aircraft, the PrP burns approximately double the amount of fuel of the CSR, as illustrated in Figure 4.6. Since the cost of burning fuel is the same, but the amount of fuel available is very different, a unit CI emphasizes fuel over time performance in a different manner for each aircraft. The PrP is driven to a slightly more fuel-efficient trajectory, whereas the CSR tends towards a faster mission. Hence, the PrP climbs during cruise for fuel economy, whilst the CSR seeks greater temporal gain.

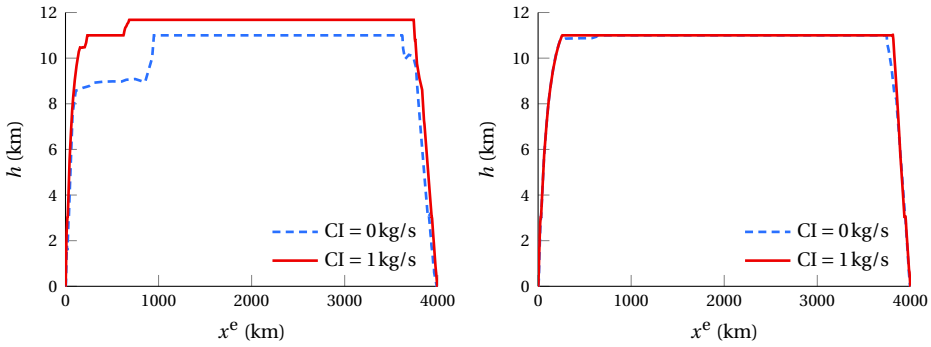

a) PrandtlPlane (PrP) **b)** CeRAS Short Range (CSR)

Figure 4.5 Design mission profile for the PrP and CSR, for different CIs.

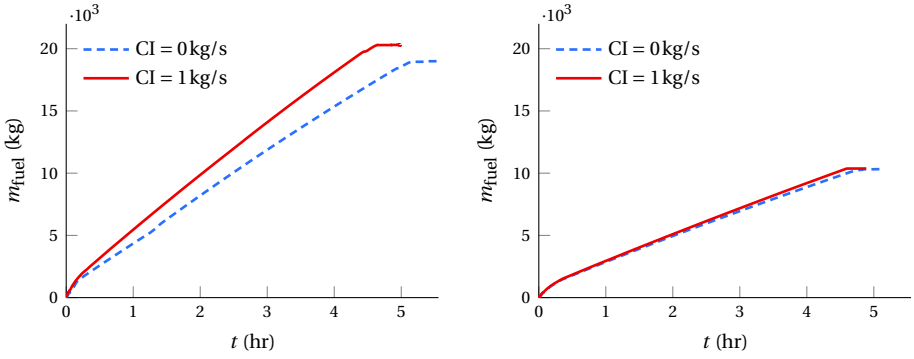

a) PrandtlPlane (PrP) **b)** CeRAS Short Range (CSR)

Figure 4.6 Design mission fuel consumption for the PrP and CSR, for different CIs.

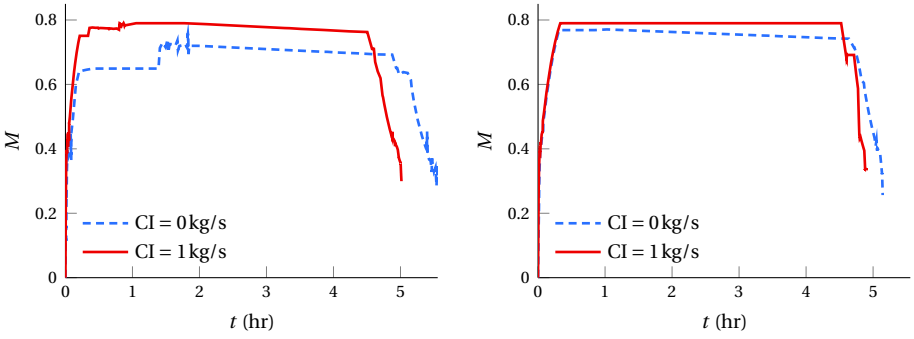

a) PrandtlPlane (PrP) **b)** CeRAS Short Range (CSR)

Figure 4.7 Design mission Mach number for the PrP and CSR, for different CIs.

Additional simulations have been performed with an initial cruise altitude which is left free to be determined by the optimizer. For the fuel efficient mission, Figure 4.8a confirms the aforementioned hypothesis according to which the design altitude of 11 km is not optimal in absolute terms. Instead, the trajectory optimization indicates that an altitude of approximately 9.3 km is more appropriate, as it results in a 2.2% fuel savings with respect to the efficient mission with the imposed cruise altitude. On the other hand, the aircraft flies even more slowly ($M \approx 0.63$) than in the previous case, as shown in Figure 4.8b. This results in an increase of the mission duration of approximately 7%.

For the balanced mission profile, the optimizer converges to a cruise altitude of just 10 m below the design cruise altitude of 11 km. This indicates that in the case both time and fuel considerations are of similar importance to the optimizer, the design cruise altitude can be deemed appropriate. In spite of the seemingly minor trajectory differences, the effects on the fuel performance of the aircraft are notable: flying level cruise at an altitude of 10 990 m gives the aircraft an approximate fuel gain of 1.7% over the design mission for CI = 1 kg/s. The overall objective function value for this optimal mission is however nearly equal, since the fuel gain is offset by the nearly 2.7% increased mission time.

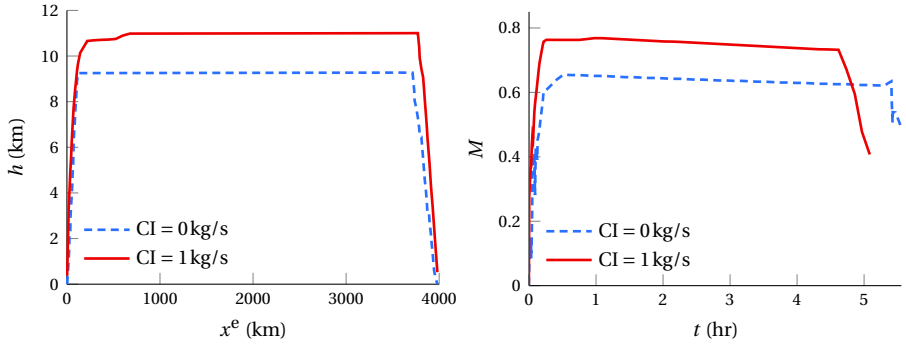

a) Altitude **b)** Mach number

Figure 4.8 Optimal trajectory and speed profile over a mission with imposed design range and free cruise altitude, for the PrP, for different CIs.

4.4.2. HARMONIC RANGE PERFORMANCE

For the harmonic mission profile — the mission for maximum range at maximum payload — no boundary condition is imposed on the final position $x^e(t_{fin})$. Instead, the objective function is defined as $\mathcal{J} = -x^e(t_{fin})$ to maximize the range. In this analysis, therefore, no distinction is made between the efficient or balanced flight schedules.

The 2D trajectories of the PrP and CSR are shown in Figure 4.9a, in which the range advantage of the CSR is clearly recognizable. Unsurprisingly, the trends in the altitude profiles show striking resemblance to those in the design mission trajectories for minimum fuel. After all, both maximum-range and minimum-fuel missions seek to maximize the specific air range. The same resemblance holds for the time histories of the Mach number, shown in Figure 4.9b. Whilst the CSR flies at or near its design cruise Mach

number for fuel-economic travel, the PrP flies notably slower. Both aircraft make full use of their fuel capacity at maximum payload, as shown in Figures 4.9c and 4.9d.

A summary of the performance metrics of the PrP and CSR corresponding to the harmonic range mission is shown in Table 4.5.

Table 4.5 Harmonic range performance of the PrP with respect to the CSR.

Aircraft	Range (km)	Fuel (kg)	Fuel/pax/km (kg/km)	Duration (h:mm:ss)
PrP	5417.2	27000	0.0146	7:27:42
CSR	6218.6	16500	0.0162	7:39:48
Δ	-12.9 %	+63.6 %	-8.5 %	-2.6 %

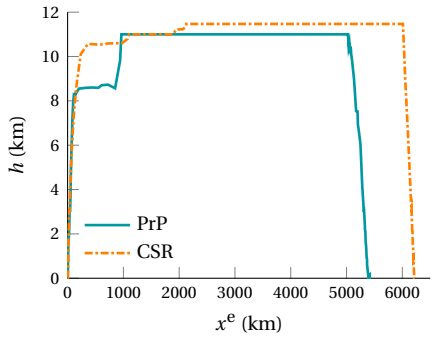

a) Mission profile

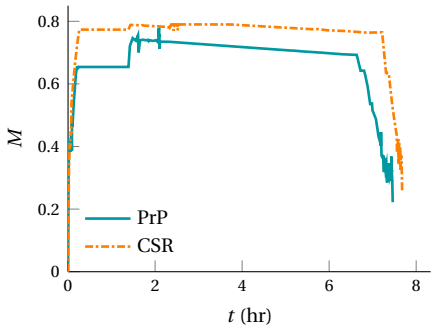

b) Mach number time history

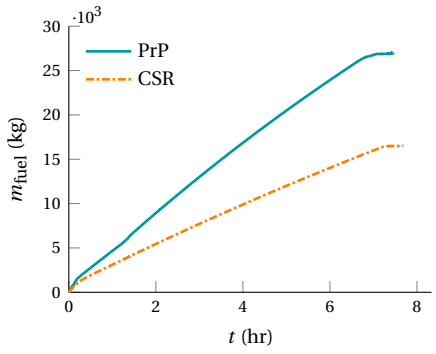

c) Fuel consumption time history

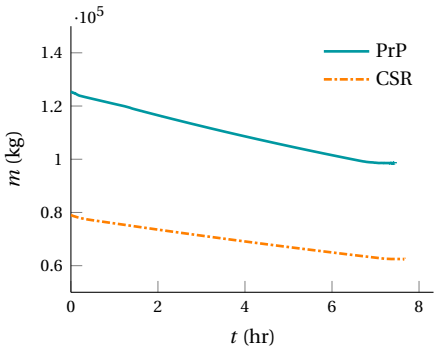

d) Aircraft mass time history

Figure 4.9 Harmonic mission performance of the PrP and CSR.

4.4.3. TOP-LEVEL MISSION PERFORMANCE SUMMARY

The top-level performance metrics of an additional 2000 km mission simulation, the details of which are not reported to promote brevity, are aggregated to those presented in

the previous sections and summarized here.

The time and fuel performance of both aircraft is shown in Figures 4.10a and 4.10b. Earlier findings according to which the PrP tends to fly slower than its competitor are confirmed. The CSR has an approximately 10 % higher average velocity on the minimum fuel missions. Although the fuel consumption of the PrP is obviously higher in absolute terms, it must be remembered that it also carries over twice as many passengers as the CSR. As shown in Figures 4.10c and 4.10d, the PrP outperforms the CSR in terms of fuel consumption per number of passengers. At a fuel consumption of approximately 15 g/pax/km, the PrP is 14.5 % more efficient than its competitor on the short-range, minimum fuel mission, 10 % on the design range minimum fuel mission, and nearly 8.5 % on the maximum range mission.

In summary, the CSR is more versatile than the PrP due to its higher maximum range. On the other hand, the PrP does confirm the expected performance for which it was conceived and designed: more efficient flight in the short-range segment.

4.5. CONCLUSIONS

The aim of this chapter has been to assess the mission performance of a box-wing aircraft under the constraint of common air traffic management procedures and practices. A unified approach has been presented to model commercial aviation missions, from a realistic point of view, in the framework of multi-phase optimal control theory. The implemented analysis framework is completely aircraft configuration-agnostic, hence allowing the evaluation and comparison of mission performance for aircraft with very distinct geometries.

Several analyses have been carried out to compare the mission performance of the PrandtlPlane (PrP) to the one of a conventional aircraft with a similar design range: the CeRAS Short Range (CSR), which is intended to replicate an Airbus A320. Both aircraft under consideration have been modelled as a point mass with 6 DoFs and variable weight. Trim and rotational inertia have been neglected, as angular rates are treated as the top-level control input for the aircraft system, together with the engine throttle. With only slight adaptations to the problem setup, mission profiles have been analyzed for various ranges and two flight strategies. The analysis has shown that the PrP outperforms its competitor in terms of fuel consumption per number of passengers, when flying on a minimum fuel schedule. Nonetheless, this benefit comes at the price of a harmonic range of 5400 km, which is significantly lower than the one of the CSR, equal to 6200 km.

A question remains about whether the comparison between the PrP and the CSR is indeed fair, and useful to draw meaningful conclusions. Since the PrP has been conceived to tackle a design range of 4000 km while accommodating about 300 passengers, it occupies a completely empty region of the payload-range diagram. For this reason, a perfectly matching competitor does not really exist at this moment in time. The choice of a A320-like aircraft as potential competitors of the PrP can be justified by similar design ranges and wing span limits. These shared characteristics result in the possibility to exploit already existing airport infrastructure, and grant the PrP the potential to be adopted in already existing markets. Larger aircraft models, such as the Airbus A330 or A350, have similar passenger capacity to the one of the PrP, but miss on the other aforementioned top-level design requirements. As observed in early preliminary studies per-

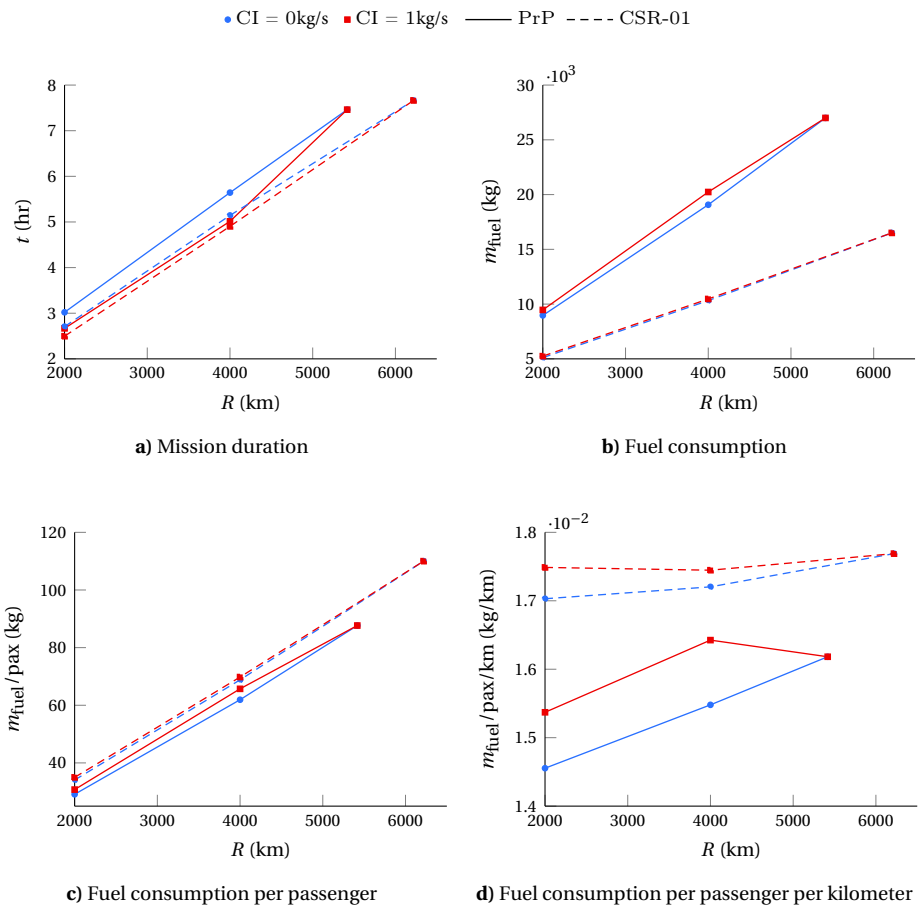

a) Mission duration

b) Fuel consumption

c) Fuel consumption per passenger

d) Fuel consumption per passenger per kilometer

Figure 4.10 Top-level mission performance metrics of the PrP and CSR, as a function of CI and range.

formed within the PARSIFAL project, the latter discrepancies would jeopardize the comparison with the PrP even more. In particular, a comparison based on fuel consumption — either in absolute terms, or normalized to the number of passengers and/or kilometers — would be made especially unfair by operating a long-range aircraft on a short-haul mission, thereby in severely off-design conditions [150].

Further research can be devoted to studying the performance of advanced box-wing configurations featuring innovative propulsive system technologies, such as electric or hydrogen, and/or distributed architectures. Also, in order to gain an operative advantage out of its control surface redundancy, it would be interesting to explore whether the employment of DLC could be beneficial towards the adoption of unconventional flight strategies, such as continuous descents procedures for approach and landing. Lastly, it could be helpful to quantify the impact of employing DLC not only as a means for fast attitude control, but also as an additional device to optimize trim drag in cruise phases.

Later on in this dissertation, Chapter 6 constitutes a first attempt in these regards, as it looks at trim conditions for minimum aerodynamic drag. Before that, the next chapter is devoted to designing a meaningful control surface layout for the box-wing architecture, which can be then exploited to perform more complex flight mechanics simulations.

5

CONTROL SURFACE LAYOUTS

When you find a good move,
look out for a better one.

William Wayte
The Chess Player's Chronicle
1878

To have breakthroughs,
you must have confidence in nonsense, okay?

Elbert L. "Burt" Rutan
Inside the New Space Race
2017

After having assessed the mission performance of the PrP as a point mass, and before being able to perform any type of flight control task, it is first necessary to have the aircraft model equipped with a set of control effectors. For conventional aircraft configurations, the specific roles of elevators, ailerons or rudders can be explicitly assigned to each Control Surface (CS). This allows to conceptually separate the available control power on each motion axis, and makes it easier to conceive an iterative procedure to position and size Control Surfaces (CSs). As already mentioned in Section 2.1, such decision cannot be taken for granted in the case of box-wings, and the CS design problem is therefore not trivial.

This chapter presents a completely physics-based and aircraft configuration-agnostic methodology to optimize an initial CS layout, in order to obtain desired Flying Qualities (FQs) according to a selection of classic, well-established criteria. It is applied to the PrP aircraft configuration, but is suitable to any conventional aircraft geometry as well. Making use of the AAS concept, the methodology proposes a way to quantify the impact of

different CA methods on top-level CS layout parameters, such as cumulative CS span width. Additionally, it explores novel CS layouts for the box-wing geometry, evaluating the performance and design benefits of a mid-wing CS on the rear wing.

The following Section 5.1 presents an overview of the CS design problem for box-wing aircraft, and briefly contrasts it to the one of conventional aircraft geometries with ganged CSs. Section 5.2 describes the optimization framework developed to perform the CS sizing iteration. In particular, Section 5.2.3 presents the FQs requirements enforced to make sure that the CS layout complies with common performance standards. The overall design optimization problem is then formulated in Section 5.2.4. The first application study, in Section 5.3.1, presents the comparison of different CA methods, and a quantification of their impact on the final CS layout. The second investigation regarding improved CS layouts is reported in Section 5.3.2. Lastly, conclusions are provided in Section 5.4.

5.1. INTRODUCTION

It has already been mentioned in Chapter 1 that the double-wing system of box-wing aircraft allows additional space and design freedom for the positioning and sizing of CSs [23, 42]. Section 1.2 has highlighted the opportunities linked to the fact that a staggered box-wing, such as the one of the PrP, can accommodate more CSs than strictly required for controllability, both in front and behind the aircraft center of gravity. Such arrangement of redundant CSs can be desired to increase safety in case of failure, distribute the aerodynamic load between the two wings, minimize trim drag, or allow innovative techniques in maneuvering flight, such as DLC [151].

While many research studies have been dedicated to the preliminary design of the box-wing aircraft configuration and to the optimization of its aerodynamic behavior, the newly available design space for CS positioning and sizing has rarely been explored [42, 152–154]. An interesting recent effort has investigated the effects of placing the elevator on only one or both front and aft wings [152]. Conclusions highlight that having CSs on both wings yields the lowest trim drag, and substantiate the idea that it is advantageous to fully exploit the additional design space offered by two full-size wings. In all cases, including the latter, existing studies are limited to explicitly assigning a determined role to CSs, hence utilizing each of them as an elevator or an aileron, responding only to pitch and roll commands, respectively [42, 153, 154].

This is equivalent to establishing an arbitrary mechanical FCS architecture — which gangs CSs together and links them to the pilot input with pre-defined gearing ratios — and is analogous to the design approach commonly adopted for conventional aircraft configurations [155]. Some considerations in these regards have already been made in Section 2.1. But while the standard ganging approach may lead to non efficient control allocation in all possible flight scenarios, it can tend to simplify the design problem. As a matter of fact, since a specific role is assigned to each control surface a priori, it is easier to understand what role it will have during a particular maneuver, and to anticipate the required control power that it must supply to achieve good FQs.

But with a set of redundant CSs that spread over the entire surface of the box-wing, the control function of each one of them does not need to be determined a priori. For example, an outboard surface on the rear wing can be used for roll control as well as for

pitch control, due to its significant longitudinal distance to the aircraft center of gravity. This flexibility should definitely be exploited to improve the control and handling qualities characteristics of the aircraft. Moreover, since an improved CS arrangements may also lead to other weight and performance benefits, it should be taken into account from the early stages of aircraft conceptual and preliminary design. A possible way to exploit the newly available design space, in conjunction with the CS redundancy of the box-wing configuration, is through the use of CA methods.

As explained in Chapter 2, CA methods exploit all available control effectors by utilizing them independently, on the basis of their control effectiveness. In the case of CSs, they find the best combination of CS deflections which results in the aerodynamic forces and moments required by the FCS, and optionally optimize other performance parameters, such as total control effort or control drag, for example. With the employment of CA methods, assigning a predetermined function to each CSs is not necessary anymore, as each effector can individually contribute to the aircraft control in the best way possible according to its own capabilities [41, 54].

The impact of different CA methods have already been compared, from the pure point of view of flight control, for over-actuated unconventional configurations such as tailless aircraft [55] and BWBs [61]. A classic CA method has been implemented in the preliminary design of the CS layout of a BWB aircraft [44]. In a very recent effort, a design optimization study is carried out to shape the AAS of a multi-rotor aircraft, with the aim to fully encircle the set of moments required by the aircraft to fulfill selected mission tasks [156, 157].

The objective of this chapter is to assess the impact of different CA methods on the optimal design parameters of a given set of CSs. While this is especially interesting for the box-wing geometry, which constitutes the main test case of the presented applications, the purpose of this investigation remains relevant also for other conventional and unconventional aircraft configurations. A first study focuses on the minimum total CS span required for the aircraft to achieve desired flight control performance. For this study, the position of the movable surfaces on the wings is assigned, and is based on past PrP design experiences. The performance of the following CA methods are compared:

- a conventional ganging strategy, as the benchmark case;
- the CWPI method, as the example of a simple optimization-based CA approach;
- the DA method, as the example of a high-performance, optimization-based CA approach.

Together with the resulting total CS span, the volume of the AAS is used as a criterion to evaluate and compare the selected CA methods. Using the most effective CA method from the latter application, a second study is performed to evaluate two novel CS layouts on the rear wing of the PrP. The new layouts feature a CS close to the central section of the wing, which can play the role of an elevon more effectively than the one close to the symmetry plane of the aircraft.

5.2. OPTIMIZATION FRAMEWORK

To assess and compare the impact of different CA methods on aircraft design parameters, a multi-disciplinary optimization framework has been developed. The objective is to achieve the smallest set of CSs on the main wings of the PrP, under the constraints of desired FQs requirements. In particular, for a fixed number of CSs with an assigned, constant chord ratio, the design optimization problem is aimed at minimizing the total span width dedicated to CSs. The requirement of small CSs span widths, together with a contained number of CSs themselves, may be desired to reduce system complexity, reduce weight and/or reserve more space for high-lift devices [42, 158].

The top-level layout of the framework is shown in Figure 5.1, in the form of an Extended Design Structure Matrix (XDSM) [159]. This is a standard diagram format to visualize multi-disciplinary analysis and optimization processes. The formal statement of the multi-disciplinary optimization problem is provided in Section 5.2.4, after a detailed overview of all of its components. In the aforementioned Figure 5.1, the design optimizer (in blue) acts as the driver and coordinator of all the evaluations that need to be carried out to converge to an optimal solution. The disciplinary analyses (in green) are executed sequentially, while the objective function and constraints (in red) are evaluated at the same time. The diagram also shows, in a qualitative way, how variables and parameters are exchanged among the different tools within the process. Several important components can be identified:

1. The optimizer evaluates the objective function, determines the feasibility and optimality of the current design point, and finds the candidate point for the following iteration.

2. The aerodynamic analysis module uses the CS layout at each iteration to create an aerodynamic database with static and dynamic force and moment coefficients.

3. The flight mechanics module simulates different flight scenarios and evaluates the corresponding FQs performance.

4. The objective function to be minimized is formulated as the sum of all CS span widths.

5. The design variables are defined as the CS span widths $\Delta\eta_i$ $(\forall\, i = 1, \ldots, N_\delta)$; chord ratios are assigned and held fixed, as well as the number of CSs.

Span widths are subject to a combination of geometric bounds and constraints which prevent CSs to overlap, exceed assigned maximum and minimum span width limits, and clash with other airframe elements, such as the vertical tails intersection with the rear wing or wing-podded engines, if present. In all cases, only one of the inboard and outboard stations of each CS is free to shrink or extend, whereas the other is held fixed, hence anchoring the CS to its position within the layout. This approach is necessary to prevent the whole CSs from moving towards the middle of the wing section, which is a space dedicated to high-lift devices. As in the case of conventional aircraft geometries, keeping outboard CSs close to the wing tip sections helps maximizing their roll moment contribution. Additionally, given the backward sweep of the front wing and the forward

sweep of the rear wing of the PrP, keeping the inboard ones close to the root wing section also helps maximizing their pitch moment contribution.

A more traditional flow-chart representation of the optimization framework is shown in Figure 5.2. Within the flight mechanics simulation, CS deflections are determined by the selected CA method. The results of the FQs evaluations are then passed to the optimizer as nonlinear inequality constraints. All of these aspects are going to be described in more detail in the following sections.

5.2.1. AERODYNAMIC ANALYSIS

As anticipated in Section 3.2.2, the AVL solver has been chosen to characterize the aerodynamic behavior of the box-wing for this particular optimization study. This has been an almost obligated choice, in light of the very large number of aerodynamic analyses required to characterize the aircraft model, and the inclusion of the aerodynamic analysis module in an outer design iteration loop.

To increase iteration efficiency and reduce computational time, a simple database feature is also implemented. The flowchart presenting its principle of operation is shown in Figure 5.3. This database stores the aerodynamic model of a CS on the basis of the wing it belongs to, its span wise location and its span width. In the course of the optimization, if the combination of these characteristics is already in the database, the corresponding aerodynamic analysis is not performed again in AVL, but the pre-computed results are retrieved directly for the specific CS. Unless the underlying aircraft geometry is altered, this database constantly grows when more and more aerodynamic analyses are performed, hence the aerodynamic computations require less time as the design optimization progresses.

On one hand, the AVL solver allows rapid evaluation of the data point with acceptable accuracy by approximating the wing planform using two-dimensional quadrilateral panels. On the other hand, the 2D assumption restricts the analysis to wing elements only, making it fundamentally impossible to include fuselage and nacelles effects in a reliable way. For this reason, the shape and influence of the fuselage has been neglected in the present study, and only the lifting surfaces are included in the flight mechanics model. While it is true that fuselage and nacelles have significant contributions to the aircraft trim and stability, especially in the case of very large bodies [40], the aim of the present study is to compare the outcome of different CA methods on top-level aircraft design parameters. Despite absolute numerical results are probably biased by the absence of the fuselage and nacelles, the comparison among CA methods is deemed fair since the underlying flight mechanics model is the same for all applications.

The box-wing geometry under investigation is based on an early layout of a PrP designed in the PARSIFAL project, and is represented in Figure 5.4. The continuous trailing edges on the front and rear wings are beneficial for this investigation, as they allow CSs to be placed at any span wise station, without requiring additional geometric constraints, such as kinks or engine gates.

5.2.2. FLIGHT CONTROL SYSTEM ARCHITECTURE

The baseline FCS architecture and propulsive model are used for the flight mechanics module of the overall design optimization problem. They are thoroughly described in

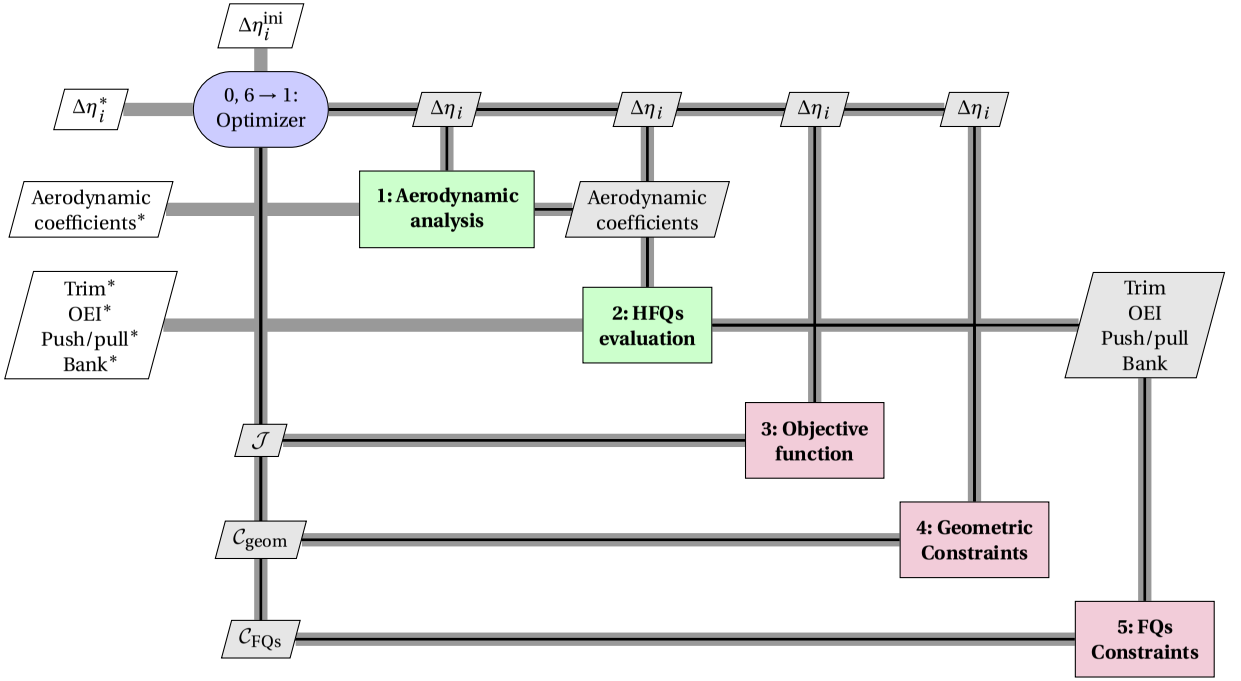

Figure 5.1 Extended Design Structure Matrix (XDSM) of the developed optimization framework. Each optimization problem in this form features a constant, assigned number of CSs.

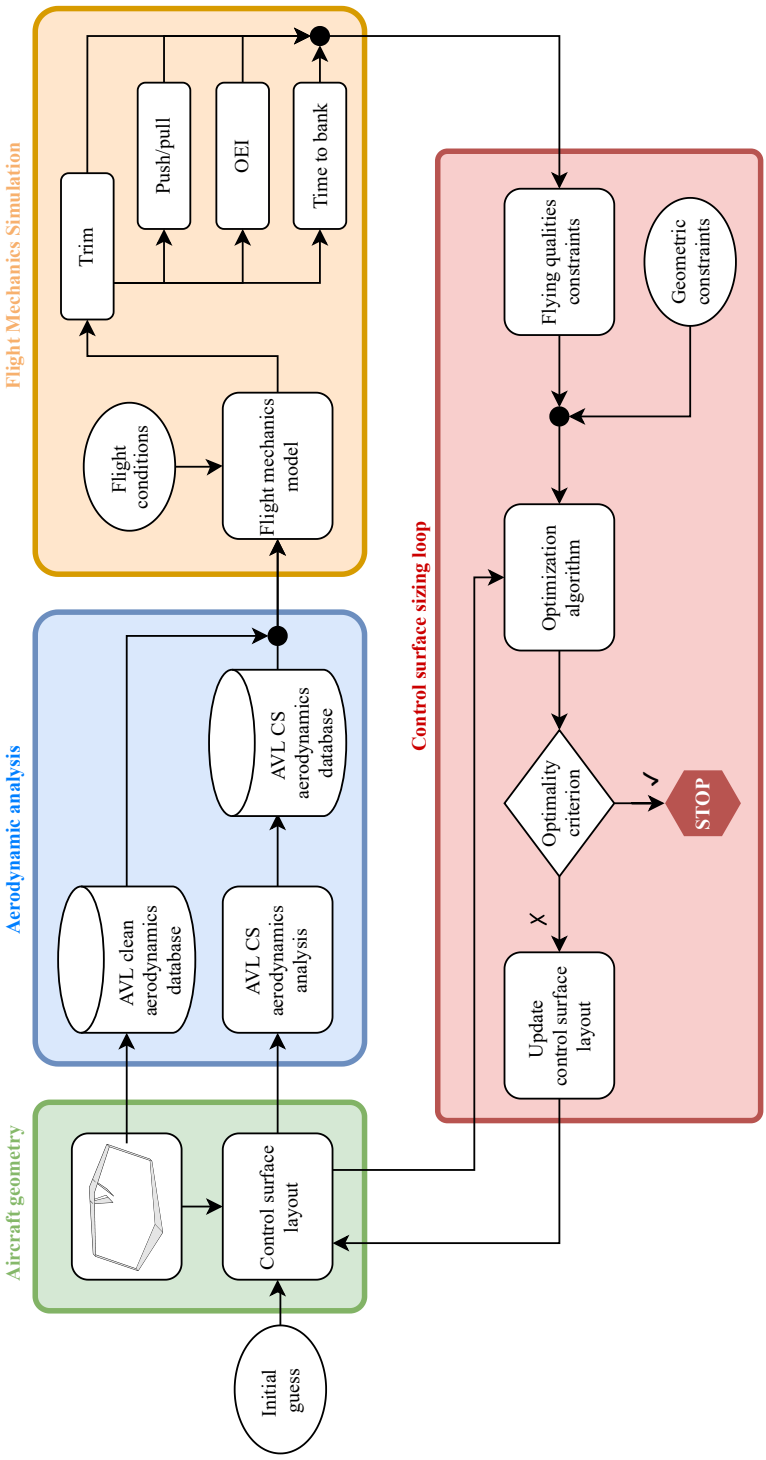

Figure 5.2 Flow chart of the developed optimization framework. Each optimization problem in this form features a constant, assigned number of CSs.

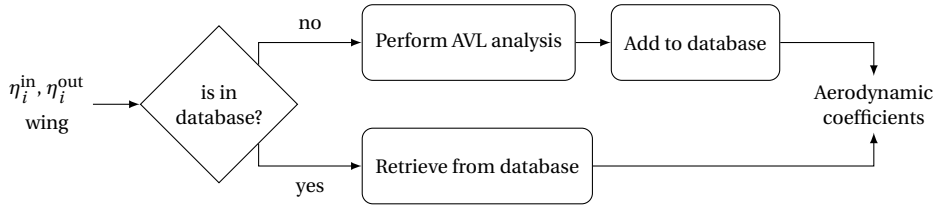

Figure 5.3 Flowchart showing the principle of operation of the aerodynamic database, conceived to speed up the aerodynamic analysis with AVL.

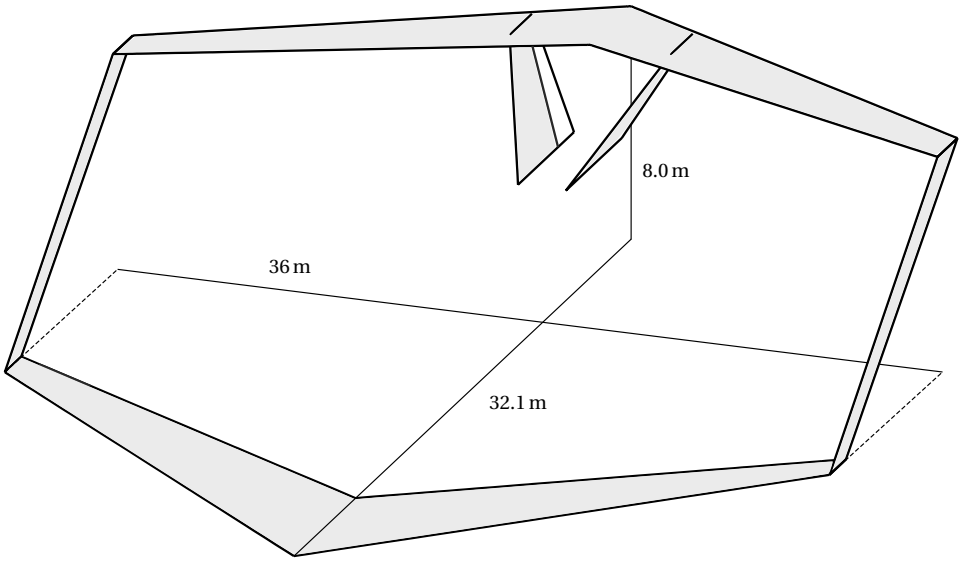

Figure 5.4 Box-wing geometry under investigation.

Section 3.3.1 and Section 3.2.3, respectively.

For all of the applications presented in this chapter, the PHALANX toolbox is used to perform open-loop flight simulations, taking pre-defined inputs in the form of pilot stick commands. No control law, or closed-loop logic has been implemented for this study. Every pilot command is given by deflecting the simulated pilot stick, pedals and throttle, and has the purpose of performing simple flight maneuvers to evaluate the inherent FQs performance of the unaugmented aircraft model.

In case the conventional ganging approach is used to distribute the pilot commands to the CS deflections, pilot inputs on the stick are simply scaled, mixed through a constant ganging matrix and routed to the effectors. An example of this approach is provided in Section 2.1, while CS ganging is presented in the scope of CA theory in Section 2.4.1. These operations correspond to the mechanical branch of the FCS in Figure 3.9.

For the other CA methods, the AFCS branch is used. First, the natural dynamics of the aircraft are eliminated by using Non-linear Dynamic Inversion (NDI) [160, 161]. This approach utilizes the dynamic equations of motion to provide a model-based transfor-

mation between the pilot inputs and the control moments that need to be allocated to the effectors. The implemented formulation is reported in Equation 5.1, where $\boldsymbol{\nu}$ is the input to the CA problem — in other words, the control moments — and the pilot inputs on the stick are interpreted as the desired angular accelerations in body axes. The aerodynamic moments that are due to angle of attack, angle of sideslip and Mach number are assumed to be know perfectly by the FCS. Methods to measure and filter their values from flight sensors are out of the scope of this dissertation.

$$\boldsymbol{\nu} = \frac{1}{q_\infty S}\begin{bmatrix} 1/b & 0 & 0 \\ 0 & 1/\bar{c} & 0 \\ 0 & 0 & 1/b \end{bmatrix}\left(J\begin{Bmatrix} \dot{p} \\ \dot{q} \\ \dot{r} \end{Bmatrix}_{\text{des}} + \begin{Bmatrix} p \\ q \\ r \end{Bmatrix} \times J\begin{Bmatrix} p \\ q \\ r \end{Bmatrix} - \begin{Bmatrix} \mathcal{L}(\alpha,\beta,M) \\ \mathcal{M}(\alpha,\beta,M) \\ \mathcal{N}(\alpha,\beta,M) \end{Bmatrix}\right) \tag{5.1}$$

Once calculated, the control moments are transformed into CS deflections by the selected CA algorithm. For both FCS architectures, control inputs to the effectors are passed through a second-order actuator model with a natural frequency of 30 rad/s, a damping ratio of 0.7, a rate limit of 45 deg/s and saturation limits of ±30 deg.

5.2.3. FLYING QUALITIES CONSTRAINTS

The term Flying Qualities (FQs) is here adopted to indicate those aircraft stability and controllability characteristics that must be assured to "provide adequate mission performance and flight safety, regardless of design implementation or FCS mechanization" [162]. Contrarily to handling qualities, which involve the pilot maneuvering experience and are therefore more subjective [163], FQs can be measured objectively through flight simulation and/or flight testing. Their values should comply with specific, quantitative criteria in order to qualify the aircraft performance as satisfying, acceptable or unacceptable.

The flight mechanics model is used to evaluate a selection of FQs criteria which are typically considered for the certification of a new aircraft design. Each of these criteria is translated into a nonlinear constraint in the overall optimization problem with total CS span as objective. Since the aim of this chapter is to assess and compare the performance of different CA methods, the focus is placed exclusively on controllability criteria. The aircraft is assumed to be statically stable, regardless of the CS layout, by imposing a convenient position of its center of gravity.

The selected flight scenarios, and the corresponding target performance metrics, are extracted from the MIL-F-8785C handbook of the U.S. Department of Defense [162]. Despite not being an official set of certification specifications, this manual and its more modern extension [164] are the *de facto* official standard in the field of FQs definition and evaluation. The following FQs tests are reproduced in PHALANX, and their outcome is evaluated against the numerical requirements for Category III transport aircraft.

- Trim in straight and level flight. The aircraft must be trimmable at a given flight condition. This test is assumed successful if the magnitude of residual accelerations after trim is lower than $\left\| \boldsymbol{a}^{\text{lim}} \right\| = 1 \times 10^{-6}\,\text{m/s}^2$.
- Push/pull maneuver. Full longitudinal stick deflections must result in normal load factors of at least $n_z^{\text{lim}} = 2.0$ for a pull-up maneuver, and $n_z^{\text{lim}} = 0.5$ for a push-down maneuver.

- Time to bank. A full lateral deflection of the stick must result in a roll angle of $\varphi^{\text{lim}} = 30\,\text{deg}$ within a time span of $\Delta t_{\varphi}^{\text{lim}} = 2.3\,\text{s}$.

- One Engine Inoperative (OEI) conditions. The aircraft must be trimmable to fly in steady flight with one engine being inoperative.

These tests are run in cruise and approach flight conditions, as well as with two different cross-wind speeds. The experiment matrix detailing the selected combinations of flight conditions and required tests is shown in Table 5.1. The cruise phase parameters are taken from the PARSIFAL mission requirements, the approach speed is chosen as a typical value for comparable commercial transport aircraft. The cross-wind magnitude is set as $V_{\text{w}} = 25\,\text{kts}$, as prescribed in current certification regulations for commercial aircraft [132]. No tests about controllability in stall and post-stall conditions have been implemented, since the underlying aerodynamic database is not able to capture such phenomena at all.

5

Table 5.1 FQs test matrix used as constraints for the design optimization study. Aircraft mass and center of gravity are assigned before each test.

	Cruise ($h = 11\,\text{km}$, $M = 0.79$)	**Approach** ($h = 0\,\text{km}$, $V = 120\,\text{kts}$)
No wind ($V_w = 0\,\text{kts}$)	Straight and level trim Push/pull Time to bank	Straight and level trim Push/pull Time to bank OEI trim
Cross-wind ($V_w = 25\,\text{kts}$)	Straight and level trim Push/pull	Straight and level trim Push/pull OEI trim

The trim test forms the basis for all subsequent maneuver simulations. If trim is not achieved, all other tests are skipped and the optimizer moves on to the next layout evaluation. The trimming routine is formulated as an optimization problem itself, with the objective to find the pilot stick inputs that minimize the residual accelerations around all motion axes. Additional insight into the trim optimization problem may be found in Chapter 6. The OEI test uses the same trim optimization algorithm, with the resultant thrust vector lying outside of the longitudinal symmetry plane. The push/pull and time-to-bank tests perform the corresponding flight maneuver by building upon the control deflections from the trim solution. For the former, the maximum and minimum values of the normal load factor are recorded. For the latter, the time interval to achieve the desired roll angle is measured.

All tests conducted within this study are deemed successful if resulting in Level 1 FQs. For each test, the limit value which guarantees Level 1 FQs is used to formulate and normalize the constraint inequalities. These are summarized in Equation 5.2.

$$\mathcal{C}_{\text{FQs}} = \begin{cases} \left\| \boldsymbol{a}^{\text{tr}} \right\| \leq \left\| \boldsymbol{a}^{\text{lim}} \right\| & \text{for each trim FQs test} \\ n_z^{\max} \geq n_z^{\text{lim}} & \text{for each pull-up FQs test} \\ n_z^{\min} \leq n_z^{\text{lim}} & \text{for each push-down FQs test} \\ \Delta t_\varphi \leq \Delta t_\varphi^{\text{lim}} & \text{for each time-to-bank FQs test} \end{cases} \tag{5.2}$$

5.2.4. OBJECTIVE FUNCTION

The objective of the present investigation is to find the CS layout, with minimum total span width, which results in satisfying FQs criteria in various flight scenarios. Having a small total CS span width reduces the weight of the control system [158], and allows more space on the trailing edge for other subsystems, such as larger high lift devices, which could be beneficial for improved take-off and landing performance. The aforementioned goal can be achieved either by assigning a given layout and iteratively reducing the span width of each CS, or by exploring different layouts entirely. Both approaches are attempted in this research effort, as presented in the following Section 5.3. Similar approaches have also been adopted already in previous studies [42, 154].

In the current study, each CS is defined by three dimensionless parameters: the inboard or outboard station (η^{in} or η^{out}), the span width $\Delta\eta$, and the chord fraction. The span wise parameters are nondimensionalized with respect to the aircraft full wing span. In all cases, the inboard station of each inboard CS is always held fixed, as well as the outboard station of each outboard CS. In this way, each CS span width is altered by moving only the side of the CS which is closer to the middle of the wing. The CS nondimensional span widths $\Delta\eta_i$ constitute the decision variables for the optimizer. They are bounded and constrained such that CSs cannot move outside of the wing limits, or intersect each other and other wing elements. The chord fraction is assigned and held constant throughout the optimization. Its value is chosen as 0.3 for all CSs, in compliance with the wing spar position foreseen for the wings in the PARSIFAL project. The formal expression of the optimization problem is reported in Equation 5.3.

$$\begin{aligned} \min_{\Delta\eta_i} \quad & \mathcal{J}_\eta = \sum_{i=1}^{N_{\text{CS}}} \Delta\eta_i \\ \text{s.t.} \quad & \mathcal{C}_{\text{FQs}} \\ & \left|\eta_i^{\text{out}}\right| > \left|\eta_i^{\text{in}}\right| \qquad \forall\, i = 1, 2, ..., N_{\text{CS}} \\ & \left|\eta_i^{\text{out}}\right| < \left|\eta_{i+1}^{\text{in}}\right| \qquad \forall\, i = 1, 2, ..., N_{\text{CS}} - 1 \\ & \Delta\eta_i^{\min} \leq \Delta\eta_i \leq \Delta\eta_i^{\max} \qquad \forall\, i = 1, 2, ..., N_{\text{CS}} \end{aligned} \tag{5.3}$$

The problem is solved using the sequential quadratic programming algorithm within the `fmincon` function in MATLAB. Such solver satisfies bound constraints at all iterations, which is important to protect the AVL aerodynamic solver from infeasible CS sizes

and layouts. Additionally, it is able to handle unconverged and infinite function values, making it possible to recover from untrimmmable flight conditions. The solver stops either by reaching an optimality tolerance of 10^{-6} or a step size of 10^{-2}. All bounds and constraints are respected with a tolerance of 10^{-6}.

5.3. APPLICATIONS AND RESULTS

Two main application studies are presented in this section. In both cases, the box-wing geometry model from Figure 5.4 is used. For both cruise and approach flight conditions, the aircraft mass has been assigned as $m = 115\,000\,\text{kg}$. This values corresponds to fuel tanks being at 75% of their full capacity, at the corresponding design stage within the PARSIFAL project. The position of the aircraft center of gravity is assigned to achieve a 10% static margin in cruise conditions, and is kept fixed throughout each study. A synthetic overview of both application studies presented in this section is reported in Table 5.2.

Table 5.2 Overview of the application studies proposed in Section 5.3.

	Section 5.3.1	**Section 5.3.2**
Purpose	Impact of CA methods on minimum CS span width	Exploration of new CS layouts for box-wing aircraft
CA methods	Ganging, CWPI, DA	DA
CS layouts	Traditional [42, 153, 154]	Traditional Traditional + central rear CS Traditional, with inboard rear CS replaced by central rear CS
Sensitivity	3 initial conditions per CA method	—

The first application study is described in Section 5.3.1, and compares the minimum total span width obtained with a conventional ganging matrix, and the CWPI and DA methods, for the most traditional box-wing CS layout [42, 153, 154]. Such a layout features one Inboard (I) and one Outboard (O) CS on each of the Front (F) and Rear (R) wings. Each optimization loop, with a given CA method, is performed three times starting from slightly different initial conditions, in order to test the sensitivity of the results to the initial guess. Because all results of this study would comply with the aforementioned set of FQs, the resulting total CS span width is used to compare the performance of the CA methods. This is done by correlating the optimal total CS span width with the AAS volume that the final layout is capable to generate using the assigned CA method.

The second application study is detailed in Section 5.3.2, and explores and evaluates a novel CS layout for box-wing aircraft, featuring a CS close to the central section of the rear wing, outside of the twin vertical tail region. The DA method is used to perform the same design optimization study as in the previous case, but starting from three different initial layouts for the rear wing. The traditional layout with only one inboard and one

outboard CS is used as a benchmark case. A second layout is obtained by adding an extra Central (C) CS, close to the mid-wing section of the rear wing. A third layout is obtained by entirely replacing the inboard CS (between the vertical tails) with the central one (outside of the vertical tail region). In all cases, the front wing always features only one inboard and one outboard CS.

All CSs are given a small clearance to other geometrically constraining elements, such as the fuselage (of the complete aircraft model), wing tips, or the vertical tail intersection with the rear wing. For both application studies, the inner stations of the inboard CSs are fixed, as well as the outer stations of the outboard ones. Thus, the optimizer only operates on the outer stations of the inboard CSs, and on the inner stations of the outboard ones. For the second application study, the central CS is treated as an inboard one, since its inner station is constrained by the wing/tail intersection. In all cases, the ruddervators on the V-tail are assumed fixed in size, and hence not included in the CS sizing process.

On the front wing, the space in between the two CSs is occupied by an additional movable surface, representing a plain flap. The flap is set to a deflection of 30 deg for the approach condition and 0 deg for cruise. The span wise position and size of this flap are not design variables, but follow from the CSs positions and span widths. Flaps are secondary flight controls and are thus not actively included in the CSs sizing process. Nevertheless, the presence of the deflected flap has a significant impact on the controllability of the aircraft, and hence on the minimum size of the CSs. For this study, it is assumed that there are no requirements on the airfield performance that would predetermine a certain flap size or type. Instead, the chosen optimization problem formulation of Equation 5.3 will result in the set of CSs with the smallest total span width and, as a consequence, in the largest possible flaps.

5.3.1. IMPACT OF CONTROL ALLOCATION METHODS

The present optimization study has been performed three times for each CA method, adopting a different initial guess for CS span widths each time. The initial values and bound constraints for the CS span widths are shown in Table 5.3. In all cases, the initial CSs are all large enough to assure good FQs, and provide the optimizer a feasible, yet improvable, solution.

The upper bound was set to limit the design space, in accordance with preliminary investigations which showed that larger values of the CS span are not necessary. By choosing these numerical values for the bounds, the additional geometric constraints reported in Equation 5.3 are not necessary anymore for this specific application, but have been left in the formulation for the purpose of generality. Figure 5.5 shows the CS layout under investigation, and summarizes how each CS span width can be altered by the optimizer.

For the conventional ganging approach, front and rear inboard CSs operate as elevators, moving in phase opposition only in response to pitch commands. The outboard surfaces deflect as ailerons, only in response to lateral commands, and the ruddervators are constrained to deflect together, acting as pure yawing moment generators. The ganging matrix used in this case is reported in the following Equation 5.4. For the other CA methods, all CSs on the main wings operate independently, whereas ruddervators are treated in the same way as before, for consistency.

Table 5.3 Different sets of initial values and bound constraints for the CS span widths of the traditional box-wing CS layout represented in Figure 5.5.

Initial guess	$\Delta\eta_{IF}$	$\Delta\eta_{OF}$	$\Delta\eta_{IR}$	$\Delta\eta_{OR}$	$\Delta\eta_i^{min}$	$\Delta\eta_i^{max}$
1	0.08	0.08	0.08	0.08	0.01	0.10
2	0.08	0.06	0.08	0.06	0.01	0.10
3	0.06	0.08	0.06	0.08	0.01	0.10

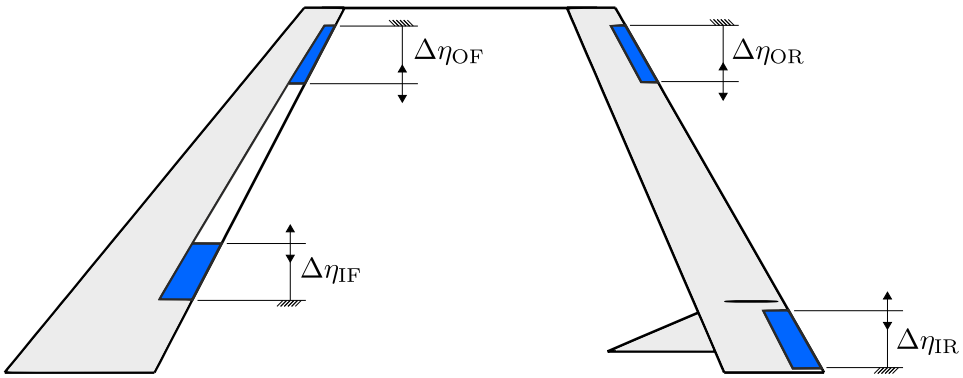

Figure 5.5 Top-view of the traditional box-wing CS layout, with visualization of how each CS span width can be altered by the optimizer.

$$\boldsymbol{u} = \begin{bmatrix} 0 & 0 & 0 & 0 & 0 & 0 & 0 & 0 & 1 & 1 \\ 1 & 1 & 0 & 0 & -1 & -1 & 0 & 0 & 0 & 0 \\ 0 & 0 & -1 & 1 & 0 & 0 & -1 & 1 & 0 & 0 \end{bmatrix}^T \begin{Bmatrix} \overline{u}_{ail} \\ \overline{u}_{ele} \\ \overline{u}_{rud} \end{Bmatrix} \tag{5.4}$$

$$\text{with } \boldsymbol{u} = \left\{ u_{IF}^{left}, u_{IF}^{right}, u_{OF}^{left}, u_{OF}^{right}, u_{IR}^{left}, u_{IR}^{right}, u_{OR}^{left}, u_{OR}^{right}, u_{rud}^{left}, u_{rud}^{right} \right\}^T$$

Results are graphically reported in Figure 5.6, and summarized in Figure 5.7 and Table 5.4. Despite significant variation in the single CS span widths, the choice of the initial point has only a minor influence on the final value of the objective function. For each CA method, the spread of the three objective function values is less than 3%. The conventional ganging approach requires the largest overall CS widths. This is expected, since roll and pitch moments are only achieved by the respective CSs, as explained at the beginning of Section 5.3. The CWPI method is able to use all effectors in combination, hence reducing the total required span width by about 9.5%. Lastly, DA reduces the required span width even further, achieving a reduction of about 17% compared to ganging. This is also an expected result, sparking from the geometric properties of the DA method, highlighted in Section 2.4.3. Since it can attain the entirety of the AAS, and is able to utilize every effector in the most efficient way, it requires less CS span width overall.

As shown in Figure 5.6a, the final CS dimensions are very similar for the three initial conditions corresponding to the ganging approach. The main differences lie in the dis-

tribution between the front and rear inner surfaces, but are consistent for all cases. On the other hand, the CWPI results present relevant differences between the CS layouts, as shown in Figure 5.6b. However, the final values of the objective function are similar. From this, it may be deduced that the design space is complex, and admits different local minima. Results for the DA method, reported in Figure 5.6c, show a similar behavior as the CWPI, albeit less pronounced. The same considerations hold true.

This investigation clearly shows that CA methods do not allow a clear choice of a specific CS layout to achieve prescribed FQs objectives. All the optimal layouts show some variation in the span widths of the individual effectors, while being equally optimal from a global standpoint. Some CSs present particularly small values of the optimum span width, for which significant non-linear aerodynamic effects could be expected. The inability to evaluate them with the selected aerodynamic model likely causes an overestimation of the overall control effectiveness and hence an underestimation of the total required CS span widths.

Table 5.4 Optimization results for the different CA methods and initial conditions. The latter are reported in Table 5.3.

CA method	Initial guess	$\sum_i \Delta\eta_i$	$\Delta\eta_{IF}$	$\Delta\eta_{OF}$	$\Delta\eta_{IR}$	$\Delta\eta_{OR}$
Ganging	1	0.259	0.076	0.057	0.080	0.051
	2	0.265	0.080	0.055	0.075	0.055
	3	0.257	0.081	0.055	0.066	0.054
CWPI	1	0.235	0.060	0.025	0.073	0.075
	2	0.241	0.047	0.053	0.098	0.043
	3	0.234	0.100	0.010	0.033	0.099
DA	1	0.214	0.097	0.027	0.016	0.074
	2	0.213	0.091	0.053	0.013	0.056
	3	0.215	0.047	0.036	0.089	0.043

Figure 5.8 correlates the total CS span width with the volume of its AAS, for every CA method and initial layout, and shows the reduction of both variables achieved through the design optimization. As explained in Section 2.5, the volume of the AAS is a common measure to quantify the total control power that a CA method can provide. For the optimal value of the total CS span width, the different CA methods are seen forming clearly distinguishable clusters in the chart. The ganging cluster is positioned at large CS span and medium AAS volume. The CWPI cluster presents smaller CS span widths than the ganging one, and the minimum AAS volume overall. The DA cluster has both the lowest required CS span width and the largest AAS volume. This confirms again that it is able to achieve the highest control power with the smallest CSs.

The inspection of the shape of the AASs in Action Space makes it possible to further analyze the performance of these CA methods. The three AASs geometries are compared in Figures 5.9 and 5.10. As explained in Section 2.5, for their respective CS layout, both

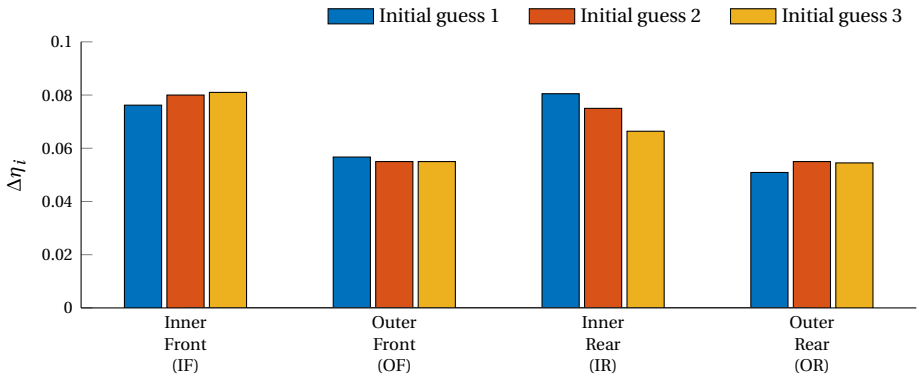

a) Ganging

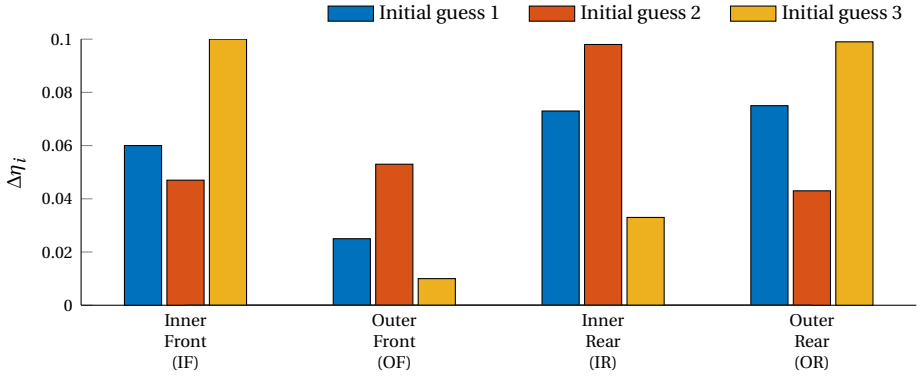

b) Constrained Weighted Pseudo Inverse (CWPI)

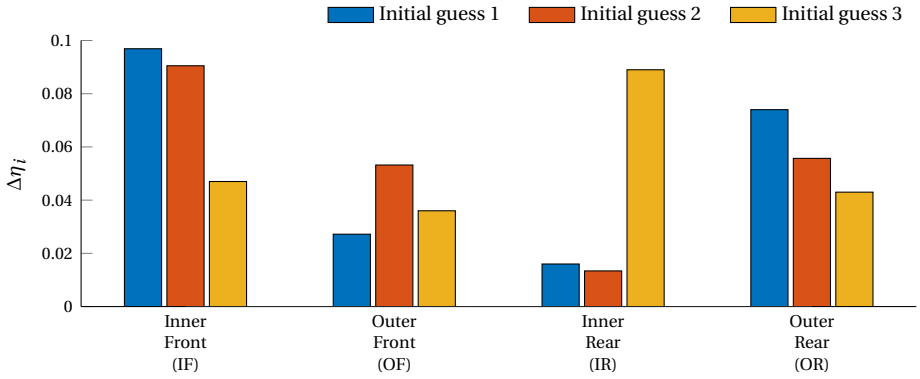

c) Direct Allocation (DA)

Figure 5.6 Comparison of optimal CS span widths for different CA methods and initial conditions. The legend refers to the initial conditions reported in Table 5.3.

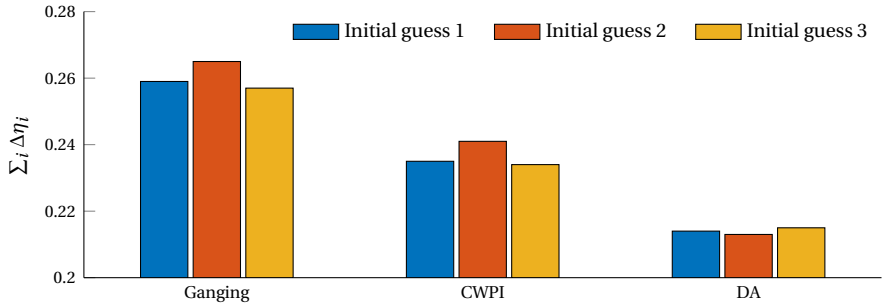

Figure 5.7 Comparison of cumulative optimal CS span widths for different CA methods and initial conditions. The legend refers to initial conditions reported in Table 5.3.

the ganging and the CWPI approaches are only able to attain a certain subset of the EAS, while the DA method is capable to attain it in its entirety. Overall, the AAS corresponding to the CWPI and DA layouts present a more rounded, oval-like shape, in comparison to the ganging method which results in a prismatic shape.

This is especially true in the roll-pitch plane of Action Space, visible in Figure 5.10. The round shape of the AASs of the the CWPI and DA layouts clearly identifies a smooth trade-off between the roll and pitch control power. This is in light of the fact that the CSs on the main wings are all employed for both of these control objectives. As the required control power increases about the roll axis, for example, the available control power about the pitch axis decreases, and vice versa. The opposite is true for the layout obtained with the ganging method, for which the roll-pitch section presents a rectangular shape. This is because the roll and pitch control tasks have been explicitly assigned to two different and independent sets of CSs, in this case. The latter behavior can also be observed in the pitch-yaw plane for all three layouts, since pitch and yaw moment generation are fundamentally uncoupled in the current setup. Lastly, a small coupling due to adverse yaw is visible in the roll-yaw plane for all three methods.

The maximum extension of all three AASs along the yaw axis is almost completely the same for all three layouts, since yaw control effectiveness is mainly ascribed to rudders, which have not been included in the design optimization problem. The AASs corresponding to the optimal layout of the ganging and CWPI method are basically overlapping in the roll-yaw plane of Action Space. On the other hand, the AAS of the layout obtained with DA is significantly more extended along the roll axis. The AAS of the ganging method is the most extended one along the pitch axis, although the difference with the other methods is smaller in this case.

In summary, the CWPI method manages to be effective for all of the FQs tests that do not require strongly coupled moments. It does need extra CS span width, as compared to the DA method, to satisfy the FQs tests in presence of side-wind. The ganging method is the most suitable to attain all combinations of coupled moments, in light of its reliance on independent sets of CSs, although it does need the largest CS span width to satisfy all FQs constraints. As the DA method accesses the entire EAS of its respective layout, it results in large moment generation capabilities, even in directions that are not specifically

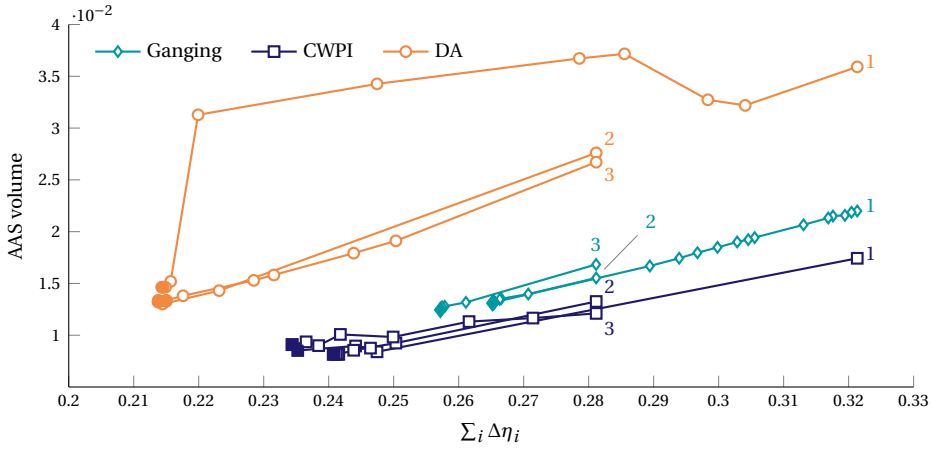

Figure 5.8 Evolution of the AAS volume and the total CS span width with the optimizer iteration, for different CA methods and initial values. The design iteration for each study starts at the respective number label. The final iteration is represented by the filled markers. Initial conditions are reported in Table 5.3

5

required for the FQs tests. This property allows such method to obtain the smallest total CS span width overall.

5.3.2. EXPLORATION OF NEW CONTROL SURFACE LAYOUTS

The baseline CS layout adopted in the previous application has its roots in the current state of the art concerning box-wing design approaches. As it is typical for FCSs using mechanically geared effectors, the wing roots represent the conventional positions of elevators, while the wing tips are the designated positions of ailerons. In combination with the two wings of the box-wing aircraft, CA methods may allow for considerably more flexible CS placements.

Moreover, for a transonic box-wing aircraft such as the PrP, the flow field around the wing/tail intersection is complex, and aerodynamic interactions can have a detrimental effect on interference drag and overall performance. In light of this, it may be in the interest of aerodynamic performance to design this complex geometry without having to mind additional complications due to CS placement. With these considerations in mind, a second investigation is performed to explore new CS layouts, featuring a CS placed outside of the vertical wing/tail intersection, and hence closer to the mid-wing section.

A design optimization is carried out for each of the three different initial layouts, on the rear wing. Namely:

Layout A is the one studied in the previous section, used now as a benchmark; it features an Inboard (I) CS, between the two vertical tails, and an Outboard (O) CS, close to the wing tip.

Layout B features an Inboard (I) CS, between the two vertical tails, an Outboard (O) CS, close to the wing tip, and a “Central” (C) CS, close to the mid-wing section and

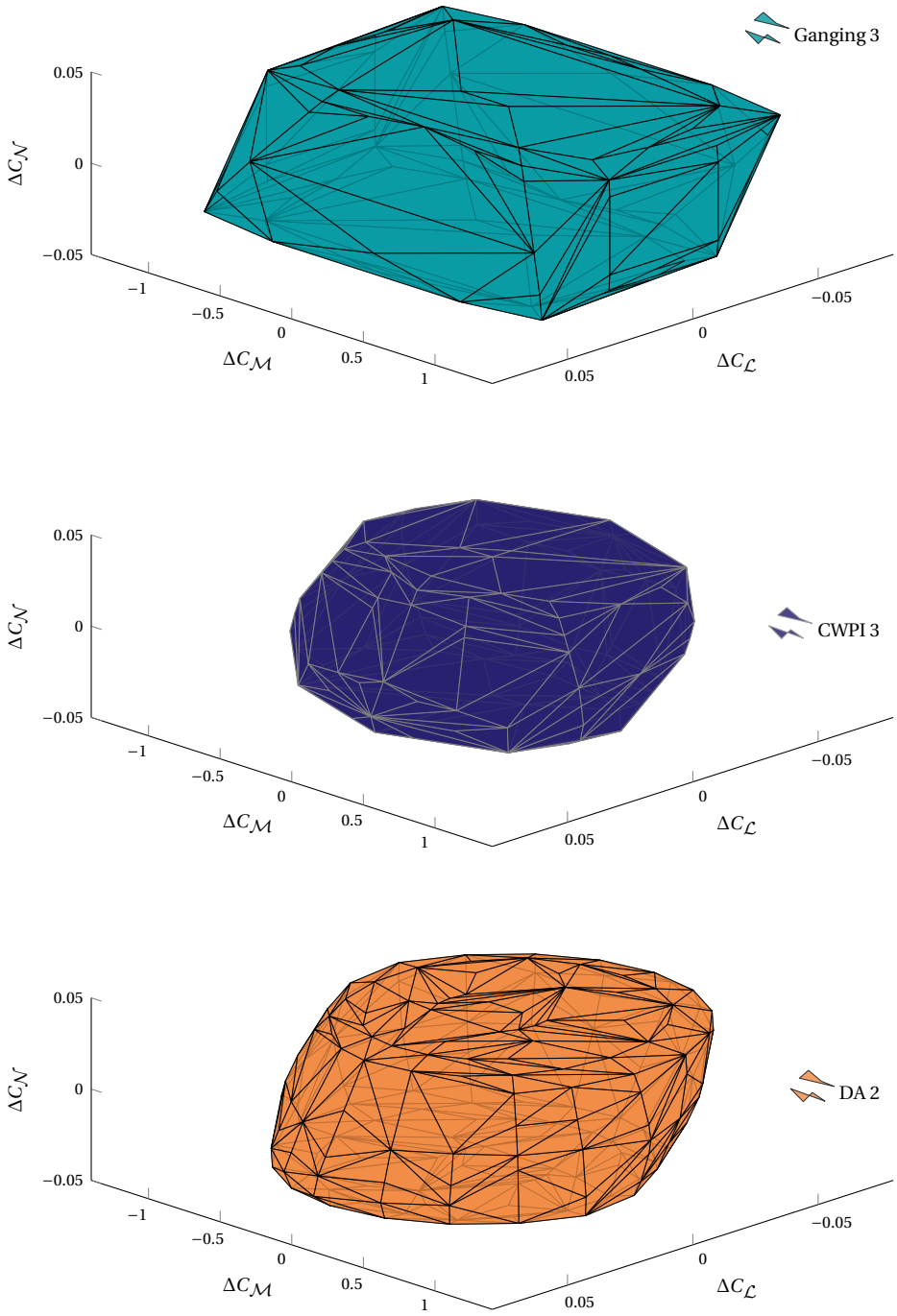

Figure 5.9 Visualization of the AASs corresponding to the optimal CS layouts obtained with each CA method. The legend entry refers to the CS layouts reported in Table 5.4.

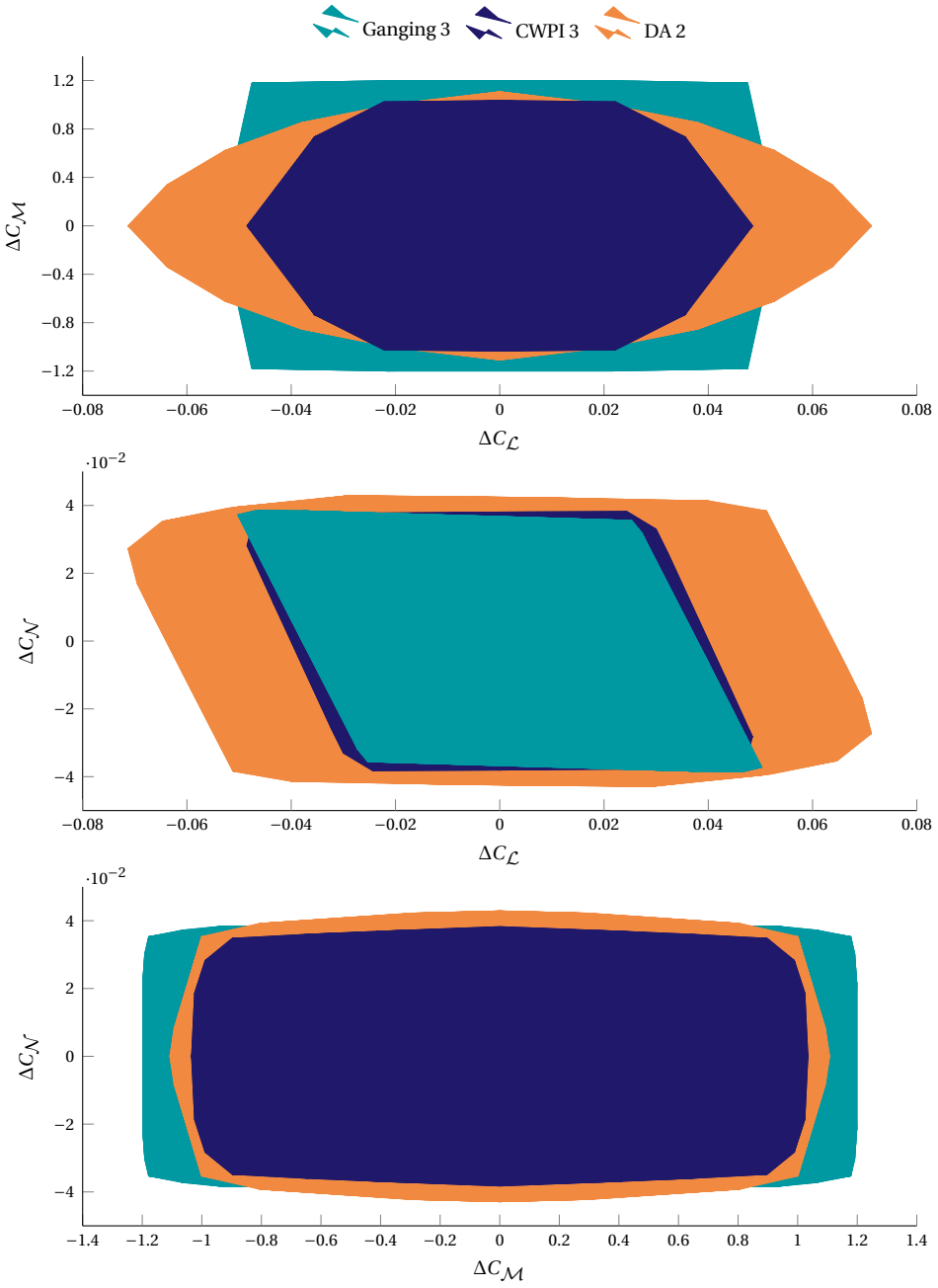

Figure 5.10 Comparison of the AASs corresponding to the optimal CS layouts obtained with each CA method. The legend entry refers to the CS layouts reported in Table 5.4.

outside of the vertical tail region;

Layout C features the aforementioned "Central" (C) CS, and an Outboard (O) CS, close to the wing tip.

For all three layouts, the CSs on the front wing retain the same arrangement and behavior as in the previous study. The DA method is employed in all cases, in light of its performance in the previous application study.

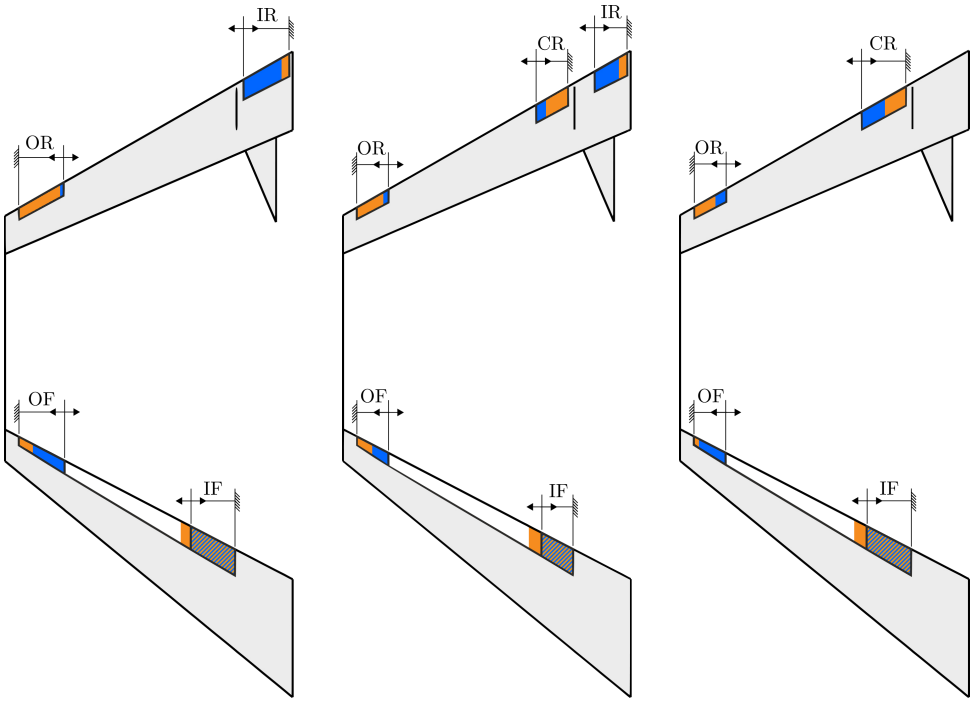

a) Layout A **b)** Layout B **c)** Layout C

Figure 5.11 Top view of CS Layouts A, B and C. Span widths are to scale and correspond to the assigned initial values (in blue), and optimum final values (in orange).

The three layouts with initial and final CS span widths are shown in Figure 5.11. Results from the three optimization studies are summarized in Table 5.5 and Figure 5.12. With respect to Layout A, Layout B shows a mere 2.3% reduction in total CS span width. In spite of this modest enhancement, it seems that the addition of an extra CS clearly leaves further margin of improvement for the selected objective function. As a matter of fact, Layout C results in about 13% decrease in total CS span, as compared to Layout A. This is due to the fact that the CS between the vertical tails has been completely replaced by the one close to the mid-wing section, outside of the vertical tail region. The new position allows the mid-wing CS to contribute to both the roll and pitch maneuvers more flexibly, effectively behaving like a proper elevon.

Table 5.5 CS span width comparison among Layouts A, B and C.

Layout	$\sum_i \Delta\eta_i$	$\Delta\eta_{IF}$	$\Delta\eta_{OF}$	$\Delta\eta_{IR}$	$\Delta\eta_{CR}$	$\Delta\eta_{OR}$	
A	0.214	—	0.097	0.027	0.016	—	0.074
B	0.209	-2.3%	0.078	0.028	0.016	0.040	0.047
C	0.186	-13.1%	0.100	0.010	—	0.038	0.038

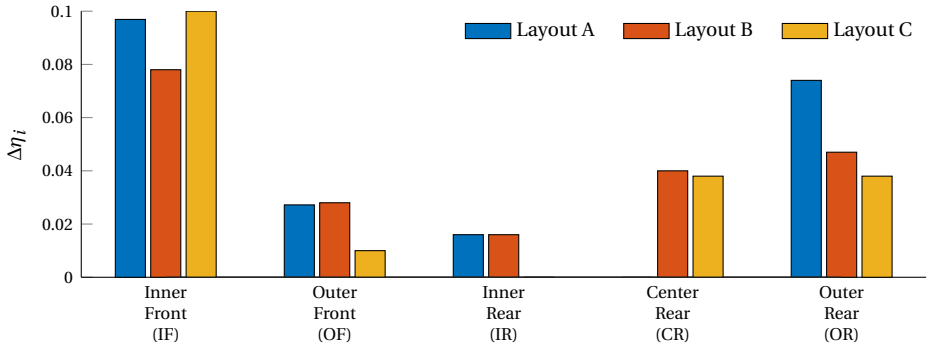

Figure 5.12 CS span width comparison among Layouts A, B and C.

For Layout B, the additional center rear CS achieves approximately the same span width of its counterpart in Layout C. Despite both the inner front and outer rear CSs are slightly smaller than in Layout A, their reduction is not sufficient to justify the addition of an extra CS. As reported in Table 5.5, the value of the objective function is reduced from 0.209 of Layout B, to 0.186 of Layout C, which corresponds to an 11% decrease in total CS span width. For Layout C, the remaining control power is provided mainly by CSs on the rear wing. Whereas those are equal in span width, the front outer surface is reduced to its minimum allowed size. This shows how the center rear surface is very effective in both pitch and roll, and can allow smaller CSs span overall.

Lastly, it is interesting to note how the optimizer retains control surfaces on both the front and rear wing for all final layouts. The inner front and the outer rear CSs, together with the center rear one (when present), seem to be the most important ones, as they are never reduced to a span width smaller than $\Delta\eta = 0.038$. The outer front and the inner rear CSs become extremely small and ineffective in all the layouts where they appear, with the former of the two reaching the minimum bound value for its span width in Layout C. This suggests that they could probably be removed from the aircraft configuration altogether, in favor of increased simplicity of its architecture. Replacing the inner rear CS with a central one has indeed proved worthy, in light of the results achieved with Layout C. Analogous investigations can be conducted for the outer front CS in the future.

5.4. CONCLUSIONS

This chapter has presented a design methodology to automatically size multiple, redundant CSs on a given wing geometry. The design task has been formulated as a multi-

disciplinary optimization problem. The problem aims to obtain a CS layout with minimum total span width, while achieving desired FQs for a specified set of flight scenarios.

FQs criteria are evaluated through flight simulation, and encoded as constraints in the overarching design optimization problem. The aircraft flight mechanics model makes it possible to render different FCS architectures, in order to link the pilot input to CS deflections. Although the proposed optimization framework is applied to a staggered box-wing configuration, it is vehicle configuration-agnostic in nature. Thus, it is suitable to any wing geometry and of particular interest to other novel configurations that offer the opportunity of installing redundant CSs (such as flying wings or BWBs).

The goal of this research has been to determine the impact of different CA methods on the optimum CS layout of a box-wing aircraft. Results have been compared for the CWPI method, the more advanced DA method, and a conventional ganging approach, which is equivalent to establishing a mechanical linkage among CSs. In line with expectations, the former two CA methods achieve CS layouts with lower total span, as compared to those obtained with conventional ganging. In particular, the DA method obtains the minimum total CS span, together with the maximum corresponding control power. This result is clearly due to the ability of the DA method to attain the entirety of the EAS, for any given CS layout. It makes it possible to extract all the control power made available by the effectors, while retaining an efficient use of each one of them, depending on the prescribed maneuver.

For this reason, the latter has then been used to explore unconventional CS layouts for the box-wing geometry. The new layout features a CS in the central region of the rear wing, which can be apposed next to, or potentially replace, the most inboard surface close to the aircraft plane of symmetry. Results show that the total CS span width is further reduced if the inboard rear surface is completely replaced by the mid-wing surface. This is because the mid-wing surface can aid in both longitudinal and lateral flight maneuvers, hence functioning as a proper elevon and providing both roll and pitch control power.

In light of these results, it is evident that CA methods should be included in similar studies, already from the conceptual and preliminary aircraft design stages. Nevertheless, the studies presented in the following chapters have been applied to the most traditional box-wing CS layout, featuring one inboard and one outboard CS per wing. This is because the present study has been concluded after the end of the PARSIFAL project, within which the PrP configuration has been researched and improved continuously.

Continuing on the presented work, additional efforts could be devoted to verifying if the findings presented in this chapter are confirmed when including fuselage aerodynamic effects. A higher fidelity aerodynamic model is advised to also account for nonlinear aerodynamic effects due to CSs, especially when very limited in span or installed next to each other (as in the case of flaps, on the front wing). A more accurate aerodynamic model would make it interesting to include trim drag as an additional design objective, as well as to validate the proposed optimization method using a conventional aircraft configuration.

Further research should generalize the proposed framework by also including stability considerations, as well as flight scenarios such as take-off and landing. In the design iteration, this would introduce a coupling between the span widths of flaps and

CSs, which could be tackled by prescribing a supplementary set of flight performance requirements. Additionally, the CS locations and/or chord ratios could be included as additional design variables in the optimization problem, to further investigate optimal CS placement on box-wing aircraft. In any manner, it is expected that the main conclusions concerning the comparison of the selected CA methods will not be hindered by the addition of these factors.

Different CA methods with more practical interest for real-life operations could be analyzed. Examples may include the unconstrained WPI, and tailored generalized inverse formulations — such as the ones for maximum AAS volume or maximum control power in a given direction — with their respective cascaded implementations. Lastly, it would be interesting to explore other design objectives, such as minimum CS area, minimum required actuator power, or maximum AAS volume.

6

TRIM AND CONTROL AUTHORITY

The best we can do then,
in response to our incomprehensible and dangerous world,
is to practice holding equilibrium internally.

Elizabeth Gilbert
Eat, Pray, Love
2006

Equilibrium is a figment of the human imagination.

Kenneth E. Boulding
The Journal of Economic Education
1988

When directly including the effects of control surfaces on aerodynamics and flight mechanics, the problem of finding the combination of their deflections that guarantees flight equilibrium must be explicitly faced. This chapter presents a novel formulation of the trim problem, based on the geometry of the AAS. Similarly to many other studies, trim conditions are found by solving an optimization problem. In the present case, the geometry of the AAS is explicitly used to define inequality constraints for a set of trim controls, among which control forces and moments, as well as to propose and exploit a definition of control authority in Action Space.

The baseline trim problem is first introduced in Section 6.2 for generic dynamic systems, with a review of common approaches used in flight mechanics applications. In particular, Section 6.1.1 presents a definition of control authority which does not depend on the number of available control surfaces, but entirely belongs to Action Space.

Parts of this chapter have been presented at the 2020 AIAA SciTech Forum and Exposition conference [165] and have been published in the CEAS Aeronautical Journal in 2021 [166].

The actual trim optimization problem is formulated in Section 6.2, where it is explained how the AAS geometry is used to enforce trim constraints and include control authority as an objective function. Trim conditions that maximize control authority about a specified motion axis are presented in Section 6.3.1, using a 3 DoFs and a 6 DoFs flight mechanics model. Sections 6.3.2 and 6.3.3 present more classic and operational trim applications, such as trim for minimum aerodynamic drag and for a prescribed pitch angle, respectively. Lastly, conclusions are drawn in Section 6.4.

6.1. INTRODUCTION

Trimming a dynamic system means finding the combination of input and state variables values which set the system in a steady-state condition [167]. In the most general case, system dynamics is expressed by non-linear, implicit or explicit equations, as shown in Eq. 6.1. If the system is trimmed, none of the states is changing in time and Equation 6.2 holds. The trim problem consists in finding the values of $\boldsymbol{\sigma}^{\text{tr}}$ and $\boldsymbol{u}^{\text{tr}}$ such that Equation 6.2 is verified.

$$\boldsymbol{f}(\dot{\boldsymbol{\sigma}}, \boldsymbol{\sigma}, \boldsymbol{u}) = \boldsymbol{0} \tag{6.1}$$

$$\boldsymbol{f}\left(\dot{\boldsymbol{\sigma}}^{\text{tr}} = \boldsymbol{0}, \boldsymbol{\sigma}^{\text{tr}}, \boldsymbol{u}^{\text{tr}}\right) = \boldsymbol{0} \tag{6.2}$$

In general, if $\mathbb{S} = \{\boldsymbol{\sigma}, \boldsymbol{u}\}$ is the set of system states and inputs, some subset $\boldsymbol{\tau}_0 \subseteq \mathbb{S}$ can (or must) be characterized explicitly in order to define the desired trim condition. The variables belonging to this subset have therefore known values. The remaining subset $\boldsymbol{\tau} = \mathbb{S} - \boldsymbol{\tau}_0$ contains unknown variables, which are referred to as "trim controls". By using these definitions, it is possible to represent $\mathbb{S}^{\text{tr}}$ either in terms of system states and inputs, or in terms of assigned and unknown variables, as done in Equation 6.3. The trim problem consists then in determining the values of the trim controls $\boldsymbol{\tau}$ such that Equation 6.2 is verified.

$$\mathbb{S}^{\text{tr}} = \left\{\boldsymbol{\sigma}^{\text{tr}}, \boldsymbol{u}^{\text{tr}}\right\} = \{\boldsymbol{\tau}_0, \boldsymbol{\tau}\} \tag{6.3}$$

Formulations of the trim problem can be classified on the basis of the number of dynamic equations $N_{\boldsymbol{f}}$ and the number of trim controls $N_{\boldsymbol{\tau}}$. The trim problem is said to be over-determined if $N_{\boldsymbol{f}} > N_{\boldsymbol{\tau}}$, determined if $N_{\boldsymbol{f}} = N_{\boldsymbol{\tau}}$, or under-determined if $N_{\boldsymbol{f}} < N_{\boldsymbol{\tau}}$. This classification does not give any indication on the number of solutions that the trim problem can have. Due to non-linearities and couplings in the dynamic equations, even a determined trim problem can have zero or more than one solution. An example of this is shown in Figure 6.1. In the figure, the leader is trimmed in straight and level flight, while the followers are trimmed in an anti-symmetric, steady forward-slip flight in the leader's wake. This attitude requires additional contemporary deflection of ailerons and rudders to maintain the asymmetric flight condition. The additional trim drag requires, in turn, a higher engine setting to maintain the horizontal trajectory. The complexity and the number of possible solutions of a given trim problem usually increases with the number of trim controls, making under-determined problems generally tougher to solve than determined ones.

An extensive and detailed analysis of the classic trim problem for rigid aircraft dynamics with 6 DoFs is presented in [168]. The trim problem is formulated as in Equation 6.4 and assumes the aircraft is trimmed when the objective function is close to zero,

Figure 6.1 Three Northrop Grumman F2F-1 fighters in steady, aerobatic, formation flight, 1939[1]. The leader is trimmed in straight and level flight, while the followers are trimmed in steady, asymmetric flight with forward slip.

within a very small tolerance. It is therefore, in essence, a root-finding problem.

$$\begin{aligned} \min_{\boldsymbol{\tau}} \quad & \mathcal{J} = \|\dot{\boldsymbol{\sigma}}\|^2 \\ \text{subj. to} \quad & \boldsymbol{\tau}_{\text{lb}} \le \boldsymbol{\tau} \le \boldsymbol{\tau}_{\text{ub}} \end{aligned} \tag{6.4}$$

For every flight condition the number of assigned trim parameters $\boldsymbol{\tau}_0$ is chosen so that the trim problem is determined. By limiting the scope to conventional aircraft configurations, each trim problem can be designed to have exactly six trim controls: the four conventional control effectors (throttle, elevator, aileron pair, and rudder), and the pitch and yaw angles of the body reference frame, θ and ψ . This solid approach may show its limitations when considering aircraft configurations with higher number of control inputs, for example with redundant or unganged sets of control effectors, for which the trim problem becomes under-determined.

An early attempt at solving an under-determined trim problem for aircraft longitudinal dynamics is provided in [169]. The trim problem is formulated as an induced drag minimization problem, with constraints on the vertical and rotational equilibrium in the longitudinal axis. The equations of motion are linearized with classic assumptions for the cruise condition and a closed form solution is derived. Examples are provided for an aircraft with three lifting surfaces and a fighter jet with thrust vectoring capabilities. The trim controls for the first application are the lifts of each surface, while those for the second application are the lifts of wing and tail, and the engines' thrust angle. In all cases, therefore, control surfaces are not included in the flight mechanics model. With this approach, $N_{\boldsymbol{\tau}} = N_{\boldsymbol{f}} + 1$ and it is possible to minimize a single scalar parameter, induced drag, while trimming the aircraft.

The case of under-determined trim problems due to control effectors redundancy

[1] Courtesy of the National Archives and Records Administration; catalog number: 80-G-409231.

has been analyzed in [170], with applications to the BWB aircraft configuration. Two trim problem formulations are proposed:

1. A Minimum Drag Trim Optimization (MDTO) applied to 6 DoFs dynamics.

2. A Root-Finding Trim with Direct Allocation (RFTDA), analogous in the objective function to the one in Equation 6.4.

For the MDTO formulation, unganged control surface deflections are directly included in the the trim controls set: $\boldsymbol{\delta} \in \boldsymbol{\tau}$. In this way, the dimension of $\boldsymbol{\tau}$ increases linearly with the amount of control effectors, making the trim problem more complex for highly redundant aircraft configurations.

For the RFTDA formulation, the trim controls set does not contain the control surface deflections, but a set of aerodynamic actions due to the control effectors $\Delta\boldsymbol{A}$. With this approach, the dimension of $\boldsymbol{\tau}$ does not depend on the control surface redundancy of the aircraft configuration. The DA method is used to establish a relation between $\Delta\boldsymbol{A}$ and $\boldsymbol{\delta}$. The dimension of $\Delta\boldsymbol{A}$, here indicated with $N_{\boldsymbol{A}}$, is somewhat arbitrary and depends on which motion axes are selected to be controlled. $\Delta\boldsymbol{A}$ contains up to two elements (lift and pitch moment) for flight simulations constrained in the longitudinal plane, or up to four elements (lift, and roll, pitch, yaw moments) for 6 DoFs simulations. It is noted that the number and type of elements in $\Delta\boldsymbol{A}$ has a significant impact on the resulting control surface deflections at trim. Lower and upper bounds for the $\Delta\boldsymbol{A}$ trim controls are selected on the basis of previously obtained solutions, or by manually inspecting particular combinations of control surface deflections for the specific problem.

A synthetic scheme of the reviewed trim problem formulations is shown in Table 6.1. Comparing the two approaches presented in [170] would be overall unfair. The MDTO is an optimization-based approach that exploits controls redundancy to minimize drag at trim conditions. The RFTDA is a root-finding trim approach that copes with control redundancy through a CA algorithm. No parameter is explicitly optimized with the latter formulation, and the method is indeed incapable of returning the minimum drag trim condition. With reference to the RFTDA approach, it is shown that introducing lift in the trim control vector results in trim conditions with lower drag, and better aerodynamic efficiency. Control drag is not explicitly included in $\boldsymbol{\tau}$ because the DA would poorly approximate its quadratic behavior with deflection angles.

Advanced CA algorithms that explicitly minimize control drag have been developed in the past, but never applied to formulations of the trim problem. An incremental, or frame-wise, expansion of the DA method is presented in [48]. A model-specific incremental CA method is presented in [57], where drag is expressed as a quadratic function of the effectors, and the CA algorithm solves a quadratic programming optimization problem.

This chapter presents a novel generic trim problem formulation, in the form of a constrained optimization problem, which employs forces and moments due to the aircraft control surfaces as trim controls. The constraints (and, optionally, the objective function) of such optimization problem are obtained by exploiting the geometric properties of the AAS. Control forces and moments are then mapped to the effectors using a linear programming formulation of the DA method [55].

Table 6.1 Summary of trim problem formulations from the reviewed literature.

Ref.	DoFs	Secondary Objective	Trim Controls	CA
[168]	6	None	$\theta, \psi, \boldsymbol{\delta}, \delta_T$	Ganging
[169]	3	Drag	$C_{L_1}, C_{L_2}, C_{L_3}$	Not modeled
	3	Drag	$C_{L_1}, C_{L_2}, \delta_T$	Not modeled
[170]	3,6	None, drag	$\alpha, \theta, \boldsymbol{\delta}, \delta_T$	None
	3	None	$\alpha, \theta, \mathcal{M}, \delta_T$	DA
	3	None	$\alpha, \theta, \mathcal{M}, L, \delta_T$	DA
	6	None	$\alpha, \theta, \psi, \varphi, \mathcal{L}, \mathcal{M}, \mathcal{N}, L, \delta_T$	DA

By using control forces and moments as decision variables, the proposed trim formulation is well suited to be applied to aircraft configurations with a high number of control surfaces. By relying on the geometry of the AAS, the formulation makes it possible to objectively define the feasible region of the trim optimization problem, exclusively on the basis of the aircraft control effectiveness. By relying on a CA method to link control forces and moments to control surface deflections, the formulation also ensures that trim solutions can automatically be obtained by an appropriate, practical realization of the aircraft FCS.

Several applications are presented for the PrP box-wing aircraft configuration. First, the possibility to trim for maximum control authority in a specific direction of one or more motion axes is explored, with examples in symmetric and asymmetric flight. For this application in particular, the AAS geometry is not only used to generate linear constraints for the trim problem, but also to calculate the objective function itself. Then, the formulation is also applied to more traditional studies on trim for minimum drag — for which control drag is also included as a decision variable — and trim for a specified pitch angle are also presented.

The standard aerodynamic model of Equation 3.1 is adopted for all of the applications. Both α and β range from -6 deg to 6 deg in steps of 3 deg, while two Mach numbers have been analyzed, namely $M = 0.3$ and $M = 0.6$. Each control surface has been deflected, independently from all the others, from -30 deg to 30 deg in steps of 10 deg.

6.1.1. CONTROL AUTHORITY

Control authority is here defined as the ability of the control effectors to generate forces and moments about one or more directions of Action Space, from a give reference flight condition. Examples may include control authority to pitch up, or to lift up and down (as in the case of spoilers). The concept of a maximum "balanced" control authority, about all motion axes, would be equivalent to the one of minimum total control effort. It is indicated with the symbol $\mathcal{A}_{\boldsymbol{A}}$, where $\boldsymbol{A}$ identifies a signed direction in Action Space. For example, pitch-up and pitch-down control authorities can be respectively calculated as in Equations 6.5 and 6.6.

$$\mathcal{A}_{+\mathcal{M}} = \left| C_{\mathcal{M}}^{\max} - C_{\mathcal{M}}^{\text{ref}} \right| \tag{6.5}$$

$$\mathcal{A}_{-\mathcal{M}} = \left| C_{\mathcal{M}}^{\min} - C_{\mathcal{M}}^{\text{ref}} \right| \tag{6.6}$$

Although control authority is a function of all flight parameters, for a given flight condition $\{\alpha, \beta, M\}$ and aircraft configuration, it only depends on the position of the control effectors. In this case, it can be expressed in terms of the aerodynamic actions due to the control effectors $\Delta C_{\boldsymbol{A}}$, as shown in Equation 6.7. It is therefore a quantity which belongs to Action Space, and in particular within the AAS.

$$\Delta\mathcal{A}_{\boldsymbol{\ell}} = \left\| \Delta C_{\boldsymbol{A}}^{\text{lim}} - \Delta C_{\boldsymbol{A}}^{\text{ref}} \right\| \tag{6.7}$$

For a given direction $\boldsymbol{\ell}$ and reference point $\Delta C_{\boldsymbol{A}}^{\text{ref}}$ in Action Space, the limit point $\Delta C_{\boldsymbol{A}}^{\text{lim}}$ is found at the intersection of the AAS boundary and a half-line starting at the reference point $\Delta C_{\boldsymbol{A}}^{\text{ref}}$ with the same direction of $\boldsymbol{\ell}$. Control authority finds its geometric representation as the distance between these two points of the AAS, as shown in Figure 6.2.

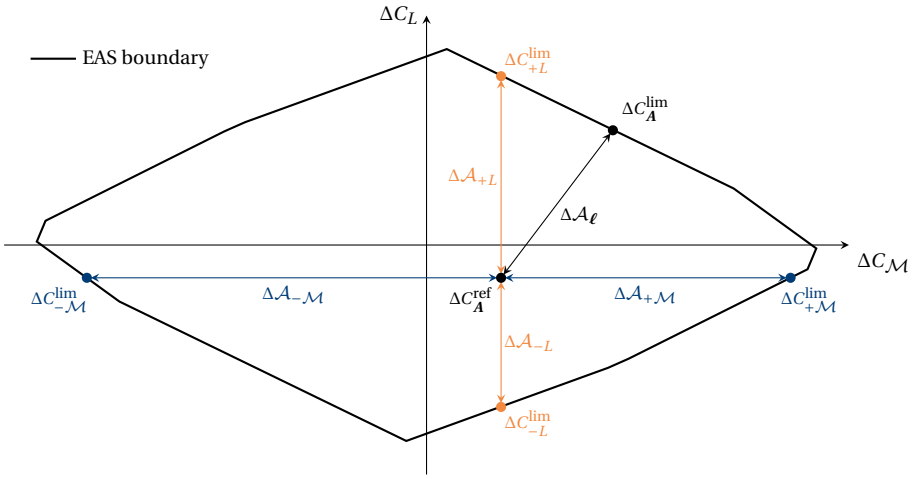

Figure 6.2 Geometric interpretation of control authority about various motion axes and directions in an $\mathbb{R}^2$ Action Space.

Searching for trim conditions which guarantee rotational equilibrium and at the same time maximize the control authority for pitch-up maneuvers could be interesting for safety purposes, for example in case of aborted landings. A similar scenario can be envisioned to justify the interest in trim with maximum lift-up control authority. Because lift lies perpendicular to the velocity vector, by definition, an increase in lift introduces a centripetal acceleration $V\dot{\gamma}$ which is the most direct way to bend the trajectory upwards. The study of control authority in the lift axis is particularly aimed at exploiting the PrP's innovative way of implementing DLC [43].

6.2. TRIM PROBLEM FORMULATION

In the context introduced by the previous section, trimming the aircraft means finding the flight condition and the set of control aerodynamic actions $\Delta C_{\boldsymbol{A}}^{\text{tr}}$, lying inside or on

the boundary of the corresponding AAS, so that Equation 6.2 is verified. Whereas trim control forces and moments must belong to the interior or to the boundary of the AAS, the inverse is obviously not true: not all points of the AAS are representative of trim conditions. This section presents a comprehensive formulation of the trim problem to find possible values of control forces and moments which trim the aircraft model.

Trim is cast as a generic constrained optimization problem, for which only the objective function has to be defined on the basis of the desired application study. The following subsections present the various parts of the optimization problem structure, while several implementations of the approach are presented in the following Section 6.3.

6.2.1. ASSIGNED TRIM PARAMETERS

The value of a certain number of variables has to be assigned to assure that the trim problem is well-posed. This is generally requested to prevent the existence of explicit relations among trim controls that are also state variables [167]. For the present formulation, these are collected in Equation 6.8. Obviously, the heading angle χ is a meaningful parameter only in geo-referenced applications or in presence of wind fields, but otherwise has no influence on the outcome of the trim problem.

$$\boldsymbol{\tau}_0 = \left\{x^{\mathrm{e}}, y^{\mathrm{e}}, z^{\mathrm{e}}, \chi, V, \dot{\psi}, \dot{\theta}, \dot{\phi}\right\}^{\mathrm{tr}} \tag{6.8}$$

Additional equality constraints may have to be imposed for other trim controls, depending on the application. These can be written in matrix form as in Equation 6.9. For example, assigning the value of β is not strictly necessary for posing the trim problem correctly, but is desired to uniquely identify the trim flight condition. Similarly, the flight path angle or throttle level may be specified to characterize a particular flight scenario, such as climbing or landing.

$$A^{\mathrm{eq}}\boldsymbol{\tau} = b^{\mathrm{eq}} \tag{6.9}$$

6.2.2. TRIM CONTROLS AND BOUNDS

The trim controls set $\boldsymbol{\tau}$ has been conceptually separated into three subsets: the pilot inputs subset $\boldsymbol{\Pi} = \{\delta_{\mathrm{lat}}, \delta_{\mathrm{lon}}, \delta_{\mathrm{dir}}, \delta_T\}$, the aircraft attitudes subset $\boldsymbol{\Theta} = \{\gamma, \psi, \theta, \varphi, \beta\}$, and the control actions subset $\Delta C_{\boldsymbol{A}} = \{\Delta C_X, \Delta C_Y, \Delta C_Z, \Delta C_{\mathcal{L}}, \Delta C_{\mathcal{M}}, \Delta C_{\mathcal{N}}\}$. Pilot inputs are normalized and bounded to the $[-1, 1]$ interval, apart from the throttle level which is bounded to $[0, 1]$. The attitude angles are bounded to the $[-\pi/6, \pi/6]$ interval, while the control actions are left unbounded.

The $\boldsymbol{\Pi}$ and $\Delta C_{\boldsymbol{A}}$ subsets share the purpose of generating control forces and moments that need to be allocated to the effectors. In these regards, and depending on the architecture of the FCS, they may have overlapping contributions to the results of the trim problem. Since the current work focuses on the application of CA methods, the latter subset is retained, and the effective subset of pilot inputs is reduced to $\boldsymbol{\Pi} = \{\delta_T\}$. The resulting generic set of trim controls, used as a baseline for all the following applications, is shown in Equation 6.10.

$$\boldsymbol{\tau} = \left\{\delta_T, \gamma, \dot{\psi}, \theta, \varphi, \beta, \Delta C_{\boldsymbol{A}}\right\} \tag{6.10}$$

6.2.3. LINEAR CONSTRAINTS DUE TO THE AAS GEOMETRY

A special set of linear inequality constraints and additional equality constraints is enforced for trim control actions, to imply that each point $\Delta C_{\boldsymbol{A}}$ has to be in the interior or on the boundary of every possible AAS. The linear constraints equations are reported in Equation 6.11. The actual value of the constraints comes as the results of the following preliminary optimization problem.

For every relevant direction of Action Space, flight parameters α and β, and control effectors positions $\boldsymbol{\delta}$ are varied to obtain the B matrix which results in the AAS spanning the most distance in that direction. Once the most extended AAS in every direction is obtained, the convex hull of all AASs is calculated. This is not an AAS itself, but rather is the smallest convex set containing all the most extended AASs. Hence, it serves well the purpose to establish the feasible region for trim control actions.

$$A_{\text{ch}}^{\text{ineq}} \Delta C_{\boldsymbol{A}} \leq b_{\text{ch}}^{\text{ineq}} \tag{6.11a}$$

$$A_{\text{ch}}^{\text{eq}} \Delta C_{\boldsymbol{A}} = b_{\text{ch}}^{\text{eq}} \tag{6.11b}$$

The inequalities are always well defined because the convex hull is, by definition, a convex set. The equalities are non-null if any of the edges, facets, or $(N_{\boldsymbol{A}}-1)$-dimensional elements constituting the boundary of the convex hull is parallel to any reference axis in Action Space. The A_{ch} matrices and b_{ch} column arrays constitute the Linear Constraint Representation (LCR) of the convex hull (Equation 6.12), and have been calculated using the `vert2lcon` [2] routine in MATLAB.

$$\text{LCR}_{\text{ch}} = \left\{ A_{\text{ch}}^{\text{ineq}}, b_{\text{ch}}^{\text{ineq}}, A_{\text{ch}}^{\text{eq}}, b_{\text{ch}}^{\text{eq}} \right\} \tag{6.12}$$

With this approach, the number of inequality constraints depends on the dimension of Action Space $N_{\boldsymbol{A}}$, and on the number of control effectors $N_{\boldsymbol{\delta}}$. For large problems, it can grow to the order of thousands. An alternative, less strict approach to construct such constraints may consist in wrapping the convex hull in its bounding hyper-rectangle. In this case, the inequality constraints would only be $2N_{\boldsymbol{A}}$, corresponding to the boundary elements of the hyper-rectangle (4 edges of a rectangle in $\mathbb{R}^2$, 6 faces of a parallelepiped in $\mathbb{R}^3$, and so on).

6.2.4. NON-LINEAR CONSTRAINTS

Most importantly, the non-linear equality constraints of Equation 6.13 enforce that the solution of the optimization problem is actually representative of a trim condition, as defined in Equation 6.2.

$$\boldsymbol{f}(\boldsymbol{\tau}_0, \boldsymbol{\tau}) = \mathbf{0} \tag{6.13}$$

Additional inequality constraints may be enforced on the angle of attack, to ensure that the resulting trim conditions are contained in the region described by the aircraft aerodynamic model. Because α is neither a trim control, nor a state variable, these have

[2] M. Jacobson (2021). Analyze N-dimensional Convex Polyhedra `https://www.mathworks.com/matlabcentral/fileexchange/` MATLAB Central File Exchange. Accessed: February 7, 2022

to be formulated as non-linear constraints for the present flight mechanics model, but are simply expressed as in Equation 6.14.

$$\alpha_{\text{lb}} \leq \alpha \leq \alpha_{\text{ub}} \tag{6.14}$$

6.2.5. SOLUTION AND ALGORITHM

A flowchart overview of the trim problem formulation and implementation is presented in Figure 6.3. At each solver iteration, the control effectiveness matrix B is calculated using the current tentative value of α and β, and the value of $\boldsymbol{\delta}$ from the previous trim iteration. Hence the AAS geometry evolves throughout the optimization routine, and is not frozen to the moment of the initialization. This is especially important for the evaluation of control authority. The effectors positions $\boldsymbol{\delta}$ are calculated at each iteration using the DA method.

The optimization problem is solved with the `fmincon` routine in MATLAB, using the interior-point algorithm. As the problem is non-smooth, also due to the sharp corners of the AAS geometry, the solver stops either by reaching an optimality tolerance of 10^{-3}, or a step size of 10^{-6}. All bounds and constraints are respected with a tolerance of 10^{-6}.

In the next section, several application studies are presented by introducing their objective function, the selected control forces and moments in Action Space, and by analyzing the resulting trim conditions. As it could be expected, the solver finds local optima that, in general, depend on the first-guess values of the trim controls. Sensitivity of the trim solution to initial conditions is hard to estimate in general terms, as it heavily depends on the set of allocated aerodynamic actions, and on the specified flight condition. Flight conditions for which the aircraft has significant control power available generally show little sensitivity to initial guesses. On the contrary, flight conditions closer to the edge of the flight envelope (low speed, for example) may result in different, more extreme trim results. For this reason, each of the following case studies has been performed twenty times by assigning random initial values to $\Delta C_{\boldsymbol{A}}$, all within the AAS. Only the results with the best value of the respective objective function are reported for brevity.

6.3. APPLICATIONS AND RESULTS

For all of the following applications, trim is performed at standard sea level conditions for a horizontal trajectory. The flight path and side-slip angles are specified as additional equality constraints, as shown in Equation 6.15. For most (but not all) applications, coordinated flight is additionally imposed by setting $\beta_0 = 0$.

$$\gamma^{\text{tr}} = 0 \tag{6.15a}$$

$$\beta^{\text{tr}} = \beta_0 \tag{6.15b}$$

The definitive baseline set of trim controls used in the following applications is then reported in Equation 6.16. The engine throttle is mainly devoted to trimming for the prescribed airspeed. Given a fixed flight path angle, the pitch angle is mainly devoted to trimming for the necessary angle of attack. The remaining attitude angles are devoted to accomplishing the prescribed side-slip and lateral-directional equilibrium. Finally, the

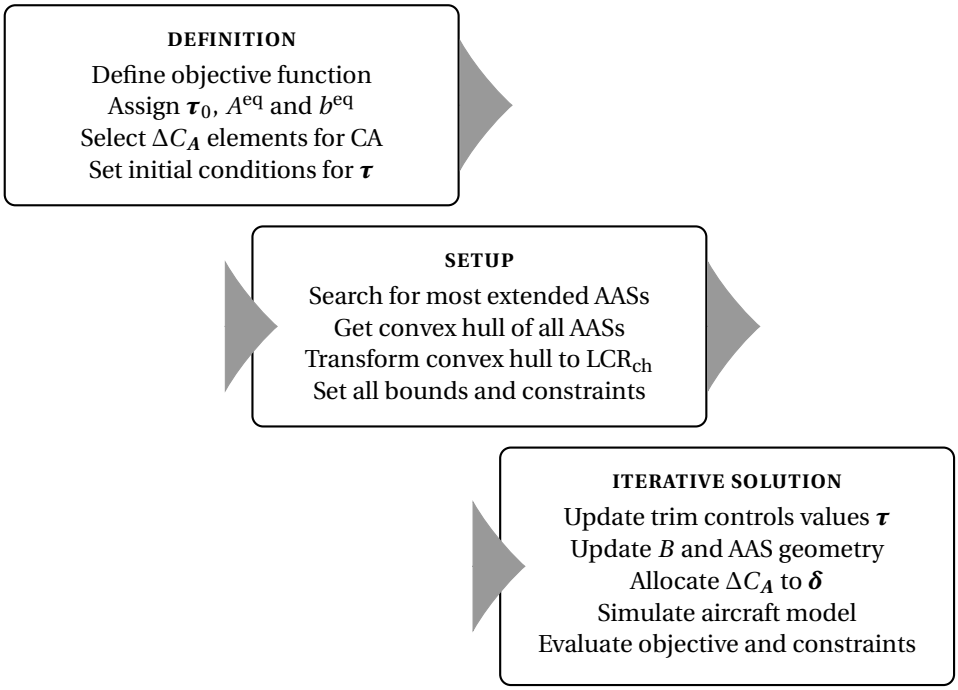

Figure 6.3 Flowchart overview of the trim problem formulation and implementation.

allocated control actions are devoted to minor force and moment adjustments, the rotational equilibrium about the aircraft center of mass, and the improvement of the value of the trim objective function.

$$\boldsymbol{\tau} = \{\delta_T, \psi, \theta, \varphi, \Delta C_{\boldsymbol{A}}\} \tag{6.16}$$

6.3.1. MAXIMUM CONTROL AUTHORITY

Two approaches are presented for the current application, based on two slightly different definitions of control authority. Both approaches revolve around the search of a limit point for the calculation of the trim objective function. The limit point is calculated by solving a simple optimization sub-problem at every step of the overarching trim problem. The objective functions and their respective limit points are briefly characterized in the following sub-sections before presenting the actual applications and results.

DEFINITION OF CONTROL AUTHORITY ABOUT A GIVEN DIRECTION

With reference to Equation 6.7, trimming the aircraft for maximum control authority about a specified motion axis (direction of Action Space) means finding $\Delta C_{\boldsymbol{A}}^{ref} = \Delta C_{\boldsymbol{A}}^{tr}$ in the interior or on the boundary of the AAS, so that its distance to $\Delta C_{\boldsymbol{A}}^{lim}$ is maximum and Equation 6.2 is verified.

As already introduced in Section 6.1.1, from a geometric perspective, $\Delta C_{\boldsymbol{A}}^{lim}$ is the furthest point from $\Delta C_{\boldsymbol{A}}^{ref}$ which simultaneously belongs to the half-line ℓ and the AAS.

Its position results from the solution of Equation 6.17, where both the AAS and ℓ can be expressed in terms of the linear equality and inequality constraints corresponding to their respective LCR representations.

Once the limit point is found, the optimal value of the objective function $\mathcal{J}_*^{\text{lim}}$ is the specified control authority for the current reference point $\Delta C_{\boldsymbol{A}}^{\text{ref}}$. This is obviously a function of $\Delta C_{\boldsymbol{A}}^{\text{ref}}$ itself, and, in order to be maximized, the objective function of the overarching trim problem has to be formulated as in Equation 6.18.

$$\Delta C_{\boldsymbol{A}}^{\text{lim}} = \arg \left\{ \begin{array}{ll} \max\limits_{\Delta C_{\boldsymbol{A}}} & \mathcal{J}^{\text{lim}} = \left\| \Delta C_{\boldsymbol{A}} - \Delta C_{\boldsymbol{A}}^{\text{ref}} \right\|^2 \\ \text{subj. to} & \Delta C_{\boldsymbol{A}} \in \{\text{AAS} \cap \ell\} \end{array} \right\} \tag{6.17}$$

$$\max_{\boldsymbol{\tau}} \quad \mathcal{J}^{\text{tr}} = \Delta \mathcal{A}_\ell = \left\| \Delta C_{\boldsymbol{A}}^{\text{lim}} - \Delta C_{\boldsymbol{A}} \right\| \tag{6.18}$$

DEFINITION OF BALANCED CONTROL AUTHORITY

Balanced control authority $\Delta \mathcal{A}_0$ is here conveniently defined as the average distance to all the vertices of the AAS. Therefore, the point of the AAS which results in the maximum $\Delta \mathcal{A}_0$ is the point with the minimum sum of distances to all of the AAS vertices. Such limit point $\Delta C_{\boldsymbol{A}}^0$ coincides with the centroid of the AAS [171] and, in case all the control effectors position limits are symmetric, with the origin of Action Space. In general, its position can be calculated by solving the optimization problem of Equation 6.19, where d_i is the distance between the candidate point $\Delta C_{\boldsymbol{A}}$ and the i-th vertex of the AAS, and n is the number of vertices of the AAS.

Once the limit point is found, the overarching trim problem to maximize $\Delta \mathcal{A}_0$ can be formulated in terms of minimizing the distance between the candidate trim point $\Delta C_{\boldsymbol{A}}^{\text{ref}}$ and $\Delta C_{\boldsymbol{A}}^0$ itself, as shown in Equation 6.20.

$$\Delta C_{\boldsymbol{A}}^0 = \arg \left\{ \begin{array}{ll} \min\limits_{\Delta C_{\boldsymbol{A}}} & \mathcal{J}^0 = \sum\limits_{i=1}^{n} d_i \\ \text{subj. to} & \Delta C_{\boldsymbol{A}} \in AAS \end{array} \right\} \tag{6.19}$$

$$\min_{\boldsymbol{\tau}} \quad \mathcal{J}^{\text{tr}} = \Delta \mathcal{A}_0 = \left\| \Delta C_{\boldsymbol{A}}^0 - \Delta C_{\boldsymbol{A}} \right\| \tag{6.20}$$

In the broader scope of flight dynamics, balanced control authority could assume an important meaning in the assessment of handling qualities characteristics. If the AAS is transformed into an Attainable Acceleration Set, by making use of the aircraft inertia tensor, a flight maneuver achieving maximum balanced control authority would also achieve minimum total acceleration. This could be relevant for handling qualities criteria which define the desired minimum acceleration value corresponding to the best performance, for a specified flight task.

APPLICATION TO SYMMETRIC FLIGHT WITH 3 DOFS

For this study case, the dynamic simulation is constrained in the vertical plane. The flight condition is longitudinal-symmetric and the aircraft has only 3 DoFs. Control surfaces are constrained to move symmetrically during the CA problem, but each left-right pair is free to move as prescribed by the DA method. These simplifications allow to set $\beta_0 = 0$,

and to allocate only the control lift and pitch moment: $\Delta C_{\boldsymbol{A}} = \{\Delta C_L, \Delta C_{\mathcal{M}}\}$. It is then possible to visualize the AAS, the trim points and the control authorities in Action Space, as shown in Figure 6.4.

In the figure, several similar AASs can be distinguished, each corresponding to the maximum control authority about a different direction of Action Space. This is due to the fact that different control authorities are obtained with different trim values of the angle of attack and control surface deflections. Because aerodynamic control actions are a function of both α and $\boldsymbol{\delta}$, as expressed in the aerodynamic model of Equation 3.1, each of the optimum trim points is associated with a slightly different control effectiveness matrix B, which results in a slightly different geometry of the AAS. The latter is exploited to calculate the maximum control authority about the prescribed axis.

The position of trim points in the AAS is in line with expectations, and their relative arrangement is preserved for all analyzed airspeed values. A preferential diagonal direction is highlighted by trim points in Action Space, taking the form of a clear tradeoff between the control lift and pitch moment that are necessary for trim at different angles of attack. For example, a negative control lift is needed to maximize the lift-up and pitch-up control authority. This corresponds to a positive pitch-up control moment, in a similar way to what happens with conventional aircraft configurations, and a relatively high trim angle of attack. The opposite is true for lift-down and pitch-down control authorities.

The trim point for balanced control authority is very close to the centroid of the AAS, but not precisely coincident with it. This is due to the fact that the aircraft is not trimmable with completely null control surface deflections. For the same reason, the trim points corresponding to the other control authorities are not on the boundary of the AAS. In such conditions, despite maximizing the prescribed objective function, they would not guarantee the compliance with the trim constraints. In all cases, it is evident how the control deflections are deployed to maximize control authority in the given direction, while the angle of attack is adjusted to guarantee vertical equilibrium.

The same study has been repeated at various airspeeds, and the results for control authority and angle of attack are synthetically reported in Figure 6.5. Optimum control authority is very different on the basis of the axis it relates to, but it is comparable for the two directions on each axis. For all airspeeds, control power about the pitch axis is greater than the one about the lift axis, while balanced control authorities lies between the two. Despite the latter comparison may be slightly improper, as it involves both forces and moments, it is dimensionally sound since control authority has been defined on the basis of dimensionless coefficients (Equation 6.7). All angles of attack decrease with increasing airspeed, as it would be expected. The most interesting insights arise when inspecting the relation between the angle of attack and control surface deflections at trim. This is the main focus of the next study case.

APPLICATION TO SYMMETRIC AND ASYMMETRIC FLIGHT WITH 6 DOFS

In the present study case, the aircraft is free to move with 6 DoFs and all control surfaces are independent, apart from the two rudders which are forced to move as one. The set of allocated actions has been chosen to be $\Delta C_{\boldsymbol{A}} = \{\Delta C_L, \Delta C_{\mathcal{L}}, \Delta C_{\mathcal{M}}, \Delta C_{\mathcal{N}}\}$, which is an extension of the classic “three moment” CA problem. The lift force has been included

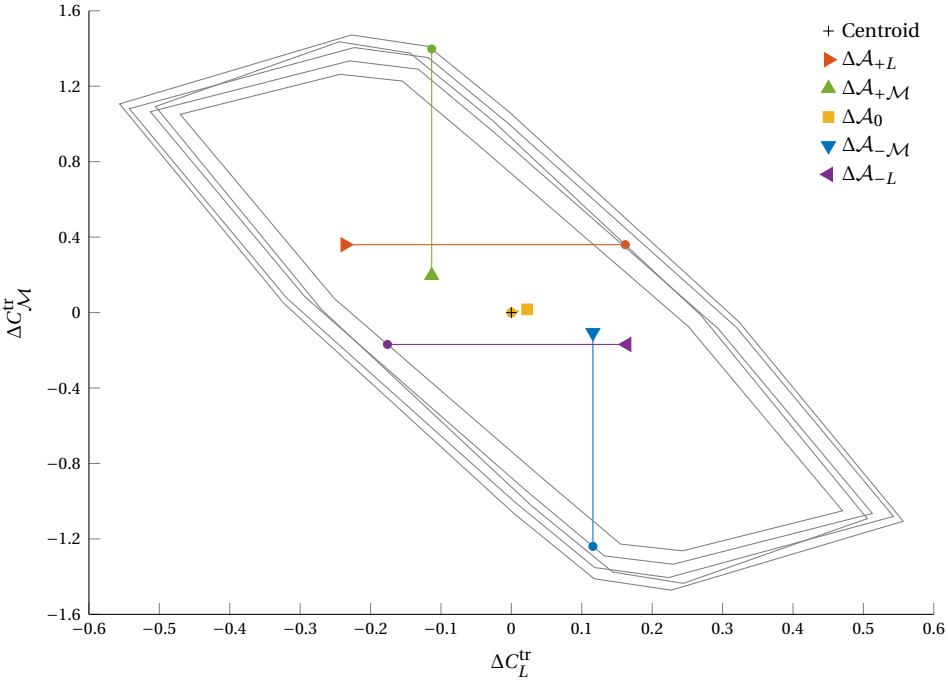

Figure 6.4 Position in Action Space of trim points maximizing control authorities about the pitch and lift axes, for $V^{\text{tr}} = 180\,\text{m/s}$.

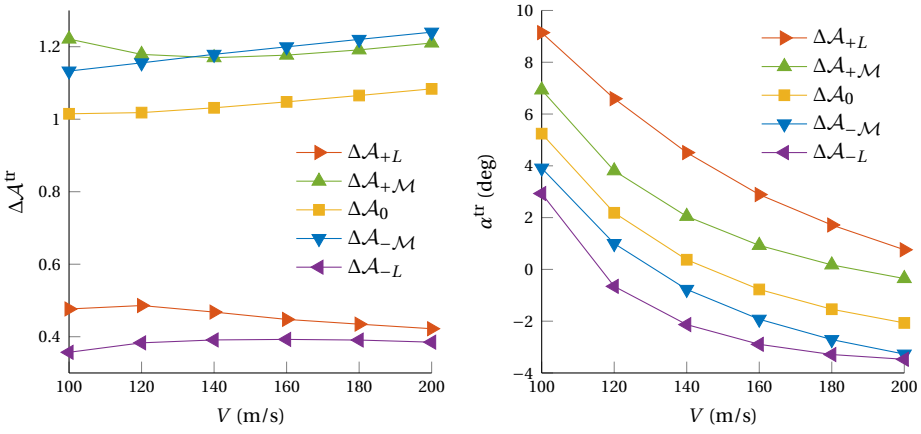

a) Control authority **b)** Angle of attack

Figure 6.5 Maximum control authority and corresponding angle of attack for various airspeeds and directions in Action Space.

in order to be able to maximize control authority about its axis. The symmetric flight condition is investigated by imposing $\beta_0 = 0$, and the asymmetric one by imposing the maximum side-slip angle allowed by regulations. In case of side-wind of magnitude V_{sw}, it is $\beta_0 = V_{sw}/V^{tr}$ [132].

As done previously, results are compared for maximum control authority in both directions of the lift and pitch axes, and for maximum balanced control authority. Since the AAS is a subset of $\mathbb{R}^4$ for this application, results cannot be shown in Action Space. Attention is focused on the optimal control surfaces deflections at trim, shown in Figure 6.6, and on the other trim controls, reported in Table 6.2. Control surface deflections on the main wings are positive if with trailing edge down, negative if with trailing edge up. The vertical axis in the figure has been inverted to reflect this convention. Rudders deflections are positive if they cause the aircraft nose to point left of the flight path.

For the symmetric flight condition, control surface deflections on the front wing range from the positive to the negative saturation limit, depending on which control authority is maximized (Figure 6.6a). Deflections are practically symmetric, although not perfectly so. This is most likely due to numerical precision, and explains the very small, non-null value of the roll angle. Maximum lift-up control authority is achieved with very negative deflections, both on the front and on the rear wing, paired up with a significant positive angle of attack $\alpha^{tr} = 5.1\,\text{deg}$. Maximum lift-down control authority is achieved with mostly large positive deflections at a negative angle of attack of $\alpha^{tr} = -4.5\,\text{deg}$. This reflects the behavior seen in the previous study case, and clearly shows how the optimizer trades α-generated lift with $\boldsymbol{\delta}$-generated lift in order to maximize the specified control authority.

In a similar way, the maximum pitch-down control authority is achieved by exploiting the pitch-down moment due to the propulsion system. By increasing the throttle level at a very low angle of attack, the solver finds a trim condition with drastic positive deflections on the front wing and negative deflections on the rear wing. Such coupling between the horizontal and rotational equilibrium is not observed for $\Delta\mathcal{A}_{\pm L}$, where the slightly higher throttle setting can be justified by the higher magnitude of the corresponding angle of attack.

Trim conditions for maximum pitch-up control authority and maximum balanced control authority are overall very similar. Both cases are characterized by the same throttle setting, and by small deflections on both the front and the rear wing. As just observed, pitch control moment can be manipulated more significantly than control lift through the alteration of thrust. But in order to maximize pitch-up control authority with a propulsive system placed above the aircraft center of gravity, thrust should be reduced as much as possible. In order to achieve horizontal equilibrium with low thrust, drag must also be kept low by employing small deflections of the control surfaces. The same reasoning in inverse order can be carried out to explain the results for the $\Delta\mathcal{A}_0$ case.

For the asymmetric flight condition, all control surface deflections show a similar behavior, slightly stretching in magnitude according to which control authority is maximized (Figure 6.6a). The front inner surfaces are adjusted asymmetrically to provide for the necessary roll moment, together with the two tail rudders correcting for the necessary yaw moment. The front outer surfaces and all the rear ones are then adjusted for optimizing control authority. Trends in the remaining flight parameters are overall

less evident and the numerical values less extreme. This happens because more control power is required to achieve basic trim, leaving less available control authority to the objective function.

Control surfaces on the front wing show more complex behavior than the ones on the rear wing, which are deflected by the same angle in all cases. This can be explained by the fact that front control surfaces have a smaller moment arm with respect to the aircraft center of gravity. Hence, they are able to alter control lift with a small impact on control pitch, and they may be preferred by the solver as they do not cause important coupling effects.

6.3.2. MINIMUM AERODYNAMIC DRAG

In each of the previous applications, the same CA method has been used to explore the properties of trim conditions maximizing control authority in different directions of Action Space. In the present section, the same objective function is optimized using different Action Space dimensions, with the intention to study the impact of the AAS geometry on the optimal objective function value. The present application aims at minimizing total aerodynamic drag at trim conditions, as expressed by Equation 6.21. Total aerodynamic drag includes the contributions of the clean aircraft geometry, as well as the one of control surfaces, and is calculated using the standard aerodynamic model presented in Equation 3.1. The dynamic simulation is constrained to 3 DoFs longitudinal-symmetric flight, with $\beta_0 = 0$.

$$\min_{\boldsymbol{\tau}} \quad \mathcal{J}^{\text{tr}} = C_D \tag{6.21}$$

In the first two study cases, the trim problem formulation presented in Section 6.2 has been implemented. The first employs the 2D CA problem already seen in Section 6.3.1. The second explores a 3D CA problem where control drag is additionally included in the trim controls set, hence setting $\Delta C_{\boldsymbol{A}} = \{\Delta C_D, \Delta C_L, \Delta C_{\mathcal{M}}\}$. As done previously, control surfaces are only constrained to move symmetrically during the CA problem, but each left-right pair is free to move according to the DA algorithm.

In the third and last study case, trim is performed by using a mechanical FCS, which links pilot inputs to the control effectors by means of a conventional gearing and ganging matrix. Therefore, only in this case, the control actions subset $\Delta C_{\boldsymbol{A}}$ is completely replaced by the pilot inputs subset $\boldsymbol{\Pi}$, introduced in Section 6.2.2. All control surfaces are constrained to move symmetrically, the inboard ones move in opposition (as conventional elevators), while the outboard ones move in agreement (as DLC effectors).

The resulting minimum trim drag has been reported in Figure 6.7 for various airspeeds. All drag coefficient curves with respect to airspeed follow the expected $C_D \propto V^{-4}$ relation. This can be easily obtained by substituting the vertical equilibrium equation in the parabolic drag polar model, as show in the following Equation 6.22.

$$C_L = \frac{2mg}{\rho_\infty V^2 S} \quad \Rightarrow \quad C_D = C_{D_0} + kC_L^2 = C_{D_0} + \frac{k}{V^4}\left(\frac{2mg}{\rho_\infty S}\right)^2 \tag{6.22}$$

The formulation with the 3D AAS is able to achieve a slightly lower minimum drag coefficient at any airspeed. This is probably due to the inclusion of information on ΔC_D in the geometry of the AAS itself. Conventional ganging gives the worst performance

Table 6.2 Trim controls for symmetric and asymmetric trimmed flight, maximizing control authority about different directions in Action Space, for $V^{\text{tr}} = 170\,\text{m/s}$.

	$\beta_0 = 0\,\text{deg}$				$\beta_0 = 4.3\,\text{deg}$			
	$\alpha^{\text{tr}} = \theta^{\text{tr}}$ deg	φ^{tr} deg	ψ^{tr} deg	δ_T^{tr} —	$\alpha^{\text{tr}} = \theta^{\text{tr}}$ deg	φ^{tr} deg	ψ^{tr} deg	δ_T^{tr} —
$\Delta\mathcal{A}_{+L}$	5.1	0.0	0.0	0.72	4.1	16.2	-3.3	0.69
$\Delta\mathcal{A}_{+\mathcal{M}}$	-1.9	0.1	0.0	0.59	0.9	19.4	-4.2	0.49
$\Delta\mathcal{A}_0$	-1.7	0.1	0.0	0.59	2.9	16.7	-3.6	0.70
$\Delta\mathcal{A}_{-\mathcal{M}}$	-0.9	-0.5	0.0	0.89	0.9	18.8	-4.2	0.47
$\Delta\mathcal{A}_{-L}$	-4.5	0.2	0.0	0.78	1.4	17.9	-4.1	0.76

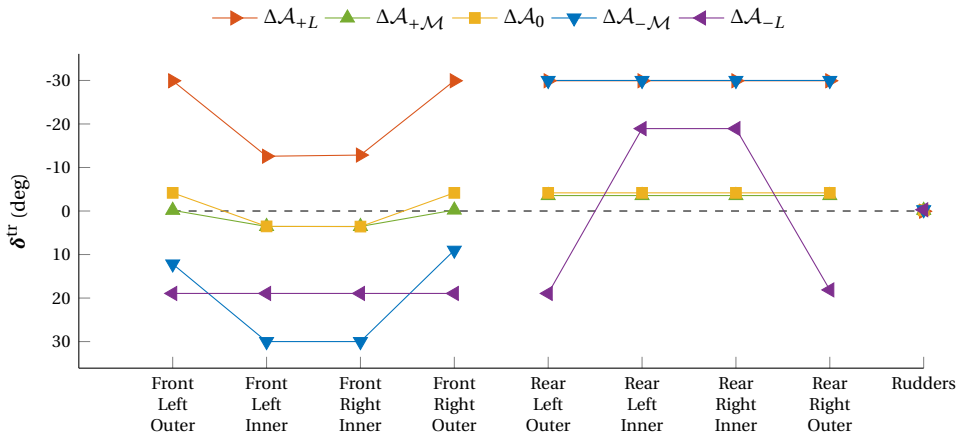

a) Symmetric flight, $\beta_0 = 0\,\text{deg}$.

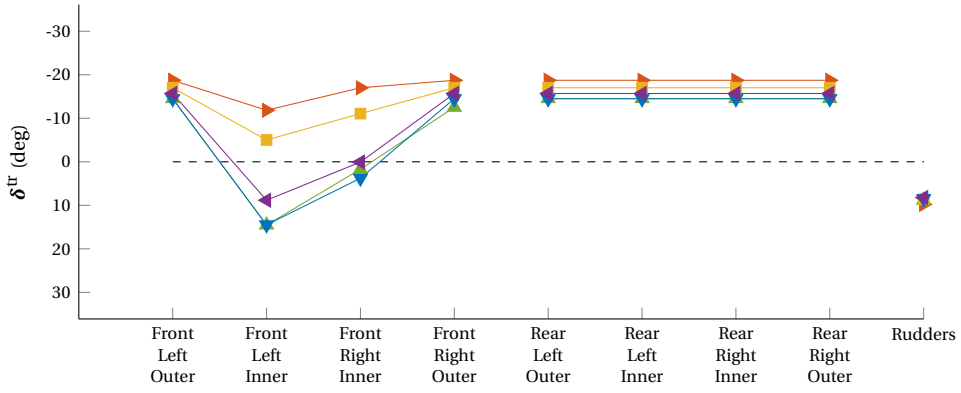

b) Asymmetric flight, $\beta_0 = 4.3\,\text{deg}$.

Figure 6.6 Control surface deflections maximizing control authorities about different directions in Action Space, for $V^{\text{tr}} = 170\,\text{m/s}$.

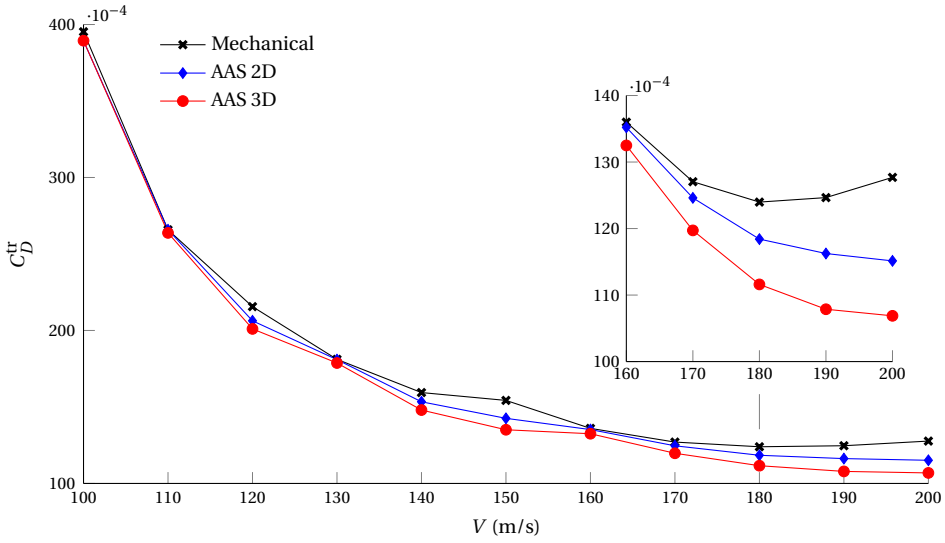

Figure 6.7 Minimum trim drag as a function of airspeed using different CA methods and allocated forces. 3 DoFs longitudinal-symmetric flight.

overall, as expected. For $V = 200\,\text{m/s}$, the corresponding drag curve has already passed its minimum, while the curve of the 3D AAS has not flattened yet. At this airspeed, the difference between drag coefficients at trim is maximum and equal to about 20 drag counts.

Figure 6.8 shows the corresponding trim angle of attack and throttle. All CA methods perform very similarly, but a trend is visible especially at higher values of the airspeed. Some numerical fluctuations are visible for the throttle values in the range of airspeeds from 130 m/s to 170 m/s. These are probably due to the underlying propulsive model, since they appear for all three CA methods, including the one using only a mechanical linkage. The conventional ganging method converges to a smaller α^{tr} if compared to the ones based on the AAS geometry. On the other hand, it requires a slightly higher throttle level for every airspeed. Interestingly, both the angle of attack and the throttle curves for the minimum drag solution are similar in shape and values, although not equal, to the solutions for the maximum balanced control authority study presented in Section 6.3.1 (only the angle of attack has been reported in Figure 6.5b, for brevity). This suggests that trim conditions achieving the maximum balanced control authority, or in other words the minimum control effort, are close to those achieving minimum drag. As a matter of fact, both optimal conditions are achieved with small deflections of control surfaces, and small values of the angle of attack.

6.3.3. ASSIGNED PITCH ANGLE

For this last application, the objective function to be minimized is the absolute difference between the achieved and a prescribed value of the pitch angle at trim. All the assumptions from the previous section hold, with the difference that only the 2D CA prob-

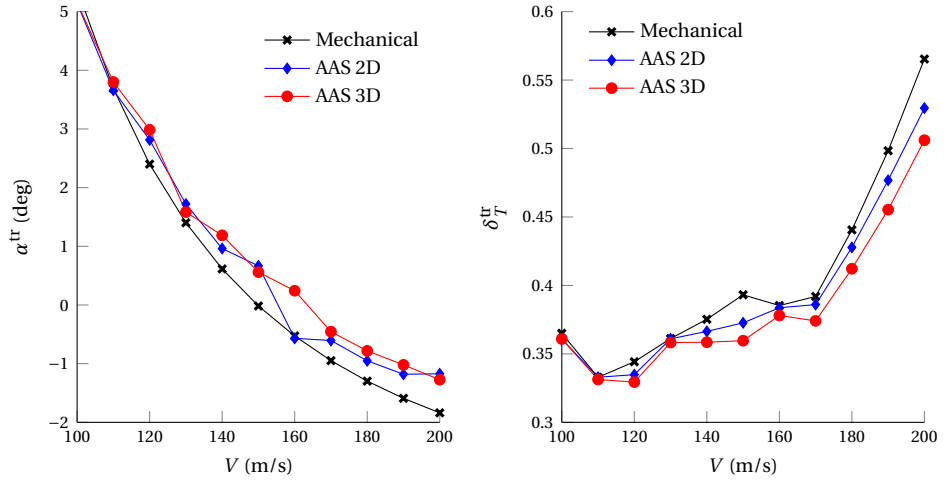

a) Angle of attack **b)** Throttle level

Figure 6.8 Trim angle of attack and throttle level as a function of airspeed using different CA methods and allocated forces. 3 DoFs longitudinal-symmetric flight.

lem with lift and pitch moment has been implemented in this case. This is in light of the small differences among results of the previous study, and due to drag being irrelevant to the analysis of the present flight scenario. Therefore, the trim control actions subset is $\Delta C_{\boldsymbol{A}} = \{\Delta C_L, \Delta C_{\mathcal{M}}\}$ and the objective function is reported in Equation 6.23.

$$\min_{\boldsymbol{\tau}} \quad \mathcal{J}^{\text{tr}} = \left|\theta - \theta^{\text{ref}}\right| \tag{6.23}$$

Such an objective function has been chosen to test the box-wing capabilities to trim the aircraft at precise body attitudes, and to obtain the limits within which this task is possible for a given aircraft model. This can be desired for flight tasks which require precise attitude hold, such air refueling, or to improve passenger comfort in landing conditions, for example.

Results are shown in Figure 6.9, in the form of a correlation between the achieved value of the trim pitch angle and an array of prescribed values for the same angle. The horizontal segments of each curve highlight the minimum and maximum pitch angle at which trim is achievable for the given airspeed. The diagonal segments between these values delineate the region for which it is possible to trim the aircraft for any specified pitch angle at the given airspeed. The same information is summarized in Figure 6.10, which shows the minimum and maximum trim pitch angles as a function of airspeed.

In almost all cases, the extreme values of θ^{tr}, which is also equal to α^{tr} because $\gamma_0 = 0$, coincide with the values of the angle of attack that maximize the control authorities shown in Figure 6.5b. This confirms, once again, that the solver presented in Section 6.3.1 is able to push α-generated lift to its limit in order to optimize $\boldsymbol{\delta}$-generated lift and pitch moment.

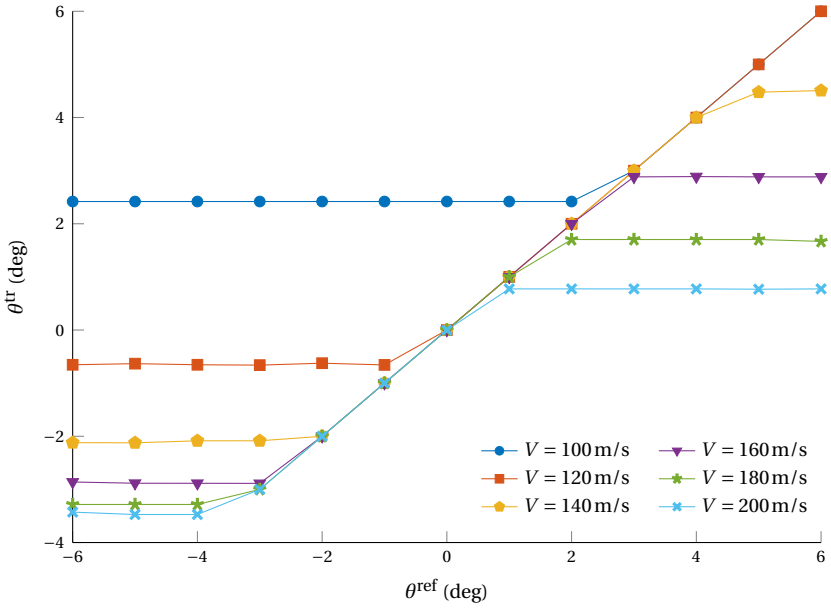

Figure 6.9 Achieved and prescribed trim pitch angles for different airspeed values, using the 2D AAS CA method.

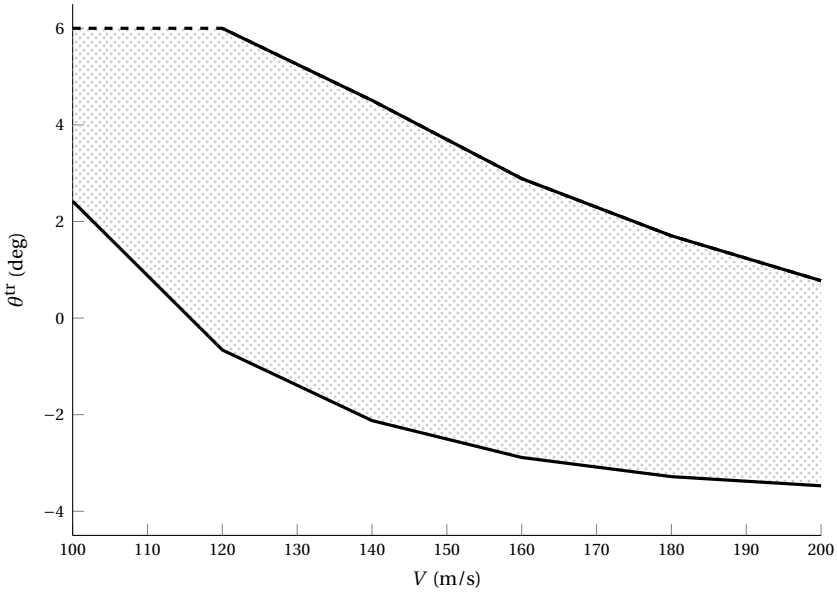

Figure 6.10 Trim pitch angle envelope as a function of airspeed, using the 2D AAS CA method. The dashed line indicates that no maximum has been explicitly found for the corresponding airspeed range with the performed numerical simulations.

6.4. CONCLUSIONS

This chapter has presented a generic trim problem formulation, in the form of a constrained optimization problem, which employs forces and moments due to the aircraft control effectors as trim controls. The linear programming formulation of the DA method has been used to map the control forces and moments to the corresponding control effectors positions. The geometry of the AAS is used in all cases for defining a set of linear equality and inequality constraints, which ensure that control forces and moments are attainable by the control effectors.

A definition of control authority has been given, which is entirely based on control forces and moments, independent of the aircraft configuration and/or number of control effectors. It has been interpreted geometrically as a distance between a reference point and a limit point within the AAS.

With application to the PrP, the trim methodology is used to compare trim conditions for maximum control authority in the pitch axis, in the lift axis, and for maximum balanced control authority about all motion axes. For these applications, the AAS geometry is also used at each solver iteration to calculate the value of the trim objective function. Results show that the method is able to capitalize on the angle of attack or the throttle setting to obtain the control surface deflections which maximize the assigned control authority.

Another application has been performed to minimize total aerodynamic drag, using a 2D or 3D AAS geometry. The former involves the allocation of control lift and pitch moment, while the latter also includes control drag. These approaches have also been compared to a standard trim problem formulation, which relies on the pilot stick input rather than control forces as trim controls, and does not employ any CA method. The three formulations all perform similarly under every point of view, but the one using the 3D AAS achieves slightly smaller drag, probably thanks to the inclusion of control drag in the AAS geometry. Trim conditions for this application are overall similar to those achieved for maximum balanced control authority.

Lastly, an application study to achieve an assigned value of the pitch angle has been carried out. This flight scenario was deemed interesting to investigate the ability of box-wing aircraft to (partially) decouple lift and pitch moment control. The extreme values of the trim pitch angle achieved coincide with the values of the angle of attack that maximize control authorities in the first study case. This confirms, once again, that the solver is able to push α-generated lift to its limit in order to optimize $\boldsymbol{\delta}$-generated lift and pitch moment.

The optimization problem is iterative and non-smooth in nature, and therefore only capable of finding local optima. These usually depend on the initial condition chosen for the selected trim controls. Therefore, several optimization runs of the same flight condition may be required to find a global optimum. Because of this, the proposed method can only be used off-line, for the generation of trim databases to be accessed at later stages, in faster applications.

Future research efforts can be devoted to improving the presented methodology when strongly non-linear aerodynamics is involved, or when searching for optimum trim conditions in the drag rise airspeed range. For example, the trim formulation has proven able to successfully minimize total aerodynamic drag, but optimization of control authority

about the drag axis is still problematic due to chattering. In particular, in proximity of the combination of control surface deflections resulting in minimum control drag, all the elements in the drag row of the control effectiveness matrix tend to zero. This leads the AAS to collapse about one dimension in Action Space (e.g. from 3D to 2D) and deteriorates the numerical calculation of the linear constraints representing its geometry, as well as the calculation of control authority as the objective function. Including control drag as an allocated force could be interesting to explore flight scenarios like trim in steep descent conditions.

Lastly, time domain simulations are recommended to study the impact of the selected control authority on maneuvering flight starting from the achieved trim condition. Given a specific maneuver to be performed after trim is achieved, a criterion to find which control authority has to be optimized to obtain best maneuver performance could be sought.

7

TRANSIENT DYNAMIC RESPONSE

The real voyage of discovery
consists not in seeking new landscapes,
but in having new eyes.

Marcel Proust
In Search of Lost Time
1923

They always say that time changes things,
but you actually have to change them yourself.

Andy Warhol
The Philosophy of Andy Warhol
1975

The previous chapter has been devoted to finding equilibrium conditions for an aircraft model equipped with redundant control surfaces. But the capability to employ DLC finds the most interesting advantages in maneuvering flight. This chapter presents a novel CA approach which is capable of shaping the transient response of the aircraft by inducing a preferred position of the Control Center of Pressure (CCoP). This is the center of pressure due to only aerodynamic control actions and, for a given flight condition $\{\alpha, \beta, M\}$, depends only on control surface deflections. By using the longitudinal position of the CCoP as a top-level FCS input, it is shown how to achieve transient response characteristics that are typical of DLC or CPC. Several applications show how DLC achieves better performance in terms of flight precision, disturbance rejection and comfort on board when performing fast, sharp maneuvers.

Parts of this chapter have been published in the Aerospace Science and Technology journal in 2021 [172].

After the following Section 7.1 briefly recaps the most relevant DLC concepts, first introduced in Chapter 1, Section 7.2 goes into more detail on the employed FCS architecture, as well as on the procedure implemented to tune it. The proposed novel CA formulation is then presented in Section 7.3, together with a formal mathematical definition of the position of the CCoP. Three relevant application studies are presented in Section 7.4, with results and discussion. A fundamental study case on a simple pull-up maneuver is performed in Section 7.4.2, with highlights on time responses of the aircraft load factor, control surface deflections, and pitch rate flying qualities. Two more study cases on an altitude shift and an altitude hold maneuver are then presented in Sections 7.4.3 and 7.4.4, respectively, with considerations on tracking precision, agility quickness and perceived comfort on board. Lastly, conclusions are drawn in Section 7.5, with an outlook on future research possibilities.

7.1. INTRODUCTION

It has already been shown in Chapter 1 how the possibility to install redundant control surfaces, both in front and behind the aircraft center of gravity, allows the PrP to make use of unconventional piloting techniques such as DLC. In Section 1.1, it has also been shown how the characteristics of the transient response majorly depend on the longitudinal position of the CCoP [27]. For example, if the CCoP is very far aft the aircraft neutral point, the transient response will resemble the one of CPC. In this case, the aircraft rotates about a point which is very close to its center of gravity. If the CCoP is ahead of the neutral point by a distance equal to the maneuver margin, the aircraft responds with a constant and sharp vertical acceleration, accompanied by a small pitch rotation to ensure no variation in the geometric angle of attack. In this case, the aircraft rotates about a point which is very far aft its center of gravity.

In the latter case, referred to as Pure DLC, the pilot is supposedly able to achieve fast and precise control of the aircraft trajectory. Such dynamic behavior can be exploited in all flight scenarios that require response quickness and maneuver accuracy. In modern commercial aviation, this is already done through the use of over-the-wing spoilers, to some extent [30, 31]. During approach and landing maneuvers, it is indeed possible to see these movable devices being deflected as one to improve tracking of the vertical descent profile prescribed by the glideslope. An example has been shown at the beginning of this dissertation, in Figure 1.10a). At the same time, differential deflections along the wing span allow spoilers to collaborate with ailerons in ensuring the right lateral-directional attitude. But since spoilers are usually close to the aircraft center of gravity, they cannot exert as much influence on pitch dynamics as elevators can do. Besides, as their actual name suggests, they fundamentally work by spoiling the aircraft aerodynamics, especially lift, hence relying on very limited control power.

With proper front and rear control surfaces, instead, it is possible to modulate their relative deflections, and achieve a desired type of longitudinal dynamics in a much more powerful way. To the authors knowledge, a single research effort has proposed a practical solution to link the tail elevator of conventional configurations with a front control device dedicated to DLC [25]. The work has explored the resulting handling qualities in the vertical and pitch axis, and proposed three new criteria for the assessment of DLC performance. Namely, a DLC “efficiency coefficient”, defined as the ratio between the initial

and steady-state load factor response; a "rate of climb increase" criterion, defined as the difference between the steady-state rate of climb, for the same aircraft, with and without DLC; and a "normalized rate of climb increase" criterion, defined as the ratio between the steady-state rate of climb of the aircraft with DLC and the rate of climb obtainable assuming a constant vertical acceleration.

The present chapter attempts to take a step further in the same direction, by relying on a CA background to achieve similar goals. In short, it presents a CA formulation which is able to alter the dynamic transient response of an aircraft. This is achieved for a given FCS architecture and tuning of its gains. Whereas the aforementioned study relies on tuning the FCS gains and the gearing ratio to obtain the optimal handling qualities performance, the antithetical approach is taken in the present chapter. The FCS parameters are systematically varied to maintain the same inner loop performance, and only the CA method formulation is changed to obtain different dynamic behaviors for the aircraft.

For all of the applications presented in the following sections, symmetric flight has been imposed by constraining the aircraft model to have only 3 DoFs in the vertical plane. The standard aerodynamic model reported in Equation 3.1 has been used, with α ranging from -6 deg to 6 deg in steps of 2 deg. Two Mach numbers have been analyzed, namely $M = 0.3$ and $M = 0.6$. Each control surface has been deflected, independently from all the others, from -30 deg to 30 deg in steps of 15 deg. Lastly, the normal load factor in body axes has been expressed as in Equation 7.1, in order to have $n_z \approx 1$ in straight and level flight.

$$n_z = -\frac{Z^{\mathrm{b}}}{mg} \tag{7.1}$$

7.2. FLIGHT CONTROL SYSTEM ARCHITECTURE

The implemented FCS architecture is reported in Figure 7.1. It consists of a simple airspeed hold, employing the throttle command, and a longitudinal control law based on NDI. The latter technique allows to neatly separate the control law from the CA components, and to use classic methods from linear control theory for tuning the controller gains [160, 161]. Control inputs for the latter are provided either from the pilot stick, with a pitch rate response type, or from an altitude control channel.

The altitude channel employs a series of linear controllers and transformations to achieve stable and robust augmented dynamics [173]. It transforms a reference altitude signal into a commanded pitch rate one. This approach has been chosen to be able to merge the altitude control channel with the pilot stick input, exploiting the same NDI formulation. It also avoids complications due to feedback of vertical acceleration in case of non-minimum phase systems [174]. For the proposed applications, this behavior would be a function of the prescribed position of the CCoP, as explained in the following Section 7.3.

The transformation between the reference vertical acceleration $\ddot{h}_{\mathrm{ref}}$ and the normal load factor assumes there is no variation in airspeed, and is expressed in Equation 7.2a. The transformation between the load factor and the desired angle of attack α_{ref} makes use of the linear approximation of the lift curve in body axes at trim conditions, and is reported in Equation 7.2b. The commanded angle of attack is clipped between -5 deg

and 5 deg to prevent the run-time values of α from exceeding the boundaries of the underlying aerodynamic dataset. Lastly, the transformation between the reference angle of attack rate $\dot{\alpha}_{\text{ref}}$ and the commanded pitch rate q_{cmd} is expressed in Equation 7.2c.

$$\ddot{h} = g\,(n_z \cos\theta - 1) \tag{7.2a}$$

$$q_\infty S\left[C_{Z_0}^{\text{tr}} + C_{Z_\alpha}^{\text{tr}}\left(\alpha - \alpha^{\text{tr}}\right)\right] = -mgn_z \tag{7.2b}$$

$$q = \dot{\alpha} - \frac{g}{V}\left(\cos\theta - n_z^{\text{tr}}\right) \tag{7.2c}$$

Each of the controllers shown in Figure 7.1 has the baseline architecture reported in Figure 7.2, consisting of two cascaded proportional-integral control loops, with a parallel feedthrough branch for improved tracking response [173]. For each controller, the feedthrough gain fraction K_f is assigned manually in order to obtain desired closed-loop characteristics. The proportional gains K_1 and K_2 are left to be determined by an automatic tuning procedure. This is formulated as an optimization problem, with the objective to find the values of the proportional gains that minimize the difference between the closed-loop dynamics of the linear aircraft model and an assigned reference model. Without loss of generality, the latter has been arbitrarily chosen as follows:

- the reference altitude dynamics is a critically damped second order system with a time constant of 2 s;
- the reference airspeed dynamics is a first order system with a time constant of 3 s.

The proprietary Control System Tuner algorithm by MathWorks has been used to solve the optimization problem and find the tuned values of the gains for every case study presented in the present chapter.

In the case of symmetric flight with three-degrees of freedom, the classic NDI of aircraft rotational dynamics resolves to the simple scalar equation reported in Equation 7.3,

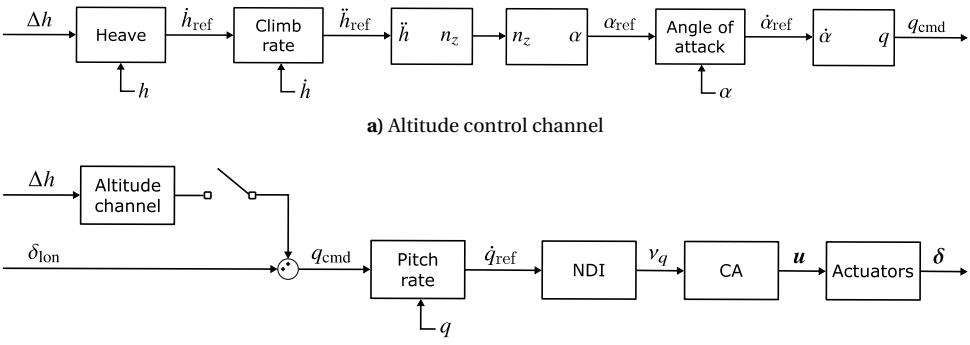

a) Altitude control channel

b) Main flight control law

Figure 7.1 Block scheme overview of the chosen FCS architecture.

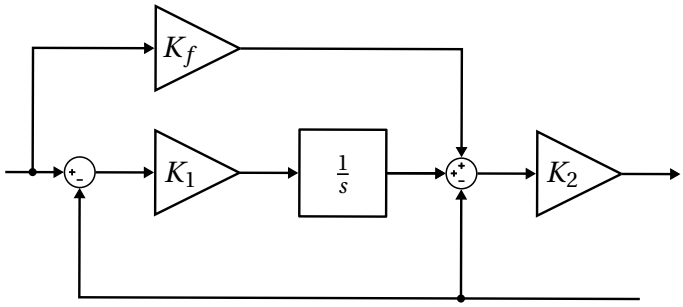

Figure 7.2 Baseline architecture for all controllers shown in Figure 7.1.

where ν_q is the non-dimensional pitch control moment required to obtain the reference pitch acceleration $\dot{q}_{\text{ref}}$.

$$J_{yy}\dot{q}_{\text{ref}} = \frac{\mathcal{M}^{\text{tr}}}{q_\infty S\bar{c}} + \nu_q \tag{7.3}$$

The pitch control moment ν_q, together with null control moments about the roll and yaw axes, is then allocated to the effectors by solving an appropriate CA problem based on Equation 7.4.

$$B\boldsymbol{u} = \boldsymbol{\nu} \quad \Longleftrightarrow \quad \begin{bmatrix} B_{\mathcal{L}} \\ B_{\mathcal{M}} \\ B_{\mathcal{N}} \end{bmatrix} \boldsymbol{u} = \begin{Bmatrix} 0 \\ \nu_q \\ 0 \end{Bmatrix} \tag{7.4}$$

The notation, explained in the following Equation 7.5, has been chosen to highlight the contribution of each row of the B matrix, and is going to be used in the next section, covering the proposed CA formulation.

$$B_H = \begin{bmatrix} \dfrac{\partial C_H}{\partial u_1} & \dfrac{\partial C_H}{\partial u_2} & \cdots & \dfrac{\partial C_H}{\partial u_{N_{\boldsymbol{u}}}} \end{bmatrix} \quad \text{for } H = \mathcal{L}, \mathcal{M}, \mathcal{N} \tag{7.5}$$

7.3. NOVEL CONTROL ALLOCATION FORMULATION

The properties of the CCoP and its relation with the control surface layout of the aircraft have been introduced and thoroughly discussed in Section 1.1 in a qualitative way. The following section provides a formal expression to calculate its longitudinal position, and makes it possible to exploit the CCoP in the formulation of a novel CA approach.

7.3.1. INDUCING THE POSITION OF THE CONTROL CENTER OF PRESSURE

In the scope of symmetric flight in a vertical plane, the non-dimensional longitudinal position of the CCoP in body axes is calculated as in the following Equation 7.6 [27].

$$\bar{x}_\delta = \frac{x_\delta}{\bar{c}} = -\frac{\sum_{i=1}^{N_{\boldsymbol{\delta}}} \Delta C_{\mathcal{M}_i}}{\sum_{i=1}^{N_{\boldsymbol{\delta}}} \Delta C_{Z_i}} \approx -\frac{\sum_{i=1}^{N_{\boldsymbol{\delta}}} C_{\mathcal{M}_{\delta_i}} \delta_i}{\sum_{i=1}^{N_{\boldsymbol{\delta}}} C_{Z_{\delta_i}} \delta_i} = -\frac{B_{\mathcal{M}}\boldsymbol{\delta}}{B_Z\boldsymbol{\delta}} \tag{7.6}$$

For $N_{\boldsymbol{\delta}} > 1$, the position of the CCoP depends on the effectiveness of all control surfaces, as well as on their instantaneous deflection angles. Therefore, it is affected by both design parameters (control surface layout, moveable surfaces size and type) and flight parameters (angle of attack, control surface deflections). Because of this, the CCoP can move extremely fast and abruptly in maneuvering flight. As shown in Equation 7.7, if it is assumed that the pitch moment contribution of each control surface is entirely due to the respective normal force contribution, the position of the CCoP can be interpreted as the weighted average of the positions of the control surfaces, where the weights are the normal forces generated by each deflection (and can be either positive or negative). From this relation, it follows that the CCoP position is more affected by moveable surfaces lying further away from the aircraft center of gravity and/or generating a larger share of control lift. In all cases, $\bar{x}_\delta$ becomes undetermined in the case of no control surface deflections ($\boldsymbol{\delta} = \mathbf{0}$).

$$C_{\mathcal{M}_{\delta_i}} = -x_i C_{Z_{\delta_i}} \quad \forall i = 1,2,\ldots,N_{\boldsymbol{\delta}} \quad \Longrightarrow \quad \bar{x}_\delta = \frac{\sum_{i=1}^{N_{\boldsymbol{\delta}}} x_i \left(C_{Z_{\delta_i}} \delta_i \right)}{\sum_{i=1}^{N_{\boldsymbol{\delta}}} C_{Z_{\delta_i}} \delta_i} \tag{7.7}$$

Several useful interpretations can also be made when only one control surface is involved (an elevator or a canard, for example). In such case, Equation 7.6 reduces to $\bar{x}_\delta = -C_{\mathcal{M}_{\delta_e}} / C_{Z_{\delta_e}}$, which indicates that the position of the CCoP does not depend on the control surface deflection at all. Moreover, if it is assumed that the pitch moment contribution is entirely due to the normal force contribution, the position of the CCoP coincides with the position of the control surface itself. Lastly, in the case of a single control surface, it is possible to show that the CCoP is also strictly related to the Instantaneous Center of Rotation (ICR) of the aircraft, which can be calculated as in Equation 7.8 in the scope of a linear dynamics formulation [174].

$$\bar{x}_{\text{ICR}} = \frac{J_{yy}}{m\bar{c}^2} \frac{C_{Z_{\delta_e}}}{C_{\mathcal{M}_{\delta_e}}} = -\frac{J_{yy}}{m\bar{c}^2} \frac{1}{\bar{x}_\delta} \quad \Longrightarrow \quad \bar{x}_\delta \bar{x}_{\text{ICR}} = -\frac{J_{yy}}{m\bar{c}^2} = \text{const} \tag{7.8}$$

In light of this, it should be evident how the position of the CCoP is capable to substantially affect the flying qualities of the aircraft in the pitch axis [164]. For a linear dynamic model, it can be derived from the previous equation that the product between the positions of the CCoP and the ICR must be constant. If the elevator is very far aft the aircraft center of gravity, the ICR falls relatively close to it. In other words, the impact of the normal control force is negligible when compared to the pitch control moment, and the aircraft motion resembles a pure rotation about its center of gravity. On the other hand, if the CCoP tends to the aircraft center of gravity, the ICR moves infinitely away from it, and the aircraft motion tends to a pure normal translation. These types of deductions, obtained in the simplified case of a single control effector and linear dynamics, motivate the effort presented herein.

As mentioned in the introductory section of the chapter, the objective of the present investigation is to shape the transient response of the aircraft by means of CA methods. This is achieved by driving the CCoP towards a prescribed reference location $\bar{x}_{\text{ref}}$, for

which the transient response is known to have desired characteristics, and translates into the following Equation 7.9.

$$\bar{x}_\delta = -\frac{B_\mathcal{M}\boldsymbol{\delta}}{B_Z\boldsymbol{\delta}} \rightarrow \bar{x}_{\text{ref}} \quad \Longleftrightarrow \quad \frac{\left(B_Z\bar{x}_{\text{ref}} + B_\mathcal{M}\right)\boldsymbol{\delta}}{B_Z\boldsymbol{\delta}} \rightarrow 0 \tag{7.9}$$

Assuming that there exists at least a combination of $\bar{x}_{\text{ref}}$ and $\boldsymbol{\delta}$ which verifies this limit, meaning that control effectors can physically drive the CCoP to its desired location, Equation 7.9 becomes an equality. Furthermore, for any realistic maneuvering scenario, which means assuming that $\boldsymbol{\delta} \neq \mathbf{0}$, the latter reduces to its numerator, as shown in the following Equation 7.10.

$$\left(B_Z\bar{x}_{\text{ref}} + B_\mathcal{M}\right)\boldsymbol{\delta} = 0 \tag{7.10}$$

The last equation can be re-written in matrix form as

$$\begin{bmatrix}\bar{x}_{\text{ref}} & 1\end{bmatrix}\begin{bmatrix}B_Z \\ B_\mathcal{M}\end{bmatrix}\boldsymbol{\delta} = RB_*\boldsymbol{\delta} = 0 \tag{7.11}$$

where $R = \left[\bar{x}_{\text{ref}}, 1\right]$ and $B_* = \left[B_Z, B_\mathcal{M}\right]^T$.

From a geometric point of view, Equation 7.11 identifies a hyperplane in Control Space, which passes through the origin, and whose orientation depends on the value of $\bar{x}_{\text{ref}}$. This linear constraint obviously maps to a much smaller AAS than the one obtained when all effectors are free to move independently. From a more practical standpoint, Equation 7.11 can be regarded in two alternative ways, which give life to two different approaches to exploit it.

7.3.2. CONTROL EFFECTIVENESS MATRIX AUGMENTATION

The first, and probably most straightforward, approach sparks out of the interpretation of Equation 7.11 as a CA problem itself, where the prescribed objective is equal to zero, and the desired position of the CCoP acts as a weight to prioritize the generation of control lift over control pitch, or vice-versa. The combined effectiveness RB_* can then be used to augment the B matrix of any standard CA problem formulation, as shown in the following Equation 7.12.

$$B\boldsymbol{u} = \boldsymbol{\nu} \longrightarrow \begin{bmatrix}B \\ RB_*\end{bmatrix}\boldsymbol{u} = \begin{Bmatrix}\boldsymbol{\nu} \\ 0\end{Bmatrix} \tag{7.12}$$

In this way, Equation 7.11 has been directly injected into the CA problem, and has been given the same dignity as the other equations for the allocation of prescribed objectives. This approach can be applied to any existing CA method, including DA, as it only needs the presence of a baseline control effectiveness matrix in the problem formulation.

On the other hand, this approach presents a major drawback: the condition number κ of the augmented effectiveness matrix increases abruptly as the CCoP tends to the aircraft center of gravity, until diverging completely at the latter position. This is due to the fact that the pitch moment row $B_\mathcal{M}$ and the extra row RB_* of the augmented effectiveness matrix become more and more similar as $\bar{x}_{\text{ref}}$ approaches zero. From a physical

point of view, this happens because the pitch effectiveness of the control effectors is used to allocate both the demanded pitch moment ν_q and the null extra objective required to prioritize the effectors.

The numerical conditioning of the augmented effectiveness matrix can be slightly improved by additionally assuming that the CA algorithm always converges, meaning that the equality for the pitch moment $B_{\mathcal{M}}\boldsymbol{u} = \nu_q$ is verified at all times. This is not true for commanded control moments outside of the AAS, for example. With this additional hypothesis, Equation 7.10 can be re-written as in Equation 7.13, and the augmented problem takes the shape presented in Equation 7.14.

$$B_Z \bar{x}_{\text{ref}} \boldsymbol{u} = -\nu_q \tag{7.13}$$

$$B\boldsymbol{u} = \boldsymbol{\nu} \longrightarrow \begin{bmatrix} B \\ B_Z \bar{x}_{\text{ref}} \end{bmatrix} \boldsymbol{u} = \begin{Bmatrix} \boldsymbol{\nu} \\ -\nu_q \end{Bmatrix} \tag{7.14}$$

As shown in Figure 7.3, also in this case the augmented effectiveness matrix becomes ill-conditioned for $\bar{x}_{\text{ref}} \to 0$. In light of this, this approach would not be suitable for any practical implementation of the proposed CA formulation. It is therefore not implemented in any of the applications presented in the remainder of this chapter. The more robust weighted prioritization method illustrated in the next section does not present any numerical instabilities, and has been used to obtain the results presented in the remainder of the article.

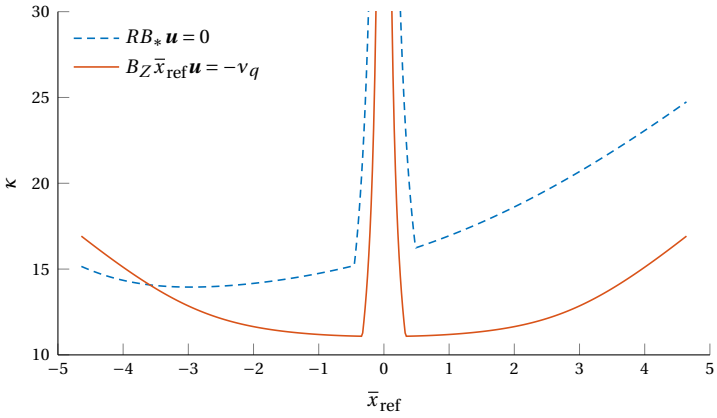

Figure 7.3 Condition number of the augmented control effectiveness matrix, for two augmentation approaches.

7.3.3. WEIGHTED PRIORITIZATION

Equation 7.11 can also be interpreted as a particular case of the classic effector prioritization expression, shown in the following Equation 7.15, used in all CA methods based on quadratic-programming algorithms.

$$RB_* \boldsymbol{u} \iff W_{\boldsymbol{u}} (\boldsymbol{u} - \boldsymbol{u}_{\text{ref}}) \tag{7.15}$$

The equivalence can be easily achieved by imposing the preferred effectors position as null, and placing the combined effectiveness vector on the diagonal of the weighting matrix, as shown in Equation 7.16.

$$\boldsymbol{u}_{\text{ref}} = 0 \qquad W_{\boldsymbol{u}} = \text{diag}\,(RB_*) \tag{7.16}$$

This approach does not present any numerical conditioning issues. On the other hand, it can only be applied to CA problems which allow some form of effectors prioritization, such as those employing the WPI method.. In case $\bar{x}_{\text{ref}}$ coincides with the aircraft center of gravity, control effectors are simply prioritized according to their pitch moment effectiveness $B_{\mathcal{M}}$.

A WPI method based on this particular formulation is going to be employed for all the applications proposed in the following Section 7.4. The control surface deflections solving such CA problem are obtained by substituting the expressions reported in Equation 7.16 into the generic WPI solution reported in Equation 2.21.

7.4. APPLICATIONS AND RESULTS

Three study cases have been performed to explore the flight mechanics possibilities of the staggered box-wing configuration:

1. an open-loop pull-up maneuver;
2. an altitude shift maneuver, using the automatic altitude control branch;
3. an altitude hold task in turbulent atmosphere, using the altitude control branch once again.

In all cases, the performance of the novel CA formulation presented in the previous Section 7.3.3 is evaluated as a function of the prescribed position of the CCoP and compared against the standard PSI formulation. The latter is simply equivalent to the WPI approach with all effectors being weighted equally, and is obtained by setting $W_{\boldsymbol{u}} = I$ and $\boldsymbol{u}_{\text{ref}} = \mathbf{0}$.

As explained in the next section, the aircraft is trimmed using the iterative methodology presented in Chapter 6. For all the subsequent applications, the control effectiveness matrix B is calculated at trim conditions and is held constant throughout each flight simulation. Actuators are modeled as first order systems with a time constant of 0.1 s, and control surface deflections are saturated at ± 30 deg. The FCS is re-tuned for each prescribed value of $\bar{x}_{\text{ref}}$, using the automatic procedure described in Section 7.2. However, if the FCS is tuned using the standard PSI method and then left unaltered when using the modified CA approach, results are substantially not affected and conclusions unhindered.

The reference trim condition is briefly illustrated in the following Section 7.4.1. Section 7.4.2 presents a simple pull-up maneuver with detailed analysis of time histories of the normal load factor and control surface deflections. In Section 7.4.3, an altitude tracking maneuver is analyzed. This is performed by closing the altitude channel switch in Figure 7.1b and prescribing a reference altitude profile. In a similar fashion, Section 7.4.4 presents an altitude holding task in turbulent atmosphere, with the estimation of a quantitative index of the comfort level on board.

7.4.1. TRIM CONDITION

The aircraft model is trimmed in straight and level flight using the CA-based methodology presented in Chapter 6. With this approach, the resulting control surface deflections are not constrained by an imposed ganging and gearing kinematic chain, but are independently set to obtain the maximum balanced control authority about the lift and pitch axes. The linear programming formulation of the standard DA method from Equation 2.23 is used in this case, because of its properties concerning the AAS. The AAS geometry at trim, and the combination of trim control forces generated by the effectors are shown in Figure 7.4a. Trim control surface deflections are reported in Figure 7.4b. The aircraft is trimmed at $V^{\text{tr}} = 170\,\text{m/s}$ at sea level altitude.

Trim control surface deflections, positive if with trailing edge down, are all symmetric and contained in magnitude, apart from the outboard ones on the rear wing, which are partially sacrificed to obtain a very small trim angle of attack $\alpha^{\text{tr}} = -0.46\,\text{deg}$. Rudders have been explicitly excluded from the CA problem, as they have a significant cant angle which makes them suitable for pitch control as well. This was judged to be undesired in a conventional flight control scenario.

7.4.2. PULL-UP MANEUVER

IMPULSIVE INPUT

An impulsive pull-up maneuver is performed by prescribing a constant pitch rate command through the pilot longitudinal control channel δ_{lon}, for the duration of 1 s, with the altitude channel switch left open, exactly as represented in Figure 7.1b. The initial instants of the arising load factor response are reported in Figure 7.5a, for several values of $\bar{x}_{\text{ref}}$ and the standard PSI formulation. Similarly, the time derivative of the load factor response at the start of the pilot maneuver is reported in Figure 7.5b and used as an indication of the sharpness of the transient response.

The standard PSI method results in the typical non-minimum phase behavior of conventional aircraft configurations. Such response corresponds to a CCoP far aft the aircraft

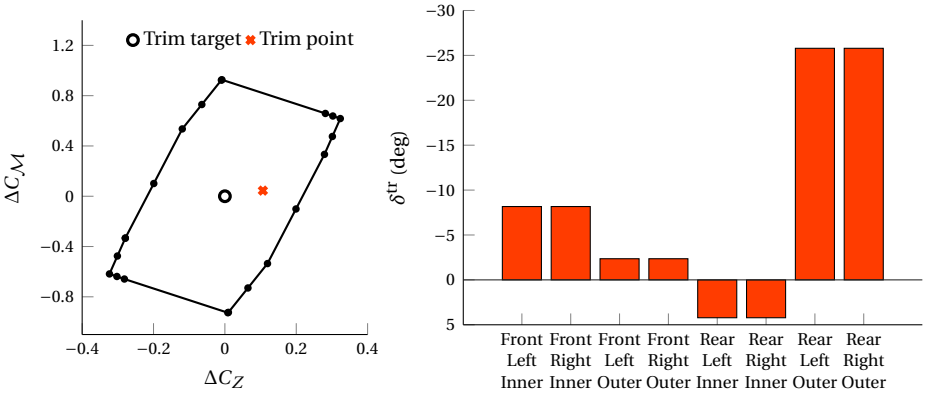

a) Control forces and AAS geometry

b) Control surface deflections

Figure 7.4 Reference trim condition: $V^{\text{tr}} = 170\,\text{m/s}$, $\alpha^{\text{tr}} = -0.46\,\text{deg}$.

center of gravity, which would be equivalent, in the modified CA formulation, to a value of $\overline{x}_{\text{ref}}$ approximately equal to -2. A similar behavior is observed with the modified CA approach, for values of $\overline{x}_{\text{ref}}$ ranging from -5 to about -0.9.

By advancing the prescribed location of the CCoP, i.e. increasing the value of $\overline{x}_{\text{ref}}$ from -5 to about 0.8, the initial decrease in load factor is progressively reduced, neutralized and converted into a sharp initial increase. The maximum response sharpness appears to plateau for $0.4 < \overline{x}_{\text{ref}} < 1$, where the transient response clearly shows the typical characteristics of DLC [27]. By further increasing $\overline{x}_{\text{ref}}$, the trend is reversed, and for $\overline{x}_{\text{ref}} = 5$ a small initial decrease in the load factor is again observed.

These results are consistent for different amplitudes and durations of the commanded input, which may be representative of different levels of pilot aggressiveness in performing the maneuver. In this specific case, for $0 < \overline{x}_{\text{ref}} < 1$, the aircraft response is so sharp that the commanded pitch rate is achieved before the end of the pilot maneuver. This forces control surfaces to be deflected back, to some extent, before reaching a steady state value, and results in the acceleration cusp visible in the corresponding curves of Figure 7.5a.

The time histories and maximum values of the pitch rate q and the angle of attack α are reported in Figures 7.6 and 7.7, respectively. Both show a similar behavior as a function of $\overline{x}_{\text{ref}}$. As it would be expected, the values of $\overline{x}_{\text{ref}}$ achieving the sharpest acceleration in Figure 7.5 also result in the fastest pitch rate and angle of attack responses. These correspond to the highest peak values in the respective quantities, in light of how the control law has been conceived (Section 7.2). In all cases, both the pitch rate and the angle of attack exhibit a significant excursion. This simply means that the aircraft does not achieve either Pure DLC or pure heave motion characteristics for any value of $\overline{x}_{\text{ref}}$ in the scope of the proposed framework.

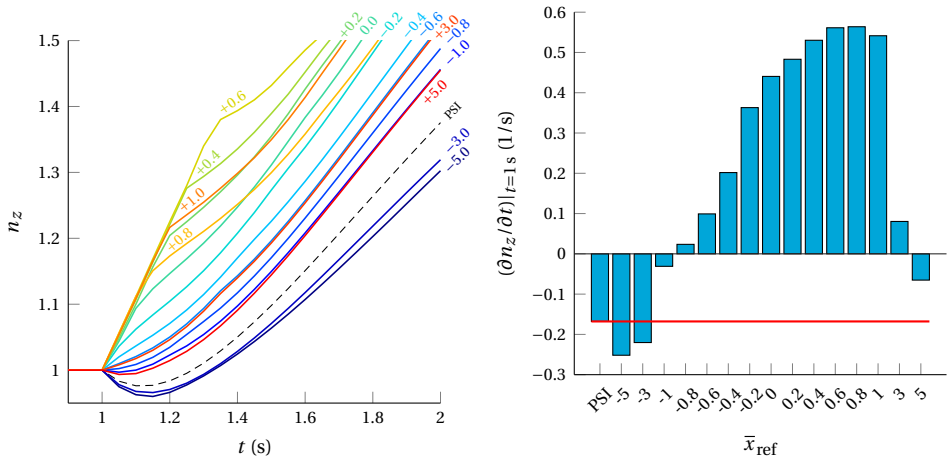

a) Time histories

b) Time derivative at $t = 1\,\text{s}$

Figure 7.5 Normal load factor response after an impulsive pull-up maneuver, for different values of the reference CCoP location and the standard PSI approach.

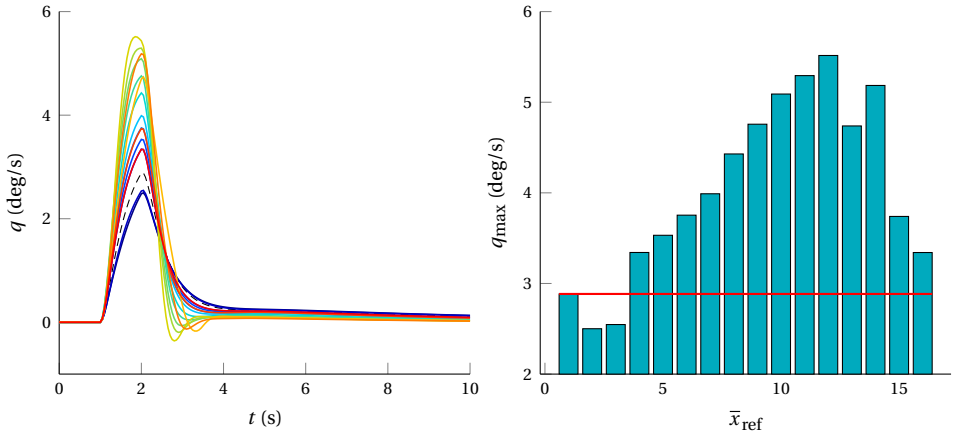

Figure 7.6 Time history and maximum value of the pitch rate, for different values of the reference CCoP location and the standard PSI approach. Same color legend as in Figure 7.5a applies to the chart on the left.

The time histories of control surface deflections are shown in Figure 7.8 for notable values of $\bar{x}_{\text{ref}}$. First, it can be seen how the standard PSI allocation mainly relies on the use of control surfaces on the rear wing. As expected, both the inner and outer rear effectors are deflected upwards in order to perform the prescribed pull-up maneuver, while the inner front effectors are only slightly activated downwards. This is in light of their lower pitch effectiveness, which is due to their smaller distance to the aircraft center of gravity as compared to their counterpart on the rear wing. The outer front effectors are left completely untouched.

Similar observations hold for the modified approach, in the case of $\bar{x}_{\text{ref}} = -5$. Such high, negative value places even more emphasis on the rear wing effectors, and in particular on their lift effectiveness. In fact, outer rear effectors are now prioritized with respect to inner ones, since they are closer to the center of gravity and their pitch effectiveness is lower. The former are deflected upwards until saturation, while the latter are now deflected less than in the previous case. All front effectors are unused.

In the case of $\bar{x}_{\text{ref}} = -0.8$, all effectors are used in a balanced way, resulting in a smooth initial load factor response. Front effectors are deflected downwards, while rear effectors are deflected upwards, so that the combined deflection generates a pitch moment about the aircraft center of gravity. The maneuver is therefore started substantially by α-generated lift.

For $0.6 < \bar{x}_{\text{ref}} < 1$, all the control effort is placed on front effectors, while rear ones are almost completely ignored. Both inner and outer effectors on the front wing are deflected significantly downwards, with the outer ones exhibiting larger deflections in light of their smaller effectiveness. For $\bar{x}_{\text{ref}} = 0.8$, inner effectors are deflected less than in the case of $\bar{x}_{\text{ref}} = 0.6$, while outer ones are deflected up almost to the saturation limit. Both $\bar{x}_{\text{ref}} = 0.6$ and $\bar{x}_{\text{ref}} = 0.8$ result in the highest response sharpness for the present application, with the former value being able to obtain a larger initial load factor excursion thanks to the more substantial use of inner front effectors.

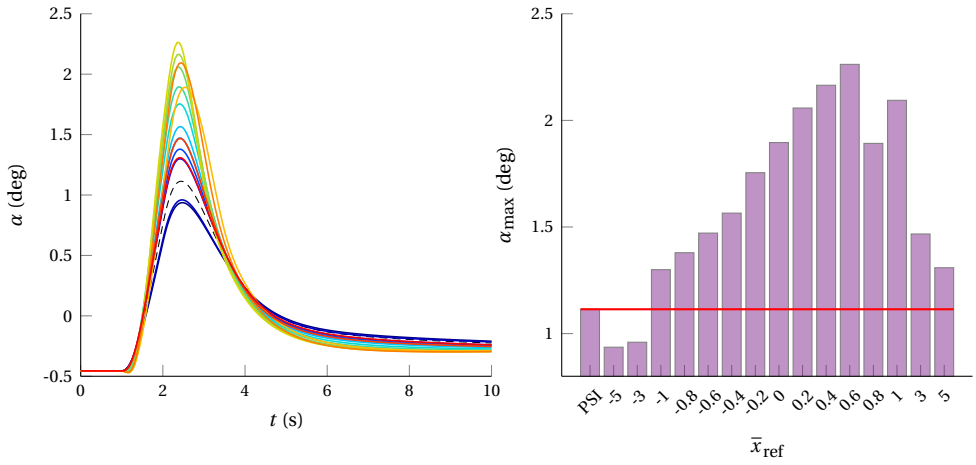

Figure 7.7 Time history and maximum value of the angle of attack, for different values of the reference CCoP location and the standard PSI approach. Same color legend as in Figure 7.5a applies to the chart on the left.

For $\bar{x}_{\text{ref}} = 1$, inner front effectors are deflected more than in the case of $\bar{x}_{\text{ref}} = 0.8$, outer front effectors reach the same final value as in the previous case, while a very slight upward deflection of all the rear effectors is once again noticeable. By further advancing the reference CCoP location, control effectors deflections result similar to the ones obtained for the $\bar{x}_{\text{ref}}$ negative value that exhibits a similar response. Notable similarities are represented by $\bar{x}_{\text{ref}} = -0.6$ and $\bar{x}_{\text{ref}} = 3$, or $\bar{x}_{\text{ref}} = -1$ and $\bar{x}_{\text{ref}} = 5$, as shown in Figure 7.5a.

STEP INPUT

A similar pull-up maneuver has been performed for a sustained duration of 10 s, with a smaller amplitude of the commanded input in order to keep the excursion of the angle of attack contained. This additional simulation was necessary to calculate the rise time and equivalent time delay of the pitch rate response, which are shown in Figure 7.9. These are two classic flying qualities metrics, used to characterize the short period pitch rate response of the aircraft to pilot commands [162, 164]. Time delay t_1 is defined as the lapse between the step command and the instant when the tangent line at the maximum pitch rate slope intersects the time axis. Rise time $\Delta t = t_2 - t_1$ is defined as the lapse between t_1 and the instant when the maximum pitch rate slope line intersects the steady state value of the pitch rate for the first time. For the presented application, these metrics have been evaluated on the basis of non-linear flight dynamics simulations.

As it can be seen in the figure, the metrics show a somewhat complementary behavior as a function of $\bar{x}_{\text{ref}}$. For basically all values of $\bar{x}_{\text{ref}}$, the modified CA approach determines a consistent improvement of the rise time with respect to the standard PSI method. All values are well within the Level 1 flying quality rating, and the minimum rise time is achieved for $\bar{x}_{\text{ref}} = 0.6$. On the other hand, a slight deterioration of the time delay can be seen for nearly all values of $\bar{x}_{\text{ref}}$, with a peak increase for $\bar{x}_{\text{ref}} = 0.6$. The latter is the only case for which the flying quality criterion results in a Level 2 rating.

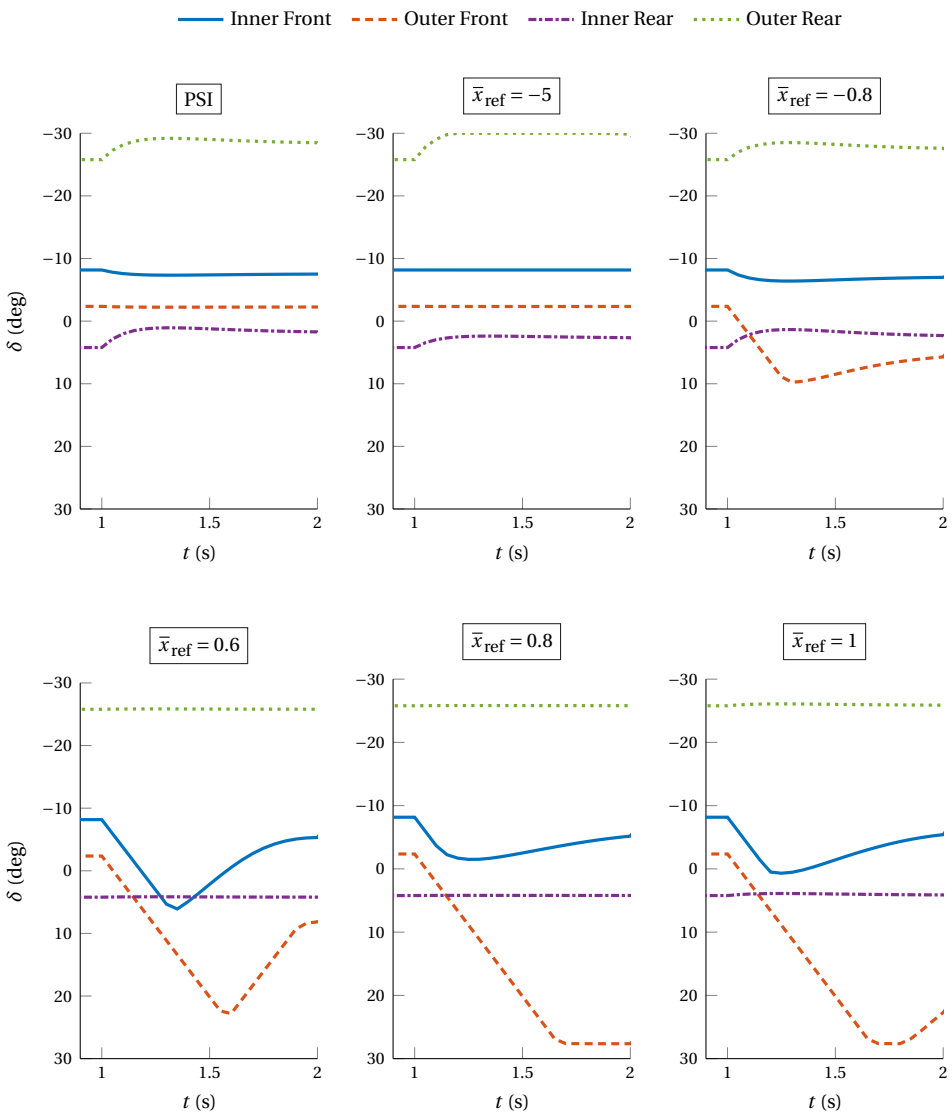

Figure 7.8 Control surface deflections time histories after an impulsive pull-up maneuver, for different values of the reference CCoP location and the standard PSI approach.

The selected metrics are deemed appropriate to characterize the dynamic behavior of the augmented aircraft model, although the criteria which prescribe their limit values have been developed for more conventional aircraft configurations. In particular, concerning their suitability for the present application, it must be reported that “several questions remain unresolved including [the fact that] effects of pilot location and blended direct lift control have been observed and need to be accounted for” [164]. This

may constitute the object of interesting future research studies.

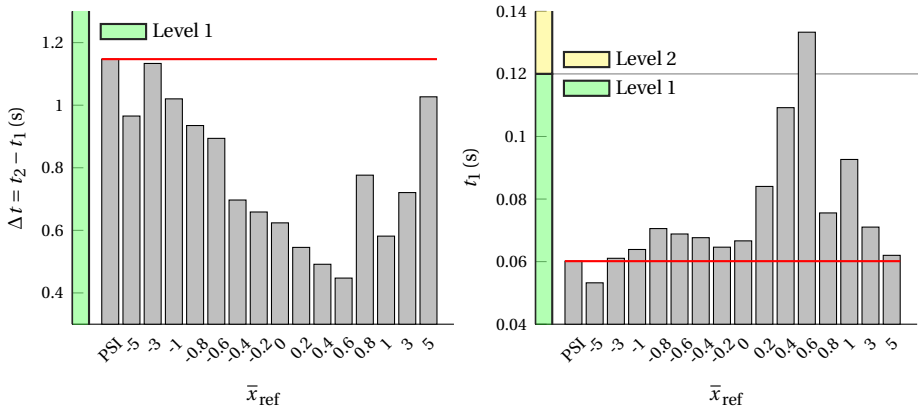

a) Rise time **b)** Equivalent time delay

Figure 7.9 Time-domain flying qualities of the short period pitch rate response q, for different values of the reference CCoP location and the standard PI approach. Criteria are valid for all aircraft categories and flight phases, but have not been defined specifically for DLC motion types [162, 164].

7.4.3. ALTITUDE SHIFT MANEUVER

The present application has the objective of estimating the impact of the modified CA approach on a practical performance metric such as tracking precision. A 10 m square wave altitude profile $h_{\text{ref}}(t)$ is prescribed for the aircraft to track. This is achieved by closing the altitude channel switch in Figure 7.1b and leaving the pilot input unaltered. The resulting altitude time histories are reported in Figure 7.10 for different values of $\overline{x}_{\text{ref}}$ and the standard PSI approach.

Apart from a very small difference during climb and descent phases, the trajectories are basically indistinguishable at the scale of the full maneuver duration. This is also in light of the fact that the FCS is re-tuned for every value of $\overline{x}_{\text{ref}}$, using the same performance requirements within the automatic procedure presented in Section 7.2.

Nevertheless, the alteration of the dynamic response achieved with the modified CA approach has a small but noticeable impact on trajectory tracking precision. The Root Mean Square (RMS) deviation $\overline{\Delta h}$ of each altitude time history with respect to the reference one is reported in Figure 7.11a. A clear trend is visible in the chart, where the cancellation of the non-minimum phase behavior clearly leads to better tracking precision due to a faster transient response. While very negative values of $\overline{x}_{\text{ref}}$ lead to a deterioration of tracking performance, the best tracking precision is obtained for $0.2 < \overline{x}_{\text{ref}} < 1$, as expected in light of the results obtained in the previous Section 7.4.2.

The same conclusions can be drawn by observing the trend in the agility quickness performance metric, reported in Figure 7.11b. This parameter, calculated as the ratio between the peak load factor and the maximum excursion of the flight path angle, has been previously proposed as a measure of moderate amplitude agility for rotorcraft maneuvering in forward flight [175]. In the opinion of the authors, it is also well suited for inter-

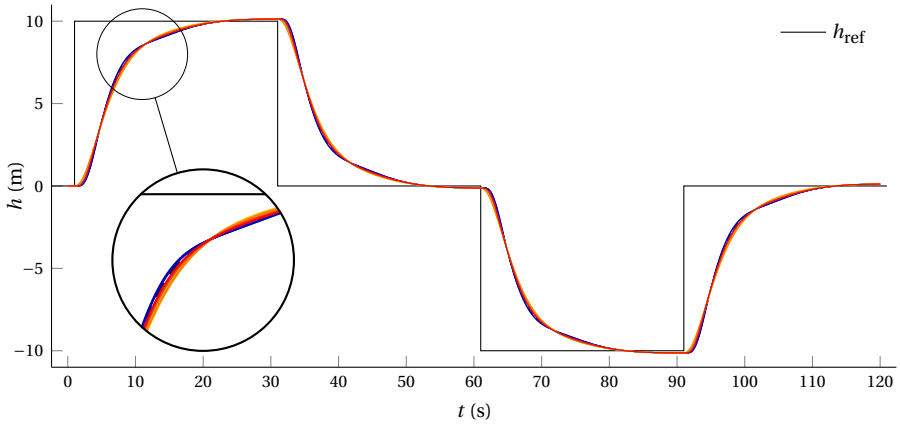

Figure 7.10 Altitude time histories for the altitude shift task, for different values of the reference CCoP location and the standard PSI approach. Trajectories are fundamentally indistinguishable and therefore have not been labeled individually.

preting the dynamic performance of aircraft capable of DLC. The highest agility quickness is achieved for $\overline{x}_{ref} = 0.8$, in line with results from all previous analyses.

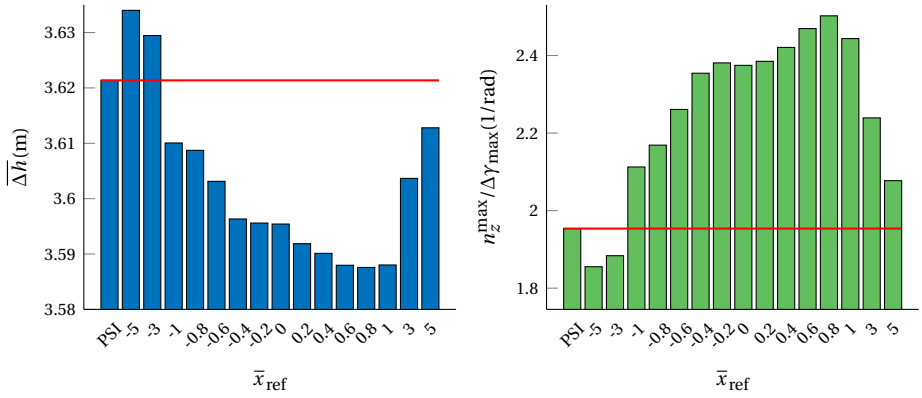

a) Altitude RMS deviation

b) Agility quickness during first climb ($t < 30$ s)

Figure 7.11 Derived performance metrics for the altitude shift task, for different values of the reference CCoP location and the standard PSI approach.

7.4.4. ALTITUDE HOLD IN TURBULENT ATMOSPHERE

In the present application, the aircraft is required to hold its initial altitude while flying in a turbulent flow. In the same way as before, the task is performed exclusively by means of the altitude control channel shown in Figure 7.1, with no input from the pilot. The von Karman turbulence model has been implemented, and a moderate turbulence intensity level has been selected for the test case [176, 177]. This is the most popular turbulence

Table 7.1 Guidelines for the interpretation of the overall frequency-weighted RMS acceleration $\overline{a}$ as an indication of the level of comfort on board [179], for a prescribed location within the aircraft.

Acceleration magnitude $\overline{a}\,(\mathrm{m/s^2})$	**Comfort level indication**
< 0.315	Not uncomfortable
$0.315 - 0.63$	A little uncomfortable
$0.5 - 1$	Fairly uncomfortable
$0.8 - 1.6$	Uncomfortable
$1.25 - 2.5$	Very uncomfortable
> 2	Extremely uncomfortable

model for aircraft design and atmospheric flight simulation applications [164]. According to this model, velocity fluctuations due to a turbulent airfield behave like spatially continuous, isotropic, stochastic processes. The model provides power spectral density functions, which can be used — with appropriate scale factors — to generate random fluctuations of the three linear and angular velocity components of the turbulent field.

Altitude time histories are shown in Figure 7.12. In this case, different features of the trajectories can be identified for different values of the prescribed position of the CCoP. As expected in light of previous results, extreme values of $\overline{x}_{\mathrm{ref}}$, as well as the classic PSI approach, result in lower frequency oscillations of greater amplitude. On the other hand, due to the cancellation of the non-minimum phase behavior, values of $\overline{x}_{\mathrm{ref}}$ between 0 and +1.0 result in higher frequency altitude oscillations of smaller amplitude, due to an overall faster and sharper response to the external disturbance. These observations are once again confirmed by the RMS deviation with respect to the reference initial altitude $h_{\mathrm{ref}}(t) = 0$, reported in Figure 7.13a. The trend of $\overline{\Delta h}$ as a function of $\overline{x}_{\mathrm{ref}}$ is completely analogous to the one seen in the previous application.

As a final analysis on these simulations, the overall frequency-weighted RMS acceleration $\overline{a}$ perceived by a passenger seated at the aircraft center of gravity location has been estimated. Because the large inertia of the PrP about the lateral axis, the longitudinal position where $\overline{a}$ has little influence on the numerical results of this study, and does not hinder the final considerations. The methodology described in [178] has been implemented, with reference to the ISO 2631-1 standard [179]. Results are reported in Figure 7.13b as a function of the prescribed position of the CCoP.

While it is hard to compare the absolute numeric values to similar studies on conventional aircraft of similar category and in similar flight scenarios, the chart once again highlights a trend analogous to all previous cases. The ISO 2631-1 standard also provides guidelines to interpret the numerical values of $\overline{a}$ as a quantitative measure of comfort on board. These are graphically represented on the left side of Figure 7.13b and additionally reported in Table 7.1. As it can be seen, the overall acceleration obtained with the standard PSI approach is classified as either “uncomfortable” or “fairly uncomfortable”. On the other hand, the proposed CA approach is able to obtain a consistent improvement, resulting in a clear classification as “little uncomfortable” in the best case.

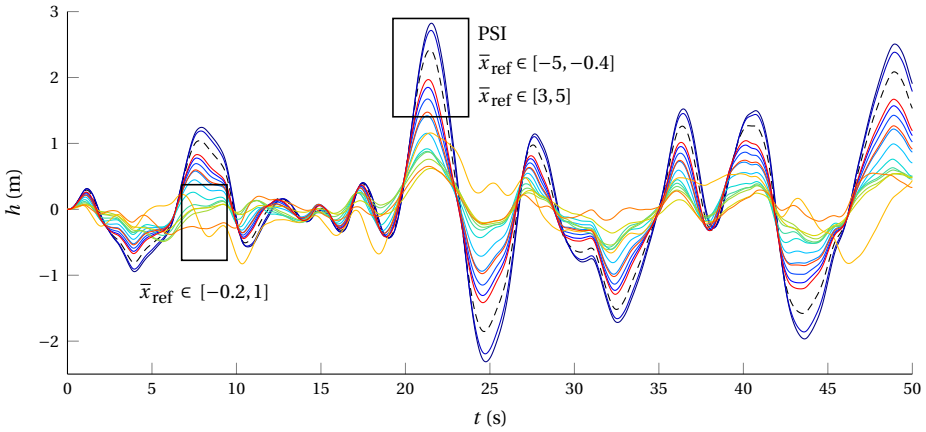

Figure 7.12 Altitude time histories for the altitude hold task in turbulent atmosphere, for different values of the reference CCoP location and the standard PSI approach. Legend labels have been aggregated, colors match Figure 7.5a.

7.5. CONCLUSIONS

A novel CA approach has been proposed with the objective of shaping the aircraft transient response by exploiting the concept of CCoP. This is the center of pressure due to only aerodynamic control actions, and is strictly related to the position of the ICR. First, a formulation based on the straightforward augmentation of the control effectiveness matrix has been presented. This can be used to modify any classic CA method already existing, but results in an ill-conditioned effectiveness matrix in some limit cases. Another formulation, based on a weighting matrix to prioritize effectors, has been outlined and implemented in three applications featuring a box-wing aircraft configuration: a pull-up maneuver, a trajectory tracking task, and an altitude holding task in turbulent air.

The performance of the proposed CA formulation is studied as a function of the prescribed position of the CCoP, and compared to a classic PSI CA method. Results show that, with the same closed-loop characteristics, the proposed approach can significantly impact performance metrics that are closely related to the aircraft transient response, such as delay due to non-minimum phase behavior, tracking precision, and capability of disturbance rejection. In the best case scenario, the aircraft is able to completely cancel the non-minimum phase behavior typical of pitch dynamics, hence achieving a sharp and more agile initial response to longitudinal commands. This results in improved tracking precision, better disturbance rejection, and ultimately in an improved feeling of comfort on board.

Although the presented CA method is applicable to any aircraft configuration, the obtained results reflect, to some extent, the flight mechanics potential of the staggered box-wing geometry. Thanks to the presence of redundant control surfaces, both fore and aft of the aircraft center of gravity, this configuration allows a large excursion of the CCoP, which is probably infeasible for more conventional architectures. Further research could be therefore devoted to assessing the benefits of the proposed CA approach on conven-

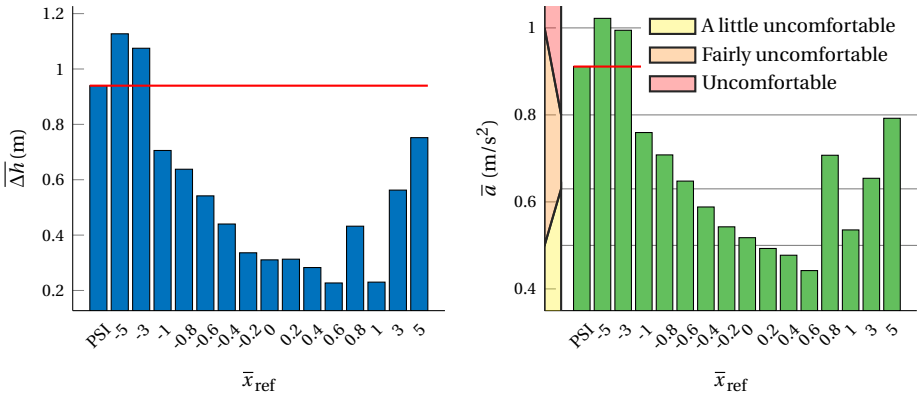

a) Altitude RMS deviation

b) Overall frequency weighted RMS acceleration perceived at the aircraft center of gravity [179]

Figure 7.13 Derived performance metrics for the altitude hold task, for different values of the reference CCoP location and the standard PSI approach.

tional aircraft configurations. This could be achieved also with pilot-in-the-loop simulations. From a more fundamental standpoint, improving the control effectiveness matrix conditioning problem could make the proposed formulation applicable to a wider range of already available CA methods. Lastly, the development of specific flying qualities metrics for DLC longitudinal response remains an open challenge.

8

CONCLUSIONS AND RECOMMENDATIONS

I am always doing that which I can not do,
in order that I may learn how to do it.

Vincent van Gogh
Letter to Anthon van Rappard
1885

Wisdom is the daughter of experience.

Leonardo da Vinci
Personal notebooks

The present dissertation has had the overarching objective to demonstrate how redundant control surfaces can be exploited to shape an aircraft dynamic response with the purpose to achieve desired flight performance and dynamic behavior. In particular, by making use of a staggered box-wing aircraft model — the PrandtlPlane (PrP) — as the main application test case, it has shown that Direct Lift Control (DLC) capabilities can be enabled by the coordinated use of conventional control surfaces located fore and aft the aircraft center of gravity. This allows the aircraft to separate the generation of lift due to variations of the angle of attack from the one due to the deflection of control surfaces, hence decoupling longitudinal stability characteristics from controllability ones, and enabling the implementation of advanced control strategies. A thorough introduction to the flight mechanics and performance of DLC, with practical and conceptual examples, and fundamental derivations, has been provided in Section 1.1. Here, the role of the Control Center of Pressure (CCoP), which is the application point of aerodynamic forces due to only control surface deflections, has also been highlighted.

The research work has been motivated by the necessity to investigate new, unconventional aircraft configurations. These have been identified as a potential, disruptive and ambitious solution towards making the aviation industry more environmentally sustainable in the near future. At the same time, such innovative aircraft concepts represent a major research and technological challenge, as they must be proven to be practically operable in all current and future flight scenarios, with good flying qualities and sufficient flight safety. In these regards, they also serve as the perfect opportunity to explore the development and application of unconventional piloting techniques, as well as of original control methods.

Within this social and scientific context, the common thread underlying all of the proposed studies, at the most fundamental level, is the exploitation and customization of Control Allocation (CA) methods. Elements from the theory of CA, such as the Attainable Actions Set (AAS) and its geometric interpretation, as well as the philosophy behind a few notable methods, have been introduced in Chapter 2 and frequently referred to throughout the dissertation. The main results illustrated in the previous chapters have been obtained by means of non-linear flight simulation, within a software environment that promotes physics-based and aircraft configuration-agnostic analyses, as much as allowed by the available computational resources. The baseline models implemented to render the aero-propulsive database of the PrP, together with a top-level presentation of the aircraft model itself, have been provided in Chapter 3.

The mission performance of the PrP has then been characterized in Chapter 4, with comparison to a competitor tube-and-wing aircraft. Chapter 5 has presented a design methodology to position and size control surfaces on a staggered box-wing geometry, and has compared the impact of different CA methods on the resulting optimal control surface layout. A trim methodology to maximize control authority about different motion axes, exploiting the properties of the AAS has been proposed in Chapter 6. In an application study aimed at finding trim conditions with minimum aerodynamic drag, the methodology has also been used to estimate the effect of the number of dimensions of the AAS on a given trim objective function. Lastly, the control surface redundancy allowed by the box-wing geometry has been fully exploited for maneuvering flight in Chapter 7. In this case, an original formulation of the classic Weighted Pseudo Inverse (WPI) CA method has been proposed, with the purpose to induce desired characteristics of the aircraft transient response by prescribing a reference position of the Control Center of Pressure (CCoP).

In the following three sections, conclusions are drawn and considerations are made on the most important aspects addressed in the previous chapters, from both a quantitative and qualitative point of view. The research questions posed in Section 1.3 are answered in the following Section 8.1. A short reflection on the way DLC can be achieved with redundant control effectors is proposed in Section 8.2. Lastly, Section 8.3 presents an outlook on possible future research studies.

8.1. CONCLUSIONS

This section recaps the most important results sparking from the technical analyses illustrated in the previous chapters, and synthesizes some final considerations. The research questions formulated at the beginning of this dissertation, in Section 1.3, are reported

below for convenience. The corresponding answers summarize the fundamental aspects related to the most important results achieved, and pave the way towards a fundamental reflection and a few recommendations for further research, presented in the next two sections.

What is the impact of different Control Allocation (CA) methods on the design of a control surface layout and on the sizing of redundant control surfaces, for a given aircraft configuration? (Chapter 5)

CA methods are able to judiciously exploit the control power available by any given aircraft configuration. They do so in the most effective way, according to a prescribed optimization criterion, and in a broad range of flight conditions. They can be tailored to virtually any specific application, and included in traditional FCS architectures with little effort. Some CA formulations are able to capitalize on all the control power made available by a given control surface layout, while other formulations are only able to attain a part of it.

Section 5.3.1 has shown that CA methods which attain a larger AAS achieve sufficient flying qualities with less span width dedicated to control surfaces. These results have been achieved in the scope of the study presented in Chapter 5, which has proposed a design methodology to automatically size multiple control surfaces on a given, fixed wing geometry. The goal of such study was to determine the impact of different CA methods on the cumulative span width required by control surfaces on a box-wing. Reducing the span width due to control surfaces can free up space for other wing-mounted devices, such as high-lift systems, and/or potentially save structural weight.

Results have been compared for the CWPI method, the more advanced DA method, and a conventional ganging approach, which is equivalent to establishing a mechanical linkage among CSs. As expected, the conventional ganging approach requires the largest cumulative control surface span width. This is due to the fact that the generation of roll and pitch moments are delegated to specific groups of control surfaces, which are constrained to deflect together according to an arbitrary, and sub-optimal, ganging matrix. The CWPI method is able to use all effectors in combination, hence reducing the required cumulative control surface span width by about 9.5% with respect to the one obtained with the ganging approach. The DA method not only achieves a reduction in cumulative control surface span of about 17% compared to the one obtained with the conventional ganging approach, but also obtains the maximum available control power as compared to all the other methods. This result is clearly due to the ability of the DA method to attain the entirety of the EAS, for any given control surface layout, and is visualized in Figure 5.8.

As mentioned before, the use of CA methods removes the necessity to assign a specific role (as elevator, aileron, rudder, for example) to each control surface in different flight phases. This convenient property has been exploited in Section 5.3.2 to search for novel control surface layouts on box-wing aircraft. The most traditional layout adopted in the literature for staggered box-wing geometries features one inboard and one outboard control surface on each of the front and rear wings. The newly investigated layout features a control surface in the central region of the rear wing, which can be apposed next to, or potentially replace, the most inboard control surface close to the aircraft plane

of symmetry. Results show that the required cumulative control surface span is further reduced if the inner rear control surface is completely replaced by the mid-wing one. This is because the mid-wing control surface can aid in both longitudinal and lateral flight maneuvers, hence functioning as a proper elevon and providing sufficient roll and pitch control power at the same time.

How can redundant control surfaces be fully exploited to obtain maximum control authority about one or more specified motion axes in trim conditions? (Chapter 6)

Section 6.3.1 has proposed a definition of control authority which is entirely based on the resultant action provided by control effectors, in terms of either forces or moments, or a combination of them. In the scope of CA theory, control authority has then been interpreted from a geometric point of view as a distance within the AAS. This formulation has allowed to exploit the DA method to find trimmed flight conditions which maximize control authority about a given motion axis, and about all motion axes at the same time. The latter case, which has been referred to as "balanced" control authority, is akin to the many classic formulations aimed at deflecting control surfaces while employing minimum control power.

For a flight mechanics model with 3 DoFs, the trim conditions that maximize control authorities to pitch-up, lift-up, pitch-down and lift-down, and the trim condition that maximizes the balanced control authority highlight a preferential diagonal direction in the two-dimensional Action Space. This suggests a clear tradeoff between the control lift and pitch moment that are necessary to trim the aircraft at a given angle of attack. Control authorities in the different directions of the same axis (pitch-up and pitch-down, for example) are comparable in magnitude, and show little variation with airspeed. Trim angles of attack show the same variation with airspeed for all control authorities, and are higher for pitch-up and lift-up control authorities, and lower for pitch-down and lift-down control authorities. In all cases, it is clear how the value of the angle of attack has a big role in determining the trim control surface deflections which would then maximize the specified control authority.

For a flight mechanics model with 6 DoFs, either in symmetric or asymmetric flight conditions, the combination of trim control surface deflections and angle of attack values are neatly distinguishable for different prescribed directions of control authority. In accordance with the behavior observed for the previous study case, maximum lift-up control authority is achieved with very negative deflections, both on the front and on the rear wing, paired up with a significant positive angle of attack of 5.1 deg. Maximum lift-down control authority is achieved with mostly large positive deflections at a negative angle of attack of -4.5 deg. Similarly, maximum pitch-down control authority is achieved at a very low angle of attack, with drastic positive deflections on the front wing and negative deflections on the rear wing. This is made possible by exploiting the pitch-down moment due to the propulsion system, which is positioned slightly above the aircraft center of gravity and has a pitch-down moment contribution. Trim conditions for maximum maximum balanced and pitch-up control authority are overall very similar, since the former case requires low drag, while the latter requires low thrust for a propulsive system placed above the aircraft center of gravity.

The presented results confirm that the proposed trim methodology is able to exploit

CA methods to capitalize on α-generated lift or engine thrust to obtain the control surface deflections which maximize the assigned control authority. This capability is clearly enabled by the geometry of the staggered box-wing geometry, which allows to install control surfaces both fore and aft the aircraft center of gravity, but can be exploited by virtually any aircraft configuration which is able to achieve DLC, to some extent.

How can the concept of Control Center of Pressure (CCoP) be leveraged to shape the aircraft transient response in a controlled manner and remove the typical non-minimum phase behavior of pitch dynamics? (Chapter 7)

As early as in Section 1.1.1, the CCoP has been defined as the center of pressure of aerodynamic actions exclusively due to control surface deflections. In Section 7.3.1, it has then been shown how, for simplified flight mechanics models, the CCoP can be closely related to the position of the Instantaneous Center of Rotation (ICR), hence having a significant impact on the characteristics of the aircraft transient response. Moving from this, an original CA approach based on the WPI method has been proposed, making use of a weighting matrix to prioritize effectors, with the objective of inducing the position of the CCoP towards a specified location of the aircraft.

Results from the simulation of a pull-up maneuver immediately highlight how the load factor response is heavily influenced by the prescribed position of the CCoP. If the latter is significantly behind the aircraft center of gravity, the vertical acceleration of the aircraft exhibits the non-minimum phase behavior typical of conventional pitch control. On the other hand, for a certain range of prescribed positions of the CCoP, the vertical acceleration raises sharply and immediately, in accordance to what is prescribed by the classic theory of DLC. This results in a load factor value 0.3 s after the pull-up ranging from a minimum of ≈ -0.95, in the worst case, to a maximum of ≈ 1.4, in the best case.

These trends in the transient response have a direct impact on integral performance metrics for assigned flight tasks. In particular, the best position of the CCoP achieves about 10% reduction in the altitude RMS error, as compared to the standard PSI method, for an altitude tracking task consisting of 10 m altitude shifts every 30 s. For the same flight scenario and position of the CCoP, the agility quickness of the aircraft, which measures its capability to swiftly change flight direction, increases by about 32%. Similar results are achieved for an altitude hold task in turbulent atmosphere. With the best prescribed position of the CCoP, a reduction of about 30% in altitude RMS error is obtained, together with a reduction of about 50% in overall perceived acceleration on board, as compared to the standard Pseudo Inverse (PSI) method.

In summary, for assigned and fixed characteristics of the closed-loop FCS, the proposed CA approach can significantly impact performance metrics that are closely related to the aircraft dynamic evolution in the short period. In the best case scenario, the aircraft is able to completely cancel the non-minimum phase behavior typical of pitch dynamics, hence achieving a sharp and more agile initial response to longitudinal commands. This translates to quantifiable improvements in the response delay due to non-minimum phase behavior, in tracking precision in terms of RMS altitude deviation, and in the capability to reject high-frequency disturbances, such as turbulence fields. In the latter case, a lower value of the overall perceived acceleration is a measurable proof of improved feeling of comfort on board.

8.2. REFLECTION

The following Section 8.2.1 provides a brief reflection on the fundamental meaning of DLC in the context of aircraft configurations featuring redundant control effectors. In Section 8.2.2, some considerations are then made on the application of DLC to the particular case of the PrP aircraft configuration.

8.2.1. DIRECT LIFT CONTROL WITH REDUNDANT EFFECTORS

The classic definition of DLC as the ability to generate lift "without, or largely without, significant change in the aircraft incidence" has been adopted since the very beginning of this dissertation. By immediately excluding the angle of attack, this definition has the advantage of giving control effectors (or, more in particular, control surfaces) the most prominent role in the task of altering the aircraft lift. This definition is satisfying when a single control device is dedicated exclusively to the realization of DLC and does not have any significant impact on the aircraft attitude, as in the case of over-the-wing spoilers, for example. In such a case, the displacement of the spoiler acts as an additional, independent degree of freedom to control the vertical motion of the aircraft, and the control- and incidence-dependent dynamics of the aircraft are clearly decoupled.

On the other hand, when redundant control effectors share both the task of controlling the aircraft attitude and the one of modulating its lift, the traditional definition of DLC loses part of its efficacy. In particular, it immediately raises additional questions about how to coordinate the motion of all the available control devices, in order to obtain a resulting control lift vector which does not give raise to variations of the aircraft angle of attack. It is clear that, for a set of control surfaces, the value of each deflection must be determined in combination with all the other ones, according to a chosen criterion. But the ultimate and most essential consequence of this process, in all cases, is a change in the position of the CCoP.

In light of this reasoning, the ability to achieve DLC with redundant control surfaces is intrinsically linked to the possibility of controlling the position of the CCoP. A single control surface is never capable to control the position of the CCoP, but it is capable to achieve DLC only if its position within the airframe allows it. Since the application point of control lift would always coincide with the control surface itself, in this case, the latter needs to be located slightly fore of the aircraft neutral point to achieve favorable DLC characteristics. On the contrary, redundant control surfaces are always able to control the position of the CCoP, and are able to achieve DLC as long as the CCoP can be driven to a certain range of positions fore of the aircraft neutral point. This is always possible if control surfaces are located both fore and aft the aircraft center of gravity, as allowed by the staggered box-wing geometry.

8.2.2. APPLICATIONS TO BOX-WING AIRCRAFT

The scientific interest in the box-wing geometry has always been justified by its optimum induced drag performance. Moving from this solid foundation, the main engineering challenge has then consisted of integrating such complex wing geometry into a complete aircraft configuration. The optimum behavior of the box-wing is the most significant for flight at low speed and relatively high angle of attack, when the aircraft needs greater lift-generating capabilities to sustain its weight, and induced drag becomes more

relevant in the total drag breakdown. Many research efforts have also been dedicated to the aerodynamic design of box-wing aircraft geometries targeted at the high-subsonic or transonic flight regime. In these cases, the design and engineering challenge typically lies in achieving optimal performance when other types of drag become relevant: parasitic drag, wave drag, or drag due to aerodynamic interference effects.

It is undeniable that the PrP configuration represents an extremely interesting and exciting case study from the perspective of flight mechanics and control. This is obviously thanks to the unique geometry of its swept and staggered box-wing, which allows the installation of conventional trailing-edge control surfaces both fore and aft of the aircraft center of gravity. The studies presented in this dissertation would have probably been impossible to conceive if they were to be applied to a Blended Wing Body (BWB) aircraft or to the Flying-V, for example, which are simply uncapable to achieve DLC because of the geometry of their configuration.

According to the most recent studies available in literature, a well-designed box-wing aircraft configuration is competitive in the modern aviation market, at least from a mission performance point of view. For example, the analyses presented in Chapter 4 have shown that the PrP is able to outperform current state-of-the-art tube-and-wing competitors in terms of fuel consumption per number of passengers, although this comes at the price of a relatively low maximum range. On the other hand, the available results all come from research studies at low or medium-low Technology Readiness Level (TRL), and feature performance evaluations at the stage of conceptual or very early preliminary design.

These studies usually tell very little about the practical feasibility of the proposed solutions, and are surely insufficient to justify the enormous risks that aircraft manufacturers would have to take to start development plans involving unconventional configurations targeted at the commercial transport sector. For example, just the possibility to operate the PrP on a smaller set of missions than its current tube-and-wing competitors — namely, the Airbus A320 and Boeing B737 — could be a reason for it to be unattractive to airliners, which currently show the tendency to operate fleets composed of many similar aircraft that can be operated flexibly on different mission ranges.

In synthesis, it may be speculated that the coexistence of optimal drag performance at high angles of attack and peculiar maneuverability characteristics makes the staggered box-wing geometry inherently more suitable for applications different from commercial transport. The aforementioned properties, together with its exotic looks, have indeed attracted some interest in the past, with projects such as the Ligeti Stratos[1] or the Airkraft Sunny[2] (now both discontinued), and more recently with the IDINTOS project[3]. These were targeted at the ultralight and microlight amateur market, for applications such as leisure and generic aerobatics. In the future, it seems sensible to envision new applications of box-wing aircraft as (possibly unmanned) vehicles for remote sensing, reconnaissance or other military applications where agility, high maneuverability, and endurance are paramount.

[1] Some details: `https://aeropedia.com.au/content/ligeti-stratos/`. Accessed on: February 7, 2022.
[2] Wikipedia: `https://en.wikipedia.org/wiki/Airkraft_Sunny`. Accessed: February 7, 2022.
[3] Homepage: `http://www.idintos.eu/eng/`. Accessed on: February 7, 2022

8.3. RECOMMENDATIONS

All of the main conclusions drawn in the present dissertation, have been made on the basis of results obtained for a staggered box-wing configuration, for which control surfaces lie both fore and aft the aircraft center of gravity. This is sufficient to verify the correctness and relevance of the proposed methods, but does not say much about the actual applicability and efficacy of the latter to real world scenarios and current state-of-art conventional aircraft configurations.

First and foremost, the development of specific flying and handling qualities metrics for DLC longitudinal response types should be addressed. Piloted simulations, with subjective evaluations from pilots, could take the current understanding of DLC transient response characteristics one step further, and could provide new insights about the applicability of already existing flying and handling qualities criteria. In these regards, a central role is going to be played by the selected structure of the control law, including the CA strategy of all control effectors involved and the response type chosen for the pilot input (pitch rate, load factor, angle of attack, pitch attitude).

From a closely related standpoint, more research should be conducted on the physical significance of the CCoP and its exploitability in engineering applications. Since its position is extremely sensitive to the deflection of each control surface, it would be interesting to determine whether monitoring the CCoP in maneuvering flight could actually be beneficial for the development of closed-loop FCS logics. In order to do so, its relation to the aircraft center of pressure and ICR should be first formalized for configurations with redundant control surfaces.

From a broader perspective, CA methods and approaches are still inherently limited by the phenomenon of control effectiveness reversal in specific flight regimes. In the longitudinal axis only, this is critical for DLC and pitch control when control surfaces are close to stall, as it can cause chattering of the effectors around the reversal point. The latter phenomenon is typically undesired, and is currently entirely avoided by either enforcing premature saturation of the effectors, or mitigated by using local control effectiveness and employing filtering logics at FCS level. The same chattering phenomenon, moreover, fundamentally hinders the possibility to employ direct drag control in fast maneuvering flight.

Despite sparking out of pure control theory, and relying almost entirely on fundamental abstract algebra, CA methods should be injected in traditional aircraft design studies more frequently. Exploiting their properties already from the conceptual and preliminary design stages may have profound consequences on several design choices, also at the whole aircraft configuration level. This type of synergy between different disciplines should be encouraged especially in the case of unconventional aircraft configurations, which are usually highly integrated and commonly require multi-disciplinary analyses to perform adequately.

Lastly, the actual role and relevance of unconventional aircraft configurations in the future aircraft market seems, at this point, still unclear. Further research, and at higher TRL, needs to be conducted to obtain better assessment of such disruptive configurations and of the innovative ways they can exploit the available technologies to reshape the aviation market as a whole. In the case of box-wing aircraft, and of the PrP configuration in particular, several questions still need to be properly addressed. The most prac-

tical one, as it also happens for other disruptive aircraft configurations, concerns the possibility of the PrP to easily generate aircraft families. The complex geometry of the staggered box-wing does not lend itself to simple approaches for redesign or adaptation. Conceiving an aircraft family based around it is not as straightforward as simply stretching the fuselage with extra cylindrical sections. This is surely one of the most important aspects to consider when proposing a disruptive configuration as a potential solution for the sustainability of future aviation, since the possibility to generate an aircraft family has constituted, and still does nowadays, a fundamental cost mitigation strategy for all commercial airliners.

ACKNOWLEDGEMENTS

It is well to remember that the entire universe,
with one trifling exception,
is composed of others.

John Andrew Holmes
Poet

To learn, to love,
to burn brightly within my circle of influence,
to leave a legacy.

David McDowell Brown
Space Shuttle Columbia Astronaut

Completing this PhD research project has been a long journey of dedication and discovery. Surely, a big part of it has consisted of reading papers, studying models and methods, making efforts to deliver small contributions to the unlimited world of science. But the most important exploration is probably the one that has taken place within myself. Either through self-reflection and mindfulness, or, most importantly, through the interaction with the many and very diverse people I've had the pleasure to meet during this adventurous quest.

This is why, first and foremost, I would like to thank my colleagues. Despite our research has taken us to different places, practically or metaphorically, we have shared the rooms and the moods of these offices for too long to pretend that we haven't left a mark on each other at all. I could not have done this without your company and your support, and I know I would not be willing to give up the after-lunch coffee break on the sixth floor, not even for some good quality coffee. Tarik, Reynard and Malcom; Sumit, Biagio, Kushagra, Reno, Fabrizio, Nando, Maurice, Tomas, Martijn, Hugo, Marco, Pedro, Nitish, Rishikesh, Sonia, Francesco, Federica, Nitish, André, Adam, Sebastian; Akshay, Imco, Anne-Liza, Pieter-Jan; Robert, Ramon, Giuseppe and Sarah. Without you, the FPP group would just be the FPP section.

I would like to thank my supervisor, for his impeccable support throughout these years. Mark, your precious suggestions have helped me to understand the type of research I like to do, as well as to get it on the right track at the very beginning. Your expert, precise and timely feedback has been fundamental to increase the quality of my studies, and to constantly push them one step beyond.

I would like to thank my promotor, for trusting me with so many responsibilities, backing me up and challenging me whenever necessary. Leo, your guidance and vision

have been invaluable to enrich and broaden the scope of my reasoning. Your experience in finding different perspectives, and to choose the right words to present them, has taught me to constantly look at the most fundamental aspects of my research, and to ask better, deeper and more "uncomfortable" questions.

I would like to reserve a special thanks to Gianfranco. Your advice has always been extremely precious to find the right way forward. In a few occasions, it has been truthfully essential to get my bearings back, to be able to focus again on what I love doing and the way I like doing it.

I would like to thank all of the MSc students that I have had the pleasure to supervise. Ester, Daniele, Davide, Luca, Francesca, Marco, Sam, Adele, Nicolas, Godert and Willy. You have gifted me with the honor and the responsibility to initiate you to the world of scientific and engineering research, and to guide you through the challenges of your first real research project. I have never given this for granted, and I hope I could contribute to the sparking of a long-lasting passion and the beginning of a brilliant career.

Of course, I would also like to thank my closest friends: Ciro, Nicolò, Lorenzo and Erasmo. Whether we meet over a video call, over a drink in the city center, on the rock by the sea, or at the park to watch the sunset, your company has the power to remind me of my dearest origins and to bring me back to the solid values that we share.

And last, but surely not least, I would like to thank my family. My parents Giovanni and Annamaria, my brother Matteo, nonna Mary, zia Antonella, zio Massimo and zio Enrico, zia Paola and my cousins Vittoria, Francesca and Francesca, my girlfriend Sarah. Your unconditional love is an immortal source of motivation to try to be a better person, every day and in all aspects of my life.

GLOSSARY

Action Space

It is a Cartesian axis system in the $\mathbb{R}^{N_A}$ space, with an aerodynamic control action — force or moment, dimensional or dimensionless — varying on each axis. Each resultant control action generated by a combination of control effector displacements is represented by a point in Action Space. The Effective Actions Set and the Attainable Actions Set belong to Action Space. It is first introduced in Section 2.3.

Admissible Controls Set

It is the set of all possible effectors displacements admitted by the physical realization of the Flight Control System and the aircraft architecture. It is a subset of Control Space. If the effectors positions are simply bounded, the Admissible Controls Set is a hyper-rectangle in Control Space. It maps to the Effective Actions Set through a linear application based on the effectiveness matrix B. It is first introduced in Section 2.3.

Attainable Actions Set

It is the subset of the Effective Actions Set which a Control Allocation method can trace to feasible positions of the effectors. Control objectives of the Effective Actions Set which are outside of the Attainable Actions Set are unattainable by the given Control Allocation algorithm, despite being actually attainable by the control power available to the aircraft. This is only dependent on the formulation of the Control Allocation problem. In classic Control Allocation literature, it is usually referred to as the "Attainable Moment Set". It is first introduced in Section 2.5, and its geometry is exploited in Chapters 5 and 6.

Constrained Weighted Pseudo Inverse

It is an alternative formulation of the Weighted Pseudo Inverse Control Allocation method, including upper and lower bounds for the effectors directly in the optimization problem. This addition makes the problem formuation inherently nonlinear. For this reason, differently from the Weighted Pseudo Inverse case, the analytic solution is not available, and the Control Allocation problem must be solved via an iterative algorithm. It is presented in Section 2.4.2 and used in Chapter 5.

Control Allocation

It is a technique used to calculate the optimal effectors displacements necessary to achieve an assigned control goal. The control goal is usually prescribed by an overarching control law or directly by the pilot. The objective of the Control Allocation problem is to associate a given point in Action Space, either inside or outside of the Effective Actions Set, to a point belonging to the Admissible Controls

Set. Control Allocation methods can be in the form of analytical functions or iterative algorithms, and almost always move from the formulation of an optimization problem. Solutions can be obtained in closed form expression or by convergence of numerical methods. The most relevant aspects of the Control Allocation problem are presented in Chapter 2.

Control Center of Pressure

It is the application point of lift generated exclusively by control effectors. It is also related to the aircraft Instantaneous Center of Rotation. Its longitudinal position heavily influences the characteristics of the longitudinal response of the aircraft, and determines the possibility to achieve Direct Lift Control more or less effectively. Its role in aircraft control is described in Section 1.1.2. Its defition is then exploited in Chapter 7 to formulate a novel Control Allocation method.

Control Effectors

Control effectors are intended as different types of physical devices which are able to generate control forces and/or moments on the aircraft, in a sufficiently small time span, for the sake of maneuvering flight. Control effectors include aerodynamic control surfaces, throttle and thrust vectoring systems; but also devices for active flow control, variable camber airfoils, or integrated architectures such as the propulsive empennage concept employed by the DUUC aircraft. It is a broad definition, exploited whenever possible throughout the entire dissertation for the sake of generality. It has been first introduced in Chapter 1, and heavily used in Chapter 2.

Control Space

It is a Cartesian axis system in the $\mathbb{R}^{N_u}$ space, with a control effector displacement varying on each axis. Each combination of control effectors displacements is represented by a point in Control Space. The Admissible Controls Set belongs to Control Space. It is first introduced in Section 2.3.

Conventional Pitch Control

It refers to the use control effectors with the aim of generating moments about the aircraft center of gravity. For all airplanes with conventional architecture, a tail elevator is used to generate a small, dislocated control lift, which is relevant only insofar it produces a significant pitch moment and gives raise to some angle of attack dynamics. Conventional Pitch Control is a very indirect control technique, which results in a time delay of the trajectory response, and non-minimum phase behaviour in the vertical axis dynamics. These aspects are first introduced in Section 1.1.

Direct Allocation

It is a Control Allocation method formulated on the basis of the geometry of the Effective Actions Set. By definition, Direct Allocation is hence capable to attain all of the prescribed control objectives within the Effective Actions Set or on its boundary. It takes into account effectors saturation limits and preserves directionality in

Action Space for unattainable desired moments, but does not allow any prioritization of effectors. It must be solved by an iterative algorithm, and the most efficient one uses linear programming techniques. It is introduced in Section 2.4.3, implemented in Chapters 5 and 6 and considered in Chapter 7.

Direct Lift Control

It is defined as the capability to use control effectors to alter the aircraft lift "without, or largely without, significant change in the aircraft incidence, and ideally is meant not to generate pitching moment". In the case of Direct Lift Control, the lift unbalance caused by control effectors can rapidly result in a translational acceleration, and hence in a variation of the aircraft trajectory, through alteration of the flight path angle. It features more rapid trajectory response, and no non-minimum phase behaviour, as compared to Conventional Pitch Control. It is introduced in Section 1.1.

Effective Actions Set

It is the set of all control forces and moments that can be, in principle, generated by the effectors. In general, it is a function of the Admissible Controls Set and of a given flight condition. For a linear aerodynamic model, if the control effectiveness matrix B is constant and the Admissible Controls Set is a convex set, the Effective Actions Set is a bounded convex polytope in Action Space. In classic Control Allocation literature, it is usually referred to as "Largest Attainable Moment Set". It is introduced in Section 2.3 and further discussed in Section 2.5.

Flight Control System

It is the set of aircraft components, mechanisms and devices that serve to control the aircraft attitude and direction in flight. It links the pilot inputs to the control effectors, or commands the control effectors according to prescribed feedback signals and control laws. The most basic Flight Control System architecture consists of mechanical linkages which gear and gang control effectors, and directly connect them to the pilot input in the cockpit. More advanced Flight Control System architectures command the effectors through electronic interfaces (fly-by-wire) regulated by flight computers, and/or make use of different types of actuators to overcome the hinge moments due to great dynamic pressure. Some general considerations on the architecture of the Flight Control System, and specifically on ganging control surfaces, are made in Sections 1.2, 2.1 and 2.4.1. The baseline Flight Control System architecture used for all flight simulations used in the present dissertation, if not specified otherwise, is presented in Section 3.3.1. A particular Flight Control System architecture has been developed in Section 7.2 for comparing the transient response of the PrandtlPlane for different positions of the Control Center of Pressure.

Flying Qualities

They indicate the characteristics of an aircraft concerning aspects such as equilibrium, static stability, dynamic stability, control and dynamic response. All of

these disciplines have to be studied to determine if the aircraft can be flown appropriately and safely in steady and maneuvering flight, "regardless of design implementation or Flight Control System mechanization". Flying Qualities can be measured objectively through flight simulation and/or flight testing. Their values should comply with specific, quantitative criteria in order to qualify the aircraft performance as satisfying, acceptable or unacceptable. In these regards, they differ from handling qualities, which involve the pilot maneuvering experience and have to be evaluated with more subjective methods. Reference Flying Qualities requirements are used in Chapter 5, and specifically presented in Section 5.2.3.

PrandtlPlane

It is an innovative aircraft configuration, featuring a staggered box-wing geometry, and designed to be operated for commercial transport in the short and medium range segment. Thanks to the optimum induced drag properties of the box-wing, it has been identified as one of the possible solutions towards more sustainable aviation in the near future. The double wing architecture allows to position multiple control surfaces, which are redundant for the longitudinal and lateral control of the aircraft. As they fall both in front and behind the aircraft center of gravity, the PrandtlPlane represents a good test subject to explore innovative applications of Control Allocation methods and Direct Lift Control. It is first introduced in Chapter 1 and presented in more detail in Section 3.1.

Pseudo Inverse

It is a particular formulation of the Weighted Pseudo Inverse Control Allocation method, which does not prioritize the control effectors, by using an identity weighting matrix W, and uses their neutral position as the reference one. In the same way as for the Weighted Pseudo Inverse, this formulation also results in a closed form solution, but its Attainable Actions Set is always smaller than the corresponding Effective Actions Set. It is first presented in Section 2.4.2 and used in Chapters 5 and 7.

Root Mean Square

It is defined as the square root of the arithmetic mean of the squares of a given set of values, as reported in the equation below.

$$x_{\text{RMS}} = \sqrt{\frac{1}{N}\left(x_1^2 + x_2^2 + \ldots + x_N^2\right)}$$

The Root Mean Square error, where x is the error, is a common measure of the difference between two data sets, one of which can generally be treated as reference. The latter is used to evaluate the aircraft tracking performance in Chapter 7.

Weighted Pseudo Inverse

It is a Control Allocation method based on a generalized inverse formulation. It results from an optimization problem to minimize control effort while ensuring that the Control Allocation problem is satisfied. It uses a weighting matrix W to prioritize the control effectors, and a reference position of the effectors $\boldsymbol{u}_{\text{ref}}$ to drive

the Control Allocation problem to a preferred solution. Both of these parameters need to be prescribed according to some criterion, and can be shaped according to the application of interest. This Control Allocation formulation results in a closed form solution, but its Attainable Actions Set is always smaller than the corresponding Effective Actions Set, as for all generalized inverses. It is first presented in Section 2.4.2, and an original implementation of it is proposed in Chapter 7.

REFERENCES

[1] Airbus.
Global Market Forecast 2019 – 2038.
Tech. rep.
Blagnac, France: Airbus S.A.S., 2019.
URL: https://www.airbus.com/aircraft/market/global-market-forecast.html.

[2] Boeing.
Commercial Market Outlook 2020 – 2039.
Tech. rep.
Chicago, Illinois, U.S.A.: The Boeing Company, 2020.
URL: http://www.boeing.com/commercial/market/commercial-market-outlook/.

[3] European Organisation for the Safety of Air Navigation.
Comprehensive Assessment of COVID-19's Impact on European Air Traffic.
Tech. rep.
EUROCONTROL, 2021.
URL: https://www.eurocontrol.int/sites/default/files/2021-05/covid19-eurocontrol-comprehensive-air-traffic-assessment-27052021.pdf.

[4] S. Gudmundsson, M. Cattaneo, and R. Redondi.
"Forecasting temporal world recovery in air transport markets in the presence of large economic shocks: The case of COVID-19".
In: *Journal of Air Transport Management* 91 (Mar. 2021), p. 102007.
DOI: 10.1016/j.jairtraman.2020.102007.

[5] German Aerospace Center.
Report on socio-economic scenarios and expectations.
Tech. rep. PARSIFAL Deliverable 1.1.
Deutsches Zentrum fur Luft- und Raumfahrt, University of Pisa, SkyBox Engineering, 2017.
URL: https://www.parsifalproject.eu/PARSIFAL_DOWNLOAD/PARSIFAL_D11.pdf.

[6] Directorate General for Research and Innovation, Directorate General for Mobility and Transport.
Flightpath 2050: Europe's Vision for Aviation.
Tech. rep.
European Commission, 2011.
URL: https://ec.europa.eu/transport/sites/transport/files/modes/air/doc/flightpath2050.pdf.

[7] Intergovernmental Panel on Climate Change.
Mitigation of Climate Change. Contribution of Working Group III to the Fifth Assessment Report of the Intergovern-mental Panel on Climate Change.
Tech. rep.
United Nations, 2014.
Chap. Transport.
URL: https://www.ipcc.ch/site/assets/uploads/2018/02/ipcc_wg3_ar5_chapter8.pdf.

[8] M. Hoogreef, R. Vos, R. de Vries, et al.
"Conceptual Assessment of Hybrid Electric Aircraft with Distributed Propulsion and Boosted Turbofans".
In: *AIAA Scitech 2019 Forum.*
American Institute of Aeronautics and Astronautics, Jan. 2019.
DOI: 10.2514/6.2019-1807.

[9] B. J. Brelje and J. R. Martins.
"Electric, hybrid, and turboelectric fixed-wing aircraft: A review of concepts, models, and design approaches".
In: *Progress in Aerospace Sciences* 104 (Jan. 2019), pp. 1–19.
DOI: 10.1016/j.paerosci.2018.06.004.

[10] J. Ribeiro, F. Afonso, I. Ribeiro, et al.
"Environmental assessment of hybrid-electric propulsion in conceptual aircraft design".
In: *Journal of Cleaner Production* 247 (Feb. 2020), p. 119477.
DOI: 10.1016/j.jclepro.2019.119477.

[11] E. O. Osigwe, A. Gad-Briggs, T. Nikolaidis, et al.
"Thermodynamic Performance and Creep Life Assessment Comparing Hydrogen- and Jet-Fueled Turbofan Aero Engine".
In: *Applied Sciences* 11.9 (Apr. 2021), p. 3873.
DOI: 10.3390/app11093873.

[12] Y. Liu, A. Elham, P. Horst, et al.
"Exploring Vehicle Level Benefits of Revolutionary Technology Progress via Aircraft Design and Optimization".
In: *Energies* 11.1 (Jan. 2018), p. 166.
DOI: 10.3390/en11010166.

[13] P. Okonkwo and H. Smith.
"Review of evolving trends in blended wing body aircraft design".
In: *Progress in Aerospace Sciences* 82 (Apr. 2016), pp. 1–23.
DOI: 10.1016/j.paerosci.2015.12.002.

[14] R. Martinez-Val, E. Perez, P. Alfaro, et al.
"Conceptual design of a medium size flying wing".
In: *Proceedings of the Institution of Mechanical Engineers, Part G: Journal of Aerospace Engineering* 221.1 (Jan. 2007), pp. 57–66.
DOI: 10.1243/09544100jaero90.

[15] R. H. Liebeck.
"Design of the Blended Wing Body Subsonic Transport".
In: *Journal of Aircraft* 41.1 (Jan. 2004), pp. 10–25.
DOI: 10.2514/1.9084.

[16] A. R. Garcia, R. Vos, and C. de Visser.
"Aerodynamic Model Identification of the Flying V from Wind Tunnel Data".
In: *AIAA Aviation 2020 Forum*.
American Institute of Aeronautics and Astronautics, June 2020.
DOI: 10.2514/6.2020-2739.

[17] R. Cavallaro and L. Demasi.
"Challenges, Ideas, and Innovations of Joined-Wing Configurations: A Concept from the Past, an Opportunity for the Future".
In: *Progress in Aerospace Sciences* 87 (Nov. 2016), pp. 1–93.
DOI: 10.1016/j.paerosci.2016.07.002.

[18] S. A. Andrews.
"Multidisciplinary Analysis of Closed Nonplanar Wing Configurations for Transport Aircraft".
PhD thesis. Royal Military College of Canada, 2016.
URL: https://central.bac-lac.gc.ca/.item?id=TC-OKR-981&op=pdf&app=Library&oclc_number=1032934227.

[19] L. Prandtl.
Induced Drag of Multiplanes.
NACA Technical Note 182.
National Advisory Committee for Aeronautics, 1924.
URL: http://digital.library.unt.edu/ark:/67531/metadc53856.

[20] M. M. Munk.
The Minimum Induced Drag of Aerofoils.
Tech. rep. NACA-TR-121.
National Advisory Committee for Aeronautics, 1923.
URL: https://ntrs.nasa.gov/citations/19930091456.

[21] L. Demasi, G. Monegato, and R. Cavallaro.
"Minimum Induced Drag Theorems for Multi-Wing Systems".
In: *57th AIAA/ASCE/AHS/ASC Structures, Structural Dynamics, and Materials Conference.*
American Institute of Aeronautics and Astronautics, Jan. 2016.
DOI: 10.2514/6.2016-0236.

[22] A. Frediani, V. Cipolla, and E. Rizzo.
"The PrandtlPlane Configuration: Overview on Possible Applications to Civil Aviation".
In: *Springer Optimization and Its Applications.*
Springer US, 2012,
Pp. 179–210.
DOI: 10.1007/978-1-4614-2435-2_8.

[23] A. Frediani, V. Cipolla, and F. Oliviero.
"Design of a prototype of light amphibious PrandtlPlane".
In: *56th AIAA/ASCE/AHS/ASC Structures, Structural Dynamics, and Materials Conference.*
Kissimmee, Florida, Jan. 2015.
DOI: 10.2514/6.2015-0700.

[24] P. O. Jemitola.
"Conceptual design and optimization methodology for box wing aircraft".
PhD thesis. School of Aerospace Engineering, Cranfield University, 2012.
URL: http://dspace.lib.cranfield.ac.uk/handle/1826/7938.

[25] A. Tomczyk.
"Aircraft maneuverability improvement by direct lift control system application".
In: *Aerospace Science and Technology* 9.8 (Nov. 2005), pp. 692–700.
DOI: 10.1016/j.ast.2005.09.004.

[26] R. M. Wood and S. X. S. Bauer.
Advanced Aerodynamic Control Effectors.
Report Rept-1999-01-5619.
NASA Langley Research Center, 1999.
URL: https://ntrs.nasa.gov/citations/20040086755.

[27] W. J. G. Pinsker.
The Control Characteristics of Aircraft Employing Direct-Lift Control.
Reports and Memoranda 3629.
Ministry of Aviation, Aeronautical Research Council, 1968.
URL: https://reports.aerade.cranfield.ac.uk/handle/1826.2/2896.

[28] L. O. Lykken and N. M. Shah.
"Direct Lift Control for Improved Automatic Landing and Performance of Transport Aircraft".
In: *Journal of Aircraft* 9.5 (May 1972), pp. 325–332.
DOI: 10.2514/3.58988.

[29] W. E. McNeill, R. M. Gerdes, R. C. Innis, et al.
A flight study of the use of direct-lift-control flaps to improve station keeping during in-flight refueling.
Technical Memorandum NASA-TM-X-2936.
NASA Ames Research Center, 1973.
URL: https://ntrs.nasa.gov/citations/19730024237.

[30] R. Merat.
"Study of a Direct Lift Control System Based on the A380 Aircraft".
In: *46th AIAA Aerospace Sciences Meeting and Exhibit.*
American Institute of Aeronautics and Astronautics, Jan. 2008.
DOI: 10.2514/6.2008-1432.

[31] T. Lombaerts and G. Looye.
"Design and Flight Testing of Nonlinear Autoflight Control Laws Incorporating Direct Lift Control".
In: *Advances in Aerospace Guidance, Navigation and Control*.
Springer Berlin Heidelberg, 2013,
Pp. 549–568.
DOI: 10.1007/978-3-642-38253-6_32.

[32] D. L. Mallick and P. W. Merlin.
The Smell of Kerosene: A Test Pilot's Odyssey.
NASA History Series, NASA SP Series 4108.
National Aeronautics and Space Administration, 2013.
ISBN: 9781481990172.
URL: https://www.nasa.gov/centers/dryden/pdf/88797main_kerosene.pdf.

[33] C. S. Barnes.
A Developed Theory of Spoilers on Aerofoils.
Tech. rep. 887.
Ministry of Aviation, Aeronautical Research Council, 1966.
URL: http://naca.central.cranfield.ac.uk/reports/arc/rm/3629.pdf.

[34] D. Loebl, M. Weiss, F. Holzapfel, et al.
"Cooperative Docking Guidance and Control with Application to Autonomous Aerial Refueling".
In: *2018 AIAA Guidance, Navigation, and Control Conference*.
American Institute of Aeronautics and Astronautics, Jan. 2018.
DOI: 10.2514/6.2018-1598.

[35] D. M. Shafer, R. C. Paul, M. J. King, et al.
"Aircraft Carrier Landing Demonstration using Manual Control by a Ship-based Observer".
In: *AIAA Scitech 2019 Forum*.
American Institute of Aeronautics and Astronautics, Jan. 2019.
DOI: 10.2514/6.2019-0010.

[36] A. Galffy, M. Bock, and A. Kugi.
"Nonlinear 3D path following control of a fixed-wing aircraft based on acceleration control".
In: *Control Engineering Practice* 86 (May 2019), pp. 56–69.
DOI: 10.1016/j.conengprac.2019.03.006.

[37] J. Pravitra and E. N. Johnson.
"Adaptive Control for Attitude Match Station-Keeping and Landing of a Fixed-Wing UAV onto a Maneuvering Platform".
In: *AIAA Scitech 2020 Forum*.
American Institute of Aeronautics and Astronautics, Jan. 2020.
DOI: 10.2514/6.2020-1082.

[38] C. Harley.
"Aerodynamic Performance of Low Form Factor Spoilers".
PhD thesis. The University of Manchester, 2011.
URL: https://www.escholar.manchester.ac.uk/uk-ac-man-scw:121110.

[39] M. DeSalvo, D. Heathcote, M. J. Smith, et al.
"Direct Lift Control using Distributed Aerodynamic Bleed".
In: *AIAA Scitech 2019 Forum*.
American Institute of Aeronautics and Astronautics, Jan. 2019.
DOI: 10.2514/6.2019-0591.

[40] C. Perkins and R. Hage.
Airplane Performance, Stability and Control.
John Wiley and Sons, 1949.
ISBN: 047168046X.

[41] W. Durham, K. A. Bordignon, and R. Beck.
Aircraft Control Allocation.
Wiley, Jan. 2017.

312 pp.
ISBN: 1118827791.

[42] D. van Ginneken, M. Voskuijl, M. van Tooren, et al.
"Automated Control Surface Design and Sizing for the Prandtl Plane".
In: *51st AIAA/ASME/ASCE/AHS/ASC Structures, Structural Dynamics, and Materials Conference*.
American Institute of Aeronautics and Astronautics, Apr. 2010.
DOI: 10.2514/6.2010-3060.

[43] M. Voskuijl, J. de Klerk, and D. van Ginneken.
"Flight Mechanics Modeling of the PrandtlPlane for Conceptual and Preliminary Design".
In: *Springer Optimization and Its Applications*.
Springer US, 2012,
Pp. 435–462.
DOI: 10.1007/978-1-4614-2435-2_19.

[44] Y. Denieul, J. Bordeneuve, D. Alazard, et al.
"Multicontrol Surface Optimization for Blended Wing–Body Under Handling Quality Constraints".
In: *Journal of Aircraft* 55.2 (Mar. 2018), pp. 638–651.
DOI: 10.2514/1.c034268.

[45] D. Cameron and N. Princen.
"Control allocation challenges and requirements for the Blended Wing Body".
In: *AIAA Guidance, Navigation, and Control Conference and Exhibit*.
American Institute of Aeronautics and Astronautics, Aug. 2000.
DOI: 10.2514/6.2000-4539.

[46] M. Oppenheimer and D. Doman.
"A Method for Including Control Effector Interactions in the Control Allocation Problem".
In: *AIAA Guidance, Navigation and Control Conference and Exhibit*.
American Institute of Aeronautics and Astronautics, Aug. 2007.
DOI: 10.2514/6.2007-6418.

[47] C. Varriale, K. Hameeteman, M. Voskuijl, et al.
"A Thrust-Elevator Interaction Criterion for Aircraft Optimal Longitudinal Control".
In: *AIAA Aviation 2019 Forum*.
American Institute of Aeronautics and Astronautics, June 2019.
DOI: 10.2514/6.2019-3001.

[48] W. C. Durham, J. G. Bolling, and K. A. Bordignon.
"Minimum Drag Control Allocation".
In: *Journal of Guidance, Control, and Dynamics* 20.1 (Jan. 1997), pp. 190–193.
DOI: 10.2514/2.4018.

[49] R. E. Beck.
"Application of Control Allocation Methods to Linear Systems with Four or More Objectives".
PhD thesis. Virginia Tech, 2002.
URL: http://hdl.handle.net/10919/28088.

[50] M. Bolender and D. Doman.
"A method for the determination of the attainable moment set for nonlinear control effectors".
In: *IEEE Aerospace Conference Proceedings*.
2003.
DOI: 10.1109/AERO.2003.1235203.

[51] T. A. Johansen, T. P. Fuglseth, P. Tøndel, et al.
"Optimal constrained control allocation in marine surface vessels with rudders".
In: *IFAC Proceedings Volumes* 36.21 (Sept. 2003), pp. 181–186.
DOI: 10.1016/s1474-6670(17)37804-7.

[52] F. A. de Almeida.
"Robust off-line control allocation".
In: *Aerospace Science and Technology* 52 (May 2016), pp. 1–9.
DOI: 10.1016/j.ast.2016.02.002.

[53] K. A. Bordignon.
"Constrained control allocation for systems with redundant control effectors".
PhD thesis. Virginia Tech, 1996.
URL: http://hdl.handle.net/10919/28570.

[54] T. A. Johansen and T. I. Fossen.
"Control allocation—A survey".
In: *Automatica* 49.5 (May 2013), pp. 1087–1103.
DOI: 10.1016/j.automatica.2013.01.035.

[55] M. Bodson.
"Evaluation of Optimization Methods for Control Allocation".
In: *Journal of Guidance, Control, and Dynamics* 25.4 (July 2002), pp. 703–711.
DOI: 10.2514/2.4937.

[56] M. Bodson and S. A. Frost.
"Load Balancing in Control Allocation".
In: *Journal of Guidance, Control, and Dynamics* 34.2 (Mar. 2011), pp. 380–387.
DOI: 10.2514/1.51952.

[57] R. Stolk and C. de Visser.
"Minimum drag control allocation for the Innovative Control Effector aircraft".
In: *5th CEAS Conference on Guidance, Navigation and Control*.
2019.

[58] S. A. Frost, M. Bodson, J. J. Burken, et al.
"Flight Control with Optimal Control Allocation Incorporating Structural Load Feedback".
In: *Journal of Aerospace Information Systems* 12.12 (2015), pp. 825–834.
DOI: 10.2514/1.I010278.

[59] D. C. Garmendia.
"A multi-disciplinary conceptual design methodology for assessing control authority on a hybrid wing body configuration".
PhD thesis. Georgia Tech, 2015.
URL: http://hdl.handle.net/1853/54328.

[60] I. Matamoros and C. C. de Visser.
"Incremental Nonlinear Control Allocation for a Tailless Aircraft with Innovative Control Effectors".
In: *2018 AIAA Guidance, Navigation, and Control Conference*.
American Institute of Aeronautics and Astronautics, Jan. 2018.
DOI: 10.2514/6.2018-1116.

[61] S. M. Waters, M. Voskuijl, L. L. Veldhuis, et al.
"Control allocation performance for blended wing body aircraft and its impact on control surface design".
In: *Aerospace Science and Technology* 29.1 (Aug. 2013), pp. 18–27.
DOI: 10.1016/j.ast.2013.01.004.

[62] C. Huijts and M. Voskuijl.
"The impact of control allocation on trim drag of blended wing body aircraft".
In: *Aerospace Science and Technology* 46 (Oct. 2015), pp. 72–81.
DOI: 10.1016/j.ast.2015.07.001.

[63] D. Doman and M. Oppenheimer.
"Improving Control Allocation Accuracy for Nonlinear Aircraft Dynamics".
In: *AIAA Guidance, Navigation, and Control Conference and Exhibit*.
American Institute of Aeronautics and Astronautics, Aug. 2002.
DOI: 10.2514/6.2002-4667.

[64] O. Härkegård.
"Dynamic Control Allocation Using Constrained Quadratic Programming".
In: *Journal of Guidance, Control, and Dynamics* 27.6 (Nov. 2004), pp. 1028–1034.
DOI: 10.2514/1.11607.

[65] K. Bordignon and J. Bessolo.
"Control Allocation for the X-35B".
In: *2002 Biennial International Powered Lift Conference and Exhibit*.
American Institute of Aeronautics and Astronautics, June 2002.
DOI: 10.2514/6.2002-6020.

[66] J. J. Harris.
"F-35 Flight Control Law Design, Development and Verification".
In: *2018 Aviation Technology, Integration, and Operations Conference*.
American Institute of Aeronautics and Astronautics, June 2018.
DOI: 10.2514/6.2018-3516.

[67] A. Frediani, V. Cipolla, K. A. Salem, et al.
"Conceptual design of PrandtlPlane civil transport aircraft".
In: *Proceedings of the Institution of Mechanical Engineers, Part G: Journal of Aerospace Engineering* 234.10 (Feb. 2019), pp. 1675–1687.
DOI: 10.1177/0954410019826435.

[68] R. Martinez-Val and E. Schoep.
"Flying Wing versus Conventional Transport Airplane: The 300 Seat Case".
In: *Proceedings of the 22nd ICAS Congress*.
2000.
URL: http://www.icas.org/ICAS_ARCHIVE/ICAS2000/PAPERS/ICA0113.PDF.

[69] University of Pisa, Delft University of Technology, and Skybox Engineering.
Requirements for the adoption of the PrandtlPlane as a means of transport.
Tech. rep. PARSIFAL Deliverable 2.1.
2017.
URL: https://www.parsifalproject.eu/PARSIFAL_DOWNLOAD/PARSIFAL_D21.pdf.

[70] V. Cipolla, A. Frediani, K. Abu Salem, et al.
"Conceptual design of a box-wing aircraft for the air transport of the future".
In: *2018 Aviation Technology, Integration, and Operations Conference*.
2018.
DOI: 10.2514/6.2018-3660.

[71] K. Abu Salem, V. Cipolla, M. Carini, et al.
"Aerodynamic design and preliminary optimization of a commercial PrandtlPlane aircraft".
In: *Proceedings of the 8th European Conference for Aeronautics and Space Sciences*.
2019.
DOI: 10.13009/EUCASS2019-741.

[72] G. La Rocca.
"Knowledge based engineering techniques to support aircraft design and optimization".
PhD thesis. Delft University of Technology, 2011.
URL: http://resolver.tudelft.nl/uuid:45ed17b3-4743-4adc-bd65-65dd203e4a09.

[73] A. R. Kulkarni, C. Varriale, M. Voskuijl, et al.
"Assessment of Sub-scale Designs for Scaled Flight Testing".
In: *AIAA Aviation 2019 Forum*.
American Institute of Aeronautics and Astronautics, June 2019.
DOI: 10.2514/6.2019-3089.

[74] A. R. Kulkarni, G. L. Rocca, and L. L. Veldhuis.
"Degree of similitude estimation for sub-scale flight testing".
In: *AIAA Scitech 2019 Forum*.
American Institute of Aeronautics and Astronautics, Jan. 2019.
DOI: 10.2514/6.2019-1208.

[75] A. Rizzi, M. Zhang, B. Nagel, et al.
"Towards a Unified Framework using CPACS for Geometry Management in Aircraft Design".
In: *50th AIAA Aerospace Sciences Meeting including the New Horizons Forum and Aerospace Exposition*.
American Institute of Aeronautics and Astronautics, Jan. 2012.
DOI: 10.2514/6.2012-549.

[76] E. J. Schut and M. J. L. van Tooren.
"Design "Feasilization" Using Knowledge-Based Engineering and Optimization Techniques".
In: *Journal of Aircraft* 44.6 (Nov. 2007), pp. 1776–1786.
DOI: 10.2514/1.24688.

[77] R. Vos and M. Hoogreef.
"Semi-Analytical Weight Estimation Method for Fuselages with Oval Cross-Section".
In: *54th AIAA/ASME/ASCE/AHS/ASC Structures, Structural Dynamics, and Materials Conference*.
American Institute of Aeronautics and Astronautics, Apr. 2013.
DOI: 10.2514/6.2013-1719.

[78] R. J. M. Elmendorp, R. Vos, and G. La Rocca.
"A Conceptual Design and Analysis Method for Conventional and Unconventional Airplanes".
In: *ICAS 2014 : Proceedings of the 29th Congress of the International Council of the Aeronautical Sciences, St. Peterburg, Russia*.
International Council of the Aeronautical Sciences, 2014.
URL: http://resolver.tudelft.nl/uuid:1dc55ce5-18c3-4986-b668-f70d9b24aac0.

[79] M. Hoogreef, R. de Vries, T. Sinnige, et al.
"Synthesis of Aero-Propulsive Interaction Studies Applied to Conceptual Hybrid-Electric Aircraft Design".
In: *AIAA Scitech 2020 Forum*.
American Institute of Aeronautics and Astronautics, Jan. 2020.
DOI: 10.2514/6.2020-0503.

[80] G. La Rocca.
"Knowledge based engineering: Between AI and CAD. Review of a language based technology to support engineering design".
In: *Advanced Engineering Informatics* 26.2 (Apr. 2012), pp. 159–179.
DOI: 10.1016/j.aei.2012.02.002.

[81] M. Tobak.
Mathematical Modeling of the Aerodynamic Characteristics in Flight Dynamics.
Tech. rep. NASA-TM-85880.
NASA, 1984.
URL: https://ntrs.nasa.gov/citations/19840009073.

[82] M. Ghoreyshi, K. J. Badcock, and M. A. Woodgate.
"Accelerating the Numerical Generation of Aerodynamic Models for Flight Simulation".
In: *Journal of Aircraft* 46.3 (May 2009), pp. 972–980.
DOI: 10.2514/1.39626.

[83] A. Da Ronch, M. Ghoreyshi, and K. J. Badcock.
"On the generation of flight dynamics aerodynamic tables by computational fluid dynamics".
In: *Progress in Aerospace Sciences* 47.8 (Nov. 2011), pp. 597–620.
DOI: 10.1016/j.paerosci.2011.09.001.

[84] L. L. Erickson.
Panel methods: An introduction.
Technical Publication NASA-TP-2995.
NASA Ames Research Center, 1990.
URL: https://ntrs.nasa.gov/citations/19910009745.

[85] J. K. Nathman.
VSAERO 7.9: A Computer Program for Calculating the Nonlinear Aerodynamic Characteristics of Arbitrary Configurations.
Stark Aerospace, Inc. 8440 154th Avenue NE, Redmond,Washington, DC, USA, 2016.

[86] P. Boschetti, E. Cárdenas, A. Amerio, et al.
"Stability and Performance of a Light Unmanned Airplane in Ground Effect".
In: *48th AIAA Aerospace Sciences Meeting Including the New Horizons Forum and Aerospace Exposition*.
American Institute of Aeronautics and Astronautics, Jan. 2010.
DOI: 10.2514/6.2010-293.

[87] R. Lykins, R. Riley, G. Garcia, et al.
"Modal Analysis of 1/3-Scale Yak-54 Aircraft Through Simulation and Flight Testing".
In: *AIAA Atmospheric Flight Mechanics Conference*.
American Institute of Aeronautics and Astronautics, June 2011.
DOI: 10.2514/6.2011-6443.

[88] B. Mialon, A. Khrabrov, S. B. Khelil, et al.
"Validation of numerical prediction of dynamic derivatives: The DLR-F12 and the Transcruiser test cases".
In: *Progress in Aerospace Sciences* 47.8 (Nov. 2011), pp. 674–694.
DOI: 10.1016/j.paerosci.2011.08.010.

[89] T. S. Richardson, C. Beaverstock, A. Isikveren, et al.
Analysis of the Boeing 747-100 using CEASIOM.
Tech. rep. 8.
Nov. 2011,
Pp. 660–673.
DOI: 10.1016/j.paerosci.2011.08.009.

[90] T. Goetzendorf-Grabowski, D. Mieszalski, and E. Marcinkiewicz.
"Stability analysis using SDSA tool".
In: *Progress in Aerospace Sciences* 47.8 (Nov. 2011), pp. 636–646.
DOI: 10.1016/j.paerosci.2011.08.007.

[91] A. Da Ronch, M. Ghoreyshi, D. Vallespin, et al.
"A Framework for Constrained Control Allocation Using CFD-based Tabular Data".
In: *49th AIAA Aerospace Sciences Meeting including the New Horizons Forum and Aerospace Exposition*.
American Institute of Aeronautics and Astronautics, Jan. 2011.
DOI: 10.2514/6.2011-925.

[92] P. Thomas, T. Richardson, and A. Cooke.
"Estimation of Stability and Control Derivatives for a Piper Cub J-3 Remotely Piloted Vehicle".
In: *AIAA Modeling and Simulation Technologies Conference*.
American Institute of Aeronautics and Astronautics, Aug. 2012.
DOI: 10.2514/6.2012-5013.

[93] M. Salichon and K. Tumer.
"A neuro-evolutionary approach to control surface segmentation for micro aerial vehicles".
In: *International Journal of General Systems* 42.7 (Oct. 2013), pp. 793–805.
DOI: 10.1080/03081079.2013.776203.

[94] D. Lee, N. V. Nguyen, M. Tyan, et al.
"Enhanced multi-fidelity model for flight simulation using global exploration and the Kriging method".
In: *Proceedings of the Institution of Mechanical Engineers, Part G: Journal of Aerospace Engineering* 231.4 (Aug. 2016), pp. 606–620.
DOI: 10.1177/0954410016641441.

[95] M. W. Lee and K. D. Visser.
"Towards an Effective Nonplanar Wing Design Strategy".
In: *34th AIAA Applied Aerodynamics Conference*.
American Institute of Aeronautics and Astronautics, June 2016.
DOI: 10.2514/6.2016-4328.

[96] O. Dantsker and M. Vahora.
"Comparison of Aerodynamic Characterization Methods for Design of Unmanned Aerial Vehicles".
In: *2018 AIAA Aerospace Sciences Meeting*.
American Institute of Aeronautics and Astronautics, Jan. 2018.
DOI: 10.2514/6.2018-0272.

[97] M. Carini, M. Meheut, S. Kanellopoulos, et al.
"Aerodynamic analysis and optimization of a boxwing architecture for commercial airplanes".
In: *AIAA Scitech 2020 Forum*.
American Institute of Aeronautics and Astronautics, Jan. 2020.
DOI: 10.2514/6.2020-1285.

[98] M. Carini, M. Méheut, L. Sanders, et al.
Aerodynamic and Acoustic Analysis of the baseline PrandtlPlane.
Tech. rep. PARSIFAL Deliverable 4.1.
Office National d'Etudes et de Recherches Aérospatiales (ONERA), 2020.
URL: https://www.parsifalproject.eu/PARSIFAL_DOWNLOAD/PARSIFAL_D41.pdf.

[99] M. Ghoreyshi, K. J. Badcock, A. D. Ronch, et al.
"Framework for Establishing Limits of Tabular Aerodynamic Models for Flight Dynamics Analysis".
In: *Journal of Aircraft* 48.1 (Jan. 2011), pp. 42–55.
DOI: 10.2514/1.c001003.

[100] B. Etkin and L. D. Reid.
Dynamics of Flight.
John Wiley & Sons, Oct. 1995.
396 pp.
ISBN: 0471034185.

[101] D. Greenwell.
"A Review of Unsteady Aerodynamic Modelling for Flight Dynamics of Manoeuvrable Aircraft".
In: *AIAA Atmospheric Flight Mechanics Conference and Exhibit.*
American Institute of Aeronautics and Astronautics, June 2004.
DOI: 10.2514/6.2004-5276.

[102] C. A. Mader and J. R. R. A. Martins.
"Computing Stability Derivatives and Their Gradients for Aerodynamic Shape Optimization".
In: *AIAA Journal* 52.11 (Nov. 2014), pp. 2533–2546.
DOI: 10.2514/1.j052922.

[103] H. Kyle, M. Lowenberg, and D. Greenwell.
"Comparative Evaluation of Unsteady Aerodynamic Modelling Approaches".
In: *AIAA Atmospheric Flight Mechanics Conference and Exhibit.*
American Institute of Aeronautics and Astronautics, June 2004.
DOI: 10.2514/6.2004-5272.

[104] P. Proesmans.
"Preliminary Propulsion System Design and Integration for a Box-Wing Aircraft Configuration, A Knowledge Based Engineering Approach".
Thesis. Delft University of Technology, 2019.
URL: http://resolver.tudelft.nl/uuid:0d2ebc46-09ee-493f-bb4c-c871133bff6f.

[105] W. Visser.
"Generic Analysis Methods for Gas Turbine Engine Performance: The development of the gas turbine simulation program GSP".
PhD thesis. Delft University of Technology, Jan. 2015.
URL: 10.4233/uuid:f95da308-e7ef-47de-abf2-aedbfa30cf63.

[106] E. M. Greitzer, P. A. Bonnefoy, E. de la Rosa Blanco, et al.
N+3 Aircraft Concept Designs and Trade Studies. Volume 2; Appendices-Design Methodologies for Aerodynamics, Structures, Weight, and Thermodynamic Cycles.
Report.
NASA Glenn Research Center, 2010.

[107] R. J. M. Elmendorp.
Feasibility study on the use of very large bypass ratio turbofan engines for the PrandtlPlane.
Tech. rep. PARSIFAL Deliverable 7.2.
Delft University of Technology, 2020.
URL: https://www.parsifalproject.eu/PARSIFAL_DOWNLOAD/PARSIFAL_D72.pdf.

[108] M. Voskuijl, G. La Rocca, and F. Dircken.
"Controllability of Blended Wing Body Aircraft".
In: *26th Congress of International Council of the Aeronautical Sciences.*
2008.

[109] C. Varriale, K. Hameeteman, M. Voskuijl, et al.
"A Thrust-Elevator Interaction Criterion for Aircraft Optimal Longitudinal Control".
In: *AIAA Aviation 2019 Forum*.
American Institute of Aeronautics and Astronautics, June 2019.
DOI: 10.2514/6.2019-3001.

[110] A. R. Abdulghany.
"Generalization of parallel axis theorem for rotational inertia".
In: *American Journal of Physics* 85.10 (Oct. 2017), pp. 791–795.
DOI: 10.1119/1.4994835.

[111] S. de Wringer, C. Varriale, and F. Oliviero.
"A Generalized Approach to Operational, Globally Optimal Aircraft Mission Performance Evaluation, with Application to Direct Lift Control".
In: *Aerospace* 7.9 (Sept. 2020), p. 134.
DOI: 10.3390/aerospace7090134.

[112] S. Alam, M. H. Nguyen, H. A. Abbass, et al.
"Multi-Aircraft Dynamic Continuous Descent Approach Methodology for Low-Noise and Emission Guidance".
In: *Journal of Aircraft* 48.4 (July 2011), pp. 1225–1237.
DOI: 10.2514/1.c031241.

[113] International Civil Aviation Organization.
Continuous Descent Operations (CDO) Manual.
Tech. rep. 9931.
ICAO, 2010.
URL: https://applications.icao.int/tools/ATMiKIT/story_content/external_files/102600063919931_en.pdf.

[114] A. Nuic.
User manual for the Base of Aircraft Data (BADA) revision 3.10.
Tech. rep.
European Organisation for the Safety of Air Navigation, 2010.

[115] Y. Zhao and R. A. Slattery.
"Capture conditions for merging trajectory segments to model realistic aircraft descents".
In: *Journal of Guidance, Control, and Dynamics* 19.2 (Mar. 1996), pp. 453–460.
DOI: 10.2514/3.21639.

[116] N. Vinh.
Optimal Trajectories in Atmospheric Flight.
Elsevier Science & Techn., Dec. 2012.
420 pp.
ISBN: 9780444601452.

[117] S. Hartjes and H. Visser.
"Efficient trajectory parameterization for environmental optimization of departure flight paths using a genetic algorithm".
In: *Proceedings of the Institution of Mechanical Engineers, Part G: Journal of Aerospace Engineering* 231.6 (May 2016), pp. 1115–1123.
DOI: 10.1177/0954410016648980.

[118] S. Hartjes, M. E. G. van Hellenberg Hubar, and H. G. Visser.
"Multiple-phase trajectory optimization for formation flight in civil aviation".
In: *CEAS Aeronautical Journal* 10.2 (Sept. 2018), pp. 453–462.
DOI: 10.1007/s13272-018-0329-9.

[119] H. G. Visser and S. Hartjes.
"Economic and environmental optimization of flight trajectories connecting a city-pair".
In: *Proceedings of the Institution of Mechanical Engineers, Part G: Journal of Aerospace Engineering* 228.6 (July 2013), pp. 980–993.
DOI: 10.1177/0954410013485348.

[120] F. Fisch.
"Development of a framework for the solution of high-fidelity trajectory optimization problems and bilevel optimal control problems".
PhD thesis. Technische Universität München, 2011.
URL: https://mediatum.ub.tum.de/doc/1001868/1001868.pdf.

[121] O. von Stryk and R. Bulirsch.
"Direct and indirect methods for trajectory optimization".
In: *Annals of Operations Research* 37.1 (1992), pp. 357–373.
DOI: 10.1007/BF02071065.

[122] J. T. Betts.
"Survey of Numerical Methods for Trajectory Optimization".
In: *Journal of Guidance, Control, and Dynamics* 21.2 (Mar. 1998), pp. 193–207.
DOI: 10.2514/2.4231.

[123] J. T. Betts.
Practical Methods for Optimal Control and Estimation Using Nonlinear Programming.
Society for Industrial and Applied Mathematics, Jan. 2010.
DOI: 10.1137/1.9780898718577.

[124] V. M. Becerra.
"Practical Direct Collocation Methods for Computational Optimal Control".
In: *Springer Optimization and Its Applications.*
Springer New York, 2012,
Pp. 33–60.
DOI: 10.1007/978-1-4614-4469-5_2.

[125] A. Bryson.
Applied optimal control : optimization, estimation, and control.
New York Oxon: CRC Press LLC Routledge, 2018.
ISBN: 9781315137667.

[126] D. E. Kirk.
Optimal Control Theory.
Dover Publications Inc., Apr. 2004.
464 pp.
ISBN: 0486434842.

[127] J. T. Betts and E. J. Cramer.
"Application of Direct Transcription to Commercial Aircraft Trajectory Optimization".
In: *Journal of Guidance, Control, and Dynamics* 18.1 (Jan. 1995), pp. 151–159.
DOI: 10.2514/3.56670.

[128] D. Wu and Y. Zhao.
"Optimization and Sensitivity Analysis of Climb and Descent Trajectories for Reducing Fuel Burn and Emissions".
In: *11th AIAA Aviation Technology, Integration, and Operations (ATIO) Conference.*
American Institute of Aeronautics and Astronautics, June 2011.
DOI: 10.2514/6.2011-6879.

[129] M. Soler, A. Olivares, and E. Staffetti.
"Multiphase Optimal Control Framework for Commercial Aircraft Four-Dimensional Flight-Planning Problems".
In: *Journal of Aircraft* 52.1 (2015), pp. 274–286.
DOI: 10.2514/1.C032697.

[130] A. Nuic, D. Poles, and V. Mouillet.
"BADA: An advanced aircraft performance model for present and future ATM systems".
In: *International Journal of Adaptive Control and Signal Processing* 24.10 (2010), pp. 850–866.
DOI: 10.1002/acs.1176.

[131] H. G. Visser.
"Terminal area traffic management".

In: *Progress in Aerospace Sciences* 28.4 (1991), pp. 323–368.
DOI: https://doi.org/10.1016/0376-0421(91)90004-N.

[132] European Aviation Safety Agency.
Certification Specifications for Large Aeroplanes CS-25A19.
EASA. 2017.

[133] Federal Aviation Administration.
Federal Aviation Regulation, Part 91: General Operating and Flight Rules, Section 117: Aircraft Speed.
FAA. 2020.

[134] J. Gagne, A. Murrieta, R. M. Botez, et al.
"New method for aircraft fuel saving using Flight Management System and its validation on the L-1011 aircraft".
In: *2013 Aviation Technology, Integration, and Operations Conference*.
American Institute of Aeronautics and Astronautics, Aug. 2013.
DOI: 10.2514/6.2013-4290.

[135] R. S. F. Patrón, R. M. Botez, and D. Labour.
"New altitude optimisation algorithm for the flight management system CMA-9000 improvement on the A310 and L-1011 aircraft".
In: *The Aeronautical Journal (1968)* 117.1194 (2013), pp. 787–805.
DOI: 10.1017/S0001924000008459.

[136] International Civil Aviation Organization.
Rules of the Air.
ICAO. 2005.

[137] Federal Aviation Administration.
Instrument Procedures Handbook, FAA-H-8083-16B, Chapter 2: En Route Operations.
FAA. 2020.

[138] Federal Aviation Administration.
Airplane Flying Handbook, FAA-H-8083-3B, Chapter 8: Approaches and Landings.
FAA. 2020.

[139] K. Abu Salem, V. Cipolla, G. Palaia, et al.
"A Physics-Based Multidisciplinary Approach for the Preliminary Design and Performance Analysis of a Medium Range Aircraft with Box-Wing Architecture".
In: *Aerospace* 8.10 (Oct. 2021), p. 292.
DOI: 10.3390/aerospace8100292.

[140] K. Risse, K. Schäfer, F. Schültke, et al.
"Central Reference Aircraft data System (CeRAS) for research community".
In: *CEAS Aeronautical Journal* 7.1 (Nov. 2015), pp. 121–133.
DOI: 10.1007/s13272-015-0177-9.

[141] L. Fogarty and R. Howe.
"Computer mechanization of six-degree of freedom flight equations".
In: *Simulation* 11.4 (Oct. 1968), pp. 187–193.
DOI: 10.1177/003754976801100407.

[142] W. F. Phillips, C. E. Hailey, and G. A. Gebert.
"Review of Attitude Representations Used for Aircraft Kinematics".
In: *Journal of Aircraft* 38.4 (2001), pp. 718–737.
DOI: 10.2514/2.2824.

[143] A. Olivares, M. Soler, and E. Staffetti.
"Multiphase Mixed-Integer Optimal Control Applied to 4D Trajectory Planning in Air Traffic Management".
In: *Proceedings of the 3rd International Conference on Application and Theory of Automation in Command and Control Systems*.
Association for Computing Machinery, 2013,
Pp. 85–94.
DOI: 10.1145/2494493.2494505.

[144] J. Sun, J. M. Hoekstra, and J. Ellerbroek.
"Aircraft drag polar estimation based on a stochastic hierarchical model".
In: *Eighth SESAR Innovation Days, University of Salzburg, Salzburg, Austria*.
2018.
URL: http://resolver.tudelft.nl/uuid:9977a616-4506-4acb-9d27-b9e27f9ddb8d.

[145] Safran Aircraft Engines.
URL: https://www.safran-aircraft-engines.com/commercial-engines/single-aisle-commercial-jets/leap/.

[146] S. Hartjes and H. G. Visser.
"Optimal Control Approach to Helicopter Noise Abatement Trajectories in Nonstandard Atmospheric Conditions".
In: *Journal of Aircraft* 56.1 (2019), pp. 43–52.
DOI: 10.2514/1.C034751.

[147] M. A. Patterson and A. V. Rao.
"GPOPS-II: A MATLAB Software for Solving Multiple-Phase Optimal Control Problems Using Hp-Adaptive Gaussian Quadrature Collocation Methods and Sparse Nonlinear Programming".
In: *ACM Transactions on Mathematical Software (TOMS)* 41.1 (2014), p. 1.
DOI: 10.1145/2558904.

[148] A. Wächter and L. T. Biegler.
"On the implementation of an interior-point filter line-search algorithm for large-scale nonlinear programming".
In: *Mathematical Programming* 106.1 (Apr. 2005), pp. 25–57.
DOI: 10.1007/s10107-004-0559-y.

[149] D. G. Hull.
Fundamentals of Airplane Flight Mechanics.
Springer-Verlag GmbH, Jan. 2007.
URL: https://www.ebook.de/de/product/8898107/david_g_hull_fundamentals_of_airplane_flight_mechanics.html.

[150] C. Varriale.
Aircraft Performance Analysis and Mission Profile Optimization.
Tech. rep. PARSIFAL Deliverable 6.1.
Delft University of Technology, 2017.
URL: https://www.parsifalproject.eu/PARSIFAL_DOWNLOAD/PARSIFAL_D61.pdf.

[151] M. H. Sadraey.
"Design of Control Surfaces".
In:
Aircraft Design.
John Wiley & Sons, Ltd, 2012.
Chap. 12, pp. 631–753.
ISBN: 9781118352700.
DOI: 10.1002/9781118352700.ch12.

[152] A. N. Sousa, A. A. de Paula, F. C. Ribeiro, et al.
"Box wing longitudinal flight quality evaluation".
In: *AIAA Aviation 2019 Forum*.
Dallas, Texas, June 2019.
DOI: 10.2514/6.2019-3490.

[153] F. Oliviero, D. Zanetti, and V. Cipolla.
"Flight dynamics model for preliminary design of PrandtlPlane wing configuration with sizing of the control surfaces".
In: *Aerotecnica Missili & Spazio* 95.4 (Oct. 2016), pp. 201–210.
DOI: 10.1007/BF03404728.

[154] C. Varriale, A. Raju Kulkarni, G. La Rocca, et al.
"A Hybrid, Configuration-Agnostic Approach to Aircraft Control Surface Sizing".

In: *25th International Congress of the Italian Association of Aeronautics and Astronautics (AIDAA)*. 2019.

[155] C. Sánchez, D. Franco, and R. Munjulury.
"Hurricane-CS: Control Surfaces and High Lift Devices Modeling And Sizing Program".
In: *Proceedings of the 31st Congress of the International Council of the Aeronautical Sciences (ICAS)*. 2018.
URL: https://www.icas.org/ICAS_ARCHIVE/ICAS2018/data/papers/ICAS2018_0627_paper.pdf.

[156] M. Söpper, J. Zhang, N. Bähr, et al.
"Required Moment Sets: Enhanced Controllability Analysis for Nonlinear Aircraft Models".
In: *Applied Sciences* 11.8 (2021).
ISSN: 2076-3417.
DOI: 10.3390/app11083456.

[157] J. Zhang, M. Söpper, and F. Holzapfel.
"Attainable Moment Set Optimization to Support Configuration Design: A Required Moment Set Based Approach".
In: *Applied Sciences* 11.8 (Apr. 2021), p. 3685.
DOI: 10.3390/app11083685.

[158] G. X. Dussart, M. M. Lone, and C. O'Rourke.
"Size Estimation Tools for Conventional Actuator System Prototyping in Aerospace".
In: *AIAA Scitech 2019 Forum*.
American Institute of Aeronautics and Astronautics, Jan. 2019.
DOI: 10.2514/6.2019-1634.

[159] A. B. Lambe and J. R. R. A. Martins.
"Extensions to the design structure matrix for the description of multidisciplinary design, analysis, and optimization processes".
In: *Structural and Multidisciplinary Optimization* 46.2 (Jan. 2012), pp. 273–284.
DOI: 10.1007/s00158-012-0763-y.

[160] C. Miller.
"Nonlinear Dynamic Inversion Baseline Control Law: Architecture and Performance Predictions".
In: *AIAA Guidance, Navigation, and Control Conference*.
American Institute of Aeronautics and Astronautics, Aug. 2011.
DOI: 10.2514/6.2011-6467.

[161] T. Lombaerts, J. Kaneshige, S. Schuet, et al.
"Dynamic Inversion based Full Envelope Flight Control for an eVTOL Vehicle using a Unified Framework".
In: *AIAA Scitech 2020 Forum*.
American Institute of Aeronautics and Astronautics, Jan. 2020.
DOI: 10.2514/6.2020-1619.

[162] US Department of Defense.
Flying Qualities of Piloted Airplanes.
MIL-F-8785C Handbook.
US Department of Defenses, 1969.

[163] G. E. Cooper and R. P. Harper.
The use of pilot rating in the evaluation of aircraft handling qualities.
Tech. rep. NASA-TN-D-5153.
NASA Ames Research Center, 1969.
URL: https://ntrs.nasa.gov/citations/19690013177.

[164] US Department of Defense.
Flying Qualities of Piloted Aircraft.
MIL-STD-1797A Handbook.
US Department of Defenses, 1997.

[165] C. Varriale, M. Voskuijl, and L. L. M. Veldhuis.
"Trim for Maximum Control Authority using the Attainable Moment Set".
In: *AIAA Scitech Forum*.
American Institute of Aeronautics and Astronautics, Jan. 2020.
DOI: 10.2514/6.2020-1265.

[166] C. Varriale and M. Voskuijl.
"A trim problem formulation for maximum control authority using the Attainable Moment Set geometry".
In: *CEAS Aeronautical Journal* (Nov. 2021).
DOI: 10.1007/s13272-021-00560-4.

[167] B. L. Stevens, F. L. Lewis, and E. N. Johnson.
Aircraft Control and Simulation: Dynamics, Controls Design, and Autonomous Systems.
Blackwell Publications, Nov. 2015.
768 pp.
ISBN: 1118870980.

[168] A. De Marco, E. Duke, and J. Berndt.
"A General Solution to the Aircraft Trim Problem".
In: *AIAA Modeling and Simulation Technologies Conference and Exhibit*.
2007.
DOI: 10.2514/6.2007-6703.

[169] K. H. Goodrich, S. M. Sliwa, and F. J. Lallman.
A closed-form trim solution yielding minimum trim drag for airplanes with multiple longitudinal-control effectors.
Technical Publication NASA-TP-2907.
NASA Langley Research Center, 1989.
URL: https://ntrs.nasa.gov/citations/19890014097.

[170] D. C. Garmendia and D. N. Mavris.
"Alternative Trim Analysis Formulations for Vehicles with Redundant Multi-Axis Control Surfaces".
In: *Journal of Aircraft* 53.1 (Jan. 2016), pp. 60–72.
DOI: 10.2514/1.c033184.

[171] R. Carbó-Dorca.
"A study on the centroid vector of a polyhedron".
In: *Journal of Mathematical Chemistry* 54.1 (Sept. 2015), pp. 61–71.
DOI: 10.1007/s10910-015-0548-9.

[172] C. Varriale and M. Voskuijl.
"A Control Allocation approach to induce the center of pressure position and shape the aircraft transient response".
In: *Aerospace Science and Technology* (Sept. 2021), p. 107092.
DOI: 10.1016/j.ast.2021.107092.

[173] G. J. J. Ducard.
Fault-tolerant Flight Control and Guidance Systems.
Springer-Verlag GmbH, May 2009.
ISBN: 1848825617.

[174] S. Kim and K. R. Horspool.
Nonlinear Controller Design for Non-minimum Phase Flight System Enhanced by Adaptive Elevator Algorithm.
American Institute of Aeronautics and Astronautics, Jan. 2020.
DOI: 10.2514/6.2020-0603.

[175] M. D. Pavel and G. D. Padfield.
"The Extension of ADS-33—Metrics for Agility Enhancement and Structural Load Alleviation".
In: *Journal of the American Helicopter Society* 51.4 (2006), p. 319.
DOI: 10.4050/jahs.51.319.

[176] T. von Karman and L. Howarth.
"On the Statistical Theory of Isotropic Turbulence".
In: *Proceedings of the Royal Society of London. Series A - Mathematical and Physical Sciences* 164.917 (Jan. 1938), pp. 192–215.
DOI: 10.1098/rspa.1938.0013.

[177] T. von Karman.
"Progress in the Statistical Theory of Turbulence".
In: *Proceedings of the National Academy of Sciences* 34.11 (Nov. 1948), pp. 530–539.
DOI: 10.1073/pnas.34.11.530.

[178] E. F. Trollip and J. A. A. Engelbrecht.
"Ride comfort in commercial aircraft during formation flight using conventional flight control".
In: *2016 IEEE Aerospace Conference*.
Institute of Electrical and Electronics Engineers, Mar. 2016.
DOI: 10.1109/aero.2016.7500886.

[179] *ISO 2631-1, Mechanical vibration and shock — Evaluation of human exposure to whole-body vibration.*
International Organization for Standardization. 1997.
URL: https://www.iso.org/standard/7612.html.

Curriculum Vitæ

Carmine Varriale was born on August 11th, 1992 in Naples, Italy, where he has been living until he was 24 years old. He obtained his high school diploma in scientific studies at the Liceo Scientifico Statale "Giuseppe Mercalli" in 2011. For this, he was granted a small scholarship for "great results and dedication". His university studies have been almost entirely conducted at the University of Naples "Federico II". Here, he obtained his BSc and MSc degrees, respectively in 2014 and 2017, both cum laude, honorable mentions and scholarships for "excellence and promptness" throughout the studies. During his MSc thesis project, he performed flight dynamics and CFD simulations to investigate flight encounters of light aircraft with wind turbine wakes. He carried it out during an internship at the Fraunhofer Institute for Wind Energy Systems in Oldenburg, Germany, with the purpose of providing safety guidelines for the construction of wind farms in proximity of small airports.

Carmine started his PhD research project at the Flight Performance and Propulsion section of TU Delft in 2017. His main research interests have covered flight mechanics and control of novel aircraft configurations. This has brought him to investigate the dynamic behavior of innovative aircraft with redundant and/or interacting control effectors, and to supervise a small number of MSc thesis projects related to these topics. He performed his research work in the framework of the European Union Horizon2020 program, for which he has been leader of the flight dynamics activities within the PARSIFAL project. To support his research studies, as well as other multi-disciplinary research and development activities, he has expanded and re-structured the "Performance, Handling Qualities and Loads Analysis Toolbox", so that colleagues and MSc students under his supervision could use it effectively and independently. Lastly, he has been the (co-)instructor of the online course "Aircraft Performance: Physics and Simulation", target at professional education.

Carmine's interest for flight mechanics and simulation was born in the early years of university, and has been constantly sparkled by the amazing preparation and burning passion of his supervisors and colleagues. He currently has a tenure track position as Assistant Professor at the Flight Performance and Propulsion section of TU Delft, where he performs research activities in the fields of direct lift control, flight dynamics, and modelling and simulation techniques. In his free time, he enjoys hiking, being by the sea, taking photos of natural landscapes, playing chess and other board games.

EXPERIENCE

2021–current **Assistant Professor (Tenure Track) of Flight Mechanics**
Delft University of Technology, Delft, the Netherlands
Course: Flight and Orbital Mechanics
Course: Aircraft Performance: Physics and Simulation

2017–2021 **PhD in Aerospace Engineering**
Delft University of Technology, Delft, the Netherlands
Dissertation: Flight Mechanics and Performance of Direct Lift Control — Applying Control Allocation Methods to a Staggered Box-Wing Aircraft Configuration
Promotor: Prof. dr. ir. L.L.M.Veldhuis
Co-promotor: Prof. dr. ir. M.Voskuijl

2017–2019 **Online Instructor**
Delft University of Technology, Delft, the Netherlands
Course: Aircraft Performance: Physics and Simulation

2016–2017 **Research Intern**
Fraunhofer-Institut für Windenergie (IWES), Oldenburg, Germany

EDUCATION

2017–2021 **Doctoral Education Program**
Delft University of Technology, Delft, the Netherlands

2014–2017 **Master's Degree in Aerospace Engineering (with distinction)**
Università degli Studi di Napoli *Federico II*, Naples, Italy
Thesis: Risk assessment for light aircraft landing trajectories in windy atmosphere and near windfarms
Supervisors: Prof. A.De Marco, Dr. E.Daniele

2011–2014 **Bachelor's Degree in Aerospace Engineering (with distinction)**
Università degli Studi di Napoli *Federico II*, Naples, Italy
Thesis: Aircraft Stability and Control Calculations with a Mathcad-Excel Software Framework
Supervisor: Prof. A.De Marco

2006–2011 **High School Diploma in Scientific Studies (with distinction)**
Liceo Scientifico Statale "Giuseppe Mercalli", Naples, Italy

AWARDS

2017	Master's Degree honorable mention and scholarship for "excellence and promptness" throughout the studies
2014	Bachelor's Degree honorable mention and scholarship for "excellence and promptness" throughout the studies
2011	High School scholarship for "great results and dedication"

List of Publications

Journal Articles

5. N. F. M. Wahler, C. Varriale and G. La Rocca, "Impact of Control Allocation Methods on the Optimal Control Surface Layout of a Box-wing Aircraft" *(under review).*

4. C. Varriale and M. Voskuijl, "A Trim Problem Formulation for Maximum Control Authority using the Attainable Moment Set Geometry", CEAS Aeronautical Journal, 2021.
DOI: https://doi.org/10.1007/s13272-021-00560-4.

3. C. Varriale and M. Voskuijl, "A Control Allocation approach to induce the center of pressure position and shape the aircraft transient response", Aerospace Science and Technology, vol. 119, 2021.
DOI: 10.1016/j.ast.2021.107092.

2. S. de Wringer, C. Varriale, and F. Oliviero, "A Generalized Approach to Operational, Globally Optimal Aircraft Mission Performance Evaluation, with Application to Direct Lift Control", Aerospace, vol. 7, no. 9, 2020.
DOI: 10.3390/aerospace7090134.

1. C. Varriale, A. De Marco, E. Daniele, J. Schmidt, and B. Stoevesandt, "Flight Load Assessment for Light Aircraft Landing Trajectories in Windy Atmosphere and Near Wind Farms", Aerospace, vol. 5, no. 2, 2018.
DOI: 10.3390/aerospace5020042.

Conference Papers

4. C. Varriale, M. Voskuijl, and L. L. M. Veldhuis, "Trim for Maximum Control Authority using the Attainable Moment Set", AIAA Scitech Forum and Exposition, 2020.
DOI: 10.2514/6.2020-1265.

3. C. Varriale, A. Raju Kulkarni, G. La Rocca, and M. Voskuijl, "A Hybrid, Configuration-Agnostic Approach to Aircraft Control Surface Sizing", 25th International Congress of the Italian Association of Aeronautics and Astronautics (AIDAA), 2019.

2. A. Raju Kulkarni, C. Varriale, M. Voskuijl, G. La Rocca, and L. L. M. Veldhuis, "Assessment of Sub-scale Designs for Scaled Flight Testing", AIAA Aviation Forum, 2019.
DOI: 10.2514/6.2019-3089.

1. C. Varriale, K. Hameeteman, M. Voskuijl, and L. L. M. Veldhuis, "A Thrust-Elevator Interaction Criterion for Aircraft Optimal Longitudinal Control", AIAA Aviation Forum, 2019.
DOI: 10.2514/6.2019-3001.

PROJECT REPORTS

3. C. Varriale, "Advanced flight control concepts for the PrandtlPlane to increase safety and passenger comfort"
   PARSIFAL Project Deliverable D6.3, 2020.

2. C. Varriale, "Design optimization for stability and control of a PrandtlPlane"
   PARSIFAL Project Deliverable D6.2, 2020.

1. C. Varriale, "Aircraft Performance Analysis and Mission Profile Optimization"
   PARSIFAL Project Deliverable D6.1, 2018.